Theses and Dissertations

August 2017

Polymer Foam /Fly Ash Composites: Evaluation of Mechanical, Interfacial, Thermal, Viscoelastic and Microstructural Properties

Parisa Khoshnoud
University of Wisconsin-Milwaukee

Follow this and additional works at: https://dc.uwm.edu/etd

Part of the Materials Science and Engineering Commons

Recommended Citation

POLYMER FOAM /FLY ASH COMPOSITES:

EVALUATION OF MECHANICAL, INTERFACIAL, THERMAL,

VISCOELASTIC AND MICROSTRUCTURAL PROPERTIES

by

Parisa Khoshnoud

A Dissertation Submitted in

Partial Fulfillment of the

Requirements for the Degree of

Doctoral of Philosophy

in Engineering

at

The University of Wisconsin-Milwaukee

August 2017

ABSTRACT

POLYMER FOAM /FLY ASH COMPOSITES:
EVALUATION OF MECHANICAL, INTERFACIAL, THERMAL, VISCOELASTIC, AND
MICROSTRUCTURAL PROPERTIES

by

Parisa Khoshnoud

The University of Wisconsin-Milwaukee, 2017
Under the Supervision of Dr. Nidal H Abu-Zahra

Fly ash, a byproduct of coal combustion process in power plants, consists of fine, powdery particles that are predominantly spherical in shape, either solid or hollow, and mostly glassy (amorphous) in nature. It is capable of being recovered and used as a low-cost reinforcing filler. Adding fly ash particles to a thermoplastic foam poses many challenges to understanding the physical, mechanical, viscoelastic, thermal, and morphological changes to the composite. The effects of fly ash particles on the foaming process; e.g. nucleating and growth steps, cell types and size, and microstructure need to be evaluated in order to develop a commercial composite material. The main goal of this work is to evaluate the use of fly ash as a cost-effective and reinforcing filler in polymer foam composites. PVC foam is selected as the base polymer and it is expected that the research findings can be generalized to other polymer foam systems.

Initially, two classes of fly ash, class-C and class-F (two different particle sizes) are well characterized and studied. Their elemental, chemical, structural, thermal and morphological properties are evaluated. Although both classes of fly ash have almost the same surface area, Class-C contains more quartz and lime content than class-F; whereas class-F is highly concentrated with iron oxides. In addition, 25 micron sized class-F fly ash possesses different chemical composition compared with 50 micron class-F fly ash. Structural analysis showed the presence of hydroxyl functional groups in both types of fly ash particles.

In the second phase, PVC foam/fly ash composites containing various levels of fly ash are prepared using extrusion as a processing method. To understand all performance aspects of fly ash, a wide range of characterizing methods was used to evaluate the physical, mechanical, thermal, and morphological properties of the composites. The experimental results showed that the density increases with increasing the amount of fly ash, while the cell size decreases. Tensile and flexural properties increased by adding fly ash, which indicates that fly ash particles are properly incorporated into the polymer. However, the elongation and impact strength of the composites decreased with increasing fly ash due to the higher rigidity of the polymer composites. Thermal analysis shows that the glass transition temperature of the composites is not significantly affected by the addition of fly ash. Thermal decomposition studies show that the dehydrochlorination of PVC is accelerated in the presence of fly ash, while the main backbone crack is enhanced.

Kinetic studies were carried out on the loaded and unloaded fly ash composites and the activation energies of both decomposition steps were estimated using Flynn-Wall model. A higher activation energy in the first step of decomposition of the pure PVC foam is noticed compared with that of fly ash loaded, while the estimated activation energy of the second step in the composites is significantly higher. Dynamic mechanical analysis confirmed the increase in stiffness as fly ash content increased in the composites due to good interfacial adhesion between the filler and the matrix. Dimensional stability of the composites improved considerably with the addition of fly ash at high loadings and morphological studies confirmed good dispersion, distribution, and interaction between fly ash and PVC matrix.

The effect of the chemical composition of fly ash on the final properties of the foam composites are studied using both classes of fly ash, C and F. The experimental results show that class-C fly ash interacts better with the polymer matrix and improves the mechanical and thermal properties significantly when compared to class-F. This is attributed to a higher SiO_2 and CaO content in class-C fly ash. Interfacial interaction of the composites reinforced with both classes of fly ash was estimated using Pukanszky model

to confirm. Structural analysis confirmed the presence of hydroxyl (–OH) functional groups on the surface of SiO_2, which plays a significant role in the formation of physical bonding and therefore interfacial interactions between fly ash particles and the polymer matrix. Morphological studies of the fracture surfaces using SEM/EDS line-scan also confirmed the effectiveness of silicon and calcium elements in the properties improvement due to their high concentration in the well-bonded particles.

The effect of the particle size of fly ash on the composites structure and performance was also evaluated. Two pre-sieved fly ash particles in the size range of 25 micron and 50 micron were used to prepare rigid PVC/fly ash composites and examine the dependency of the composites performance on the filler size and composition. It was found that at the same fly ash loadings (10wt%), 25 micron sized loaded composites show better mechanical properties due to their higher surface area and the amount of hydroxyl groups. The interfacial interaction between the two different fly ash particle sizes with rigid PVC was evaluated experimentally, using nanoindentor, and quantitatively, using models developed by Pukanszky and Kubat.

Recyclability and reprocess-ability of the fly ash filled composites were also investigated. The experimental results achieved by processing measurements showed that the maximum and minimum torque values increase by adding more regrind. Whereas, increasing fly ash content decreases the melt viscosity and improves processability. It was also observed that the mechanical properties of the reprocessed composites improve by adding more regrind, which indicates a good gelation in the composites containing both virgin and regrind of PVC/fly ash foam. SEM images confirmed a good level of mixing and gelation between virgin and regrind foam matrix up to 40wt% regrind content.

To my loving and supportive Father and Mother,
who guided me to where I am today

TABLE OF CONTENTS

LIST OF FIGURES

LIST OF TABLES

ACKNOWLEDGEMENTS

I would like to express my sincere gratitude to my advisor Prof. Nidal Abu-Zahra for the continuous support of my Ph.D. study. Without his guidance and persistent help this dissertation would not have been possible.

Special thanks goes to my committee members: Dr. Benjamin Church, Dr. Changsoo Kim, Dr. Hong Chang and Dr. Wilkistar Otieno for their valuable advice and guidance.

In addition, a thanks to Dr. Steve Hardcastle, the manager of the Advanced Analysis Facility (AAF) in the College of Engineering & Applied Science, who provided insight and expertise that greatly assisted this research.

Chapter 1- Introduction

1-1- Introduction to Polyvinyl Chloride (PVC) Foam

Polyvinyl Chloride (PVC) is one of the most valuable plastic materials in the chemical industry and as compared to other building materials, it is more inexpensive and easier to assemble and therefore is mainly used in construction. PVC is widely used in window frames and blinds, decorative trimming, furniture components, advertising boards and other applications [Lee et al. (2000)]. PVC as the second most used plastic materials in the world, has a well-established market which globally makes up twenty percent of all the sold resins. In 2007, the PVC universal market size was around 32.2 million tonnes, and based on researched data the expectancy for 2011 was about 39 million tonnes. Twenty five percent of all PVC resin consumption in the world was mainly due to the U.S. and Canada, which was the largest worldwide consumption market in 2007. Asia and Europe are the prominent regions in terms of PVC production. By the end 2009, global PVC production achieved the level of 29,924,000 ton/year that is equivalent to the utilization level of 62%. Meanwhile, the share of North America in producing PVC is 17% [Lee et al. (2000); Deloitte & Touche Regional Consulting Services (2010)]. Breakdown of production is shown in Figure 1-1.
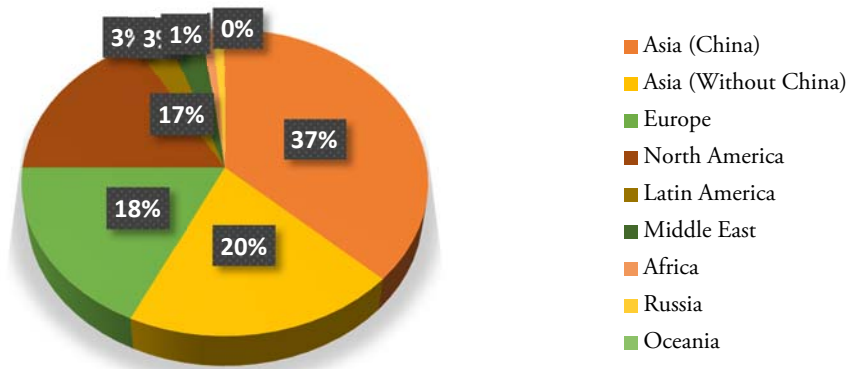
Figure 0-1- Global production capacities of PVC by region [Deloitte & Touche Regional Consulting Services (2010)]

Polymer foams are made up of a solid and gas phase mixed together. The used gas phase is known as a blowing agent, and can be either chemical or physical. Chemical blowing agents take part in a chemical reaction or decompose and produce gas, while physical blowing agents are inert gases that do not react [Wallenberger et al. (2001)]. They have many advantages over solid polymers. For example their low density make them more cost effective due to the significant weight reduction, low heat transfer make them optimal insulators, their flexibility make them comfort for furniture and bedding applications and etc. Therefore in the past few years, polymer foam processing attracted many researchers' attractions [Lee et al. (2006)]. Polymer foams are found virtually everywhere in our modern world and are used in a wide variety of applications such as disposable packaging of fast-food, the cushioning of your furniture and insulation material [Wallenberger et al. (2001)]. The market size of polymer foams reached out 20.1 million tons in 2014, and it is expected to reach 26.9 million tons in 2020. The global polymer foam market has been segmented into five types including polyurethane, polystyrene, polyvinyl chloride (PVC), polyolefin and others (such as, phenolic, melamine and silicone) [Ceskaa (2016)].

The market for rigid PVC foam can be categorized into three main applications as profile, sheet, and pipe which is shown in Figure 1-2. Within Europe the current sizes of the earlier mentioned sectors are estimated to be 60, 50, and 180 Kilotonnes, respectively. These markets are regional, reflecting the differences throughout Europe of both building design and construction regulations. For instance, the UK is by far the largest market for foam profile, whereas foam sheet is predominantly produced in Germany, with additional production in Switzerland and Eire. The most important market for foam pipe has always been France, although now significant quantities are also manufactured and used in Germany, the Netherlands and Spain [NEXTOOL (2009)].
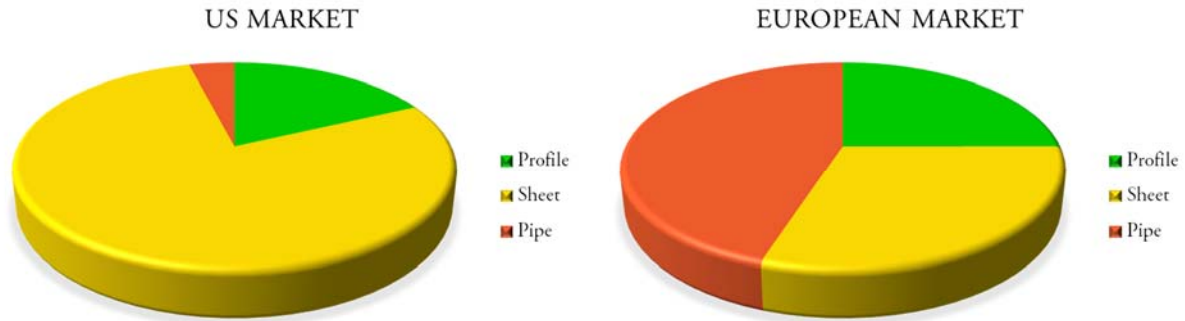
Figure 0-2- PVC Foam market [NEXTOOL (2009)].

1-1-1- PVC Foam General Aspects

Polymer foams can be viewed from different practical perspectives, such products, technology, and components. They can be categorized in different ways, for instance, by nature as flexible and rigid, by dimension as sheet and board, by weight as low density and high density, by structure as open cell and close cell, and by cell size as foam and microcellular [Lee et al. (2006)]. Polymer foams can be also categorized into either thermoplastics or thermosets. The thermoplastics can usually be broken down and recycled; while thermosets are harder to recycle because they are usually heavily cross-linked. In addition, Closed-cell foams are generally more rigid, while open-cell foams are usually flexible [Lee et al. (2000)]. PVC foam mostly has "closed cells," which makes this material water-resistant and anticorrosive. It is also considered as a non-toxic pollutant (heavy metal-free materials) and eco-friendly material. Respectively in Table 1-1 and Figure 1-3 summery of foaming prospective and polymeric foam performance dependency is represented.

Table 0-1- Foaming prospective [Lee et al. (2000)]

Perspective	Terminology
Material	Thermoplastic and Thermoset
Mechanism	Soluble Foaming and Reactive Foaming
Nature	Flexible and Rigid
Structure	Closed Cell and Open Cell
Cell Size	Microcellular and Cellular
Density	High Density and Low Density
Dimension	Broad and Thin Sheet

PVC foam provides many advantages over solid rigid PVC which are listed as follows:

1) Lower cost per unit volume

2) Less density than solid rigid PVC

3) Greater rigidity (which gives the possibility of thicker panel production)

4) Wood substitute with easier handling and machining

5) Better insulating and acoustic properties (due to the presence of air pockets)
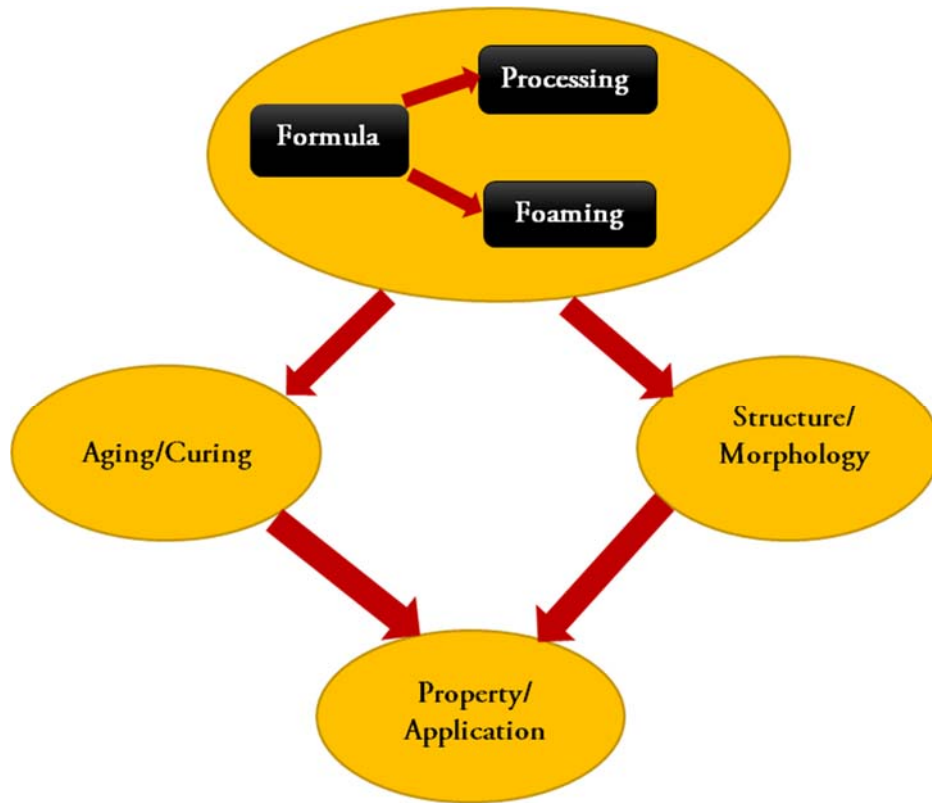
Figure 0-3- Polymeric foam performance dependency summary chart[Lee et al. (2000)].

Rigid PVC foam is excellent replacement for wood products in window frames, window blinds, decorative trimming, furniture components, advertising boards, and other applications. In addition, PVC foam has many advantages over wood such as a good chemical resistance, good weather ability, and good fire retardancy [Rabinovich et al. (1997); Thomas (2004a); Thomas (2004b)]. PVC foams are used in many different sandwich structure applications varying from thermal insulation to aerospace applications and are probably the most widely used core material. They have 95% closed-cell structure at lower densities and completely closed-cell at higher densities [Carnachan (2004)].

1-1-2- PVC Foam structure and properties

Structurally PVC is a vinyl polymer that on every other carbon in the backbone chain, one of the hydrogen atoms is replaced with a chlorine atom and it is polymerized via free radical polymerization of vinyl chloride. The polymerization reaction is highly exothermic and the number of monomers as a repeat unit in PVC can be in a range of 500 to 4000. Figure 1-4 shows PVC structure.

$$n \begin{bmatrix} \underset{H}{\overset{H}{C}} = \underset{H}{\overset{Cl}{C}} \end{bmatrix} \xrightarrow[\text{13atm}]{\text{325-350k}} \left(\underset{H\ \ H}{\overset{H\ \ Cl}{C\text{—}C}} \right)_n \quad \Delta H = -96 \text{ kJ mol}^{-1}$$
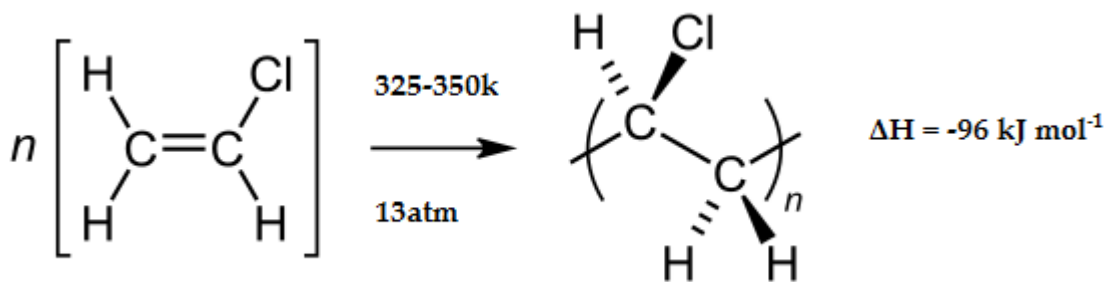
Figure 0-4- PVC polymerization mechanism [Wikipedia (2017)]

PVC foam is produced by introducing gas into the polymer melt. At nucleation sites, the release of external pressure results in the expansion the gas to form cells within the polymer melt. When the temperature decreases below the glass transition point the expansion of the cells ceases forming a solid foam [Hess (2014)].

PVC foam can be classified into two different types, a thermoplastic, called linear, and a cross-linked isocyanate. Linear PVC foam has great ductility, but softens at elevated temperatures. The cross-linked PVC is more rigid, has higher mechanical properties and better thermal stability, but is more brittle. PVC is also non-flammable, but HCl gas will be released when it is burned [Carnachan (2004)]. In order to produce a light weight rigid PVC foam with a sufficient stiffness,

7

strength and impact properties, it is important to control parameters such as foam density, skin thickness, surface finish and cell size. A polymeric foam structure possesses unique physical, mechanical, and thermal properties, which are governed by polymer matrix, the cellular structure and the gas composition [Throne (2004)]. According to the model of Gibson and Ashby, the mechanical properties (Figure 1-5), i.e., the tensile modulus of foams are determined by three factors [Eaves (2004)]:

      1)   Density of the foam

      2)   Tensile modulus of the blend used, and

      3)   Foam structure
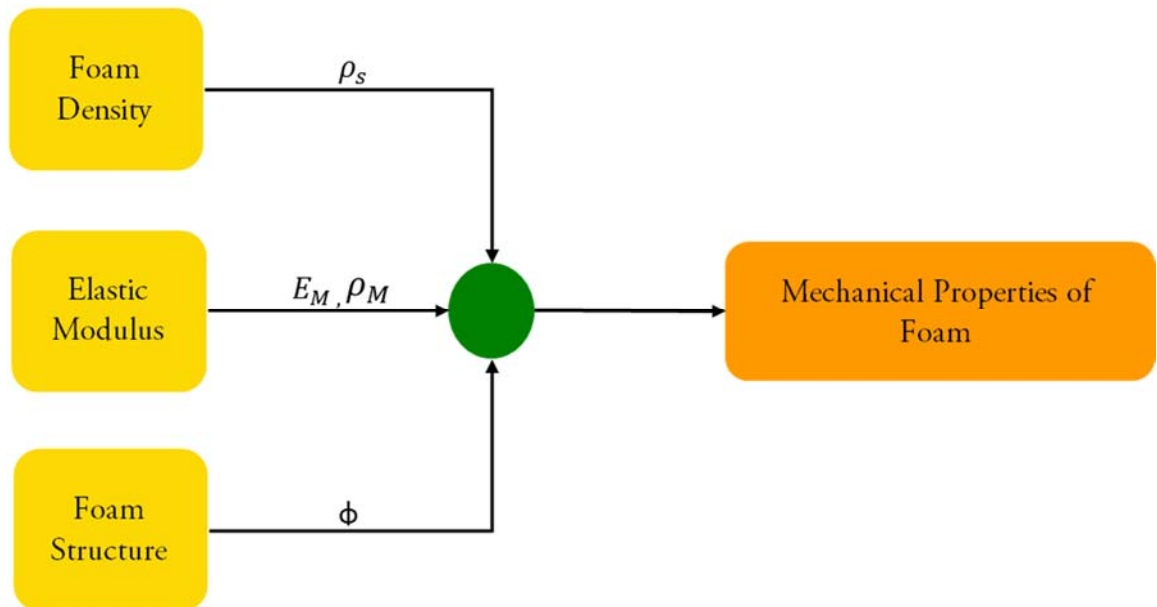
Figure 0-5-Influence factors for mechanical properties of foams [Eaves (2004)].

8

Polymer foams can also be counted as a composite as it is prepared by dispersing a spherical gas phase within a polymeric matrix, thus the properties of this composite are determined by its constituents and their distributions. Since the weight of gas is negligible, the properties of gas/polymer composite often volumetrically depend on participating components. The density is a typical example of this, especially in cases where the bubble phase dominates. However, the thermodynamic properties such as the specific heat, the equilibrium constant, and the heat conductivity, would still remain gravimetrically dependent on the individual elements, i.e., by weight of each element [Lee (2000)].

1-1-3- Formulation of Polymer Foams

Formulation of polymer foam system is a critical factor that determines the produced foam density and morphology. The key ingredients in the recipe are blowing agent and processing aid, although the type of PVC, lubricants and stabilizers are also important [Eaves (2004)]. In Table 1-2, raw material considerations are shown.

Table 0-2- Raw Material Considerations, [Eaves (2004)].

Material Name	Roles
PVC Resin	Viscosity affects the final performance
Stabilizer	Dual role of heat stabilizer and active the blowing agent
Blowing agent	Endothermic blowing agent- $NaHCO_3$
	Exothermic blowing agent- $C_2H_4O_2N_4$
Nucleating agent	Promote optimum gas evaluation and develop the finer cell structure
Impact factor	Modify the elasticity of the melt
Process aid	Enhance the elasticity of the melt, good elasticity allow individual bubbles to expand in the melt without breaking
Lubricants	Control the fusion rate and heat generation rate, to avoid premature gas evaluation
Filler	Positive effect on the activation of blowing agents

1-1-3-1 Blowing agent

The cellular structure of polymer foams is generated by either decomposition of chemical blowing agents (CBA), which are organic or inorganic compounds that decompose on heating to evolve one or more gases applying physical blowing agents (PBA), which are gases or low boiling point liquids, are not widely used in the production of rigid PVC foam [Thomas (2004a); Thomas (2004b); NEXTOOL (2009); Annapragada (2007)]. Two commonly used blowing agents in the production of rigid PVC foams are azodicarbonamide and sodium bicarbonate.

Azodicarbonamide (AZO) is widely used in the polymer industry, specifically in PVC foam production. It has the advantage of being a highly efficient exothermic blowing agent, which gives

a high rate of gas expansion and fine, uniform cell structure. Its gas yield is about 220cm^3/g, which mainly contains N_2, NH_3, CO and CO_2 during decomposition [Eaves (2004)]. Its structure is shown in Figure 1-6.
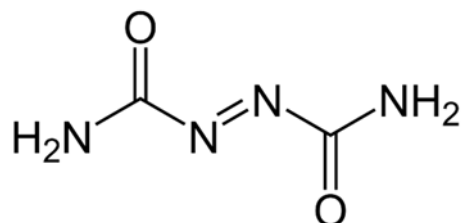
Figure 0-6-Azodicarbonamide structure [Wikipedia (2017)].

Sodium bicarbonate (SBC) is also another well-known blowing agent as its main usage is in baking. Its decomposition is endothermic and reversible and takes place over a wide temperature range, which fortunately coincides with the processing window for rigid PVC (160-190℃). The decomposition products are CO_2, H_2O, and Na_2CO_3 and its gas yield is about 125cm^3/g. However, compared with AZO, its decomposition has been described as slow and erratic. SBC is less efficient blowing agent than AZO [Thomas (2004a); Thomas (2004b); NEXTOOL (2009); Annapragada (2007)].

Researches showed that combination of both AZO and SBC has a synergistic effect which leads producing a very low density foam. Morphological studies confirmed that foam produced by using SBC alone have a coarse cell structure, while cell structure of the foams resulted from both AZO and SBC blowing agents were finer and more uniform [Thomas (2004b)]. Optimized formulation of rigid PVC foam profile, which results in a low density foam with optimum property contains high level of SBC along with a low level of AZO, which acts as 'nucleating agent' to

ensure reasonably fine cell structure. These foams are mainly produced for applications that a particularly fine cell structure is needed and for products produced by the free-foaming method [Thomas (2004a); NEXTOOL (2009)].

1-1-4- Foam Processing

Structural parameters such as cell density, expansion ratio, cell size distribution, open-cell content, and cell integrity will determine the characteristics of polymeric foams. These cellular structural parameters are governed by the foaming technology used in processing, and the foaming technology often heavily depends on the type of polymer to be foamed. In other words, different polymers display different properties, and thus distinct processing systems are required to accommodate these discrepancies. This is why various foaming technologies, such as batch (single-stage, multi-stage), semi-continuous, and continuous processes, have been gradually developed over years for each specific polymer foam [Lee (2000)].

Generally, polymer foam processing includes three main stages including implantation of gas, expansion of gas, and stabilization of polymer. Governing mechanisms and parameters in various stages are mostly different and changing the surrounding conditions may cause in competing mechanisms and make the kinetic process more complex [Lee et al. (2006)]. Selected processing parameters and their effects are listed in Table 1-3.

Table 0-3- Processing parameters and their effects at different stages, [Lee et al. (2006)]

	Implementation	Expansion	Stabilization
Temperature	Solubility ↑	Volatility ↑	Solidification ↓
Viscosity ↓	Surface tension ↑	Permeability ↑	
Reactivity ↑	Viscosity ↓		
Diffusivity ↑			
Interaction parameter ↓			
Pressure	Solubility ↑	Shear heat ↑	Solidification -
Viscosity -	Surface tension -		
Homogenization↑	Nucleation ↑		
Shear	Solubility -	Nucleation ↑	Solidification ↓
Dissolution ↑	Growth ↑		
Dispersion ↑	Cell distribution ↑		

1-1-4-1- Foam Extrusion

The principal method for the production of PVC foam profile, sheet and pipe is extrusion, which is a process of forcing a highly viscous liquid under pressure through a shaped orifice. Commercial foams are usually produced by foaming the polymer containing gas outside the extruder and die [Thomas (2004a); Thomas (2004b); Throne (2003)].

Foaming process includes two straightforward steps; generating bubbles and stabilizing them within a polymeric matrix [Lee et al. (2006)]. Main steps in foaming process in shown in Figure 1-7. Any gas can serve as a blowing agent, but not all can be easily implemented in the foaming process. In terms of solubility, volatility, and diffusivity some gases are more preferred. Therefore,

the blowing agent quality, quantity, and nature are key parameters in the production of a foamed structure with certain desired properties. The blowing agent governs the selection of the foaming methodology, which more often than not becomes a limiting factor in industrial practice [Lee et al. (2006)].
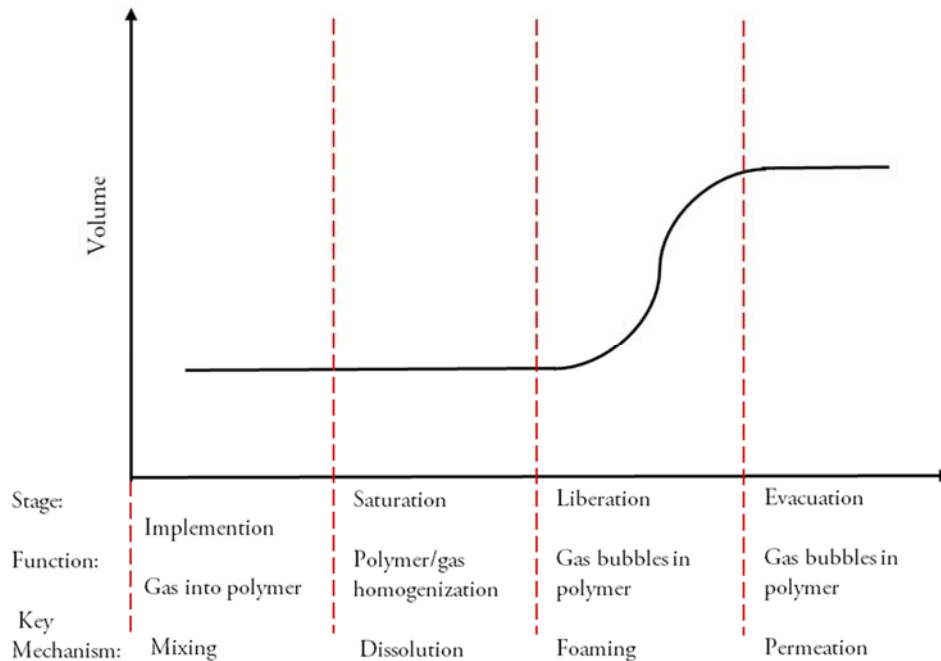
Figure 0-7- Foaming process main steps, [Annapragada (2007)].

Gas is introduced into the molten polymer in extruder barrel either by thermal decomposition of chemical blowing agents (CBA) or by direct injection of physical blowing agents (PBA). In order to achieve an optimum foaming process, it is necessary that bubble nucleation is delayed until the polymer melt emerged from die. Hence high pressure must be maintained throughout the barrel and die to keep the gas in solution. Therefore, appropriate screw and die design, as well as good temperature control is needed. Decreasing the die temperature causes both melt viscosity and

pressure increase, which will suppress any undesirable, premature foaming [Thomas (2004a); Thomas (2004b); Throne (2003)].

Rapid pressure drop occurs when the polymer melt exits the die, which leads the polymer to become supersaturated with gas. Then, phase separation takes place and almost instantaneous nucleation of bubbles occurs. Bubbles will nucleate at irregularities in the polymer melt such as CBA solid residues, pigments, fillers, etc. and their growth rate is rapid at first and then drops as pressure within them diminishes. Bubble growth is also retarded as the polymer cools down and its viscosity increases. Rapid cooling of the final polymer foam product is essential to prevent the foam structure from collapsing, which will be done by passing the foam through chilled calibration unit. The surface quality, density, and thickness of the outer skin are influenced by the distance between the die and the calibration unit as well as the intensity of the cooling [Lee (2000); Eaves (2004); Thomas (2004a); Throne (2003); Annapragada (2007)]. Figure 1-8 shows general foam extrusion process.
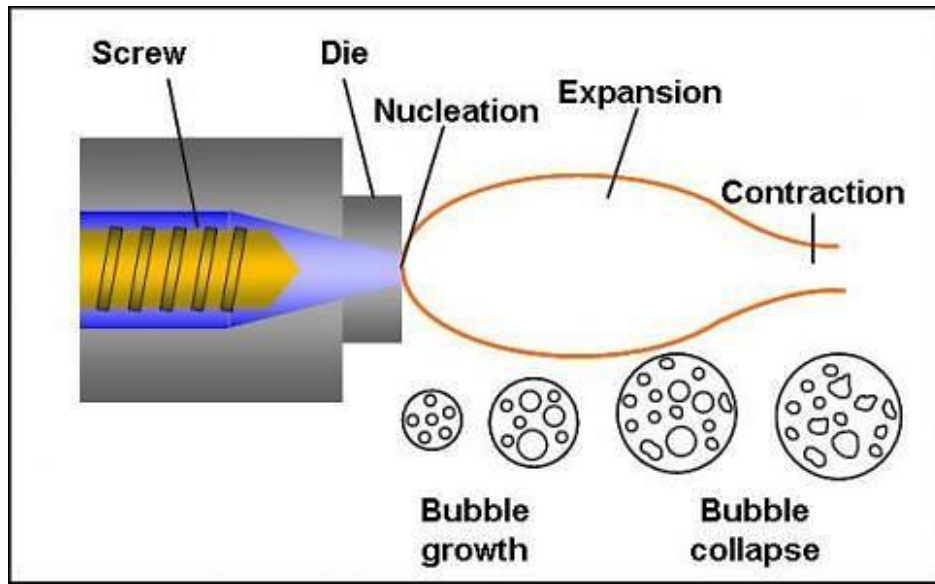
Figure 0-8- Foam extrusion process, [Aurora plastics (2017)]

Rigid PVC foam is processed from dry blend on parallel or conical, contra-rotating, twin-screw extruder, which generally can be produced according to two different foaming methods, free-foaming and Celuka methods, which are described as follows [Thomas (2004a); NEXTOOL (2009)].

1-1-4-2- Free Foam Process

Melt expands freely upon emerging from the die in free foam process, which let free expansion in the both cross section and extrusion directions. Density and thickness of the final product can be controlled by varying the drawdown rate. The final product performance affected by processing conditions, formulation, and the blowing agent type preferred for simple geometry profiles. Schematic of free foam processing is shown in Figure 1-9 [Thomas (2004a); NEXTOOL (2009)].

16
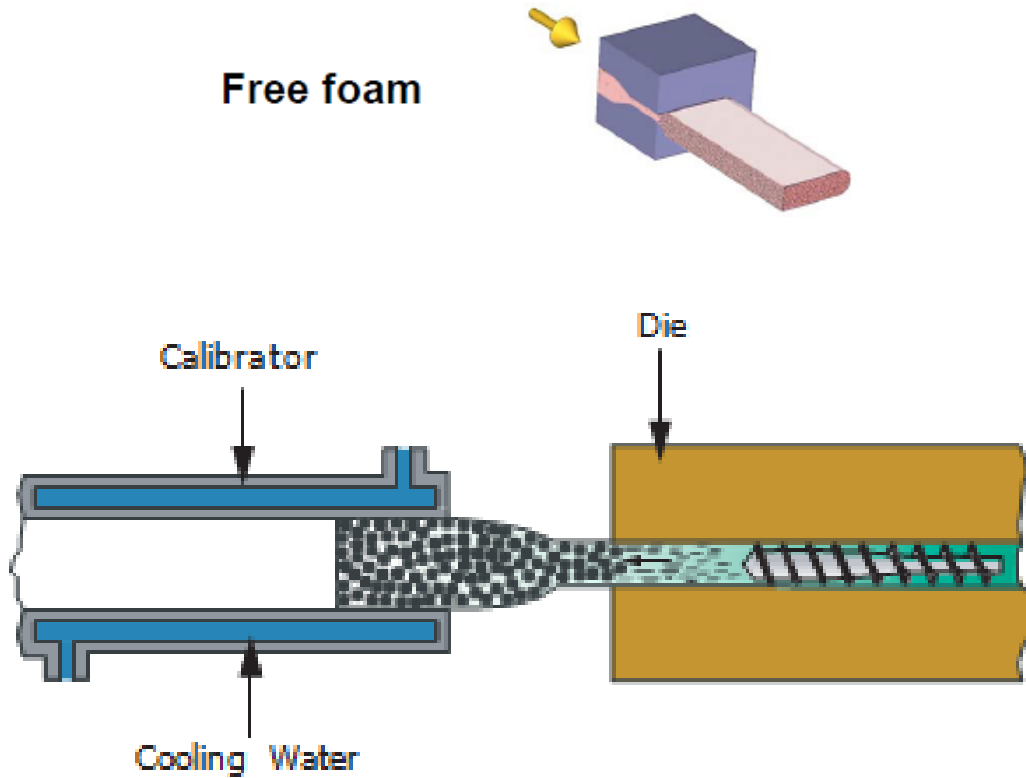
Figure 0-9- Free foam process, [Qingdao extrusion Technology (2017); Aurora plastics (2017)]

1-1-4-3- Celuka Foam Process

The Celuka is also called as inward foaming process which is shown schematically in Figure 1-10. In this process, the extruded product surface is immediately cooled upon exiting through the die. The cell formation suppressed on the surface, the hard finish skin created while the foam allowed to expand toward the center of the melt and rejoined after passing around a mandrel.

The process involves simultaneous calibration of the final shape. The Celuka process is preferred for thicker and relatively complicated products, such as boards, sheets, and profiles [Qingdao extrusion Technology (2017); Aurora plastics (2017)].

17
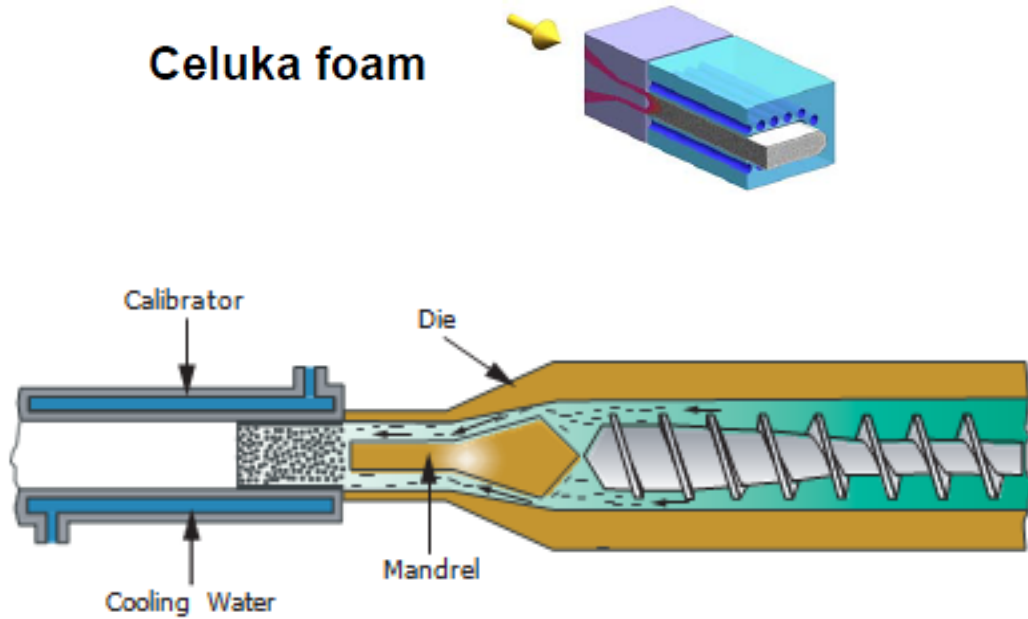
Figure 0-10- Celuka foam process, [Qingdao extrusion Technology (2017); Aurora plastics (2017)].

1-1-4-4- Comparison between free foam and Celuka

Free foam has thin skin with higher density and also less rigid and textured surface finish. However, Celuka foam has nearly solid surface and low density core and also in these type of foam density gradually decrease from surface to center. Free Foam is also faster and has easier operation than Celuka. In Free foam, surface quality is poor, while in Celuka voids in center of products are inevitable during the extrusion [Qingdao extrusion Technology (2017); Aurora plastics (2017)]. The distribution of density across the cross section is shown in Figure 1-11.
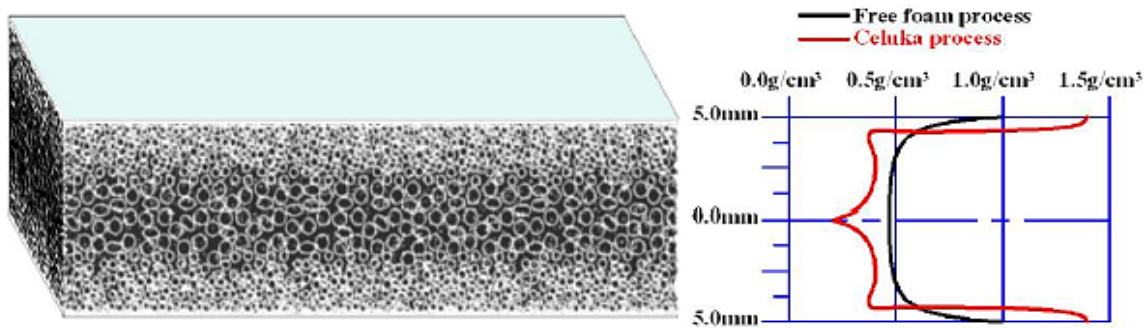
Figure 0-11- Comparison between the distribution of density across the cross section of Free and Celuka Foams,

[Qingdao extrusion Technology (2017); Aurora plastics (2017)].

1-1-5-PVC Foam recycling

One particular criticism often levelled at PVC products is that it cannot be recycled. Specifically recycling of rigid PVC foam usually with a very complicated formulation; containing processing aid, thermal stabilizer, blowing agent, lubricants, pigment and filler is even more complicated. In fact, all PVC foam ingredients can influence melt flow, gelation behavior, thermal stability, melt rheology and strength and therefore will define the final properties of the product [Thomas (2004a)].

Generally, PVC has a lower thermal degradation temperature than other polymers and it should not be processed above 200℃. Increasing the regrind percentage of PVC in plastic waste increases the possibility for thermal breakdown of the whole compound [Materion (2011)] as PVC may have degraded before some other polymers have reached their melting point [Lee (2000); Thomas (2004a)]. In addition, each time the material is processed, some of the heat stabilizers will be used. Therefore, the heat stabilizer in the virgin material must also protect some portion of the regrinds and as higher amount of regrind is used, more heat stabilizer should be added to the virgin resin

19

during compounding. A common mistake is to reprocess large amounts of regrind, which is no longer adequately heat stabilized, causing temporary problems such as the generation of HCl [Materion (2011)]. One of the advantages of producing co-extruded PVC foam profile or pipe is the opportunity that it provides to use recycled material in the foamed core. The recyclate may be industrial scrap recovered from pipe production or foam production processes, or it may be material recovered alter consumer use [Tomaszewska (2005)].

1-2- Introduction to Fly Ash

Fly ash is a by-product of the pulverized coal combustion in thermal power plants [Ramezanpour (2014)]. The pulverized coal, when blown with air into the boiler's combustion chamber immediately ignites generating heat and producing a molten mineral residue. Boiler tubes extract the heat from the boiler, cooling the flue gas and causing the molten mineral residue to harden and form ash [Anantharaman (2008)]. Schematic layout of a fly ash production is shown in Figure 1-12 [Thomas (2007)].

Fly ash is defined as "the finely divided residue that results from the combustion of ground or powdered coal and that is transported by flue gasses from the combustion zone to the particle removal system" [Thomas (2007)]. The heavier unburned materials drop to the bottom of the furnace, referred to as "bottom ash" or 'slag" which looks similar to sand, while the lighter fine ash particles, termed "fly ash", remain suspended in the flue gas [American Coal Ash Association (2003); Thomas (2007)]. The dust-collection system removes the fly ash, either mechanically or by using electrostatic precipitators, as a fine particulate residue, from the combustion gases before they are discharged into the atmosphere [Thomas (2004c), Thomas (2007)].

Coal Fired Power Station
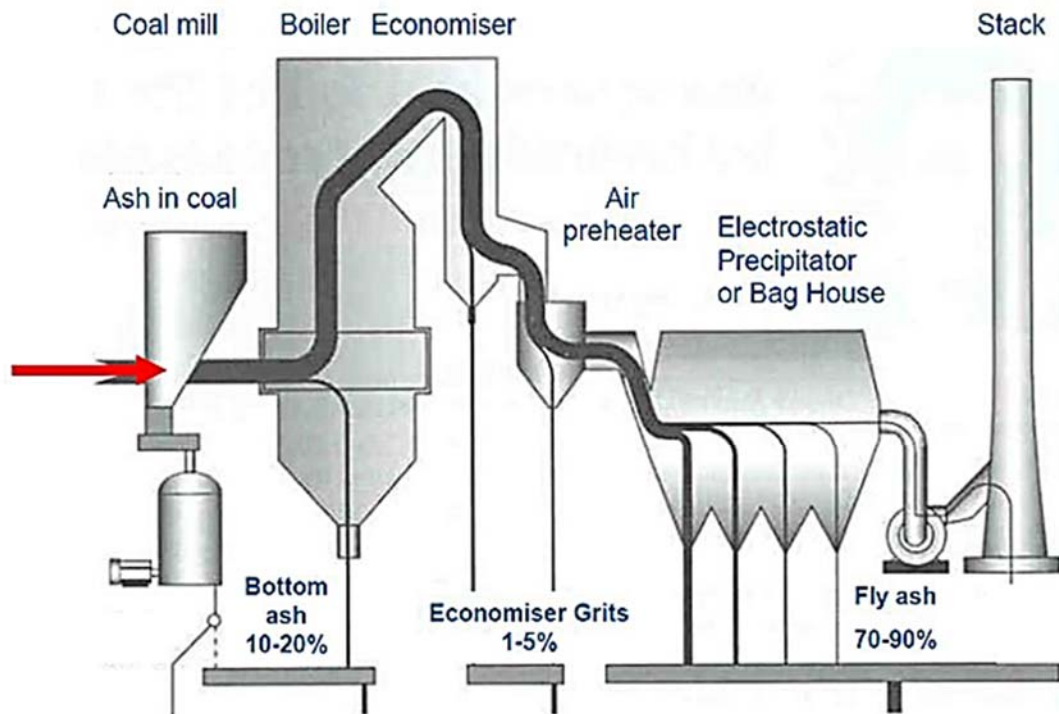
Figure 0-12- Fly ash production schematic [Thomas (2007)].

Fly ash is also known as a pozzolanic material, which is defined by the American Society for Testing and Materials (ASTM) as "a siliceous or siliceous and aluminous material which in itself possesses little or no cementitious value but which will, in finely divided form and in the presence of moisture, chemically react with calcium hydroxide at ordinary temperature to form compounds possessing cementitious properties" [ASTM C618-92a].

US congress has classified fly ash as the sixth most abundant resource in the United States of America [Anantharaman (2008)]. In 2001, 62 million metric tons (68 million tons) of fly ash was produced, while only 20 million metric tons (22 million tons), or 32 percent of total production,

22

was used and the remaining amounts of 68% of the total produced fly ash were disposed in landfills [American Coal Ash Association (2003)]. As shown in Figure 1-13, the utilization rate of fly ash has grown from 8.4 percent of coal combustion production in 1974 to 43.7 percent in 2013, when 23.3 million tons were beneficially used. "Based on ready mixed concrete market projections, fly ash utilization is forecast to increase to 35.7 million tons in 2033—a 53 percent cumulative increase. The existence of such significant amounts forms a serious problem that has negative impacts on the society and the environment. Hence, the optimum utilization of the fly ash will contribute in solving this problem [Mining Media International (2017)].
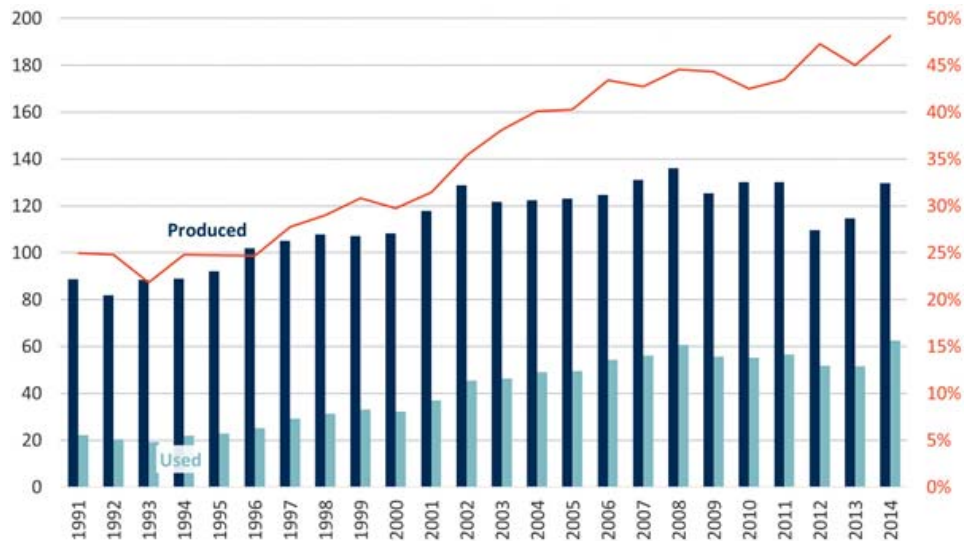
Figure 0-13- Rate of fly ash production and utilization, 1991-2014 [Mining Media International (2017)].

One of the major fly ash utilization is in concrete, which has significant environmental benefits including increasing the life of concrete roads and structures by improving concrete durability and net reduction in energy use and greenhouse gas and other adverse air emissions when fly ash is used to replace or displace manufactured cement. In addition, generally utilization fly ash in any

application will cause in a reduction in amount of coal combustion products that must be disposed in landfills and conservation of other natural resources and materials [Hardjito and Rangan (2005); American Coal Ash Association (2003), Anantharaman (2008)].

1-2-1- Fly Ash Characteristics

1-2-1-1- Shape and Size

Fly ash typically has a unique spherical particles and some ashes also contain irregular of angular particles. Its typical spherical microscopic structure is mainly related to the equilibrium of the forces on the molten inorganic particle as it is forced up the furnace or smoke stack against gravity. The molten particles cool down rapidly, maintaining their equilibrium shape. A similar situation is found in spherical drops of water falling from a faucet [Anantharaman (2008)]. The size of particles varies depending on the sources, ranging in diameter from less than $1\mu m$ up to $150\mu m$ with specific gravity in a range of 1.8-2.8 g/cm³. Some of these particles appear to be solid, whereas some larger particles appear to be portions of thin, hollow spheres containing many smaller particles, which is called cenosphere [Thomas (2008); Hardjito and Rangan (2005); Ramme (2013)]. Cenospheres are lightweight, idle, and empty circles basically comprising of silica and alumina, are loaded with air or gasses, and are by results of the ignition of pulverized coal at the warm power plants. It fluctuates from light black color to practically white shade and their specific gravity extends in the middle of 0.4–0.8g/cm³, which offers them extraordinary lightness [Sen (2014)].

The type of dust collection equipment used largely determines the range of particle sizes in any given fly ash. The fly ash from boilers at some older plants using mechanical collectors alone

is coarser than from plants using electrostatic precipitators. Fineness of fly ash mostly depends on the operating conditions of coal crushers and the grinding process of the coal itself. Finer gradation generally results in a more reactive ash and contains less carbon. It is found that high-calcium fly ashes were finer than the low calcium ones, and this difference is related to the presence of larger amounts of alkali sulphates in high-calcium fly ashes [Thomas (2004c); Thomas (2007)].

1-2-1-2- Mineralogical and Chemical Composition

Chemical composition of fly ash will determine its type and relative amounts of incombustible matters [Thomas (20044), Hardjito and Rangan (2005)]. Fly ash consists mainly the oxides of silicon (SiO_2), aluminum (Al_2O_3), iron (Fe_2O_3), and calcium (CaO) and lesser degree of magnesium (MgO), potassium (K_2O), sodium (Na_2O), titanium (TiO_2) and sulfur (SO_3) [Thomas (2004c); American Coal Ash Association (2003)]. The main influence on the fly ash chemical composition comes from the type of coal. Generally, fly ash produced from the combustion of subbituminous coals contains more calcium and less iron than fly ash from bituminous coal [Thomas (2004c); Hardjito and Rangan (2005); American Coal Ash Association (2003)].

The physical and chemical characteristics of fly ash depend on the combustion methods, coal source and particle shape. The chemical compositions of various fly ashes show a wide range, indicating that there is a wide variations in the coal (anthracite, bituminous, sub-bituminous and lignite) used in power plants all over the world [Hardjito and Rangan (2005); Ramme (2013); Thomas (2007)].

The Canadian Standards Association (CSA) [Canadian Standards Association (1982)] and ASTM [ASTM C618-92a] recognize two general classes of fly ash:

25

- Class C or high-calcium fly ash, normally produced from lignite of sub-bituminous coals; and

- Class F, normally produced from bituminous and anthracite coals.

Class C fly ash typically contains more than 20 percent of CaO and usually contains a less amount of unburned carbon (less than 1%), while Class F mainly consists of an alumino silicate glass, and has less than 10 percent of CaO. The color of fly ash can be tan to dark grey, depending upon the chemical and mineral constituents. For example, Class F has some shade of gray as of the presence of high amount of unburned carbon [Thomas (2004c); Hardjito and Rangan (2005); Anantharaman (2008)].

The most important minerals found in fly ashes from bituminous coal are mainly quartz, mullite, hematite, magnetite, free calcium oxide and in lesser degree of calcite, anhydrite and periclase range from trace amounts to 2.5%. In sub-bituminous fly ashes, the crystalline phases may include tricalcium aluminate (C3A) and calcium sulphate, and alkali sulphate [Thomas (2004c); Sayhan (2010)].

Quartz, (SiO_2), is a transparent crystal has a molar mass and density of 60.08 g/mol and 2.648g/cm^3, respectively. It has high thermal resistivity and hardness of about 7 Mohs. Its structure is shown in Figure 1-14. Quartz is used in the production of Portland cement, drinking glasses, glass for windows and beverage bottles. It finds its application in telecommunication industry in the manufacture of optical fiber. For removal of tooth plaque it can be used in hydrated form in toothpaste [Sen (2014); Ciullo (1996)].
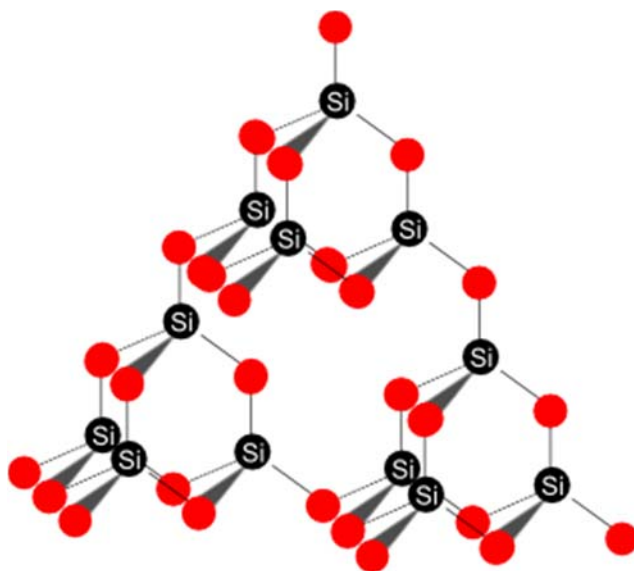
Figure 0-14-Quartz Crystal Structure [BetterChemText (2017)]

Alumina (Al_2O_3) has molecular mass of 101.96 g/mol. Its density and melting points are 4.1 g/cm^3 and 2072°C, respectively, with a high compressive strength value of 1900-2000 N/mm^2. It has been used as a filler in plastic industry because of its inertness and for its high electrical resistivity as electrical insulator [Sen (2014)]. Alumina crystal structure is shown in Figure 1-15.
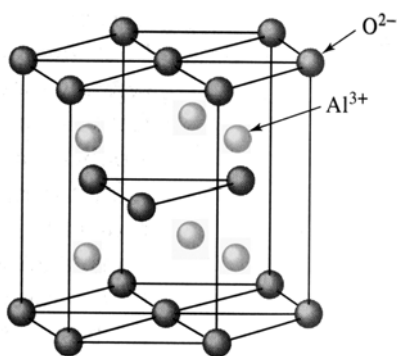
Figure 0-15- Aluminum oxide crystal structure [StackExchange (2017)]

Hematite (Fe_2O_3) is a rhombohedral crystal structure material (as shown in Figure 1-16) with higher density of 5.24 g/cm^3 and having molecular mass of 159.69 g/mol. Hematite is harder than pure iron (Mohs hardness 5.5-6.5), but much more brittle. It is the main raw material for steel and iron industries. It is used in final polishing of lenses and jewelry [Sen (2014)].
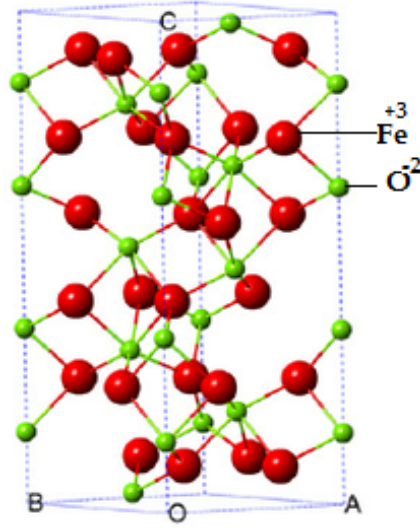
Figure 0-16- Hematite crystal structure [Wu (2015)].

Calcium oxide (CaO) is a widely used compound commonly known as quicklime. It is an alkaline crystal solid and soluble in water with density of 3.34g/cm^3. It has molecular mass of 56.0774 g/mol and possess of higher melting point of 2613°C. Quicklime finds its application in numerous industries like light, cement, paper, chemical production etc. It is used in light industry for its ability to produce intense glow when the material is heated to 2400°C [Sen (2014)]. Lime crystal structure is shown in Figure 1-17.
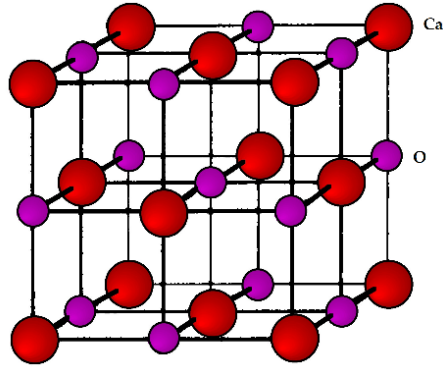
Figure 0-17-Lime crystal structure [123Stock Photos (2017)].

Periclase (MgO) has molar mass of 40.3044g/mol, density around of 3.85g/cm^3 and melting point of 2852°C. It has two useful attributes including high thermal conductivity and low electrical conductivity. MgO is used extensively in the soil and groundwater remediation, wastewater treatment, drinking water treatment, air emissions treatment, and waste treatment industries for its acid buffering capacity and related effectiveness in stabilizing dissolved heavy metal species Periclase mineral is used in fire refractory, medicine, desiccant and cement industries[Sen (2014)]. Its crystal structure is shown in Figure 1-18.
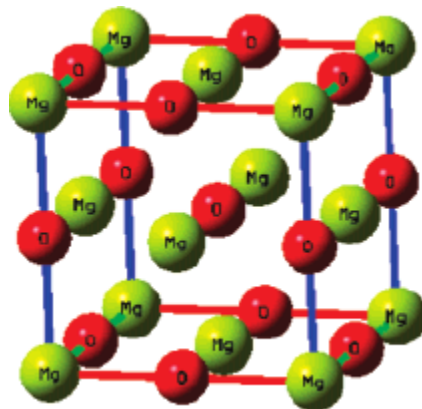
Figure 0-18- Periclase crystal structure [Liu (2007)].

29

The reactivity of fly ashes is related to its amorphous phase. Somewhere it is mentioned that the reasons for the high reactivity of high-calcium fly ashes used in cement application may partially lie in the chemical composition of the glass, which is different from that of the glass in low calcium fly ashes [Thomas (2004c)].

1-3- Outline

The remainder of this thesis is structured as follows:

Chapter 2: Literature Review. This chapter is a detailed survey of relevant literature on PVC processing, PVC composites and polymer/fly ash incorporated composites.

Chapter 3: Research Objectives, Motivation and Novelty are mentioned in details in this chapter. Five main objective of this study and their goals are listed at the end of this chapter.

Chapter 4: Experimental Work including materials properties, fabrication methods of both rigid and foam PVC composites and their characterization techniques are discussed in this chapter. Recipes of all prepared composites are also disclosed here.

Chapter 5: Results and Discussion of all objectives are presented in this chapter. First of all, two precipitator classes of fly ash (F and C) that are mainly used in this study are characterized using different techniques and their physical, structural, thermal, elemental and chemical compositional properties are well discussed. Then, the results of each research objective are expressed one by one and the reasons of the each observations are well addressed.

Chapter 6: Conclusions and Recommendations for the Future Work of this research are summarized.

Results and outcomes of further studies on PVC/fly ash foam composites are reported in Appendices of this thesis, which are as follows.

Appendix A: Preliminary results on Fly Ash surface treatment

Appendix B: Evaluating the effect of fly ash hollow type, Cenosphere, on PVC foam composites properties

Appendix C: Studying the effect of filler shape and geometry on mechanical, thermal, morphological properties

Chapter 2- Literature Review

As mentioned earlier in the chapter 1, PVC foam is one of the highly demanded polymer foams, which made it to become the subject of many researches. One of the main concerns about PVC is its processing conditions due to its low thermal stability, so many researchers focused on understanding effect of various processing factors on its gelation behavior, which significantly influence the final properties of PVC products.

2-1- Literature review on PVC Processing

One of the most common methods to study melt behavior of PVC during processing is using HAAKE and/or Brabender mixing bowl to get torque rheometer curve. General type of PVC torque rheometer curve is shown in Figure 2-1. The first maximum peak is the loading peak (point A). Afterwards, the torque curve drops to a minimum value (point B), where PVC subgrains and agglomerates slide over each other and the gelation process begins. This value is a relative value for the melt viscosity. Following point B, the torque reaches its maximum at point X, which is known as the fusion or gelation torque. At point X, the polymer is in a void-free state and starts to melt at the interface between the compacted polymer and the hot mixer chamber surface. The torque curve starts to drop until it reaches a constant value after a certain time, t_E. At this point, the polymer melt is in a homogenous state where an equilibrium between the friction heat and the temperature of the chamber is reached [Piszczek et al. (2009); Tomaszewska et al. (2005); Tomaszewska et al. (2004); Tomaszewska et al. (2005); Piszczek et al. (2007); Tomaszewska et al. (2008); Tomaszewska et al. (2010); Tomaszewska et al. (2012)].

Due to low thermal stability of PVC, stabilizers need to be added to the compound to catch polymer chains separated chlorine ions. Each stabilizer has a certain capacity to tie to the free

chlorine ions and after reaching its saturation limit, further chlorine ions separation will cause the PVC degradation along with crosslinking. The point where the torque value starts to rise again is called the "Onset of Degradation" which is noted as "On" in Figure 2-1. Time between the stable point (S) and the Onset of Degradation point (On) is called stable time (D), which is generally taken to be a relative measure for the compound stability against thermal degradation [Jährling et al, 2009].
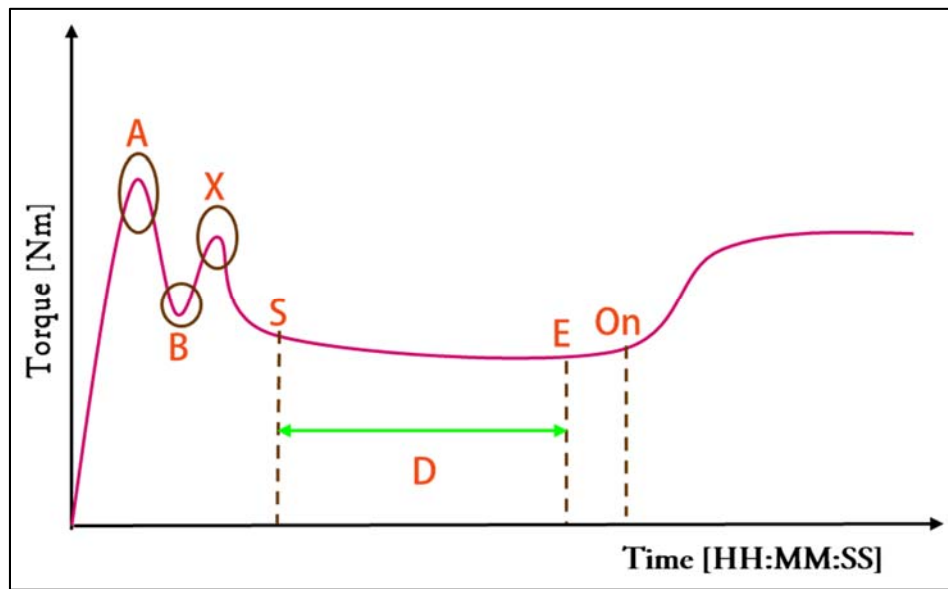
Figure 0-1-Torque rheometer curve of a PVC foam composite

Degradation behavior of two PVC compounds with respect to 0.1% stabilizer content were studied using HAAKE mixer [Jährling et al, (2009)]. As shown in Figure 2-2, the sample with a higher stabilizer content of 2% has a longer stable time. It is also noticeable that change of stabilizer content has a significant effect on the fusion behavior and the compound with the higher stabilizer content needs a longer time to reach the fusion maximum and therefore has a remarkable effect on the degree of gelation and consequently the mechanical property of the final product.

34
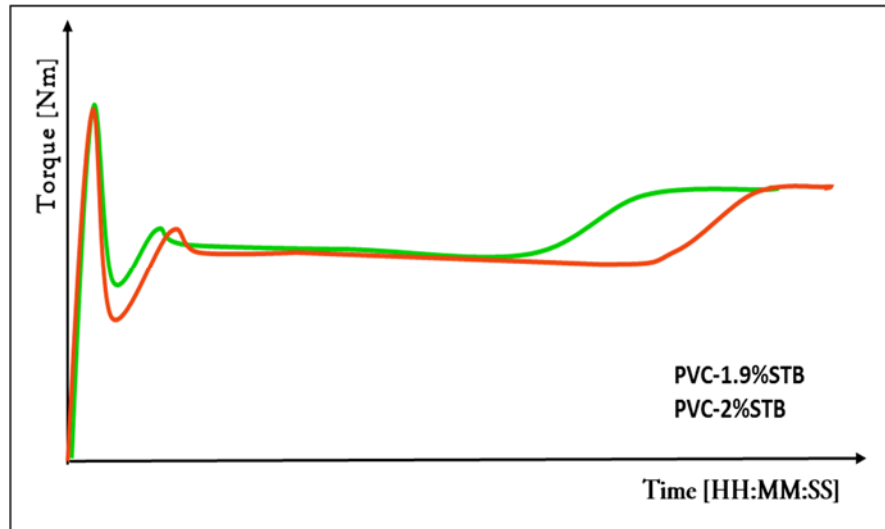
Figure 0-2-The torque versus time curves of both PVC compounds with 1.9% and 2% stabilizer [Jährling et al, (2009)].

Effect of PVC K-value (intrinsic viscosity) on its mixing behavior was also studied using Brabender machine [Piszczek et al. (2004)]. PVC K-values has the most tangible effect on evaluating X-point as a maximum torque rather than mixing temperature and rotation speed. It means that for PVC with defined intrinsic viscosity the maximum of the torque appears in the same temperature, independent of the temperature of the chamber wall and of the rotation speed of the rotors.

Gelation behavior of plasticized and un-plasticized PVC was also investigated [Tomaszewska et al. (2005)]. As shown in Figure 2-3a, after loading the temperature and torque of the un-plasticizer PVC compound remain almost constant during mixing. While in the plasticized PVC (Figure 2-3b) the mixing temperature increases to adjust 170°C during first 5 min, and in the next 2 min raises still about 13°C. At this time torque reaches a characteristic maximum correlated to the gelation of PVC (point X). The further processing caused the reduction of the torque to the

state of its equilibrium (point E). Therefore, it can be concluded plasticizer content and mixing temperature are two main factors in defining gelation point.
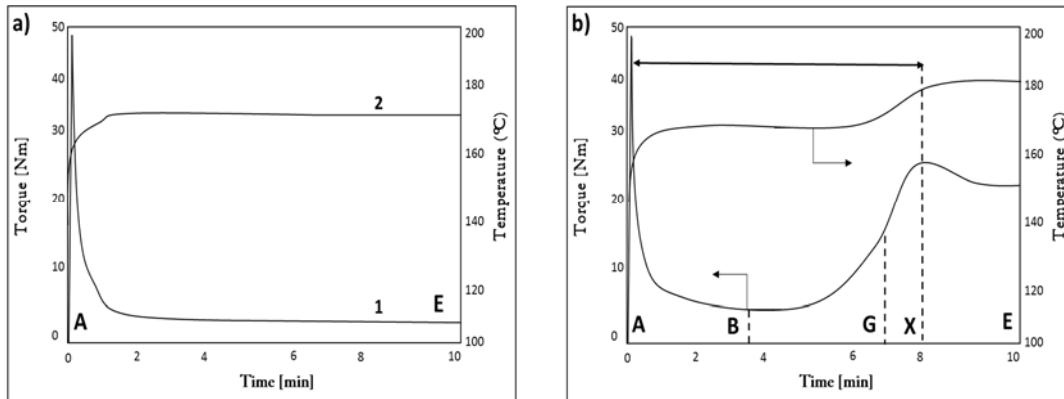
Figure 0-3- Torque rheometer process curves of PVC compound processed at adjusted temperature 170℃;
a) without plasticizer; b)with 2.5 phr of DOP plasticizer [Tomaszewska et al. (2004)].

Studies on temperature effect on inflation point (called point G), where PVC compound structure is significantly inhomogeneous, indicated that the time of reaching this point (t_G) decreases with increasing the chamber temperature [Piszczek et al. (2007)]. t_G also decreased as shear rate increases and the most noticeable t_G shortening, with an increase of shear rate, was reported for the chamber temperature of 160℃ and 170℃. Above 180℃, the necessary time to reach point G is about 2min and practically does not depend on shear rate. It was also observed that the increase of the chamber temperature and the range of shear rate cause a small rise of the torque value at point G and simultaneously a considerable time shortening to reach this point.

Relationship between the minimum torque value (point B) and the time necessary to reach this point and between the shear rate ($\dot{\gamma}$) and the chamber temperature (T_{ch}) was also investigated [Piszczek et al. (2007)]. As represented in Figure 2-4, point B values increase as processing temperature increases, whereas the time necessary to reach this point is significantly decreases. Similar results were observed in the case of increasing shear rate, which confirmed the necessary

36

time to reach the minimum torque is shorter at higher shear rates. Therefore, it is evident that the value of minimum of torque, and the time necessary to reach this characteristic point on the Brabender processing curve, depends on both the temperature and the shearing rate and also this value may be treated as representative for a transitory equilibrium state between sliding of broken grains and increasing degree of gelation of the compound.
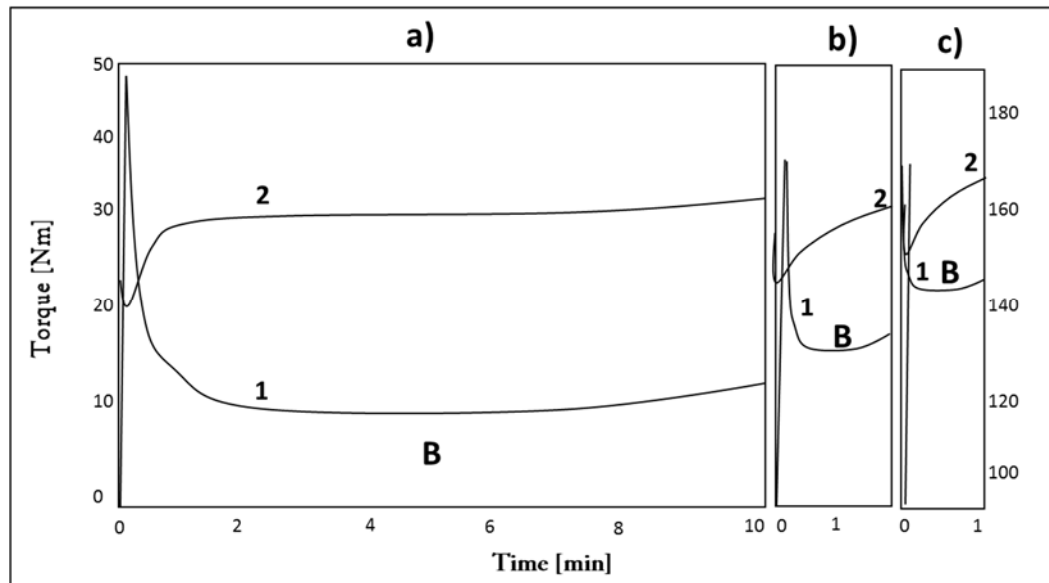
Figure 0-4- Torque rheometer process curves of PVC compound processed at shear rate 8.69 s^{-1} and temperatures (a) 160; (b) 175; (c) 185°C [Piszczek et al. (2007)].

Influence of the chamber temperature (T_{ch}) on the values of torque (τ_E) and time (t_E) at point E (equilibrium state) indicated that increasing T_{ch} causes a considerable decrease in τ_E and t_E. [Tomaszewska et al. (2008)]. Researches on the real temperature of the compound at point X (T_X), showed that maximum torque (τ_X) occurs in a specific range of compound temperatures independently of the chamber temperature [Tomaszewska et al. (2007)].

Degree of gelation (G) of PVC compounds at the equilibrium state was measured to evaluate the effects of shear rate and temperature on the structure and properties of PVC compounds. A typical DSC of processed PVC shows a broad endotherm in the range of 140 to 230°C during a partial melting of the crystalline region as seen in Figure 2-5. Crystallites that did not melt during processing also create secondary endotherms at higher temperatures than its processing temperature [White (1990); Mudassir and Lee (2014); Fillot and Hajji (2006)].
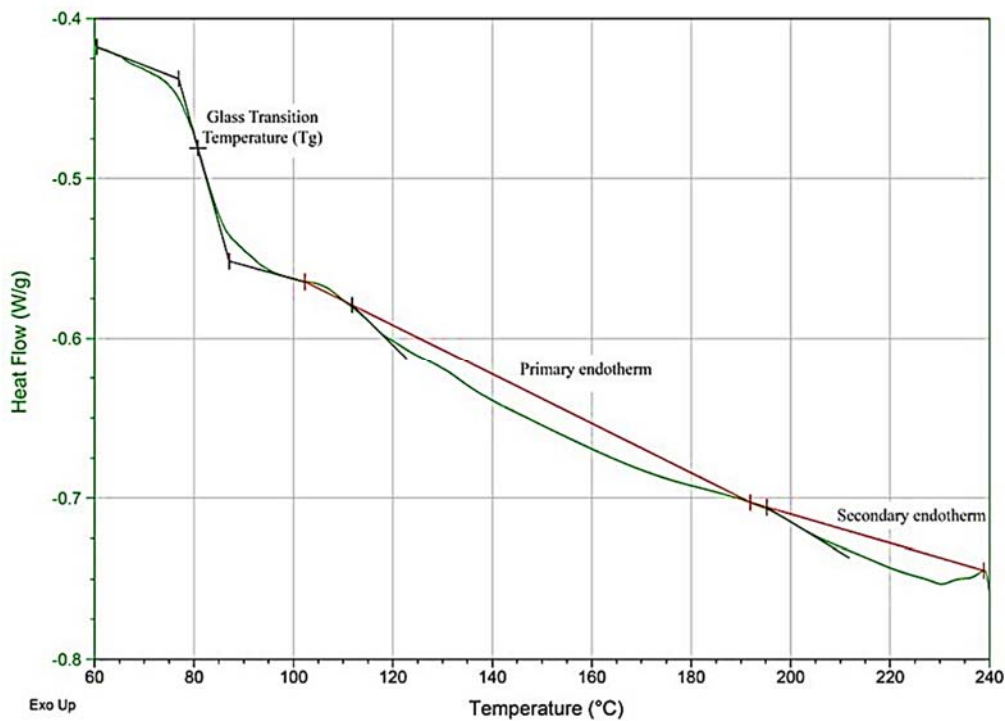
Figure 0-5- Typical DSC plot of processed PVC

Degree of gelation (G) can be estimated according to the formula proposed by Potente, based on the melting enthalpy (J/g) of the primary (ΔH_A) and secondary (ΔH_B) crystallites as shown in Equation 2-1.

$$G = \frac{\Delta H_A}{\Delta H_A + \Delta H_B} \times 100 \qquad \qquad \textbf{Equation 0-1}$$

38

It was found that the degree of gelation increases as shear rate increase, mainly in the range of 160°C to 200°C of the chamber temperature [Piszczek et al. (2010)]. It was also concluded the real residence time of the compound in specific conditions of temperature and mechanical charges seems to be less important for the high gelation. SEM results of the fracture surfaces, as shown in Figure 2-6, reveals a significant inhomogeneity in the compounds processed at higher shear rates. This observation was explained by an insufficient grinding (disintegration) of grains at the earlier stage of the processing, such as minimum torque.
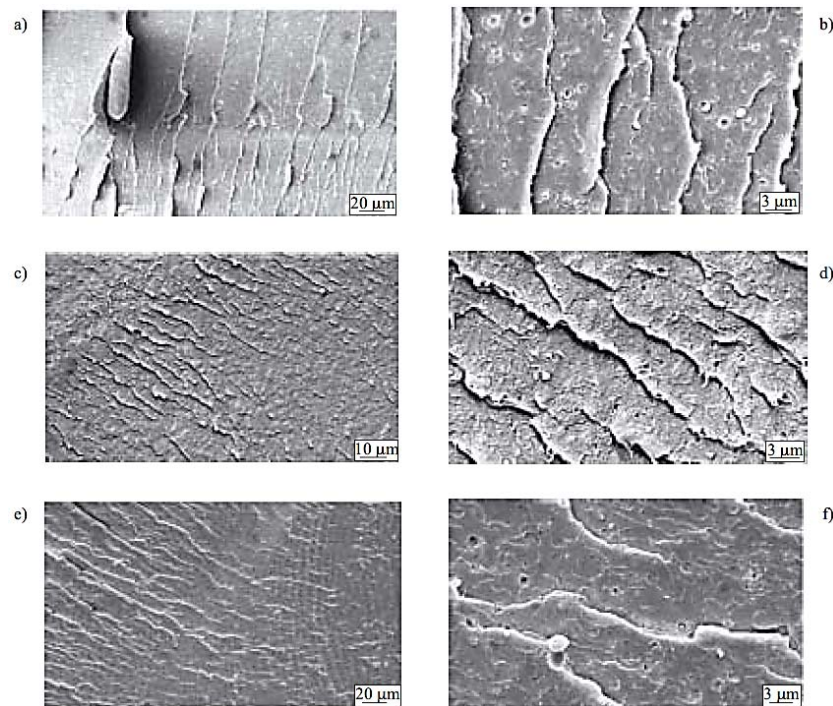
Figure 0-6- SEM images of PVC compounds after processing to equilibrium state of torque in the Brabender measuring mixer in the following conditions: a, b) 150 ℃, 17.38s⁻¹; c, d) 170 ℃, 2.18s⁻¹; e, f) 170 ℃, 17.38s⁻¹ [Piszczek et al. (2010)].

39

Studies on the processing of non-granular PVC (PVCp) and a commercial PVC (PVC-S61) showed that dimension of PVCp lumps and therefore the grain size are much less than PVC-S61, which means PVC-S61 aggregates more than PVCp at same processing temperature [Tomaszewska et al. (2012)]. As mutual friction of grains increase, more heat will be generated and so time necessary to reach point-X will decrease. Addition of lubricant decreases the friction in between the grains which results in an increase in time of reaching point X.

Many researches also conducted on PVC recycling and reprocessing. Effect of regrind amount (0 to 80wt%) in PVC pipes recipes on their rheological, morphological, mechanical, and thermal properties was also studied [Sombatsompop et al. (2001)]. It is reported with an increase of recycled PVC content, melt viscosity increases, while the ratio of die swelling remains almost the same. It was also concluded the maximum amount of regrind to be added to the virgin PVC bottle and PVC pipe grades in order to achieve the optimum mechanical properties is respectively 40wt% and 80wt%.

Surface properties studies of PVC regrind-contained products showed that reprocessing of the regrind-incorporated products needs to be done at 8 to 10℃ higher than its previous heat history to reach a smooth surface [Rabinovich et al. (1997)]. It is believed that the reason behind the decreasing roughness by increasing temperature is PVC semi-crystallinity, where primary particle melt flow units are held together by a three dimensional network structure.

It is also found melt temperature has a direct influence on melt viscosity, degree of fusion, and gas generation from the blowing agent during foaming process [Rabinovich et al. (1990)]. It is suggested that melt temperature of the foaming process must be low enough to allow cell formation

and expansion, but high enough to avoid cell rupture and so increasing foam density and surface roughness. It is said the optimum range of temperatures for obtaining uniform low density PVC foam is 190-196°C.

Studies on evaluating recyclability of post-consumer unplasticized PVC (U-PVC) window profiles over several repeated extrusion cycles showed that the tensile properties of 20-year old, outdoor used, profiles are almost the same as virgin materials [Ditta et al. (2004)]. An exfoliated structure in 10wt% clay/recycled PVC composite was achieved, which showed an eleven times improvement in the storage modulus compared to pure samples [Yoo et al. (2004)].

It is also reported somewhere that careful characterization of used PVC is one of the main necessities before recycling [Sombatsompop et al. (2004)]. It was suggested that reprocess-ability of PVC scraps can be improved by adding calcium carbonate to PVC wastes with low thermal stability. Studies on virgin PVC bottle compounds blended with two different types of post-consumer PVC bottles showed that mechanical properties and hardness represents decreasing and increasing trends; respectively, with increasing UV exposure time.

Heat impact studies on post-consumer PVC bottles during recycling revealed a significant impact during heat treatment at 180°C, and a slight impact at 160°C, with a 30min processing time [Ulutan (1998)]. It was also reported that, under less than 30min processing times, reprocessing without a need for excess additives is possible.

Processing behavior and product quality of unplasticized PVC (UPVC) window frame waste with different recyclate grades were also evaluated [Kelly et al. (2002)]. Results showed that the samples prepared with recycled grades have higher tensile strength (up to 14%), elongation to break

(up to 300%), and flexural strength (up to 20%) than virgin compounds. The impact strength of the recyclates was comparable to that of virgin compounds and in all cases above the minimum value of 12 kJ/m^2 specified in industry standards.

2-2- Literature Review on PVC Reinforced Composites

Polymer composites received significant attention during the past few decades due to their enhanced properties and wide applications. Polymer matrices reinforced with mineral fillers exhibit improved mechanical, morphological, thermal, and processing properties [Ghanbar et al. (2014); Gdoutos et al. (2001); Matuana et al. (2004); Kord (2012); Mohammadian et al. (2016); Ma et al. (2013); Parvaiz et al. (2010); Gummadi et al. (2012); Zarandi and Pillai (2017); Bosand and Mahanwar (2004)]. Polyvinyl Chloride (PVC) foam is one of the most commonly used polymers in building industry due to its low cost, low density, fire retardancy, high insulation and damping properties [Rabinovich et al. (1997); Thomas (2004a); Eaves (2004); Thomas, (2004b)]. Selection of fillers, as in the case with other compounding ingredients, involves consideration of available types and their effects on processing, product properties, and economics [British plastic and rubber (2003)]. Fillers; such as mica, calcium carbonate, glass fibers and wood fibers are commonly used in PVC improve the composites properties [British plastic and rubber (2003); Jiang and Kamdem (2004); Ráthy et al. (2012)].

Calcium carbonate, $CaCO_3$ is one of the most common and popular mineral fillers used in polyvinyl chloride compounding. It is widely available all over the world, which is easy to grind or reduce to a specific particle size and economical. It helps to decrease surface energy and provides opacity and surface gloss, which improves surface finish. In addition, when the particle size is

carefully controlled using this filler improves both impact strength and flexural modulus [Liu et al. (2006)]. Mica is a flaky like crystalline alumino-silicate with a high aspect ratio. It has excellent chemical and corrosion resistance, good electric properties, low thermal expansion, and it causes low wear and abrasion to the processing equipment. The high aspect ratio of the platy particles provides an excellent balance of mechanical, thermal, and dimensional properties when used as functional fillers in plastics; thus providing increased stiffness, superior high temperature performance, improved scratch resistance, lower coefficient of linear thermal expansion (CLTE) and improved acoustic damping properties and dimensional stability [Deshmukh et al. (2011)]. Glass fibers are among the most versatile fillers and, by far, the most predominant class of fibers used in reinforced polymers. They are made from virgin glass, which is alkali-free and produces a uniform diameter; and contain oxides of silicon, calcium, aluminum, magnesium, and boron, fused in an amorphous hyaline phase [Katz and Mileski (1987); White (1990)]. Glass fibers are strong, lightweight, and robust materials and their bulk strength and weight properties are favorable when compared to metals [Kinsella et al. (2001); Wallenberger (2001)].

Different properties of PVC composites reinforced with mica and glass fiber have been studied by a number of researchers. Effect of adding mica and glass fibers to PVC-Wood composites were reviewed and reported that the mechanical properties of PVC-wood composites can be improved by combining mica or glass fiber with wood fibers to make hybrid reinforcements [Jiang and Kamdem (2004)]. Study the effect of various parameters; such as particle size, concentration, and silane surface treatment on the mechanical properties of mica reinforced PVC composites showed that young modulus, stiffness, hardness, and dielectric properties improved with increasing mica content, while tensile strength and elongation at break decreased with increasing mica concentration. Their

results also showed that mechanical and electrical properties were enhanced slightly with the use of silane-treated mica [Deshmukh et al. (2011)]. Deshmukh and Rao [Deshmukh and Rao (2012)] also studied the dielectric properties of silane treated and untreated water ground PVC/mica composites. They reported that the dielectric strength and surface resistance of PVC composites increases more in silane treated mica filled composites with an optimum mica loading of 30 weight percent. Wang et al. [Wang et al. (2011)] studied the effect of dioctyl phthalate (DOP) and mica loading (0-50wt%) on the sound insulation properties of PVC composites. Their results showed that the stiffness and surface density are the main influencing factors in improving sound transmission loss (STL) and the addition of mica results in more significant improvement in the acoustic insulation ability. It was reported that the average STL value increases in stiffness-controlled region up to 40wt% mica loading in PVC, while further increasing of mica content results in decreasing uniformity of mica dispersion and consequently decreases STL. However, the maximum average STL increase in the mass-controlled region was only 12.8%, due to small improvement in surface densities of composites with increasing the mica content.

Jiang et al. [Jiang et al. (2003)] studied the influence of glass fiber length on the impact strength of PVC/wood flour/glass fiber hybrid composites. They reported an improvement of 66% in notched impact strength and 36% in unnotched impact strength using 5% long type glass fiber at 55% PVC content; whereas, no significant improvement was reported in the impact strength of short glass fiber filled composites. Tungjitpornkull et al. [Tungjitpornkull et al. (2009)] prepared glass fiber/wood/PVC composites using a twin-screw extruder and compression molding methods to study the effect of fiber forms and orientation angle. They claimed that compression molding is the most effective method in producing glass fiber/wood/PVC composites. They also reported that the

orientation angle of glass fibers has more effect on impact properties. In a similar work, Tungjitpornkull et al. [Tungjitpornkull et al. (2007)] prepared PVC/wood/glass fiber composites at different glass fiber loadings (10, 20, and 30phr) and lengths (3, 6, and 12mm). They concluded that at 10 and 20phr glass fiber loadings, tensile and flexural properties are strongly dependent on carbonyl content on the fiber surface; whereas at 30phr glass fiber content, the average length of glass fibers mainly affects these properties. Matuana et al. [Matuana et al. (1998)] studied the effect of surface treatment on the mechanical properties of foamed PVC/wood-fiber composites. They reported that tensile and impact properties of the composites are strongly related to the cell morphology and surface treatment of glass fibers. They also observed a reduction in tensile properties of the composites at higher glass fiber loading, which was attributed to higher void fraction in the composites structure and weak interaction between the matrix and glass fiber.

2-3-   Literature Review on Polymer-Fly Ash Composites

Fly ash (FA) is widely studied as reinforcing filler in metal, polymer, and cement matrices due to its unique properties; such as low density, low cost, and smooth spherical surface [Sreekanth and Bambole (2009)]. Effect of FA on different properties of polymer composites has been studied by a number of researchers. Anandhan et al. [Anandhan et al. (2012)] studied the mechanical and thermal properties of extruded ethylene-octene random copolymer/FA composites; they reported 50% increase in tensile strength in a sample with 20% FA loading, while there was no significant change in thermal properties.

Deepthi et al. [Deepthi et al. (2010)] studied High Density Poly Ethylene (HDPE)/cenosphere FA composites using maleate ester modified HPDE; they reported improvement in mechanical and

thermal properties and decrease in crystallinity. Jute-epoxy sandwiches reinforced with FA to make functionally gradient (FG) composites were prepared [Doddamani et al. (2011)]; they derived a correlation between FA content and their mechanical properties using a Taguchi design of experiments. Nath et al. [Nath et al. (2009)] prepared isotactic semicrystalline polypropylene/ FA composites using injection molding. The composites contained 20, 45 and 60% FA by weight. They reported enhancement in tensile modulus of all composites independent of the testing temperatures. Wide angle XRD (WAXRD) and DSC observations indicated that FA particles act as nucleation sites for the crystalline phase and the amount of crystallinity increased up to 11% with increasing FA. In a similar work, Nath et al. [Nath et al. (2010a) and (2010b)] studied the kinetics of non-isothermal crystallization of the prepared isotactic polypropylene/ FA composites; adding FA to neat PP caused partial trans-crystallization of α crystalline phase into β, therefore the presence of FA has led to a change in crystallinity. In addition, Nath et al. [Nath et al. (2010c) and (2010d)] studied biodegradable composites of Poly Vinyl Alcohol (PVA)/ FA ranging between 5 and 25wt.% concentration. Tensile strength and tensile modulus increased proportionally to 193% and 212%; respectively, by the addition of 20% fly ash to the polymer. Dynamic mechanical analysis also showed an improvement in both storage and loss modulus, and a shift in tan δ peaks towards higher temperatures.

Vijaykumar et al. [Vijaykumar et al. (2014)] prepared FA-epoxy core sandwiched composites with three different proportions of epoxy and FA. Their studies on tensile and compressive strengths indicated that the composite with 60% FA had the best properties. Guhanathan et al. [Guhanathan et al. (2004)] studied the mechanical, thermal, and morphological properties of polyester/surface treated FA composites. An improvement in tensile, flexural, and impact properties of composites in

the presence of FA was reported. Bishoyee et al. [Bishoyee et al. (2010)] prepared FA filled polyester-glass fiber composites and studied their erosion properties using a grey-based Taguchi approach.

Some researchers mainly focused on studying cenosphere reinforced composites. Labella et al. [Labella et al. (2014)] prepared cenosphere/vinyl ester syntactic foams to study their mechanical and thermal properties. They reported that the flexural modulus increased by 47% at 60 vol% cenosphere loading, while the flexural strength and coefficient of thermal expansion (CTE) decreased by 73% and 48%; respectively. Similarly, Qiao et al. [Qiao et al. (2011)] showed that the dynamic mechanical properties were enhanced in Polyurea/cenosphere composites.

The effect of cenosphere concentration on the mechanical, thermal, rheological, and morphological properties of Nylon6 was studied by Wasekar et al. [Wasekar et al. (2012)]; they reported an improvement in the elongation at break, impact, and flexural strengths by the addition of a small amount of cenospheres. Rohatgi et al. [Rohatgi et al. (2009)] reported an increase in the compression modulus of polyester/cenosphere composites with increasing the cenospheres content. Kulkarni et al. [Kulkarni et al. (2014)] studied the effect of cenosphere particle size (100-300 mesh) on the properties of acrylonitrile butadiene styrene-filled composites. Their results showed that smaller particles yield better thermal, electrical, and mechanical properties. Manjunath et al. [Manjunath et al. (2013)] reported that the glass transition temperature (Tg), activation energy for decomposition, and Smoke Density Rating (SDR) of PVC/cenosphere composites decrease with increasing the cenosphere content without affecting their Limiting Oxygen Index (LOI) and thermal stability. Aashis et al. [Aashis et al. (2014)] added amino silane functionalized cenospheres to

poly(vinyl butyral) using melt mixing method; they reported that the dielectric properties of the composite films is dependent on the cenosphere content.

Recently, researchers focused on studying the tribological properties of cenosphere filled polymer composites. Thakur et al. [Thakur and Chauhan (2013)] studied the mechanical and tribological behavior of cenosphere/vinyl ester composites using Taguchi technique. They prepared composites with three different size cenosphere particles and their results showed that the submicron sized particles improved the mechanical properties and wear resistance of the composites significantly. Chand et al. [Chand et al. (2011)] studied abrasive wear behavior of low density polyethylene (LDPE)/silane treated cenosphere composites; they reported a maximum wear resistance of 10−11 m3/Nm in a composite containing 10wt% silane treated cenospheres. They [Chand et al. (2010)] also prepared HDPE/silane treated cenosphere composites and reported significant improvement in the impact strength and wear resistance of the composites. Sharma et al. [Sharma and Chand (2012)] prepared LDPE/cenosphere composites with inhomogeneous dispersions of cenospheres and reported that the dielectric constant decreases with increasing cenosphere content with a Maxwell–Garnet approximation. Chauhan et al. [Chauhan and Thakur (2012)] prepared vinyl ester composites containing micron sized cenospheres and reported a significant improvement in wear resistance in the presence of cenospheres.

Whereas, among all researches done so far only few focused on polymer foams with FA fillers. Usta, [Usta (2012)] investigated the flame retardancy behavior of rigid polyurethane (PU) foams containing FA using a cone calorimeter. It was reported that the incorporation of FA particles in PU foam dramatically increased the fire resistance and thermal stability of the composite foams. Chow et al. [Chow et al. (2008)] reported the usage of PU foam/FA blends as a commercial product to

encapsulate heavy metals. It was observed that PU foam- FA blends were waterproof, with good resistance to heat and light. The blends contained a maximum of 18% FA in their composition. Gupta et al. [Gupta et al. (2004)] focused on the effect of cenosphere FA radius ratio on compressive properties of syntactic foams. The results showed that compressive strength and modulus depends on the internal radius of the particles and they are higher in those specimens filled with smaller internal radius cenospheres.

2-4-   Literature Review on Rigid PVC-Fly Ash Composites

Whereas many researches are done on polymer/FA composites, there are few researchers who studied PVC/FA composites properties. Jin-hu et al. [Jin-hu et al. (2011)] studied the effect of fly ash surface modifier types, loading, and fly ash content on different properties of PVC/fly ash composites. They reported that among all surface modifiers, only using silane coupling agent KH550 could result in an improvement of tensile and impact strengths. They also reported that the optimum amount of KH550 and fly ash particles in the PVC composite were 1.5% and 10%; respectively. Yu-sheng et al. [Zhou et al. (2012)] focused on studying the rheological and mechanical properties of fly ash filled and modified PVC. They reported impact and tensile strengths of PVC composites with maximum values of 46 kJ/m2 and 42.7MPa; respectively, in the presence of 5phr fly ash. Sushma et al. [Sushma et al. (2014)] prepared PVC/fly ash composites using injection molding to evaluate the effect of fly ash loading on hardness and tensile properties. Their results showed that 10wt% and 20wt% are the maximum amounts of fly ash that can be used to reach the highest hardness and tensile properties, respectively, while further fly ash addition caused a reduction in these properties. They also claimed that the solubility of fly ash in PVC is the highest in the range of 15 to 25wt% and it can be improved by better mixing of composites.

Chapter3- Research Objectives, Motivation and Novelty

3-1- Research Motivation and Goals

Poly (vinyl chloride) (PVC) is one of the most widely used thermoplastic polymers. PVC is inexpensive, durable, flexible, chemically stable, biocompatible, possesses superior physical and mechanical properties, as well as high chemical resistance. But, brittleness and low thermal stability of a PVC, however, have limited its application at high temperatures. Therefore, improvement in these properties of PVC will broaden its application in various fields. Although PVC itself is one of the cost-effective thermoplastics, its low process-ability make it necessary to add high various types of additives such as plasticizers, processing aids, blowing agents, fillers, thermal stabilizer, which raise could raise the final price of product. Meanwhile, replacing some of the currently used fillers in PVC foam formulation with fly ash particles is even more beneficial which can reduce the final price. Therefore, the broader impact of this project will be demonstrated as developing a new avenue to absorb fly ash in commercial products, adding value to fly ash so it can be traded as an additive rather than a filler, providing industry with a knowledge base that can be used in developing individual applications of fly ash use as a low cost filler at high loadings, offsetting the costs of resin and relatively more expensive fillers with low cost fly ash, and thus improving profit margins on commodity products and price competitiveness of US products.

The motivation behind conducting this research is to examine the feasibility of using fly ash as a very low cost reinforcement filler in PVC foams at high concentrations. Particular attention is paid to evaluate final properties of PVC foam/fly ash composites as a novel system and understanding the effect of chemical compositions of both precipitator; class C and class F, on interface interaction of fly ash particles and the polymer matrix; in terms of structure, properties, processing, and performance of the composites. Moreover, properties of the particulate reinforced composites are

mainly depends on the particles size and filler-polymer interfacial interaction. As known particle size and the strength of interface interaction influence the strength of the composite, therefore; it is found necessary to evaluate fly ash particle size effects and estimate polymer and fly ash interfacial interaction strength. Besides, recyclability and reprocess-ability of PVC-FA foam composites is investigated since recycling of postconsumer products containing fly ash is of a considerable concern.

3-2- Significance and Novelty

Fly ash, a silica and alumina residue collected from the chimneys of coal-fired power plants and incinerators, is both a waste product and a promising low-cost filler for plastics. For 50 years, fly ash has been used in cement, where it improves compressive strength and curing. In addition, polymer compounders located near coal-fired power plants have put small amounts (1-2%) of ash into dark-colored compounds to save money and add stiffness. Nowadays, with record high prices of raw materials, specifically polymer resins, and short supplies evident by long lead times, there is a renewed interest in using fly ash at high loading in polymer compounds. However, this task has been proven to be challenging for foam polymers due to the complexity of the foaming process and the lack of relevant studies published in the field.

Although there is an extensive list of published work and mature applications on the use of fly ash as a reinforcing filler in cement and polymer composites, there is very few known applications or published studies of using fly ash in thermoplastic polymer foams and no publication specifically in PVC foams. The goal of this project is to conduct an extensive study on the feasibility of using fly ash in polymer foams. Since the field of polymer foams is very wide, we narrowed down the focus of this project to extruded rigid PVC foams due to its well established use in building industry.

The anticipated outcomes of this project will offer manufacturers of structural polymer foams scientific data and engineering guidelines on the use of fly ash as a very low cost filler in their products. This will reduce the cost of raw materials, particularly the resin, and improve the operating profit margins of their products (which are typically low for commodity plastics). Higher profit margins will allow manufacturers to be more competitive with pricing their products, and able to

invest in better technologies. In addition, the development of new avenues to utilize fly ash in consumer products reduces the burden on our landfills in disposing this byproduct.

3-3- Main Objectives

The main purpose of this research work is to examine the feasibility of introducing fly ash to polymer industry. Therefore, fly ash is first characterized using wide range of techniques, then various polymer/fly ash composites were prepared to be studied. The five main objectives of the current study are as follows.

1- Fly Ash characterization to determine its general properties

Extensive characterization is carried out on Fly Ash to determine its elemental and chemical composition, physical, structural, thermal and morphological properties regarding different classes and particle sizes of fly ash

2-Determine general aspects of Fly Ash performance in PVC Foam Composites

As to the best of our knowledge PVC/Fly ash foam composites are not studied before, in this objective the composites containing Class-F fly ash with various loading levels (0, 6, 9, 12, 25 and 40phr) are prepared and well characterized to determine the baseline of the composite performance in terms of physical, mechanical, thermal, structural and microstructural properties. In addition, the mechanisms of thermal degradation in PVC/Fly ash composites and their kinetics are well discussed.

3- Determine Fly Ash Chemical Composition effects on PVC foam composites performance

As fly ash properties vary type to type and class to class, in this objective two main classed of fly ash, Class F and Class C, were selected to focus more on chemical composition effects of fly ash on the composites properties and performance. Besides, Interfacial interaction between the fillers

and matrix as an important factor affecting the mechanical properties of the composites is quantified by Pukanszky model. Interface interaction between fly ash and polymer is also examined by structural and microstructural techniques. The most effective phases of the fly ash in terms of improving the composite's properties are also identified according to the analyzed results.

4-Determine effect of Fly Ash particle size on its chemical composition and polymer composites performance

Fly ash particles were sieved into two different sizes to investigate the relationship between its particle size and chemical composition and therefore examine the particle size and chemical composition dependency of the polymer composites properties. Interfacial interaction between polymer matrix and two different particle-sized fly ash in the composites are also evaluated both experimentally using nanoindentation, and quantitatively using Pukanszky and DMA models.

5- Evaluate recyclability and reprocessability of recycled-PVC/Fly Ash Foam Composites

Using fly ash as a reinforcing filler can be very cost effective; however, the recycling of postconsumer products containing fly ash is of a considerable concern, therefore the viability and main variables which govern the recyclability of fly ash reinforced PVC foam composites is investigated in this objective.

Chapter 4- Experimental work

4-1- Materials

4-1-1- Rigid PVC resin

Rigid PVC resin was purchased from Shintech, USA. PVC is mostly amorphous polymer with inherently superior fire retarding properties due to its chlorine content, even in the absence of fire retardants and with. It is a brittle, rigid with low impact strength thermoplastic with a general properties as listed in Table 4-1.

Table 0-1- General properties of rigid PVC

Properties	Value
Density	1380 kg/m^3
Young's Modulus	2900-3300 MPa
Tensile strength	50-80MPa
Elongation at break	20-40%
Impact strength	2-5KJ/m^2
Glass temperature	87°C
Melting Point	200°C
Vicat temperature	85°C
Heat transfer coefficient	0.16W/m.K
Linear expansion coefficient	8×10^{-5}/K
Specific heat	0.9KJ/(Kg.K)
Water absorption	0.04-0.4
Inherent viscosity	0.74
Maximum volatiles	0.12%

4-1-2- Additives

A major drawback of PVC is its poor resistance to heat and light. It easily decomposes under moderate heat which leads intense color formation and deterioration of the polymer properties over time. For this reason, stabilizers are added to the PVC to prevent or delay this process.

4-1-2-1- Thermal Stabilizer

Thermolite® 137 is a sulfur-containing butyltin stabilizer, which was provided by Arkema, USA. It is suitable for both single and multiple-screw extrusion systems. Its general characteristics are listed in Table 4-2.

Table 0-2- General Characteristics of Thermolite® 137

Properties	Value
Viscosity, cs (@25°C)	50
Specific Gravity	1.04
% Tin	14

4-1-2-2- Processing Aids, Lubricants and Wax

Plastistrength® 530 and 770 are acrylic processing aids that are provided by Arkema, USA. Plastistrength® 530 is a high molecular weight acrylic process aid that brings enhanced processability to high output extrusion, foam and highly filled compounds such as those found in wood-polymer composites. Whereas Plastistrength® 770 process aid is a lubricating acrylic process

aid that brings enhanced processability to vinyl compounds through exceptional metal release properties. Plastistrength® 770 process aid is a first class solution to improve the surface quality of finished articles and prevent plate-out issues. Typical physical properties of the processing aids are listed in Table 4-3.

Table 0-3- General Characteristics of Processing Aids

Properties	530	770
Specific Gravity	1.17	1.11
Bulk Density (g/cc)	0.45	0.5
Particle Size (Max on 40 mesh)	2%	2%
Percent Volatiles (wt%)	1.2%	1%

LOXIOL 2899 and 2307 lubricants are provided by Oleochemicals, USA. LOXIOL 2899 has respectively a chemistry and melting range of polyol ester and 70-80°C. LOXIOL 2307 as a strong external lubricant and release agent, has a melting point in the range of 80-90°C.

Petrac® 215 paraffin wax is provided by Ferro Corp., USA. It has a specific gravity of 0.94 and melting point of 102°C.

4-1-2-3- Filler

COAD® 10 produced by Norac Corp., USA. It is a high grade calcium stearate with a chemical composition of Ca $(C_{18}H_{35}O_2)_2$. It has low chloride content, low specific surface, exhibits excellent

heat stability properties for high temperature processing and provides mold release properties critical

for thermoplastics and thermoset molding. Its general properties are listed in Table 4-4.

Table 0-4- General properties of COAD® 10 Calcium Stearate

Properties	Value
Apparent Density	448.5 kg/m^3
Mean Particle Size, microns	11
Top Size %98, microns	35
% thru 325 Mesh	100
Moisture, %	1.0
Total Ash, %	10.3

4-1-2-4-Blowing agent

Chemical blowing agents Azodicarbonamide (AZO) and Sodium Hydrogen Carbonate (FICEL

SBH) produced by Season Corp. and Hughes Polymer Additives Corp., USA, respectively. The

general properties of blowing agents are listed in Table 4-5.

Table 0-5- General Characteristics of Blowing Agnets

Properties	AZO	SBH
Appearance	Yellow Powder	White Powder
Gas-forming Amount (ml/g $\geq$)	215$\pm$3	200$\pm$3
Dissociation Point ($\geq$)	200°$C \pm 3$	155°C$\pm$3
Ash Content ($\leq$)	0.12	0.1

4-1-3- Fly Ash

Class F (FA-F) and Class C (FA-C) precipitator Fly Ash were collected from WE Energies power plant in Oak Creek, Wisconsin, USA. As shown in Figure 4-1, the average particle size of fly ash is about 10μm but can vary from <1μm to over 150μm The reported properties of the received fly ash particles is also listed in Table 4-6.

Table 0-6- Fly Ash general properties, reported by We Energy.

Properties	Class-F	Class-C
Collected Power Plant	Elm Road, Oak Creek, WI	Elm Road, Oak Creek, WI
Specific gravity	2.5	2.5
Loss on ignition (%)	$\leq$ 3.0	$\leq$ 3.0
Moisture Content (%)	$\leq$ 3.0	$\leq$ 3.0
SO_3 (max%)	5.0	5.0

Particle Size Distribution
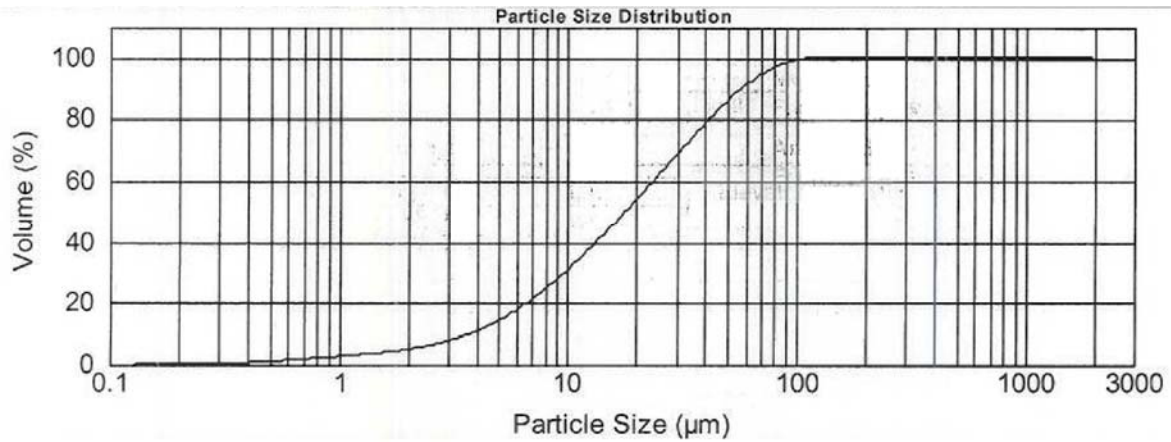
Figure 0-1-Particle size distribution of Fly Ash

To narrow down fly ash particle size, it was sieved to different particle sizes. Class F fly ash was passed through sieves with the nominal openings of 150, 100, 53, 25 and 20microns. Then the sieves were shaken well for 10minutes and the remained particles on each sieve were collected. 25miron and 50micron particle size fly ash were selected at the end for the purpose of objective 4 and they are named as 25-FA-F and 50-FA-F; respectively.

4-2- Composites Fabrication Methods

First, independent of the purpose of each objective, PVC compounds were prepared. Then according to the main goal of each objective, appropriate processing method was selected to prepare the composites which are described as follows.

4-2-1- PVC Foam Composites Compounding

Before PVC can be made into products, it has to be combined with a range of special additives through compounding process. Generally, PVC foam compounds were prepared using a high shear mixer (Gunther Pepenmeier, Machinenu. Detmoid, Type: TSHK). The stabilizer and processing aids were added to the PVC resin at 52ºC and 58ºC; respectively. In case of interest on PVC/fly ash composite preparation, fly ash at different level and classes (C and F) were also added to the compound at 52ºC.

Finally, the lubricants were added at 66ºC to the compound and the result was a dry blend which is called rigid PVC compound. In case of interest on foam composite preparation, blowing agents (AZO and SBH) were also added at 66ºC to the compound and the result is called PVC foam compound. Then the intended compound is fed into the proper processing equipment. Table 4-7 shows the general recipes of PVC foam and rigid PVC compounds.

4-2-2- PVC Foam Composites Extrusion Process

PVC foam composites in the shape of rectangular strips (1inch wide) were produced using extrusion method. Previously prepared PVC foam compounds were fed into a single screw extruder (Themoplas New England Wire Machinery Co. Inc.) with 20:1 (L/D) at 60rpm screw speed. The

barrel temperature profile in the range of 158℃ to 175℃ is used during extrusion process and the extrudates were air cooled and cut using an automated cutter. The prepared PVC foam composites were used directly in the study of objectives 2 and 3 that their recipes are also listed in Tables 4-8 and 4-9; respectively.

The mentioned extrusion process is also used in objective 5 to prepare virgin PVC foam composites. Whereas, in case of regrind contained foams, an extra step is necessary. For this purpose, previously prepared virgin extrudates were ground first using a Conair Wortex JC10 grinder with a 0.25inch screen. Then, a specific amount of each regrind was subsequently added to its original compound and was re-extruded to make foam samples containing both fly ash and regrind. At the end of this step, PVC foam extrudates containing regrind were prepared. Table 4-10 shows the formulation of the prepared samples used in objective 5.

4-2-3- Rigid PVC Composites Mixing Process

Brabender mixing chamber (Plasti-Corder torque rheometers.R.E.E.6) with the capacity of 60ml was used to mix rigid PVC compounds. This processing method was specifically selected to prepare composites used in the study of objective 4. Previously prepared pure rigid PVC compound is first blended with a desired amount (10wt%) of the intended fly ash particles (25μm sized or 50μm sized). Then, the mixture is fed to the mixing bowl at 180°C and is mixed at 40rpm rotation speed for 10minutes. The torque and stock temperature values were recorded versus mixing time. The recipe of the prepared composites regarding objective 3 is shown in Table 4-11.

4-3-Samples Coding Method

In this study a simple coding system is used to name the prepared samples. FA-F and FA-C represent the samples containing class F and C fly ash; respectively. The number in front of each sample code also states the amount of the used fly ash in each sample. For example, FA0 is a pure PVC sample. In case of regrind contained composites, samples are codes as FA0-R0, which in this case the number in front of as a symbol of regrind, represents amount of regrind. In addition, in Table 4-11, FA-F10, 25-FA-F10 and 50-FA-F10 are representing respectively the composites containing 10wt% of unsieved, 25µm sized and 50µm sized fly ash.

Table 0-7-PVC foam and Rigid PVC Compound Formulation

Ingredients (phr[1])		PVC Foam Compound	Rigid PVC Compound
Resin	PVC	100	100
Processing Aid	P530	5.2	5.2
	P770	0.52	0.52
Blowing Agent	AZO	0.4	0
	SBH	0.2	0
Lubricant	Loxial 2986	0.1	0.1
	Loxial 2307	0.5	0.5
Wax	PE Wax	0.1	0.1
Filler	Calcium Stearate	1	1

---

[1] phr or part per hundred resin is a common unit in polymer industry. In this unit the amount of additives are expressed in parts per hundred resin.

Table 0-8- Formulation of PVC Foam Composites regarding objective 2 study

Ingredients (phr)	FA-0	FA-F6	FA-F9	FA-F12	FA-F25	FA-F40
PVC Foam Compound	100	100	100	100	100	100
Fly ash	0	6	9	12	25	40

Table 0-9- Formulation of PVC Foam Composites regarding objective 3 study

Ingredients (phr)	FA-F6	FA-F40	FA-C6	FA-C40
PVC Foam Compound	100	100	100	100
FA-F	6	40	0	0
FA-C	0	0	6	40

Table 0-10- Formulation of PVC Foam Composites regarding objective 5 study

Sample Group	Samples Coding	PVC resin	Fly Ash	Regrind
FA0	FA0-R0	100	0	0
	FA0-R20		0	20
	FA0-R40		0	40
FA10	FA10-R0	100	10	0
	FA10-R20		10	20
	FA10-R40		10	40
FA20	FA20-R0	100	20	0
	FA20-R20		20	20
	FA20-R40		20	40

Table 0-11- Formulation of PVC Foam Composites regarding objective 4 study

Ingredients (wt%)	FA-F10	25-FA-F10	50-FA-F
Rigid PVC Compound	90	90	90
Unsieved FA-F	10	-	-
25µm-Sized FA-F	-	10	-
50µm-Sized FA-F	-	-	10

4-4-Characterization Techniques

4-4-1-Physical Properties

4-4-1-1- Density

The theoretical density (ρ_{th}) of the foam composites was calculated based on the rule of mixtures using Equation (4-1). The experimental density (ρ_{exp}) was calculated according to ASTM D272 by weighing and measuring the volume of a composite sample. The void content (V_{void}) was calculated using Equation (4-2), below:

$$\rho_{th} = (\rho_{FA} \times v_{FA}) + (\rho_{PVC\ compound} \times v_{PVC\ compound}) \qquad\qquad \textit{Equation 0-1}$$

$$V_{void}\% = \frac{\rho_{th} - \rho_{exp}}{\rho_{th}} \times 100 \qquad\qquad \textit{Equation 0-2}$$

where v_{FA} and $v_{compound}$ are the volume fractions of the fly ash and PVC compound; respectively. ρ_{FA} and $\rho_{compound}$ are the densities of fly ash particles and the PVC compound; respectively. ρ_{exp} and ρ_{th} are the experimentally measured and theoretical densities of the PVC foam-Fly ash composites.

4-4-3-2- Brunauer–Emmett–Teller (BET) Surface Area Analysis

BET[2] theory is based on the physical adsorption of gas on a surface and its Equation is expressed as follows:

$$\frac{p}{v(p_0-p)} = \frac{1}{v_m c} + c - \frac{p}{v_m c}\left(\frac{p}{p_0}\right) \qquad \textbf{Equation 0-3}$$

where p and p_0 are the equilibrium and the saturation pressure of adsorbates at the temperature of adsorption, v is quantity of the adsorbed gas, and ϑ_m is the quantity of monolayer adsorbed gas and c is the BET constant, which is expressed by Equation 4-4:

$$c = \frac{\exp(E_1-E_2)}{RT} \qquad \textbf{Equation 0-4}$$

where E_1 is the heat of the first layer adsorption, and E_L is that for the second and higher layers. Equation 4-3 is an adsorption isotherm and can be plotted as a straight line with $1/v$ [(P0 / P) − 1] on the y-axis and φ =P/P0 on the x-axis as shown in Figure 4-2 and is called a BET plot. A and I are respectively slope and intercept of the line that are used to calculate ϑ_m, the monolayer adsorbed gas quantity, using Equation 4-5 and then calculate BET constant using Equation 4-6.

---

[2] Brunauer, Emmett, Teller

$$v_m = \frac{1}{A} + I \qquad\qquad \textbf{Equation 0-5}$$

$$c = 1 + \frac{A}{I} \qquad\qquad \textbf{Equation 0-6}$$
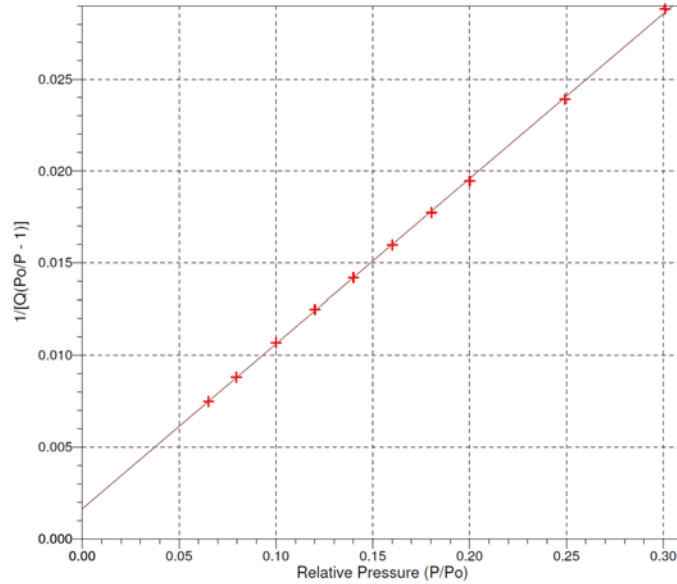
Figure 0-2- BET plot of Fly Ash

Therefore S$_{total}$, a total surface area, and S, a specific surface area, are evaluated by the following Equations:

$$S_{BET,total} = \frac{v_m Ns}{V} \qquad\qquad \textbf{Equation 0-7}$$

$$S_{BET} = S_{total/a} \qquad\qquad \textbf{Equation 0-8}$$

where N is Avogadro's number, S is adsorption cross section, V is molar volume of adsorbent gas and a is molar weight of adsorbed species [Behera (2010); Wikipedia BET theory (2017)].

The BET specific surface area (S$_{BET}$) was determined based on the shape of the vapor nitrogen adsorption/desorption isotherms in -196.15 °C. The samples were degassed at 100°C for 5h in a reduced pressure (10^{-1} Pa). S$_{BET}$ was determined based on the BET multilayer adsorption theory at a

p/p₀ between 0.06 and 0.3 (p and p₀ are the equilibrium and saturation pressure of nitrogen; respectively).

4-4-3-3- Nanoindentation Hardness Testing

Thin layer of PVC/fly ash rigid composites was cut using razor blade. Then it was mounted using a melt WAX. In case of interest on measuring fly ash properties, particles were mounted in epoxy resin and the surface was then polished to reach a smooth surface.

Nanoindentation was carried out using Agilent Technologies Nanoindenter G200. For the modulus and hardness measurements, the maximum loads were up to 250mN, which gave a maximum indentation depth of less than 250nm. The diamond indenters used in both instruments have a 90° conical shape with an approximately 1mm tip radius.

4-4-2-Mechanical Properties

Tensile properties were determined using an Instron 3365 universal testing machine according to ASTM D638 at a crosshead speed of 5mm/min. Load versus displacement were measured.

Flexural properties were determined using Instron 3365 with a three-point bending test set-up on rectangular specimens measuring 20.5×2.5×0.7cm at a crosshead speed of 0.5 in/min. The span length was kept at 4inches. The flexural stress and strains were calculated using Equations 4-9 and 4-10.

$$\sigma_f = \frac{3PL}{2bd^2}$$ *Equation 0-9*

$$\varepsilon_f = \frac{6Dd}{L^2}$$ *Equation 0-10*

Where, σ_f and ε_f are the flexural stress and strain at the midpoint; respectively, and P, L, b, d, D are the load, span length, specimen width, specimen thickness and midpoint deflection; respectively. The flexural strength was determined using the maximum stress value recorded before sample fracture and flexural modulus was determined by the slope of the initial linear region of the stress-strain curve.

Charpy impact properties were determined using Tinus Olsen impact testing machine (model IT 504) according to ASTM D 6110. The hardness was determined with a Shore-D Durometer.

4-4-3-Thermal Characterization

Thermal stability and characteristics of the composites were analyzed using TA Instrument SDT 2960 thermo gravimetric analyzer (TGA) in the temperature range of 25 to 800 ℃ at a heating rate of 10°C/min in an inert argon atmosphere.

Differential Scanning Calorimetry (DSC) was used to measure gelation degree in PVC composites. These measurements were carried out using TA Q2000 analyzer (TA Instruments, U.S.). Foam composite samples weighing 5 to 10 mg were heated in standard aluminum pans in the temperature range of 25 to 260 ℃ at a heating rate of 10°C/min.

4-4-4- Viscoelastic Properties

Dynamic Mechanical Analysis (DMA) was performed using a TA Instrument Q800 to evaluate the viscoelastic properties (storage modulus, loss modulus, and tanδ) of the composites in a solid state. The three-point bending mode was used at a test temperature range of 25 to 120 ℃ at a constant heating rate of 3°C/min and the frequency of dynamic force of 1 Hz.

4-4-5-Stuructural Characterization

4-4-5-1-X-Ray Diffraction analysis (XRD)

Elemental and chemical analysis of the fly ash particles were determined using an X-ray diffractometer (Bruker D8 Discovery) with a CuK_α radiation (λ=1.54056 Å) source. The samples were scanned at the rate of $1.25°\ 2\theta/min$ with a step size of $0.03°\ 2\theta$ from 10 to $70°\ (2\theta)$.

4-4-5-2-*Fourier Transform Infrared (FTIR) Spectroscopy*

Infrared spectroscopy of the Fly ash powders were applied using a BRUKER vector 22 FTIR/ATR system (typically 64 scans; 4cm^{-1}). ATR apparatus was used for the determination of the functional groups distribution in fly ashes. The samples were scanned in the region of 4000 to 500 cm^{-1}.

4-4-5-3-Scanning Electron Microscopy and Energy Dispersive X-Ray Analysis (SEM/EDX)

The morphology of the fly ash and composites was characterized using a JEOL JSM-6460LV Scanning Electron Microscope. Samples were fractured in liquid nitrogen and coated using a sputter coater to minimize the charging effect and to improve the conductivity of the samples prior to the analysis. In addition, SEM/EDX was used to confirm the elemental composition of fly ash particles.

4-4-4-4- X-ray Photoelectron Spectroscopy (XPS)

X-ray Photoelectron Spectroscopy (XPS) or ESCA (Electron Spectroscopy for Chemical Analysis) is one of the most widely used surface analysis techniques that was used to determine the surface chemistry of fly ash. XPS studies were carried out using a Perkin Elmer PHI 5440 system equipped with a monochromated Mg-K X-ray source and hemispherical analyzer. Binding energies

for Ca 2p and Ag 3d electrons were determined by scanning the range of 430-442 eV and 363-377

eV in calcium and silver exchanged zeolites with a step size of 0.05 eV.

Chapter 5- Results and Discussion

5.1. Fly ash Characterization

In this research work four different types of fly ash; including two different classes, F and C, and two different sizes of class F, 25µm and 50µm, are studied and well characterized. Their properties are reported in four main categories including physical, structural, morphological and thermal properties.

5.1.1 Physical Properties

The physical properties of the used fly ash particles including specific gravity and color are listed in Table 5-1. It is shown class F fly ash is slightly denser than Class C and also as expected smaller particle sized fly ash, 25-FA-F, has lower density than a fly ash with larger particle size, 50-FA-F.

Table 0-1- Physical properties of used fly ash

	FA-C	FA-F	25-FA-F	50-FA-F
Color	Light Tan	Dark grey	Light Grey	Dark Grey
Specific gravity	2.3	2.5	2.1	2.4

The BET measured surface properties of the fly ash particles are listed in Table 5-2.

Table 0-2-Surface properties of the used fly ash measured with BET

	BET Surface Area m^2/g	BJH cumulative surface area of pores (17-3000Å diameter) m^2/g	Pore Volume mm^3/g	Pore Size Å
FA-C	4.42	2.45	7.57	73.74
FA-F	4.36	2.55	7.7	70.72
25-FA-F	7.86	5.28	8.55	43.48
50-FA-F	3.18	2.1	5.66	71.33

As it is shown, both classes, C and F, have almost the same surface area and pore volume, which also confirms the results of density measurements. Comparison between of 25μm and 50μm sized class F fly ash particles shows that particles with the smaller size, 25-FA-F, has larger BET surface area and larger values of BJH[3] cumulative surface area of pores and pore volume.

Adsorption isotherms of hysteresis loops of N_2 at 77K for the used fly ash are shown in Figure 5-1. The presented isotherms belongs to type II adsorption with a hysteresis loop of H1 type according to IUPAC classification, which is mostly found when adsorption occurs on nonporous agglomerates or spherical particles. In the isotherm graphs the inflection points represents where the completion of the adsorbed first monolayer occurs.
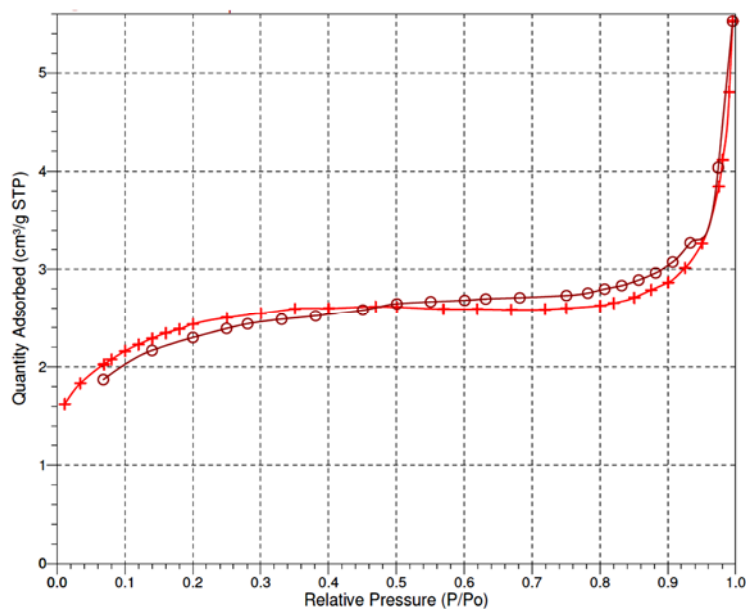
Figure 0-1- Adsorption isotherms of hysteresis loops of fly ash

[3] Barrett, Joyner, Halenda

5.1.2 Structural properties

SEM/EDX was carried out to analyze the elemental composition of the used fly ash. The reported results are the average of five different measurement in each type of fly ash, which are listed in Table 5-3.

As per weight percentage of the elements, the major elements are carbon, oxygen, silicon, aluminum, iron and calcium. Class C fly ash has general lower amount of carbon rather than class F which is also noticeable from its bright tan color. It is been also noticed also that FA-C is rich in calcium, while FA-F has more iron instead. Comparison between 25-FA-F and 50-FA-F also shows that fly ash elemental composition is particle size dependent. 25micon sized particles contains more calcium, less silicon and less iron compared to 50micron-sized fly ash.

Table 0-3- Elemental Analysis of the used fly ash, characterized by SEM/EDX

	FA-C	FA-F	25-FA-F	50-FA-F
Carbon	4.69	10.21	13.21	15.46
Oxygen	33.04	37.28	31.86	31.16
Silicon	16.15	13.45	14.94	17.54
Aluminum	9.83	9.66	8.11	8.00
Iron	5.2	10.23	7.71	10.32
Calcium	25.35	13.1	17.16	12.51
Potassium	0.53	1.01	0.86	0.54
Sodium	1.07	0.66	1.11	0.8
Sulfur	1.5	3.12	3.05	2.24
Magnesium	2.64	1.28	1.98	1.13

The chemical compositions of the used fly ash are characterized by XRD. In Figures 5-2 and 5-3 respectively XRD spectrum of two classes of fly ash, FA-F and FA-C, and class F fly ash with different particle size. The identified crystal phases and their amount in each spectrum are listed in Table 5-4. Fly ash is a mixture of amorphous and crystalline phases that the weight percentage (X_i) of its crystalline phase can be calculated using Equation 5-1.

$$X_i = \frac{1}{1+[k_i/I_i(I_j/k_j+I_k/k_k)]}$$ **Equation 0-1**

where, K =I/Ic and I is intensity of largest peak in the fly ash. The crystalline amounts of the fly ash are reported in Table 5-4.

Comparison between oxide contents reveals that in FA-C lime, tricalcium aluminate (C3A), periclase and anhydrite contents are more than FA-F, while iron oxide content, considering hematite and magnetite, in FA-F is significantly higher. Quartz and mullite contents are respectively about 5wt% higher and lower in FA-C compared to FA-F.

Take a closer look at composition of two different particle sized fly ash, 25-FA-F and 50-FA-F, shows that fly ash oxide composition is highly size dependent. Smaller particles contains more of calcium oxide regarding anhydrite, lime and C3A contents. Whereas larger particles mainly composed of quartz and iron oxide. These results are consistent with EDX results presented earlier. The chemical formula of each oxide phase and their nominal compositions are also mentioned in Table 5-5.
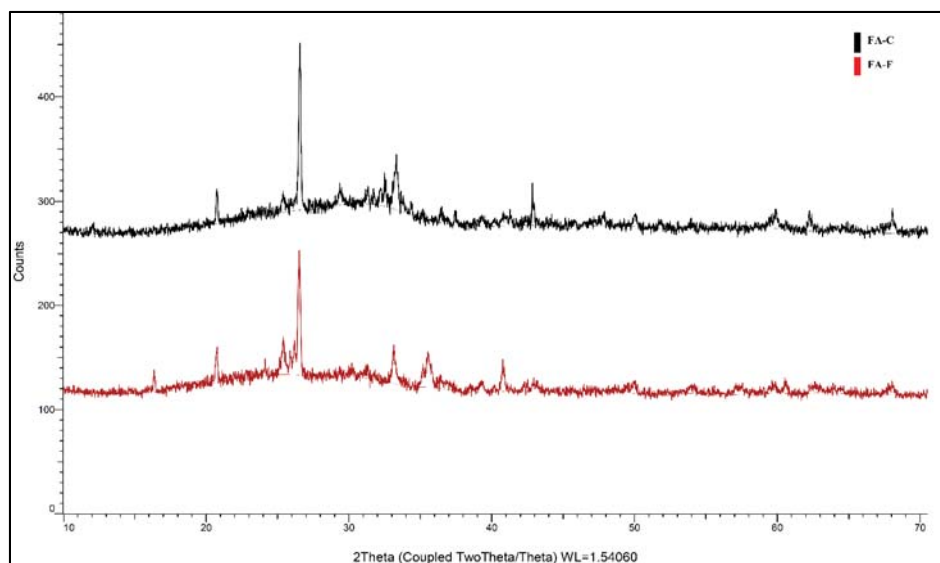
Figure 0-2- XRD Spectrum of FA-F and FA-C
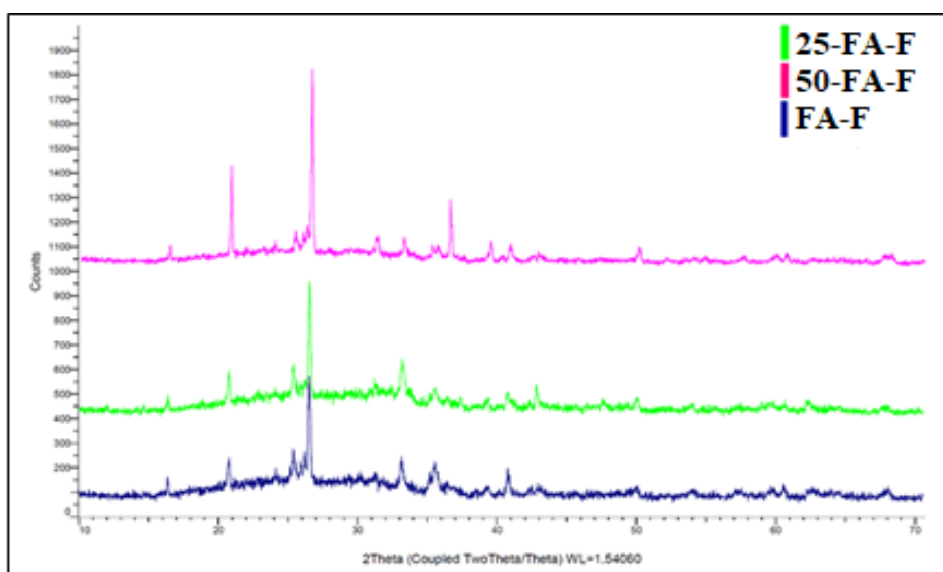
Figure 0-3- XRD Spectrum of FA-F, 25-FA-F and 50-FA-F

Table 0-4- Composition of the used fly ash, characterized by XRD

FA-C		FA-F		25-FA-F		50-FA-F	
%Crystallinity	**43.5**	%Crystallinity	**41.3**	%Crystallinity	**40.9**	%Crystallinity	**40.4**
Quartz	25.96	*Quartz*	20.19	*Quartz*	19.79	*Quartz*	29.67
Mullite	12.25	*Mullite*	17.31	*Mullite*	8.30	*Mullite*	12.83
Hematite	6.75	*Hematite*	14.84	*Hematite*	6.85	*Hematite*	1.43
Periclase	13.61	*Periclase*	6.55	*Periclase*	11.73	*Periclase*	3.38
Anhydrite	7.20	*Anhydrite*	2.80	*Anhydrite*	16.12	*Anhydrite*	9.54
Lime	6.43	*Lime*	4.86	*Lime*	5.85	*Lime*	2.50
tricalcium aluminate	19.19	*tricalcium aluminate*	7.80	*tricalcium aluminate*	21.16	*tricalcium aluminate*	9.59
Ettringite	3.10	*Ettringite*	1.38	*Ettringite*	2.76	*Ettringite*	0.71
Spinel	5.51	*Spinel*	5.77	*Spinel*	5.61	*Spinel*	29.03
		Magnetite	18.51	*Magnetite*	1.82	*Magnetite*	1.33

Table 0-5- Chemical formula of each characterized phase and their nominal composition

Name of crystalline phase	Chemical Formula	Nominal Composition
Quartz	SiO_2	SiO_2
Mullite	$Al_6 Si_2 O_{13}$	$3Al_2O_3 . 2SiO_2$
Hematite	Fe_2O_3	Fe_2O_3
Periclase	MgO	MgO
Anhydrite	$CaSO_4$	$CaO. SO_3$
Lime	CaO	CaO
Tricalcium aluminate (C3A)	$Ca_3 Al_2 O_6$	$3CaO. Al_2O_3$
Ettringite **(C3A + 3 CaSO4 =Ettringite)**	$Ca_6 Al_2 (SO_4)_3 (OH)_{12}.26H_2O$	$4CaO. Al_2O_3. 3(SO_3)$
Spinel	$Mg(Fe)_2O_4$	$MgO. Fe_2O_3$
Magnetite	Fe_3O_4	$FeO.Fe_2O_3$

The major components of fly ash reported in oxide form are silica (SiO_2), alumina (Al_2O_3), and oxides of magnesium, calcium and iron (MgO, CaO, FeO and Fe_2O_3). Considering the nominal composition of the listed crystalline phases in Table 5-4 and 5-5, total amount of the main oxides can be calculated which are reported in Table 5-6.

Comparison between oxide content in different classes and sizes of fly ash revels the same trend as was shown in Table 4. It can be noticed that of SiO_2 and CaO contents in FA-C are more than that of FA-F, while iron oxide content in FA-F is more than three times as in FA-C. Particle size dependency of fly ash chemical composition is also obvious by comparing 25-FA-F and 50-FA-F. As mentioned earlier, the larger particle size, the more recognized content of silicon and iron oxides, while the smaller particle size, the more characterized content of calcium oxide in fly ash.

	%crystalline phases							
	%SiO2	%Al2O3	%CaO	%MgO	%Fe2O3	%FeO	%SO3	Oxide total
FA-C	13.42	5.45	11.30	7.12	4.13	0.00	2.07	43.50
FA-F	11.20	5.17	5.29	3.90	11.14	3.82	4.14	44.66
FA-F25	9.45	4.34	12.74	5.94	4.32	0.37	3.72	40.90
FA-F50	14.06	4.11	5.99	7.23	6.71	0.27	2.03	40.40

Amounts of crystalline oxide phases listed in Table 5-6 are reported whereas the total oxides in each fly ash differs from one to another. Normalized content of oxides regarding to their total oxides content are reported in Table 5-7, which shows the same trend in the amount of oxides as before in all fly ash.

Table 0-6-Oxides content in fly ash in respect of their crystal phase percent

	%crystalline phases							Oxide total
	%SiO$_2$	%Al$_2$O$_3$	%CaO	%MgO	%Fe$_2$O$_3$	%FeO	%SO$_3$	
FA-C	13.42	5.45	11.30	7.12	4.13	0.00	2.07	43.50
FA-F	11.20	5.17	5.29	3.90	11.14	3.82	4.14	44.66
25-FA-F	9.45	4.34	12.74	5.94	4.32	0.37	3.72	40.90
50-FA-F	14.06	4.11	5.99	7.23	6.71	0.27	2.03	40.40

Table 0-7- Normalized content of oxides regarding to their total oxides content

	Crystalline phases (%wt)							Total
	%SiO$_2$	%Al$_2$O$_3$	%CaO	%MgO	%Fe$_2$O$_3$	%FeO	%SO$_3$	
FA-C	30.86	12.54	25.97	16.37	9.51	0.00	4.76	100
FA-F	25.08	11.57	11.84	8.73	24.95	8.56	9.28	100
25-FA-F	23.11	10.62	31.16	14.54	10.57	0.91	9.10	100
50-FA-F	34.80	10.18	14.82	17.89	16.61	0.66	5.04	100

FTIR spectra of both classes of fly ash, C and F, are shown in Figures 5-4. FA-C and FA-F show almost the same spectra, and the difference between their peak numbers is negligible, which shows the presence of almost the same type of bands in both [Fauzi et al. (2016); Patil et al. (2012)]. The important infrared bands of them with their possible assignments are listed in Table 5-8. The peak intensity at 1096 cm^{-1}, which is attributed to Si-O-Si stretching, is much sharper in FA-C than that of FA-F. It is an evidence for higher Si-O-Si content in FA-C [Patil et al. (2012)].

Table 0-8- Important IR bands of fly ash with their possible assignments

Frequency (cm^{-1})	Assignment
3759	O-H stretching
3423	Si-OH stretch
1507	C-O stretching for carbonate
1096	Si-O-Si asymmetric stretching vibration
790	Si-O-Al stretch
795	Si-O-Si symmetric stretching vibration
595	Si-O-Al stretching
535	Si-O-Fe stretching
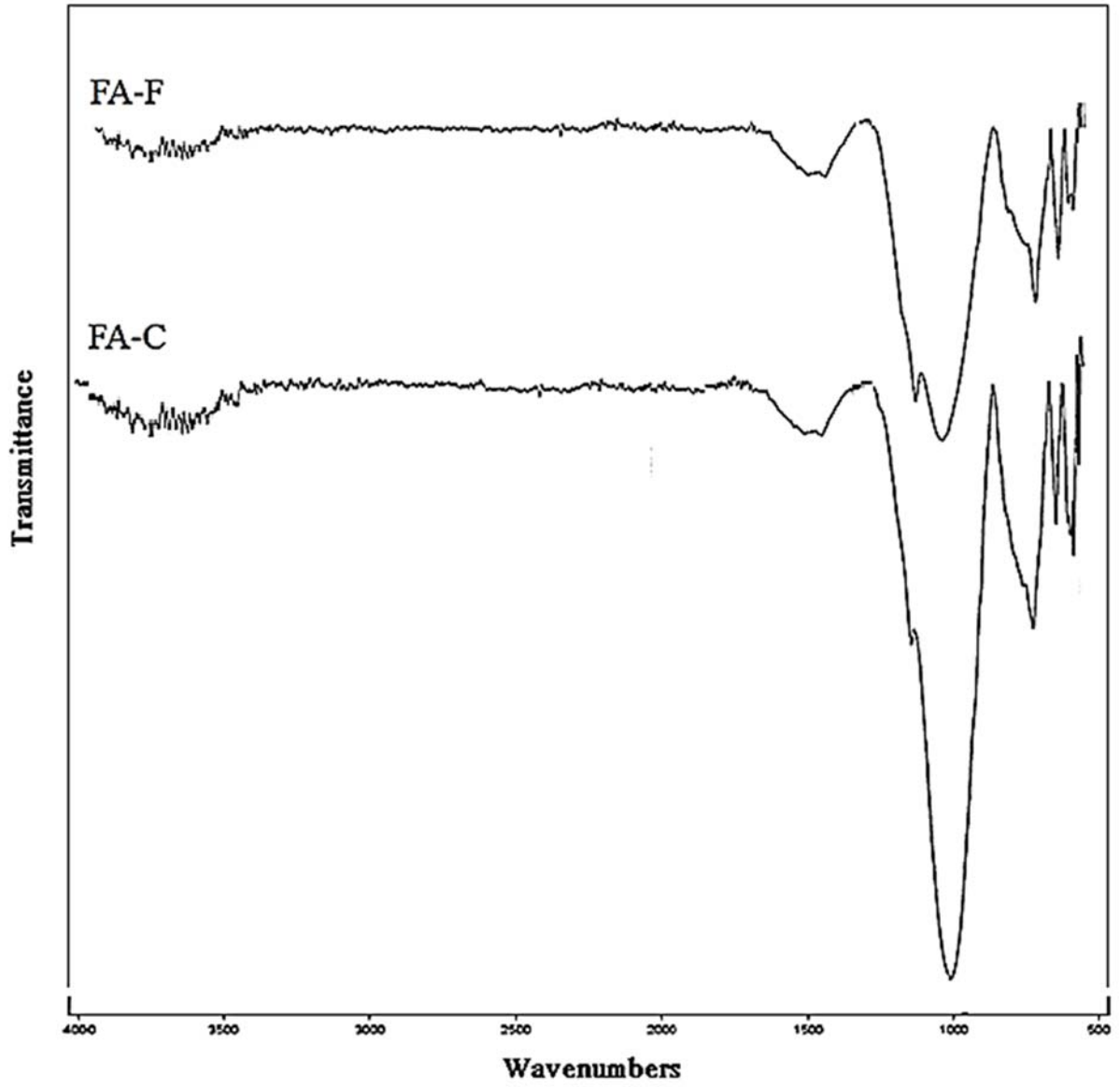
Figure 0-4-FTIR Spectrum of FA-F and FA-C

5.1.3. Morphological Properties

In order to study the particle shape of the used fly ash, investigation via SEM was conducted as shown in Figures 5-5 to 5-8. The furnace operating temperature during coal combustion is usually higher than 1400°C, which makes the inorganic materials become fluid-like and solidify, leading to different morphologies of generated fly ash. Due to rapid cooling inter-particle fusing occurs and fly ash particles agglomerate, which results in irregular shape [Patil et al. (2012)]. As observed in Figures 5-5 and 5-6, majority of particles are spherical in shape with smooth surfaces and there is no significant difference in morphology between FA-C and FA-F. The morphology of fly ash particles is controlled by combustion temperature and cooling rate.

As seen in Figures 5-7 and 5-8, majority of particles are sized respectively less than 25micron and 50micron in 25-FA-F and 50-FA-F. This confirms appropriate sieving method in them, which results in uniform particle size distribution.
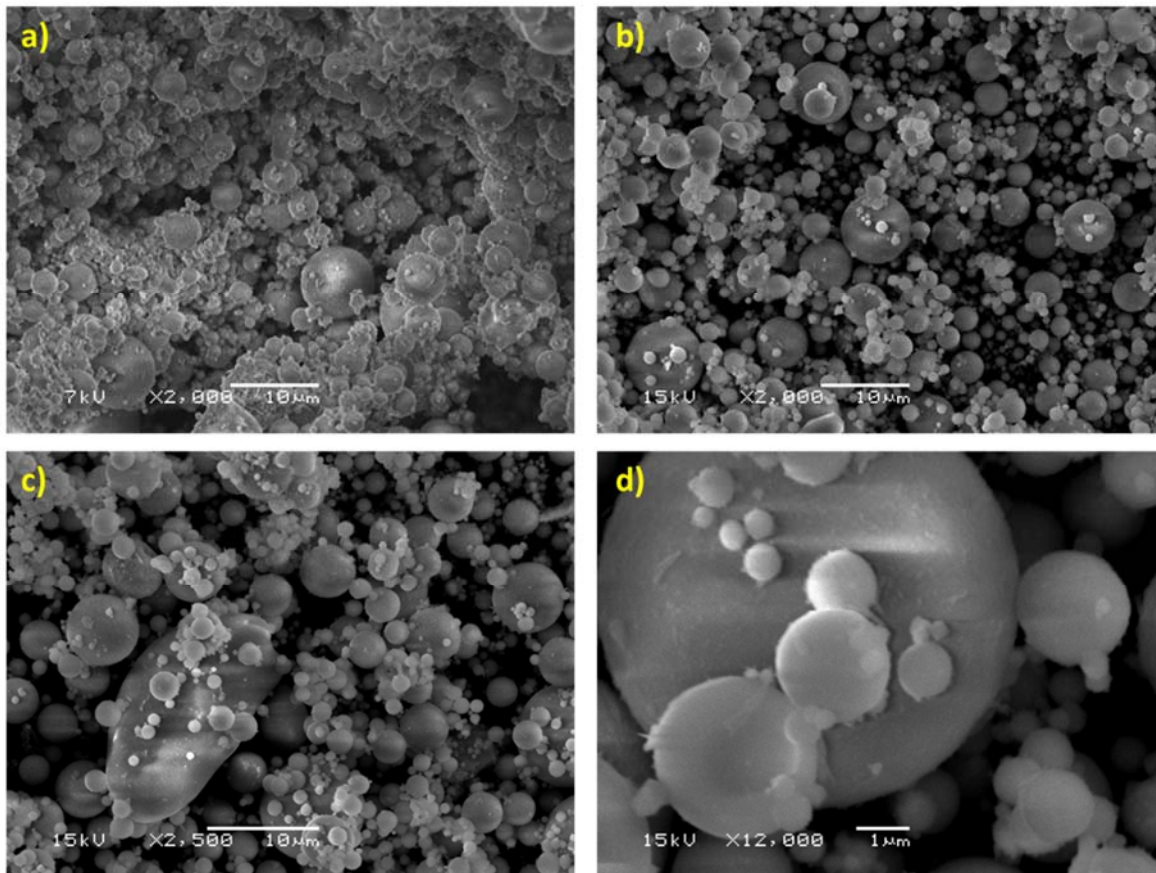
Figure 0-5- SEM of FA-C a) 2000X, b) 2000X, c) 2500X, d) 12000X
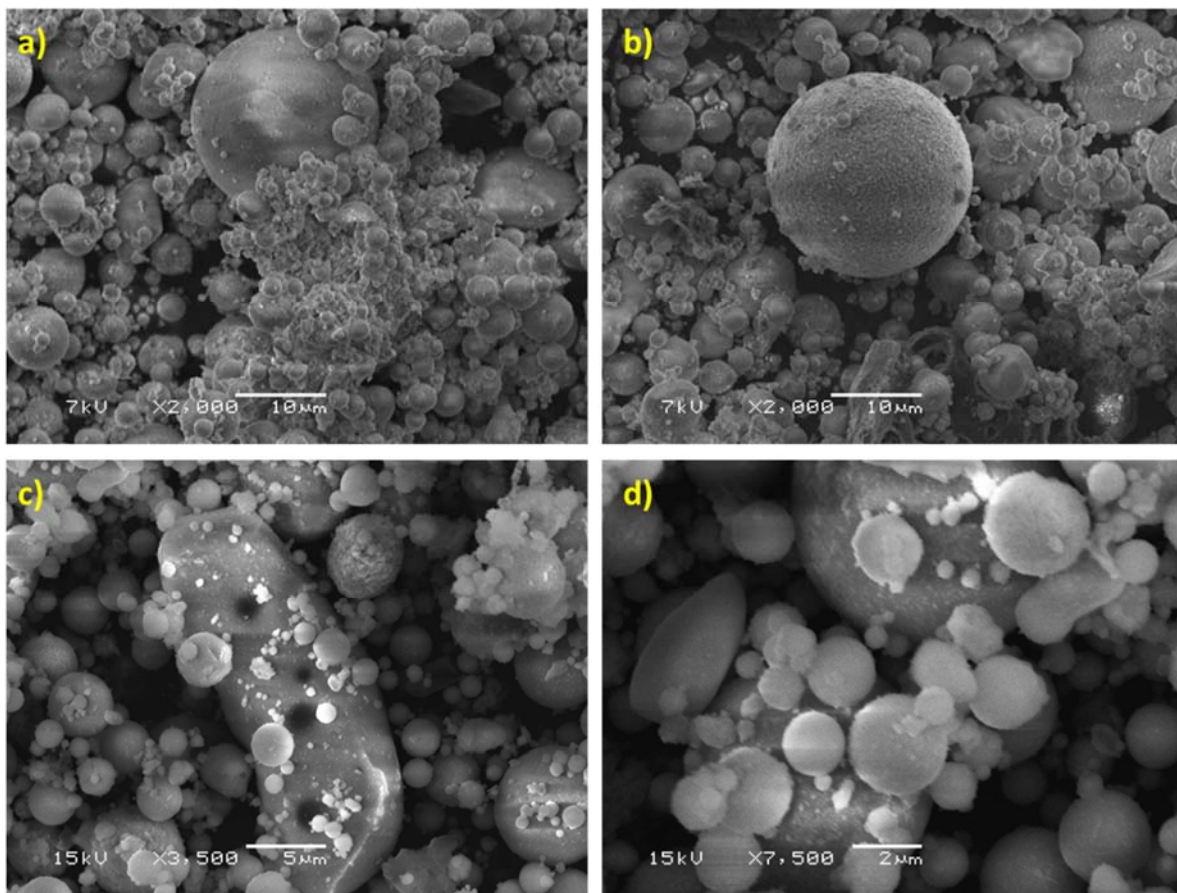
Figure 0-6-SEM of FA-F, a) 2000X, b)2000X, c)3500X, d)7500X.
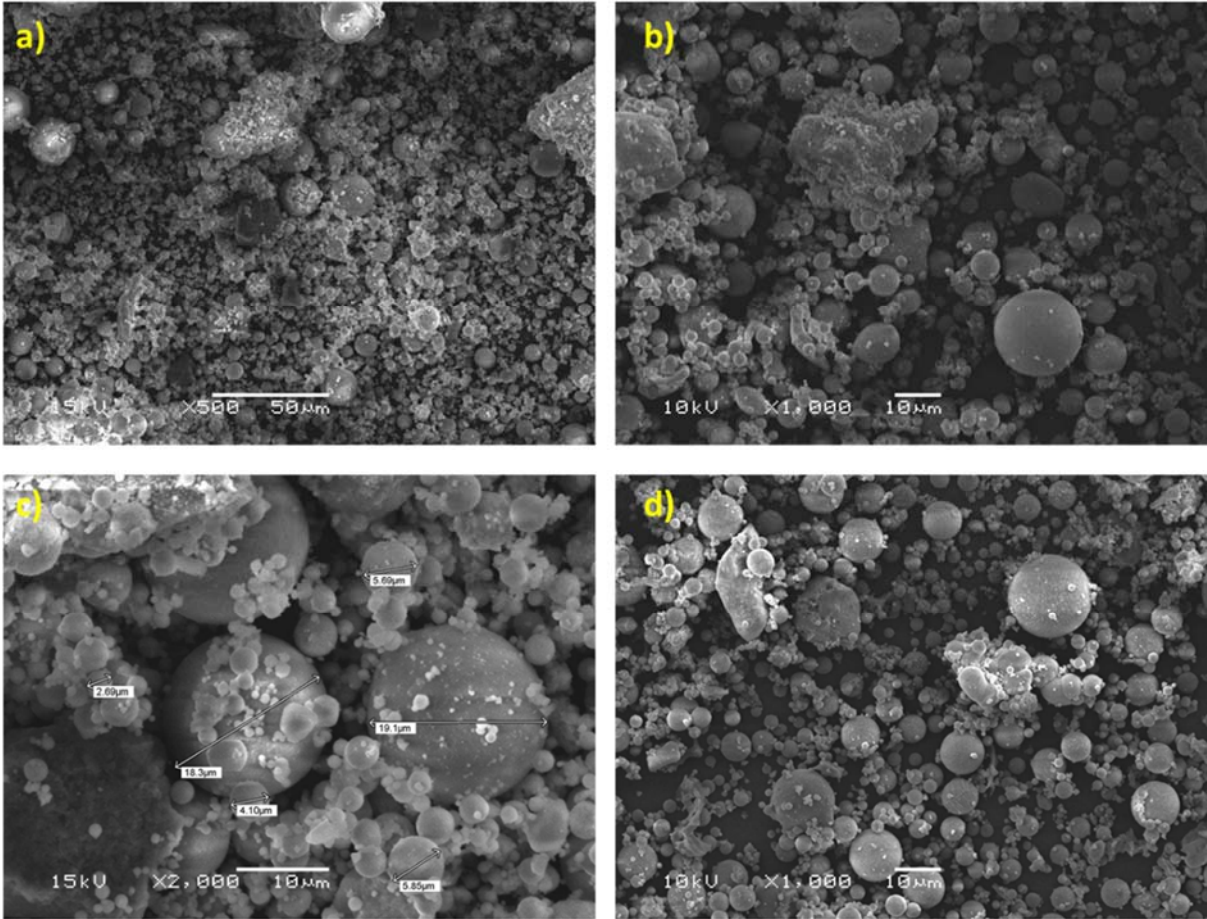
Figure 0-7- SEM of 25- FA-F a) 500X, b) 1000X, c) 2000X, d) 5000X.
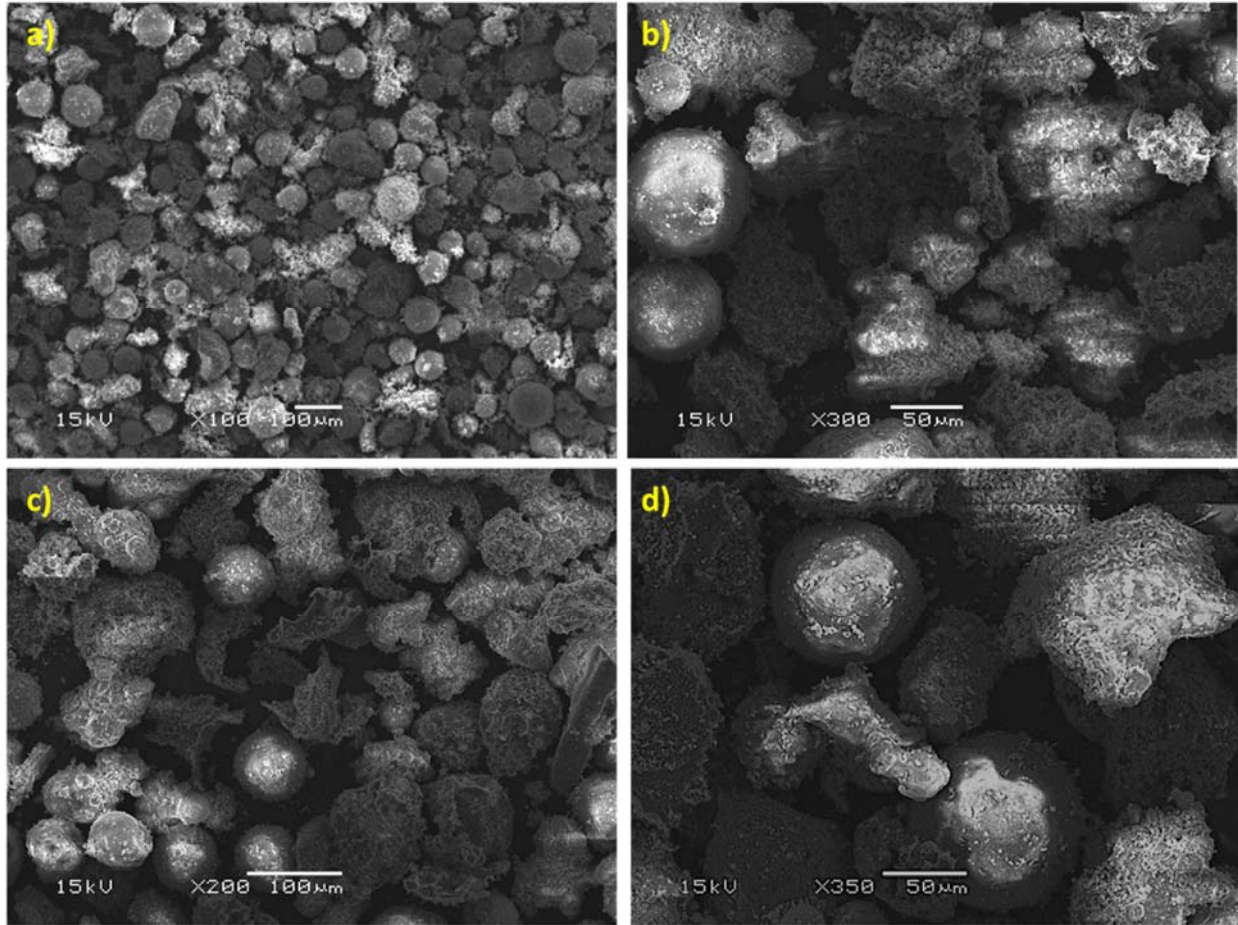
Figure 0-8- SEM of 50-FA-F a) 100X, b) 200X, c) 200X, d) 350X

5.1.4. Thermal Properties

TGA and DTA thermograms of the used fly ash with two different classes and two different particle sizes were measured at N_2 atmosphere up to 800°C, which are presented in Figures 5-9. Typically, fly ash is pretty stable up to 1000°C with negligible weight loss. Any weight loss below 200°C corresponds to water loss [Sen (2014)]. As of using dried fly ash during characterization, there is no noticeable weight loss in the TGA patterns of the fly ashes. Further increase in temperature above 550°C, a significant slope change in heat flow pattern and remarkable weight losses in TGA are observed at around 600°C which is due to evaporation of carbonaceous substances [Brown (1995)].

As FA-C contains much less carbon compared to FA-F, it is much more stable upon heating as shown in Figure 5-9a. According to EDX results reported in Table 5-3, 50micron sized class F fly ash, 50-FA-F, contains more carbon than that of unsieved FA-F and 25-FA-F, therefore the observed weight loss in its TGA thermogram is significant. Thus, the more carbon content in fly ash, the higher weight loss in TGA thermogram is expected as shown in Figure 5-9b.
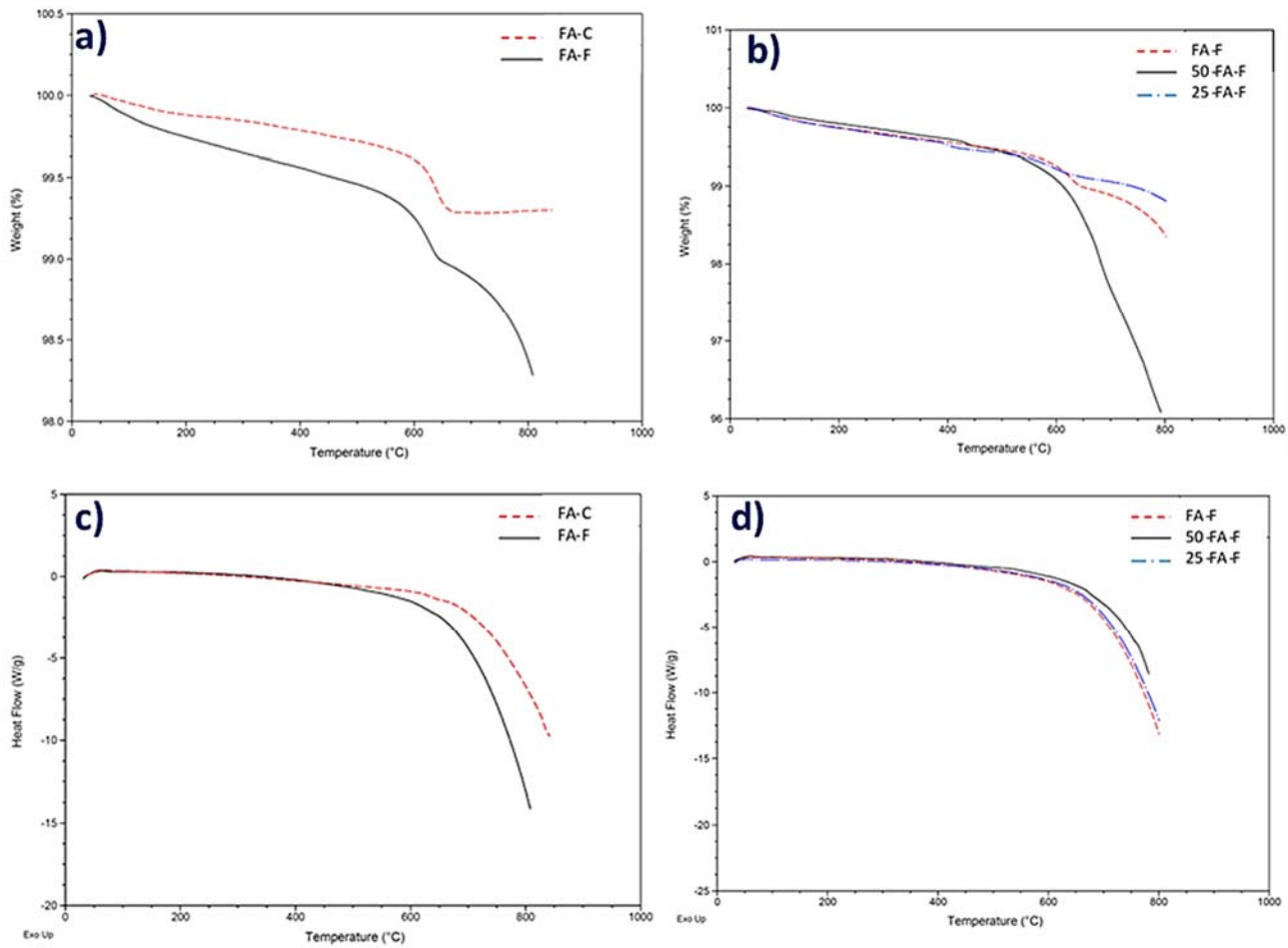
Figure 0-9- a) and c) TGA and DTA thermograms of FA-C and FA-F, b and d) TGA and DTA thermograms of FA-F, 25-FA-F and 50-FA-F.

5.2. Evaluation of the Fly Ash Performance in PVC Foam Composites using Class F

5.2.1. Physical Properties

Density and void content are considered as important parameters in controlling the mechanical and thermal properties of the foams. Experimental and theoretical density of the composites were respectively measured and calculated according to ASTM D272 and rule of mixture as presented in Equation 4-1. Void content is also calculated according to Equation 4-2. Results are shown in Figure 5-10.

It can be seen in Figure 5-11, the measured density of composites increases proportionally as the fly ash content increases, while void content had an inverse trend. Since fly ash particles have higher density than the polymer itself, the density of filled composites is higher than the pure sample. The improvement of density values with increasing fly ash content is more significant in highly loaded samples (from FA-F12 to FA-F40). In fact, cell growth can be physically hindered in the presence of fly ash particles, which may result in smaller cell size, thicker cell walls, and higher foam density and thus in highly loaded samples higher foam density is expected.

The results of tensile, flexural, dynamic mechanical and thermal shrinkage represented a direct relationship with density especially in highly loaded samples FA-F12, FA-F25 and FA-F40. Decreasing void content with increasing fly ash content may be attributed to the scarcity of resin and high amounts of fly ash particles which may hinder the foaming process. A 30% reduction in the void volume can be observed in FA-F40, which has the highest amount of fly ash in the composites. It is expected that the presence of finely dispersed filler in the PVC melt provides nucleation sites for gas evolution and activate the blowing agent at lower temperatures than its regular decomposition temperature range [Yoo and Kim (2004)].
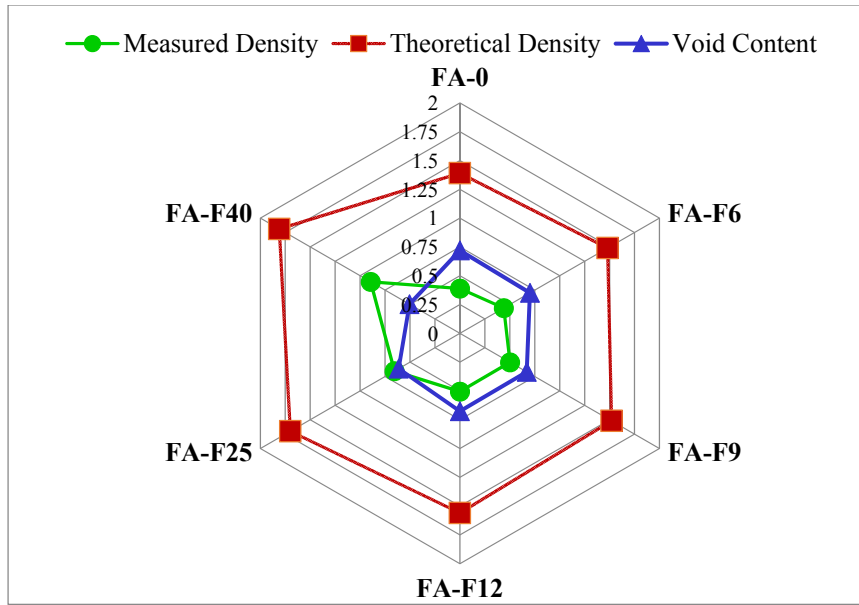
Figure 0-10- Measured density (g/cm³) and void content (%) in PVC/fly ash foam composites
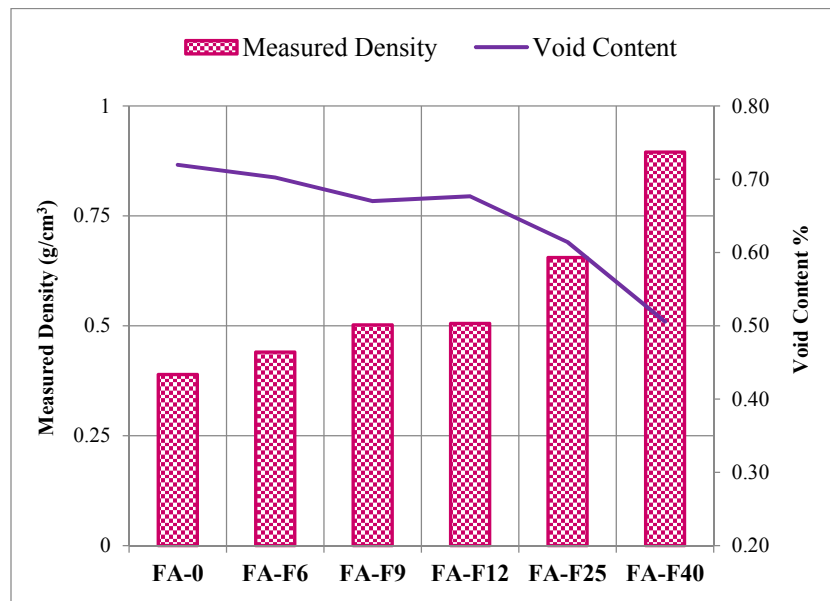
Figure 0-11- Trend of measured density (g/cm³) and void content (%) in PVC/fly ash foam composites

5.2.2. Mechanical Properties

Mechanical properties also evaluated using tensile, flexural, and impact characterization methods. Tensile modulus and strength as shown in Figure 5-12a improved with increasing fly ash content, which may be due to good dispersion of fly ash particles in the PVC foam matrix combined with a sufficient interface adhesion [Wallenberger et al. (2001); Azimpour and Marchand (2006); Swain et al. (2014)]. On the other hand, increasing the fly ash content lowers the elongation at UTS of the composites, as shown in Figure 5-12b, and increases the rigidity of the composites.

Flexural properties were also measured and the results are shown in Figure 5-13. The flexural strength increased with the incorporation of fly ash particles in the PVC foam matrix. The addition of fly ash increases the flexural strength by 14%, as seen in samples containing 40phr fly ash, indicating a good interaction between the filler and the foam matrix [Thakur and Chauhan (2013)]. In addition, well dispersed fly ash particles make the crack propagation path longer, absorb a portion of energy, and enhance the plastic deformation of the matrix, which result in higher flexural strength of the composites [Sahin et al. (2012)]. The flexural modulus was found to improve significantly upon adding fly ash into the PVC foam matrix. The modulus of the filled composites depends on the properties of components, fillers, and the matrix [Gummadi et al. (2012)]. Fly ash particles have higher modulus than PVC foam matrix, which results in higher flexural modulus in the composites compared to the rigid PVC foam (FA0). Mechanical strengthening in the foam composites can also be attributed to the decreasing cell size as the fly ash content is increased, which have been confirmed by the density measurements and SEM images shown in Figures 5-11 and 5-29; respectively. Pore size distribution of the samples also are presented in Figure 5-28, confirming density results.
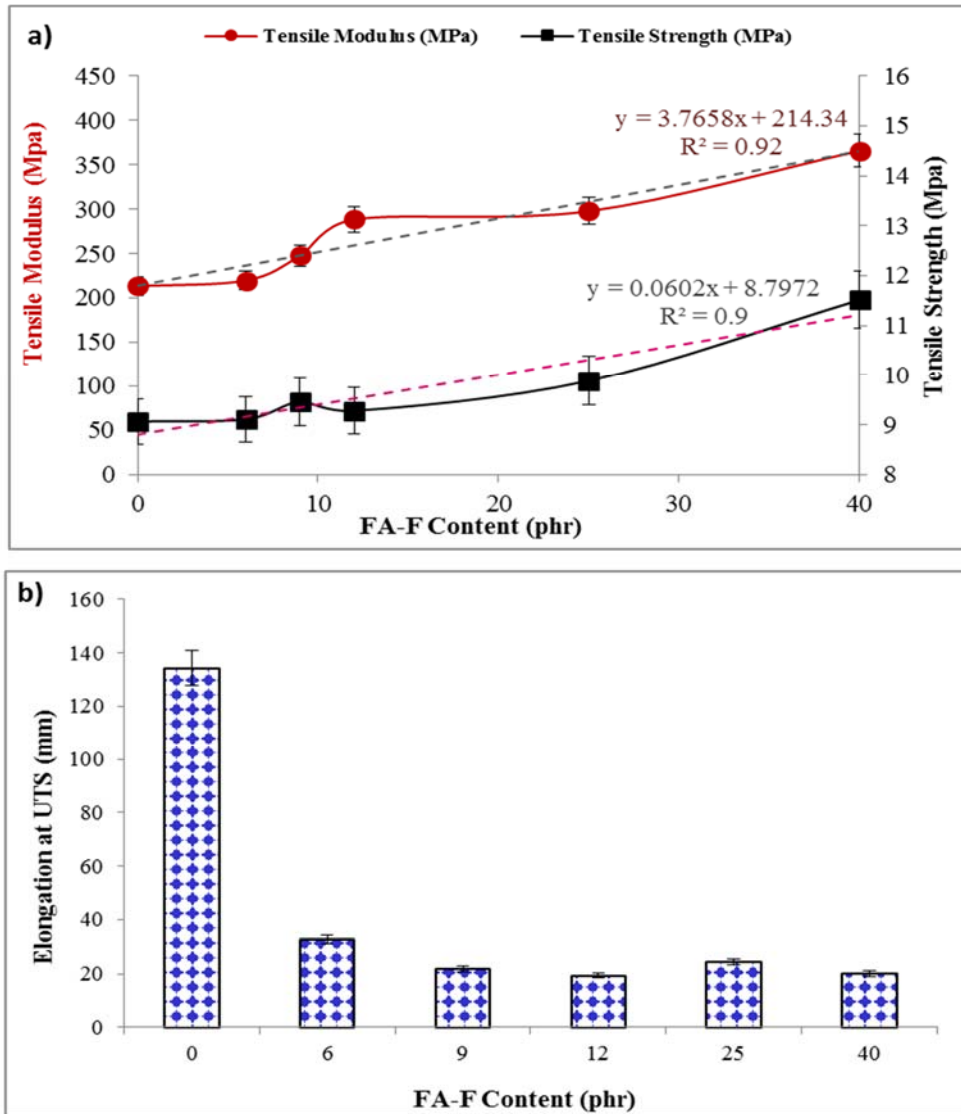
Figure 0-12- a) Tensile modulus and strength, and b) Elongation at UTS of PVC foam composites versus Fly ash
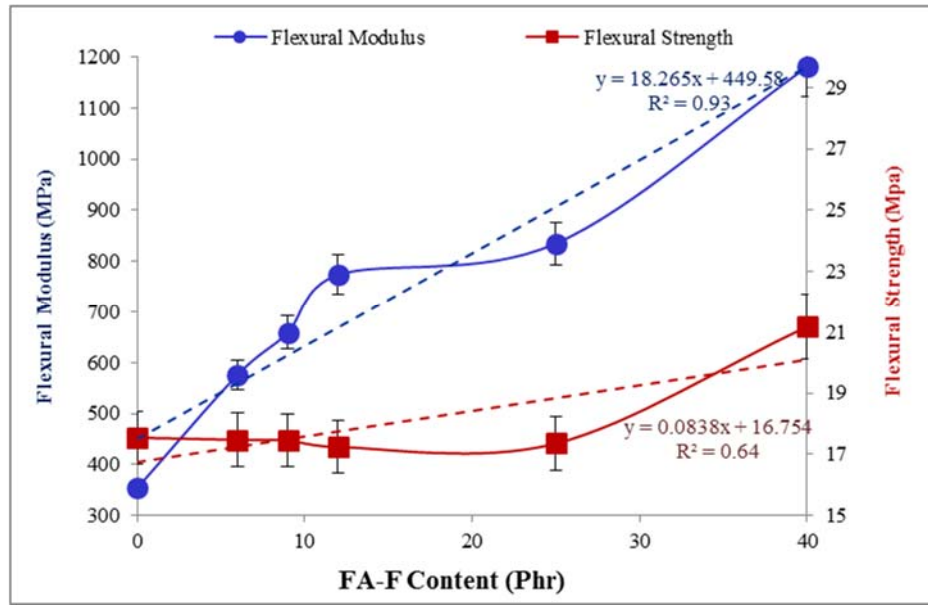
content (phr)

Figure 0-13- Flexural modulus and strength of PVC foam composites versus fly ash content (phr)

Impact strength evaluation of the foams were also done as shown in Figure 5-14. Results showed a decreasing trend as the amount of fly ash increases in the composites. This reduction might be attributed to a strong interfacial bonding between fly ash and the matrix; therefore, the polymer backbone cannot flex upon impact to absorb the energy. In addition, filler addition increases the composite stiffness, which explains the reduction in the impact strength.

In Figure 5-15, comparison between impact energy of fly ash loaded composites shows that energy of crack propagation does change significantly. For instant, impact energy in FA-F40, containing 40phr fly ash, drops only about 29% compared to FA-F6. This reveals that fly ash particles are well dispersed in the matrix and their surface are wetted with the polymer resin, whereas better wetting in solid resins are expected as foamy matrix contains a lot of air bubbles and therefore decreases surface contact between filler and polymer.
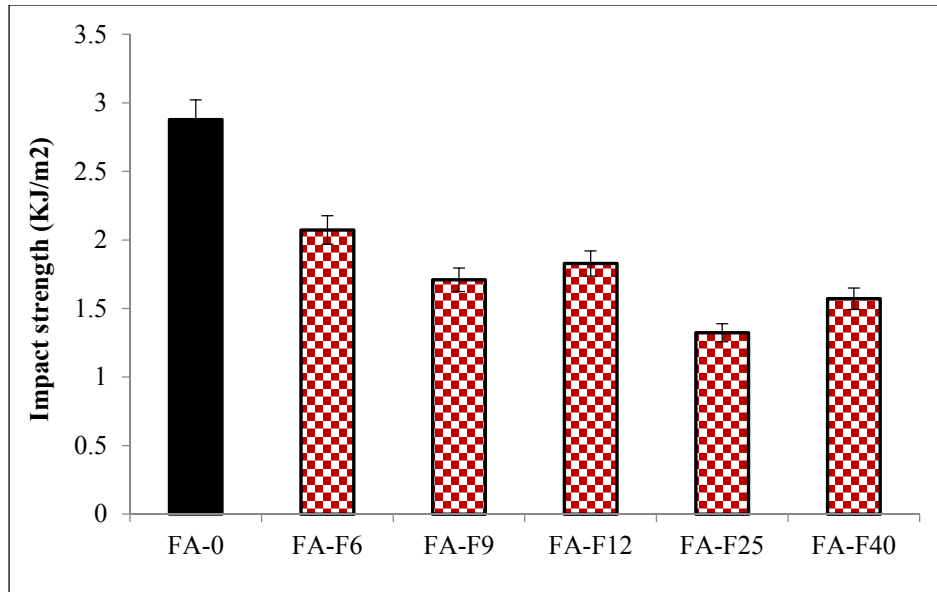
Figure 0-14- Impact strength of PVC foam composites versus Fly ash content (phr)

$$y = -0.0116x + 0.153$$
$$R^2 = 0.669$$
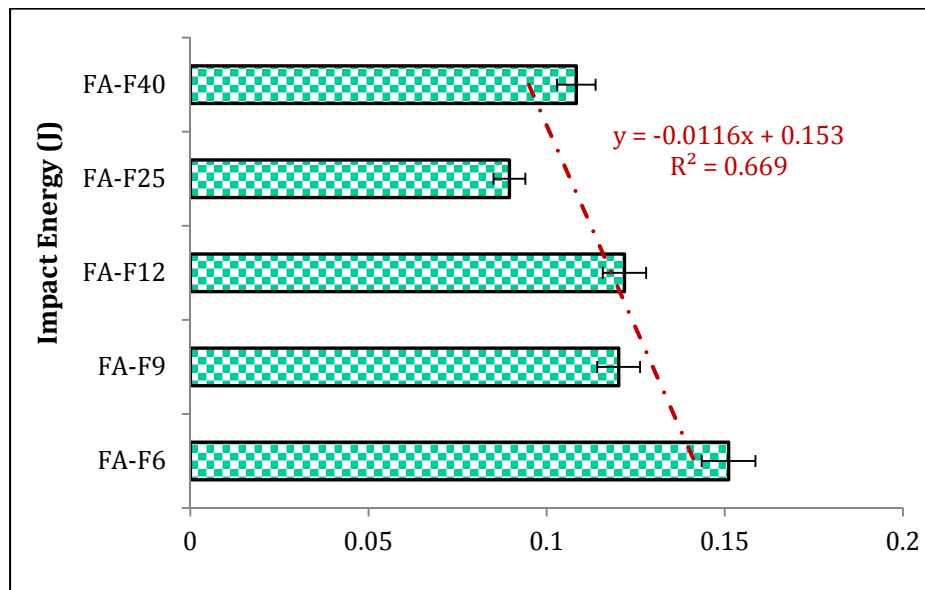
Figure 0-15-Effect of Fly ash Addition on Impact Energy of PVC Foam Composites

5.2.3. Viscoelastic Properties

Storage modulus increases significantly with the incorporation of fly ash particles as shown in Figure 5-16a. The reinforcing effect of fly ash particles is considerable at both below and above Tg temperatures. The storage modulus of filled composites below Tg is mainly affected by the filler content and stiffness [Gummadi et al. (2012)]. Therefore, with further loading of fly ash, storage modulus improves due to higher stiffness of the composites. For example, the extent of increase in storage modulus in FA-F40 at 50°C is approximately 200% compared to FA0. The increase in storage modulus at higher temperatures than Tg can be an indication of a good interfacial interaction between fly ash particles and PVC matrix [Das and Satapathy (2011); Gummadi et al. (2012)].

Loss modulus peaks of PVC foam composites are presented in Figure 5-16b. A comparison between the peak intensities shows that the addition of fly ash increases the peak intensity, which may be due to an enhancement in the energy dissipation ability in the presence of spherical filler in the composites and also an increase in the polymer-filler and filler-filler slippage at Tg [Qiao et al. (2011)].
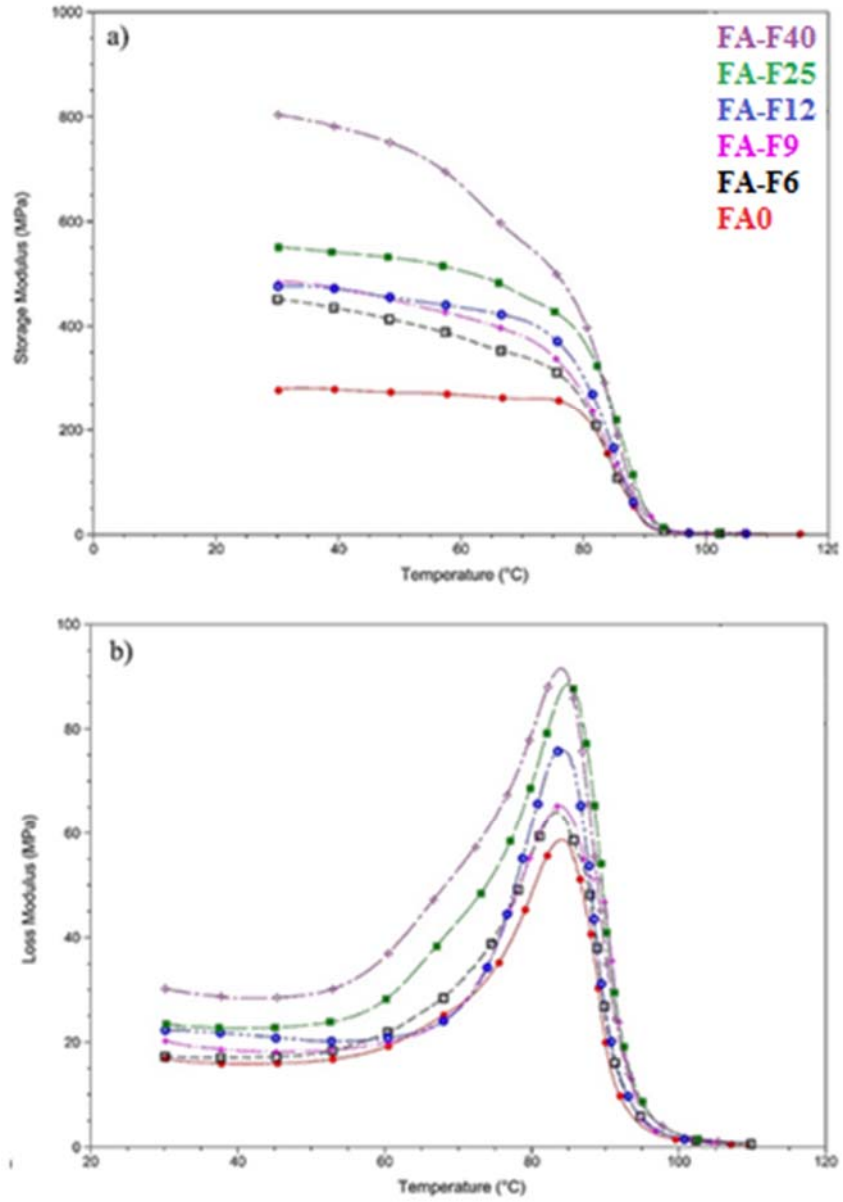
Figure 0-16- Dynamic mechanical analysis plots of PVC foam composites (a) storage modulus (E') and (b) loss

modulus (E") versus temperature

5.2.4. Thermal Properties

The degree of gelation and Tg[4] value of polymer composites are reported in Table 5-9. The addition of fly ash causes a decrease in the degree of gelation which may be attributed to the difficulty in PVC network formation. This effect is more obvious in samples with high fly ash loadings like FA-F40. The effect of fly ash on the Tg of the composites was negligible; similar findings were reported by other groups [Cruz and Garman (2009); Piszczek et al. (2010); Iulianelli et al. (2011)].

Table 0-9-Tg values and percentage of gelation obtained from DSC of PVC foam composites

Sample	Tg	Peak A (J/g)	Peak B (J/g)	%Gelation [(A/A+B)×100]
FA0	82.40	7.09	1.19	86
FA-F6	82.60	7.48	1.81	81
FA-F9	82.75	5.34	1.69	76
FA-F12	81.59	6.43	2.47	72
FA-F25	82.86	5.97	2.48	71
FA-F40	83.40	4.4	2.59	69

The dimensional stability of the foam composites was measured as a percentage of shrinkage and the results are presented in Figure 5-17. It is found that the shrinkage decreases considerably with increasing the fly ash content in the composites. The samples with 40phr fly ash (FA-F40) exhibit the lowest amount of shrinkage compared to its counterparts. This indicates that the chemical and

---

[4] Glass Transition Temperature

physical characteristics of fly ash make it suitable as a filler for PVC foam composites with applications requiring small shrinkage, such as vinyl sidings.
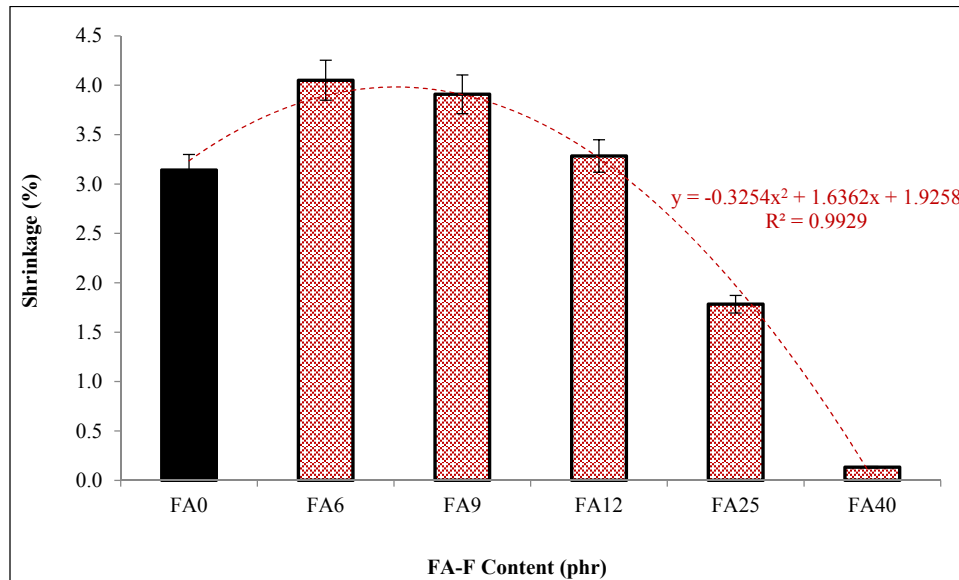
Figure 0-17- Percentage of Shrinkage in the PVC/Fly ash foam composites

PVC has a lower thermal stability compared with other major thermoplastics and its thermal degradation consists of two main steps. Dehydrochlorination occurs at the first step; which is known as the primary degradation temperature (PDT), where hydrogen chloride is eliminated, leaving behind the unsaturated hydrocarbons containing long conjugated double bonds. At the second step, which is known as the secondary degradation temperature (SDT), degradation of the $-(-CH=CH-)_n-$ hydrocarbon backbone occurs through hydrogen subtraction from the backbone via chlorine free radicals and therefore forming HCl gas as a product, which inherently results in a color change [Sin et al. (2012); Liu et al. (2006); Inoue et al. (2004); Parvaiz et al. (2010)]. The mechanism of the two-step degradation process is illustrated in Figures 5-18. A typical TGA thermogram of PVC is shown in 5-19. TGA thermograms of the fly ash reinforced composites are presented in Figure 5-20.

Figure 0-18- Mechanism of PVC degradation

Figure 0-19- General TGA thermograms of PVC
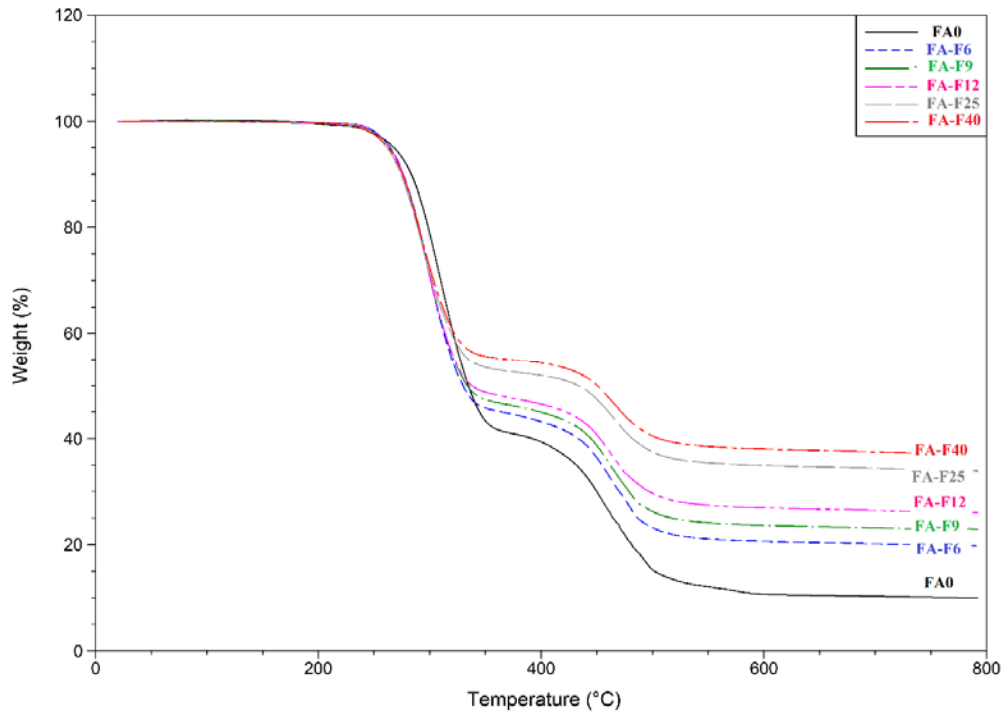
Figure 0-20- TGA thermograms of PVC/Fly ash foam composites

As illustrated in Figure 5-21, the primary degradation temperature (PDT) of the PVC composites decreases slightly in PVC/FA-F composites; the composite filled with the lowest amount of fly ash, FA-F6, shows the lowest drop in the first decomposition temperature. From the foam point of view, the addition of dispersed filler results in activating Azodicarbonamide blowing agent at temperatures lower than its regular decomposition range (195-216°C) and providing more nucleation sites for gas evolution [Yoo et al. (2004)], this may be attributed to the observed drop in PDT in FA-F6, as it has the lowest amount of fly ash particles.
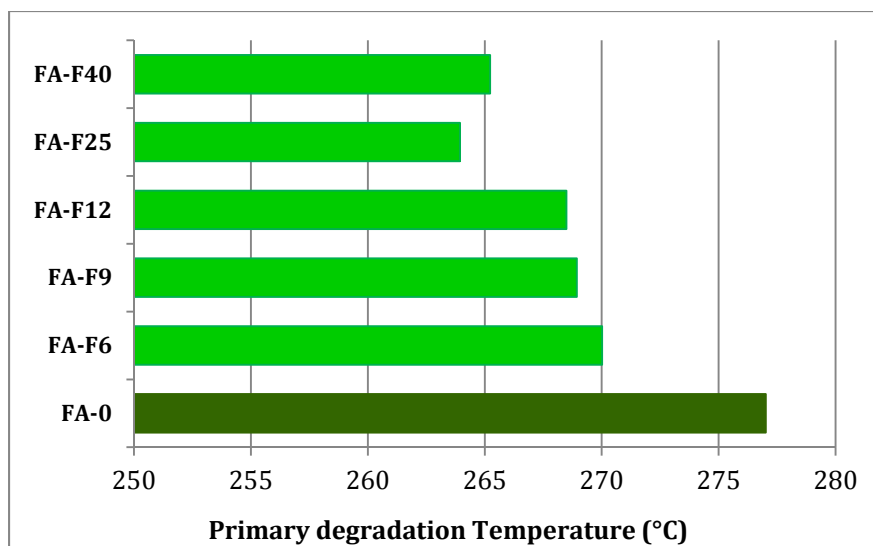
Figure 0-21- PDT of PVC/FA-F Foam Composites

Similar findings were reported by other research groups in the case of PVC composites containing various metal oxides [Sivalingam and Madras (2004); Uegaki and Nakagawa (1977)]. It has also been reported elsewhere that the oxygen, and the oxygen-containing groups like metal oxides, may function as sites for the initiation of dehydrochlorination in PVC and accelerate the degradation mechanism. Acid absorbers reduce the catalytic effects of liberated Cl radicals and the accelerating effect depends on the concentration of the oxides. Therefore, metal oxides may act as acid absorbers and result in the destabilization of PVC due to the metal oxide radical or hydrogen chloride formation during the degradation process [Sivalingam and Madras (2004); Uegaki and Nakagawa (1977); Gupta and Viswanath (1998)].

Since most fly ash contains metal oxides; such as CaO and Fe_2O_3, the formation of metal chlorides may occur during the dehydrochlorination process of PVC, which can be the main reason for the primary decomposition temperature (PDT) to drop in fly ash filled composites. The secondary

106

degradation temperature (SDT) of PVC composites is shown in Figure 5-22. SDT shifts towards the

higher temperatures with the addition of fly ash particles which means that cracking of the

hydrocarbon backbone is delayed by the addition of fly ash.
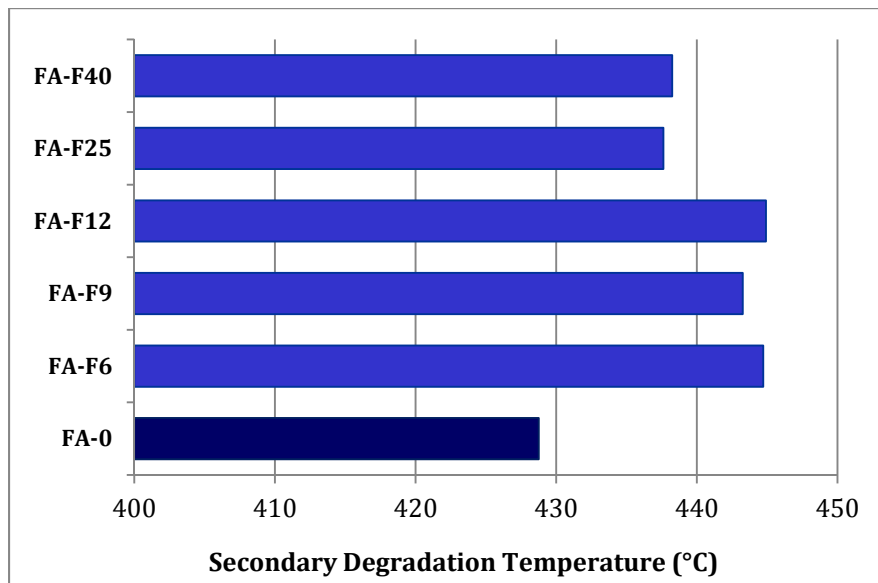
Figure 0-22-SDT of PVC/FA-F Foam Composites

In the presence of metal oxides, the mechanism of the second degradation step is much different

than what is shown earlier in Figure 5-18. The suggested degradation mechanism in the presence of

metal oxides is represented in Figure 5-23. The chlorine free radical ($Cl^{\bullet}$) reacts with the metal oxide

(M_xO_y) and replaces its oxygen to form a metal chloride (MCl_x), instead of HCl. The oxygen radical

then abstracts hydrogen from PVC to form water [Gupta and Viswanath (1998)].

Figure 0-23- *Suggested mechanism of PVC degradation in the presence of metal oxides*

$$XCl^{\bullet} + M_xO_y \rightarrow MCl_x + YO^{\bullet}$$
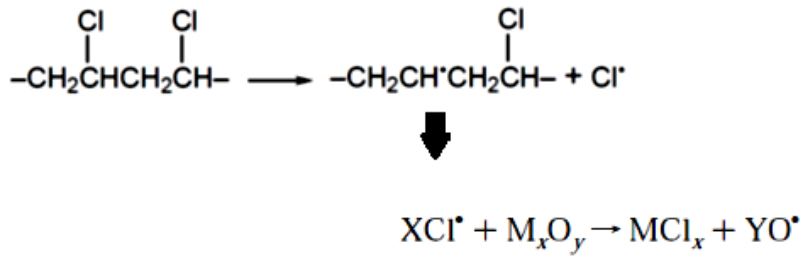
Figure 0-23- Suggested mechanism of PVC degradation in the presence of metal oxides

Among all metal oxides, CaO and Fe_2O_3 were found to be reactive to the chlorine radicals and will form metal chloride as a product. Meanwhile SiO_2 and Al_2O_3 were found to be non-reactive, and therefore HCl gas is still released during the degradation process. It is also mentioned elsewhere that the minimum change of PVC molecular weight is observed in the presence of CaO, which means that CaO reacts predominantly with Cl in PVC [Inoue et al. (2004)]. Approximately 45wt% of Class-F fly ash is composed of calcium and iron oxides, which can react with chlorine free radicals and inhibit HCl formation. Mechanisms of the reaction between PVC and the reactive oxides, CaO and Fe_2O_3, and the non-reactive ones, SiO_2 and Al_2O_3, are shown in Figure 5-24.

$$-(CH_2CHCl)- + CaO \rightarrow -(CH=CH)- + CaOHCl$$

$$4-(CH_2CHCl)- + Fe_2O_3 \rightarrow 3-(CH=CH)- + -(CHClCHCl)- + FeCl_2 \cdot 2H_2O + FeO$$

$$-(CH_2CHCl)- + SiO_2 \rightarrow -(CH=CH)- + SiO_2 + HCl$$

$$-(CH_2CHCl)- + Al_2O_3 \rightarrow -(CH=CH)- + Al_2O_3 + HCl$$
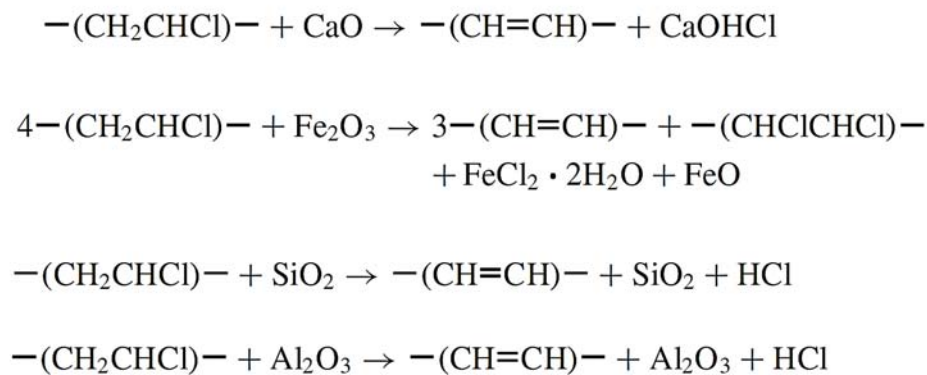
Figure 0-24- Mechanisms of reaction between PVC and reactive oxides, CaO and Fe_2O_3, and non-reactive oxides, SiO_2 and Al_2O_3.

Although the degradation mechanism is accelerated in the presence of metal oxides, hydrochloric acid, a toxic and harmful substance, will not form. One of the main issues that is pointed towards PVC products is its disposal after usage that is now applied under restricted conditions because of the emission of harmful substances such as HCl gas [Inoue et al. (2004)]. Our results show that by applying some amounts of fly ash to PVC, it can overcome the problem of HCl gas emission during PVC decomposition, thus providing a low-cost solution to an environmental problem.

It can also be noticed that the final weight loss at 800°C increases with increasing fly ash and reaches 37% in FA-F40, which has the highest amount of fly ash loading. As shown earlier in the section of fly ash characterization, Figure 5-20, fly ash is almost stable up to 1400°C, therefore the higher fly ash content, the more remained ash is left at the end.

5.2.5. Kinetics Analysis of Thermal Decomposition

The kinetics of thermal decomposition in the fly ash loaded composites are also studied to confirm the observations in TGA results. Flynn-Wall model was applied due its simplicity and short experimental requirements. TGA was run on FA0 and FA-F40 three times at different heating rates, 5, 10 and 20°C/min. The activation energy (E_A), which is the amount of energy needed to initiate a chemical process, is estimated using Equation 5-2.

$$\ln k = lnA - \frac{E_A}{RT}$$ **Equation 0-2**

where A, k, T and R, are a pre-exponential factor, heating rate constant, temperature and gas constant (8.3144 J.mol^{-1}.K^{-1}); respectively. E_A and A can be estimated, respectively, from the slope and intercept values of the linear correlation between k and 1/T. For this purpose, at a constant

109

weight fraction of conversion (α) and a constant heating rate, the weight loss temperature was determined as shown in Figure 5-25. Linear correlation between heating rate (ln k) and temperature (1000/T) at various weight fractions of conversion are shown in Figure 5-26. Weight fraction of conversion (α) is determined using Equation 5-3:

$$\alpha = \frac{W - W_f}{W_i - W_f} \qquad\qquad \textbf{Equation 0-3}$$

W = mass at a particular temperature (mg)

W_i = initial sample mass (mg)

W_f = final sample mass (mg)
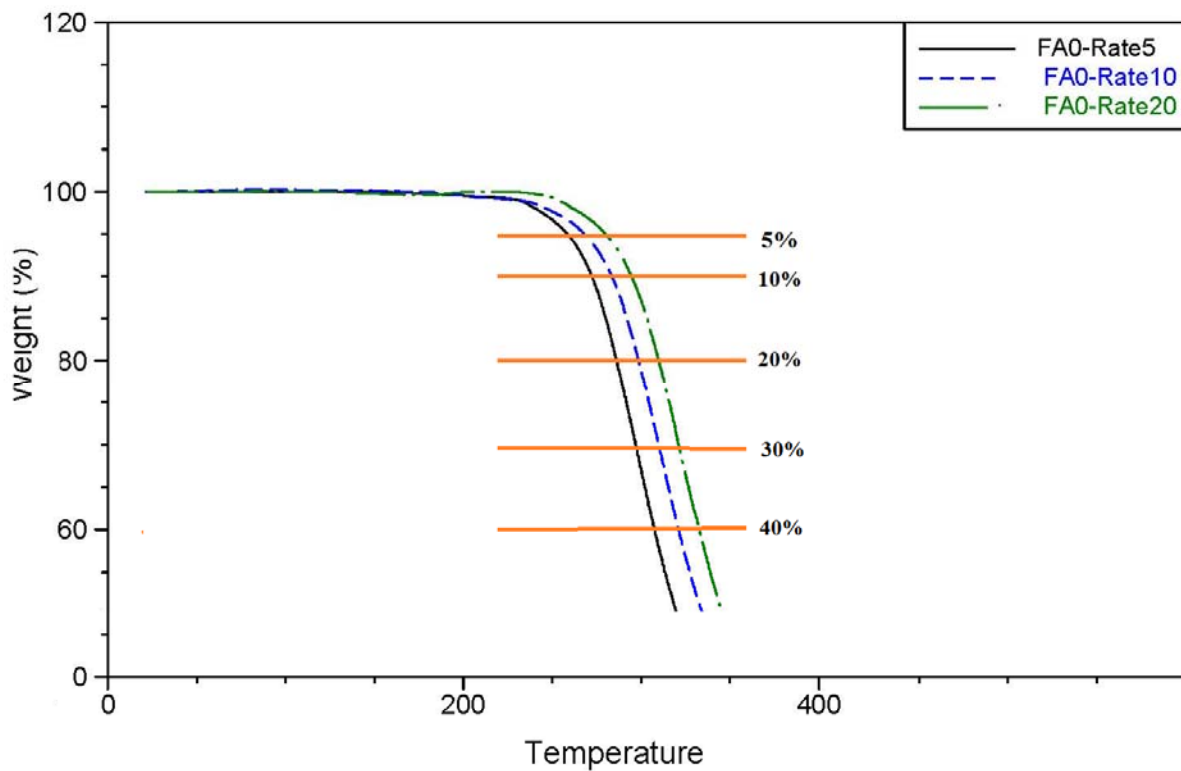
Figure 0-25-TGA Kinetics using Flynn-Wall method

110
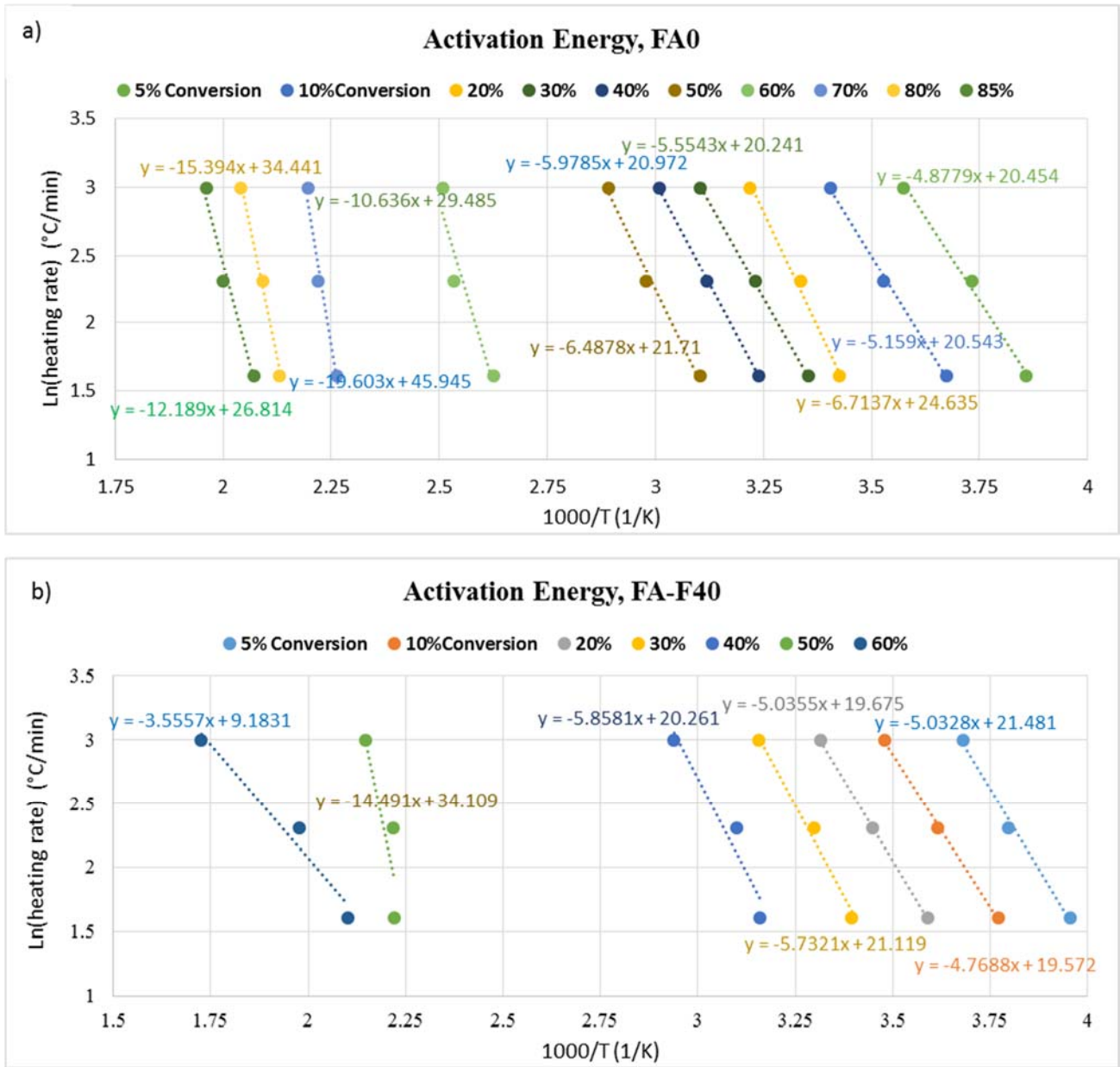
Figure 0-26- Estimated activation energy (from slope of heating rate versus temperature) of a) FA0 and b) FA-F40.

Activation energy of FA0 and FA-F40 at a constant percent of conversation is estimated from the slope of the presented lines in Figure 5-26. The estimated activation energy (E_A) is presented in 5-27. As shown in Figure 5-27, E_A in FA0 is higher than FA-F40 up to 20% weight fraction conversion and their values are almost the same at 30% conversion. As was discussed earlier, thermal

degradation of PVC compounds involves two steps, where the first step is almost completed after 30% weight loss and the second step starts right after that. The calculated activation energies are consistent with the TGA results depicted earlier in Figure 5-26. It confirms that pure PVC, i.e. FA0, has higher activation energy at the first decomposition step than those reinforced with fly ash. Whereas, the addition of fly ash results in a significant increase in the activation energy of the second decomposition step. Therefore, in the presence of fly ash, degradation of the main backbone is much slower and harder than in the case of pure PVC.

Although fly ash addition to the PVC compounds accelerates the dehydrochlorination process, which is due to the metal oxide presence, it improves thermal stability of the main backbone and prevents the formation and release of the toxic gas.
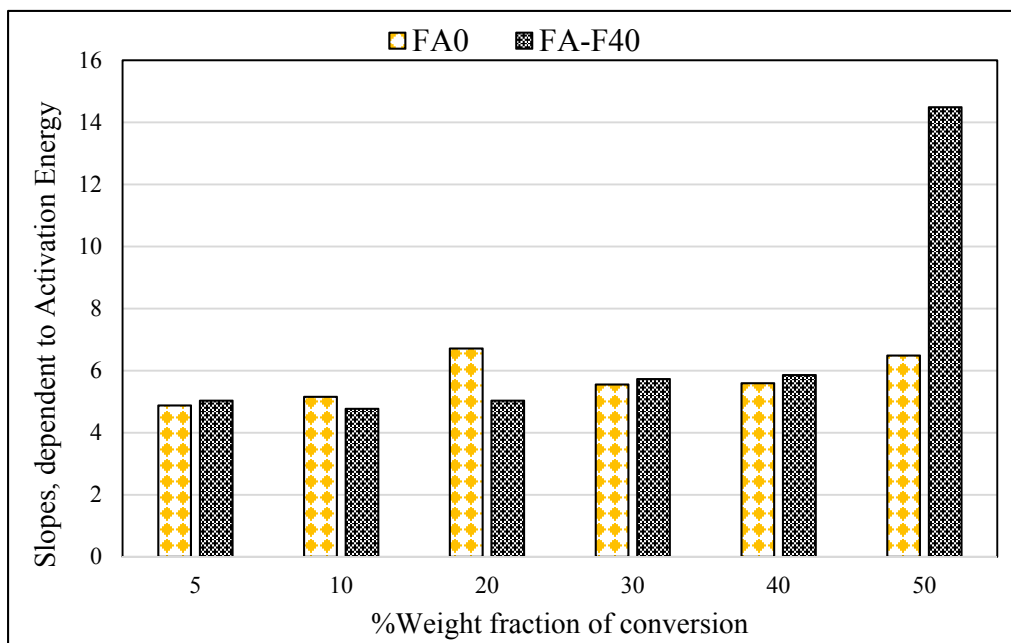
Figure 0-27- Estimated activation energy in FA0 and FA-F40

5.2.6. Morphological Properties

In Figure 5-28 pore size distribution of pure PVC foam, FA0, and 40phr loaded composite foam, FA-F40 are shown. As seen in histograms, in FA0 the pore size distribution is broad and the majority of cells are sized in the range of higher than 150μm.Whereas, in FA-F40 cell size distribution is much narrower than FA0 mainly in the range of 50μm to 100μm. This observation are consistent with density and void measurements showing that fly ash particles may hinder cell growth which results in smaller cell size, thicker cell walls, and higher foam density.

Morphological studies of the PVC/fly ash foam composites as shown in Figure 5-29, represents that fly ash particles are uniformly dispersed within the matrix, especially at lower loadings (Figure 5-29 (a)). However, the number of visible particles and aggregates are more noticeable in the case of composites with a high loading, e.g. FA-F40 (Figure 5-29 (e)). In addition, SEM images of the foam composites show that increasing fly ash particles decreases cell size and this effect can be observed by comparing Figures 5-29 (a) and 5-29 (e) which correspond to FA-F6 and FA-F40; respectively. The presence of tightly embedded and mechanically interlocked fly ash particles within the PVC matrix in all composites indicates a strong interaction between the filler and the matrix and also a good dispersion of fly ash particles. By increasing fly ash content, especially in samples FA-F25 and FA-F40, the number of filler debonding is found to be higher, which is due to high filler loading and dewetting of fly ash surface with the PVC matrix.
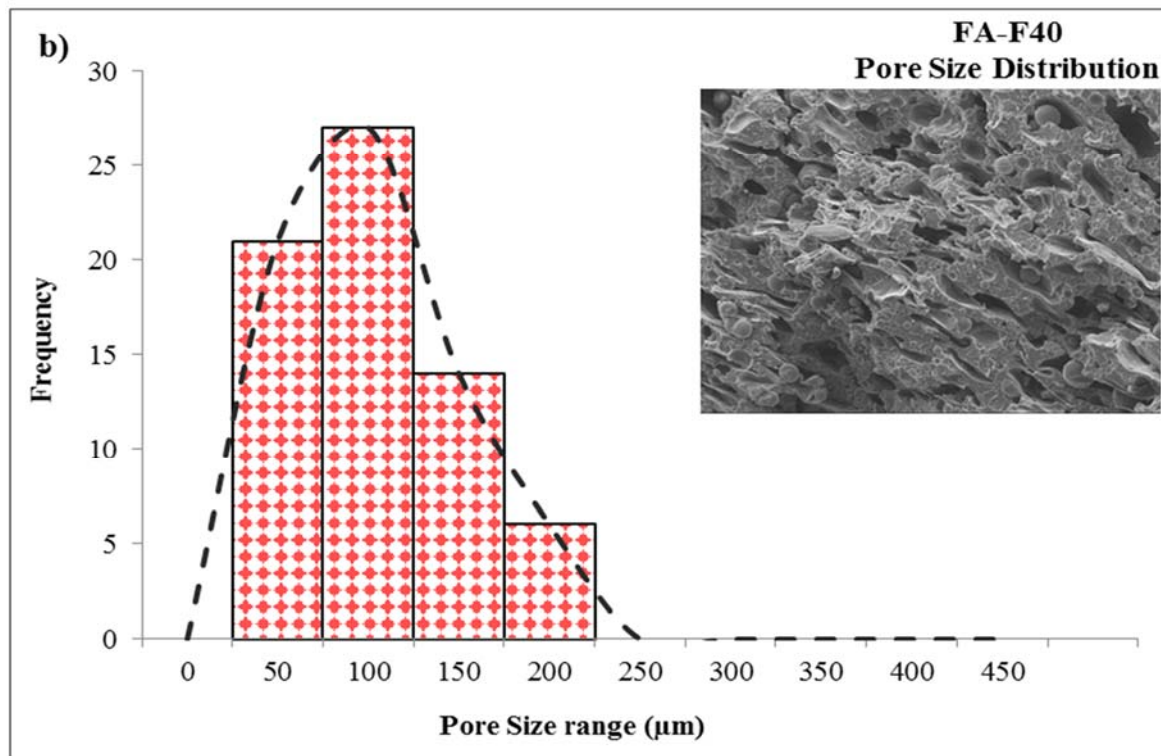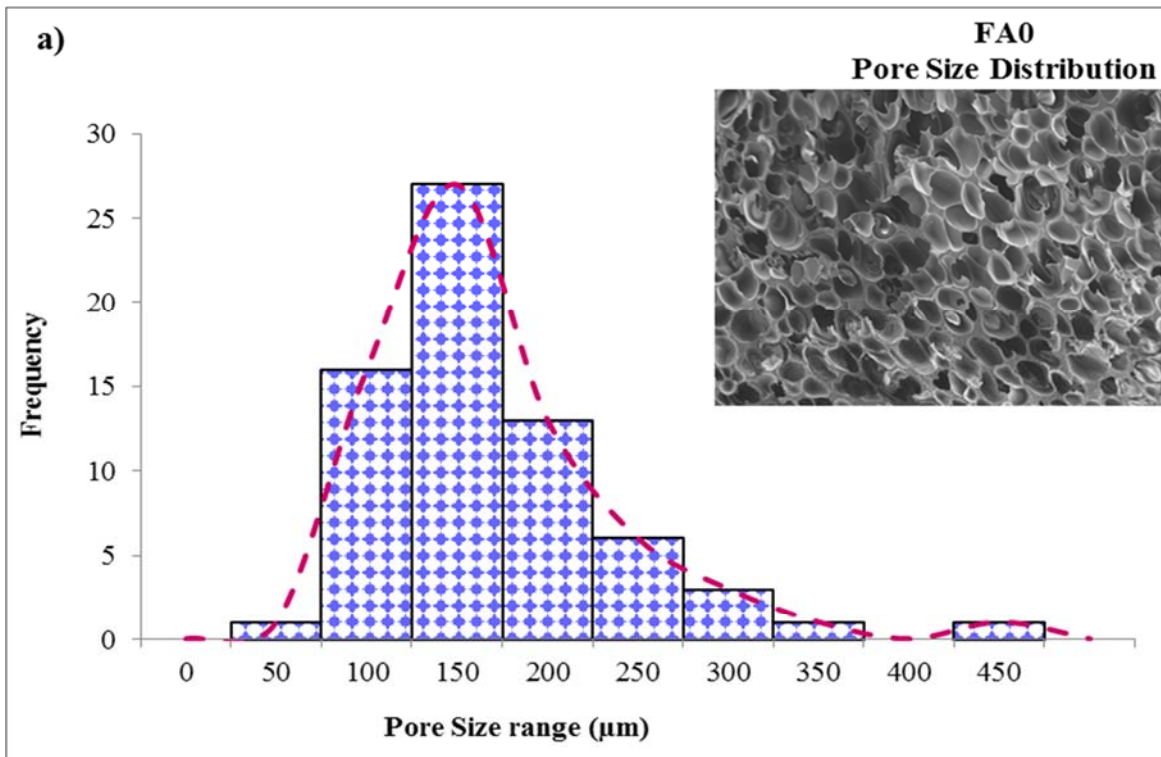
Figure 0-28- Pore size distribution of a) FA0 and b) FA-F40
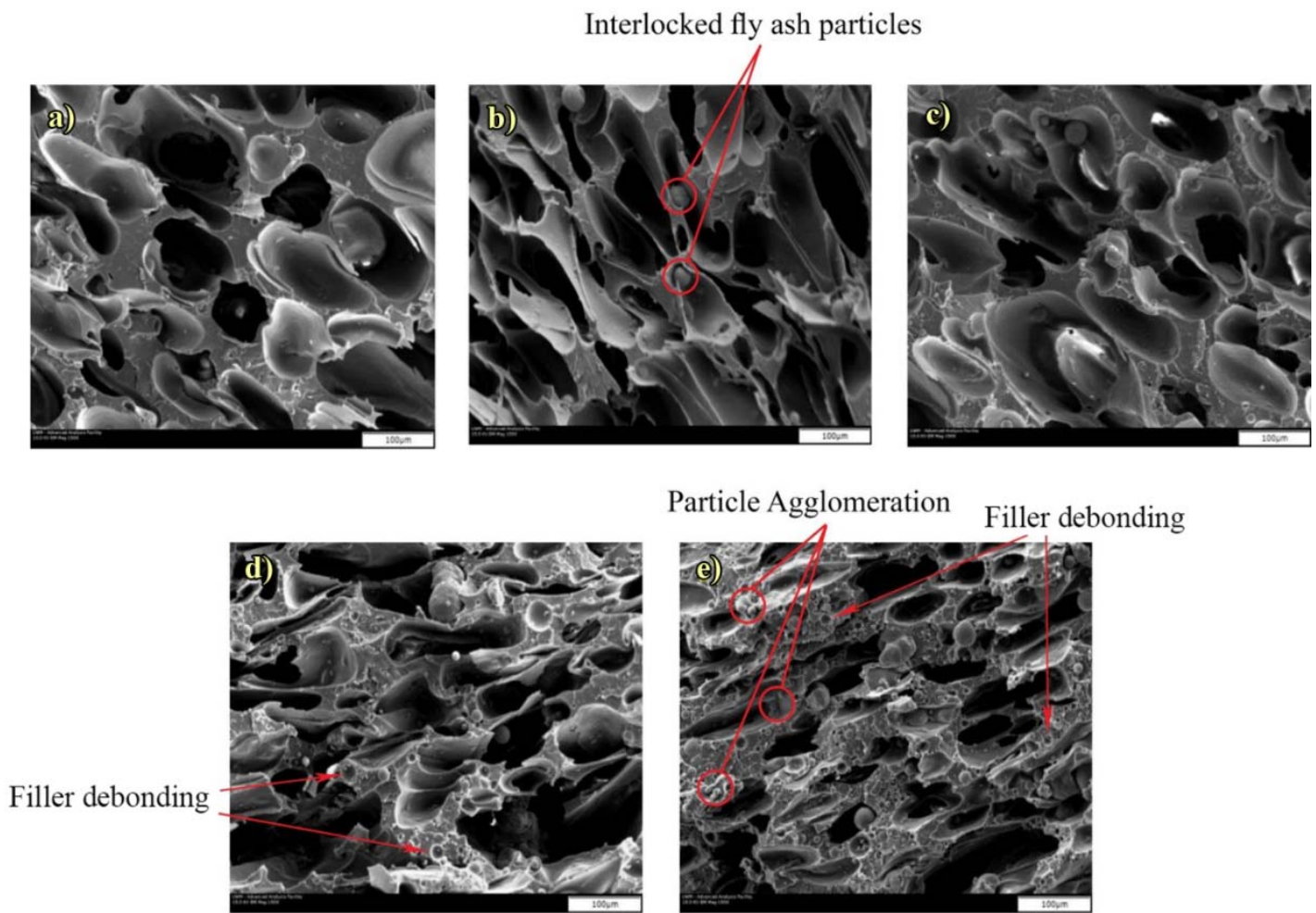
Figure 0-29- SEM micrograph of the PVC foam composites, a) FA-F6, b) FA-F9, c) FA-F12, d) FA-F25, and

e) FA-F40

5.3.   Evaluate Fly Ash Chemical Composition Effect on PVC Foam Composites Properties

5.3.1. Physical Properties

The measured density was obtained by weighing a fixed volume of the extruded foam material; whereas the theoretical density was calculated using the rule of mixtures for the un-foamed material (Equation 4-1). The values are listed in Table 5-10.

Table 0-10- Measured and theoretical density of extruded PVC-FA foam composites

Sample	Measured Density (g/cm³)	Theoretical Density (g/cm³)
FA0	0.39	1.39
FA-F6	0.44	1.43
FA-C6	0.43	1.45
FA-F-40	0.89	1.66
FA-C40	0.69	1.68

Results of measured density show that FA-C reinforced composites have lower density compared to the composites reinforced with FA-F, which is more noticeable at higher fly ash content. This can be attributed to the different elemental and chemical compositions of class C and F. Based XRD results of fly ash characterization, both FA-F and FA-C have almost the same amount of alumina. FA-C contains more than 25% calcium oxide, while more than 25% of FA-F is made of iron oxide. Comparison between specific gravity of each oxide determines that CaO is one of the lightest oxides, while iron oxides are the heaviest ones. Therefore, the higher CaO content, the lower density would be expected.

Weight percent of each oxide, their specific gravity and the calculated apparent specific gravity of each oxide are reported in Table 5-11. Comparison between total value of specific gravity of FA-

F and FA-C also confirms that FA-C is slightly lighter than FA-F, which is consistent with the measured density values reported in Table 5-1. Therefore, density of fly ash is chemical compositional dependent and the variants of densities in between different classes could be explained by their difference in chemical composition.

Table 0-11- Specific gravity of constituent oxides in fly ash, FA-F and FA-C

Oxide	Specific gravity	Amount of oxides, FA-F (wt%)	Amount of oxides, FA-C (wt%)	Apparent Specific Gravity of each oxide, FA-F	Apparent Specific Gravity of each oxide, FA-C
SiO_2	2.65	25.08	30.86	0.66	0.82
Al_2O_3	3.96	11.57	12.54	0.46	0.50
MgO	3.60	8.73	16.37	0.31	0.59
Fe_2O_3	5.30	24.95	9.51	1.32	0.50
FeO	5.20	3.82	0.00	0.20	0.00
CaO	2.71	11.84	25.97	0.32	0.70
Total Apparent Specific Gravity				3.28	3.11

5.3.2. Mechanical Properties

Effect of fly ash incorporation and its chemical composition on tensile properties of PVC foams is shown in Figure 5-30. The incorporation of fly ash, both FA-F and FA-C, improves the tensile strength and modulus of the composites, which is more significant in FA-C reinforced composites.

The increase in the modulus of composites can be caused by the resin substitution by the largely more rigid filler, which is more noticeable at higher filler content. In addition, the filler restricting the mobility and deformability of the matrix by introduction of a mechanical restraint [Leong et al. (2004)].

As mentioned before, polymer foam properties is highly dependent on their density. Whereas density of PVC foam composites loaded with two classes of fly ash are different (as listed in Table 5-10) and to be more accurate to eliminate density effect by normalizing the property. Density normalized tensile strength of the composites is presented in Figure 5-31. A comparison of the results show that in both low and high fly ash loaded composites, class-C contained composites has higher tensile strength than class-F ones which may be attributed to better filler-matrix interfacial interaction [Das and Satapathy (2011)]. Normalized tensile strength drops in the highly fly ash loaded composites, 40phr, compared to 6phr ones can be attributed to higher probability of particles agglomeration in the matrix at higher filler loading.

In the polymer composites generally mechanical properties depend on the filler's nature, size and distribution, aspect ratio, volume fraction, and the intrinsic adhesion between the surfaces of filler and polymer [Nath et al. (2009)]. Comparison between two different classes contained composites clarify that the degree of tensile properties improvement in the PVC/FA composites mainly depends on fly ash chemical composition which directly affects interfacial adhesion between matrix and filler.

Comparing the metal oxide content in each class of fly ash, C and F, as represented in Table 5-7, shows that both have almost the same amount of Al_2O_3, therefore this oxide cannot be much effective in terms of the composite mechanical properties. Whereas class-F has higher iron oxide content and much less oxides of magnesium and calcium compared to class-C. Besides, quartz content in FA-C is also 5% higher than FA-F. Therefore, the better mechanical properties in FA-C-contained composites might be due to higher SiO_2, CaO and MgO content in their fly ash.

As reported elsewhere, adding iron oxides into polymers is mainly purposed to improve polymer's ignition and burning resistance and reduce their flammability [Hashim et al. (2006)]. It

can also be used to improve paramagnetic property of polymers [Yan et al. (2014)]. In the case of PVC, it also effectively scavenge HCl gas formed during its burning [Inoue et al. (2004)]. MgO is also known as magnesia which is mainly used in numerous fields as catalysis, ceramics, and refractory as well as paint industry [Gandhi et al. (2011)]. It is reported elsewhere that MgO incorporation to polystyrene improves tensile strength and its amount also has a significant effect on tensile properties of the composites [Hachani et al. (2016)]. Calcium based compounds, mainly $CaCO_3$, were used previously as a cost-effective filler and nowadays it is more recognized as an impact modifier in PVC [Leong et al. (2004), Hassan et al. (2009), Zeng et al. (2008)]. A reduction in tensile strength was also reported in calcium carbonate incorporated polypropylene, which may be because of craze formation in deformed $CaCO_3$ loaded polymers before fracture [Leong et al. (2004)]. The literature also reported the beneficial effect of SiO_2 addition in terms of strengthening and toughnening of the polymer composite which were related to the high interfacial stress transfer efficiency [Nath et al. (2009); Mueller et al. (2003); Leong et al. (2004)]. Silica powders are widely used as fillers, catalysts, adsorbents, etc. Its surface is terminates either in siloxane group ($\equiv Si - O - Si \equiv$) with the oxygen on the surface or in one of several forms of silanol groups (($\equiv Si - OH$) [Mueller et al. (2003)].

Overall, comparison between chemical composition of FA-C and FA-F show that the improved property in the class-C contained composites might be due to higher amount of the oxides of silicon, magnesium and calcium their fly ash compared to FA-F.
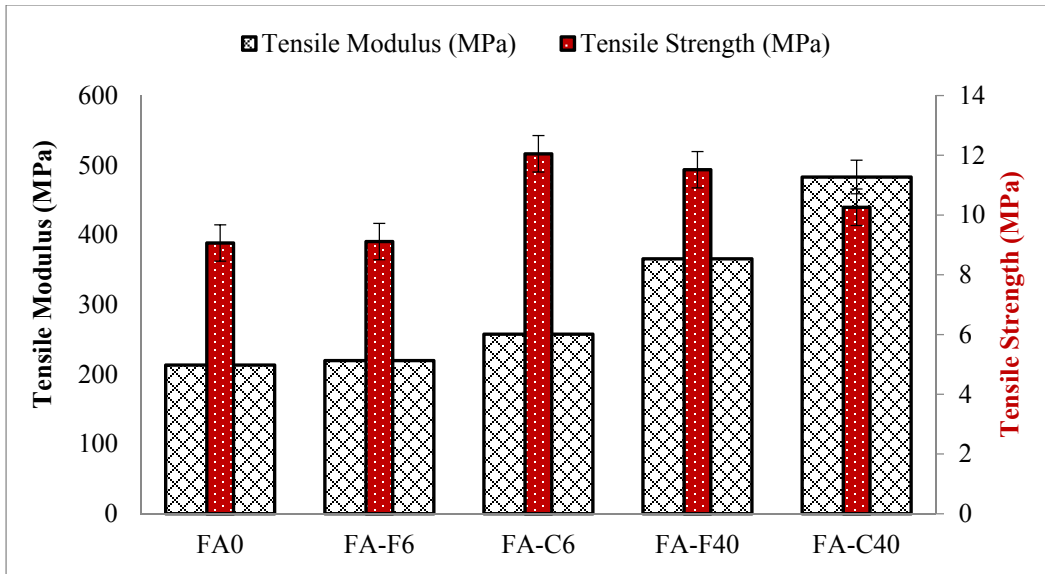
Figure 0-30- Tensile Strength and Modulus of PVC foam composites
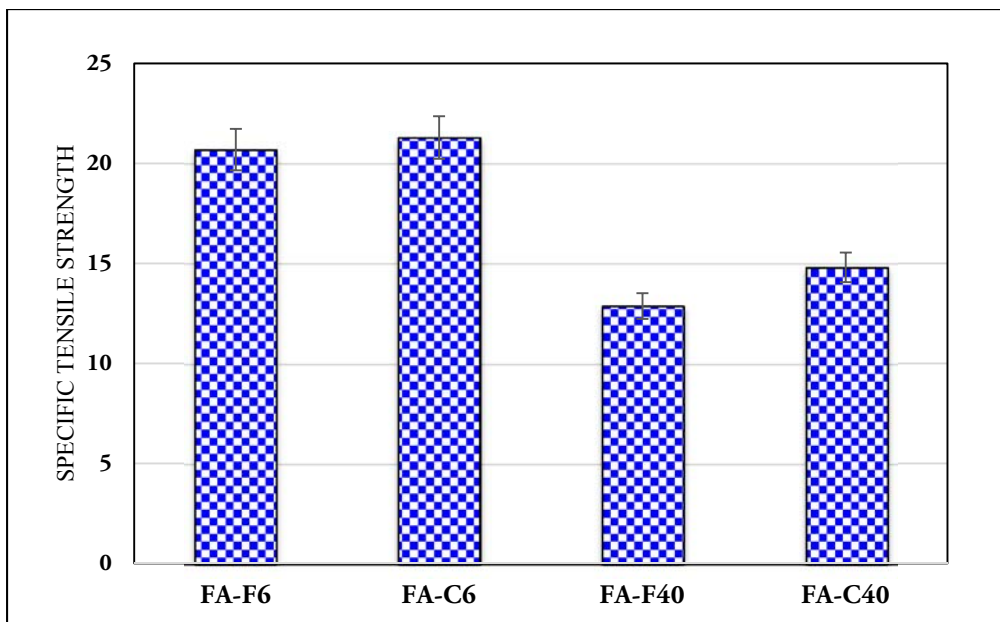
Figure 0-31- Specific Tensile Strength of PVC foam composites

As shown in Figure 5-32, elongation at UTS drops significantly by incorporation of fly ash, which indicates that the mode of failure in PVC foams changes from ductile behavior to brittle behavior [Leong et al. (2004)]. The elongation at UTS in both low (6phr) and high loading (40phr)

composites is lower in FA-C filled composites in comparison to class F composites; this may be due to increased rigidity imparted by the mineralogical phases in FA-C which may lower the polymer mobility as a result of strong interaction between FA-C filler and polymer matrix [Sreekanth and Bambole (2009)]. In other words, the weaker adhesion between fillers and matrix allows sufficient debonding of the filler from the matrix, which results in the occurrence of more plastic deformation before failure and therefore leads to the higher elongation values of the composite [Leong et al. (2004)].
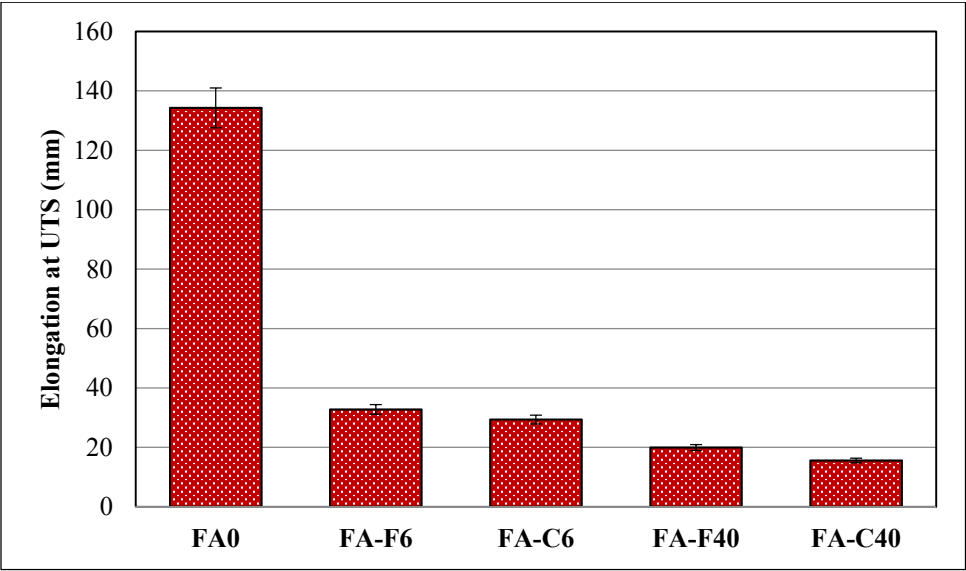
Figure 0-32- Elongation at UTS of PVC foam composites

Figures 5-33 a) and b) depict the effect of FA on the flexural modulus and strength of PVC/FA foam composites; respectively. The flexural modulus was found to improve upon adding FA into the PVC foam matrix and this improvement is slightly higher in FA-C6 than FA-F6. The increase in flexural modulus of FA filled composites is a result of the inherent rigidity of the FA filler, which is more significant in highly loaded composites. Highly loaded composites FA-F40 and FA-C40 have almost the same flexural modulus.

The addition of 6phr of FA-F to the PVC foam matrix resulted in almost no change in flexural strength, while incorporating the same amount of FA-C led to a 95% increase in the flexural strength. It can also be observed that FA-C40 yields a 46% higher flexural strength than FA-F40.

This behavior confirms that FA-C can interact better with PVC matrix than class F. It is also worth noting that FA-C6 shows higher flexural strength than FA-C40, which may be attributed to poor filler dispersion, higher stress concentration, and higher defect and agglomeration probability in highly loaded composites [Labella et al. (2014)]. At the same FA loading, either 6 or 40phr, class C filled samples exhibit higher flexural strength due to higher calcium content in class-C, which improves the reactivity and interfacial interaction between FA with the polymer matrix. Density normalized flexural strength of the composites is also presented in Figure 5-34 which shows the same trend as shown in Figure 5-33a.
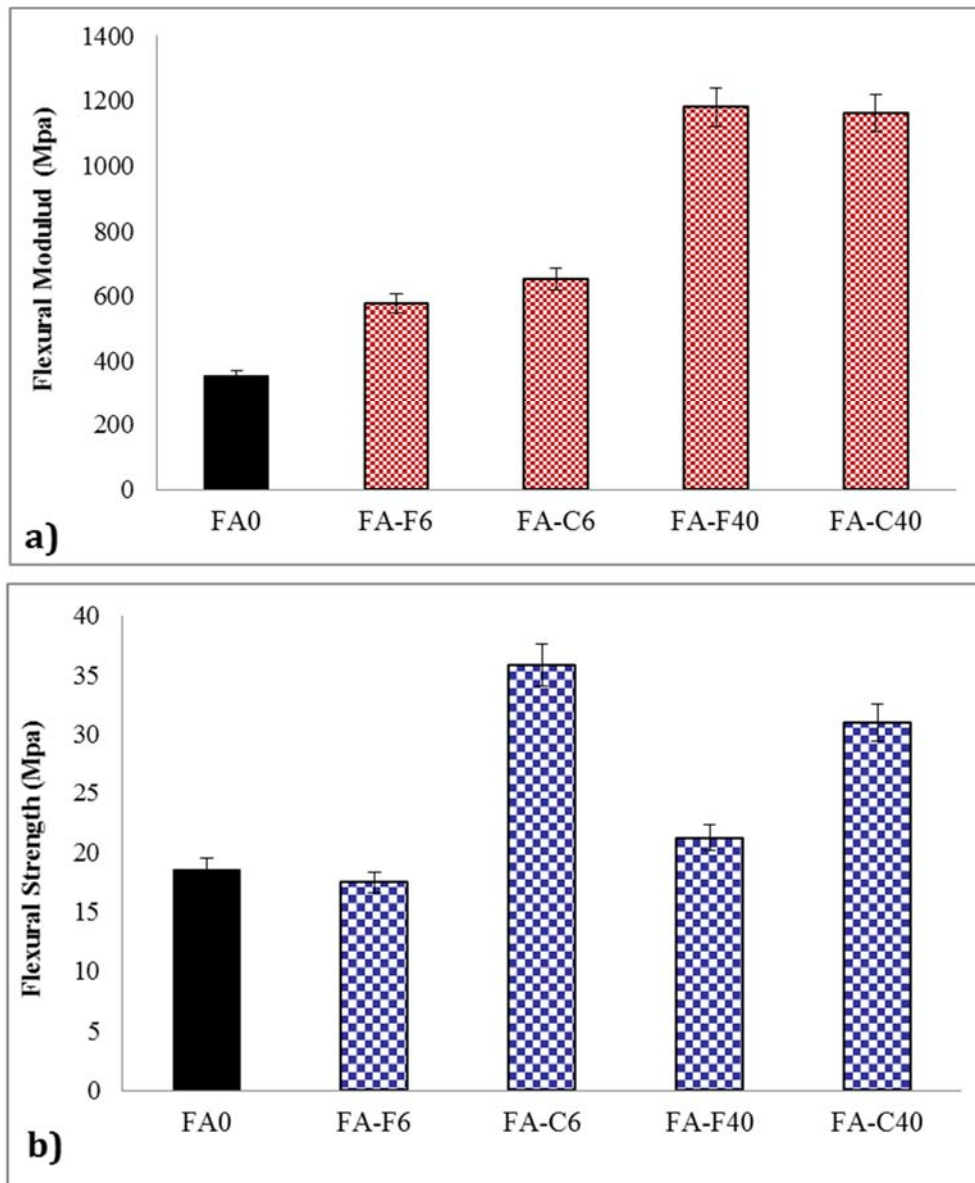
Figure 0-33- a) Flexural Modulus and b) Flexural Strength of PVC foam composites

123
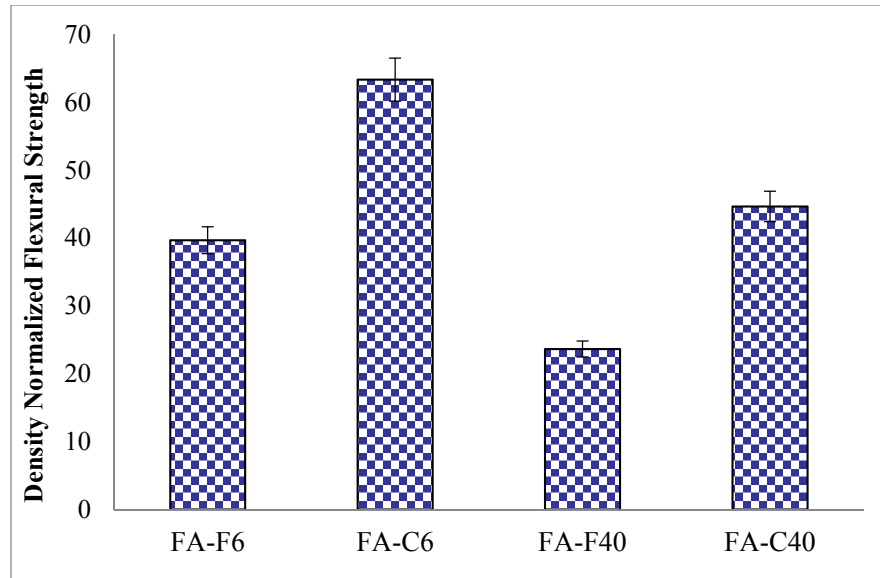
Figure 0-34- Density Normalized Flexural Strength of PVC foam composites

The effect of the type of FA on the impact strength of the composites is shown in Figure 5-35. The impact strength and impact energy decrease by incorporating FA in PVC matrix. The samples containing 6phr of FA-C show higher impact strength compared to other samples, which represent more efficient load transfer. Moreover, this observation is consistent with the flexural strength and the elongation at UTS results indicating an increase in rigidity of the composites upon reinforcing them with either type of FA. As it is also shown in Figure 5-36, class-C fly ash addition improves impact strength of the composites more than class-F, which is more noticeable is higher loaded sample and this indicates that the achieved mechanical properties in fly ash reinforced polymer composites highly depend on fly ash composition.

It is reported elsewhere that calcium-based filler, especially calcium carbonate is an effective impact modifier and toughener for PVC [Hassan et al. (2009), Zeng et al. (2008)]. $CaCO_3$ is known to promote craze formation in deformed polymers before fracture [Leong et al. (2004)], which allows

higher energy damping and therefore better impact strength. The higher impact strength in FA-C contained composites can be due to its higher calcium oxide content compared with FA-F. The reason of impact strength drop at the highly loaded composites, FA-C40 and FA-F40, may be due to higher probability of particles agglomeration and therefore poor filler dispersion, which result in an increase in stress concentration sites [Zeng et al. (2008)].
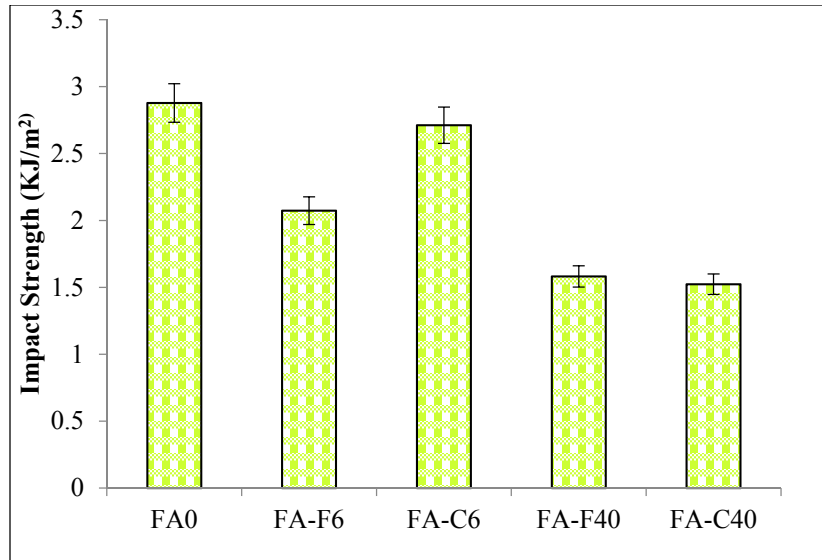
Figure 0-35- Impact strength of PVC foam composites
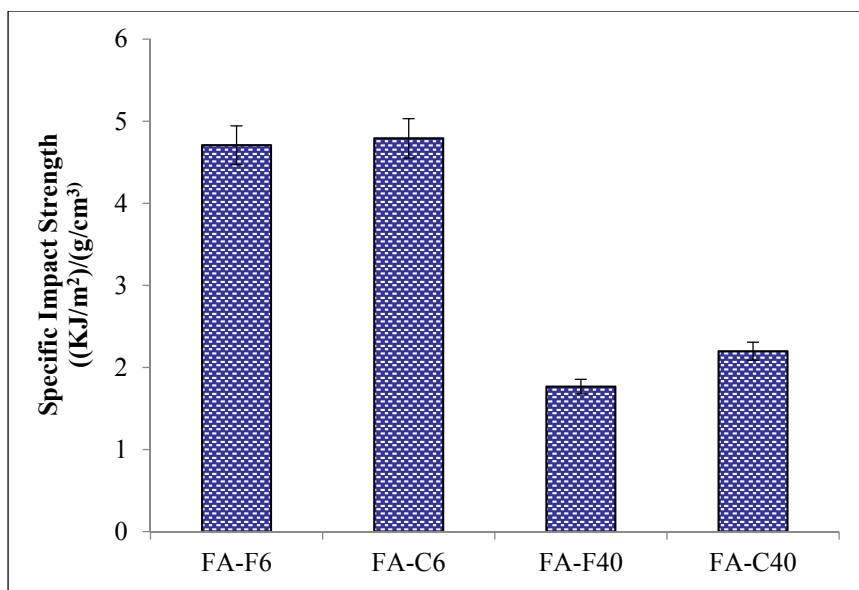
Figure 0-36- Density Normalized Impact Strength of PVC foam composites

5.3.3. Thermal Properties

To study the effect of fly ash chemical composition on the thermal degradation behavior of PVC/Fly ash composites, two different types of fly ash, namely FA-C and FA-F, with different chemical compositions, were added separately to the PVC compound at low (6 phr) and high (40 phr) loadings. The TGA thermograms of the PVC/Fly ash composites are shown in Figure 5-37. The samples without any fly ash; i.e. FA0, shows PDT and SDT at 277℃ and 429℃; respectively. PDT is found to decrease slightly with the addition of either class C or class F fly ash due to the accelerating effect of metal oxides on the dehydrochlorination process. However, the PDT drop in the FA-F loaded composites is more significant than those filled with FA-C. Studies on the role of various metal oxides in the thermal degradation of PVC show that some of the metal oxides; e.g. CaO and Fe_2O_3, can retard dehydrochlorination, while other oxides, e.g. Al_2O_3, can promote the dehydrochlorination process [Gupta and Viswanath (1998)].

126

Studies on the dehydrochlorination rates of PVC compounds filled separately with CaO and Fe_2O_3 showed that the degradation rate values in the PVC/Fe_2O_3 composites is about twice as high as PVC/CaO composites. This behavior was attributed to the amount of chlorine free radicals reacting with iron, which is twice as much as those reacting with calcium [Inoue et al. (2004)]. The reaction is shown below:

$$-(CH_2CHCl)- + CaO \rightarrow -(CH=CH)- + CaOHCl$$

$$4-(CH_2CHCl)- + Fe_2O_3 \rightarrow 3-(CH=CH)- + -(CHClCHCl)-$$
$$+ FeCl_2 \cdot 2H_2O + FeO$$
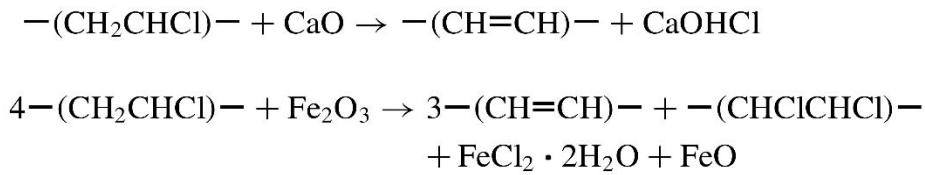
Therefore, the higher content of iron oxide in class F fly ash, in comparison with class C, can result in a higher dehydrochlorination rates in the composites, and hence a lower PDT.

SDT is found to improve significantly with both types of fly ash filled composites, i.e. it takes more energy to break the hydrocarbon backbone in the presence of fly ash particles. The maximum SDT increase is approximately 16ºC in FA-C6 compared to FA0, which indicates good interfacial interaction between the filler and the PVC matrix. Since the chemical composition of class-C fly ash is different than that of class-F fly ash, i.e. lower calcium and iron oxides, it is expected to yield a better thermal stability of the polymer backbone in the composites reinforced with class C. Therefore, class-C fly ash composites exhibit higher SDT than class-F composites at the same loading levels.

The residual weight of the composites determined by TGA analysis is the undecomposed inorganic fillers and ash [Singh and Benipal (2015)]. Residual weight at 800ºC was found to be

9.31% in FA0 which does not contain any FA. The residual weight in both FA-F6 and FA-C6 samples was around 19% and around 40% in both FA-F40 and FA-C40 samples.
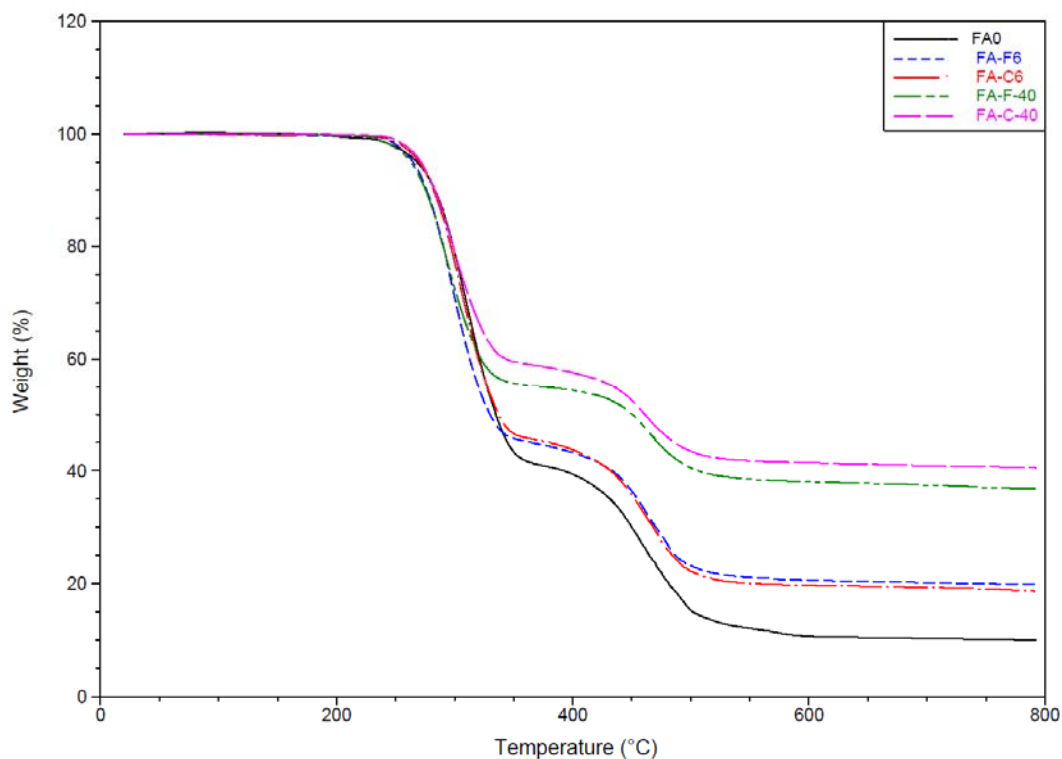
Figure 0-37- TGA curves of PVC/FA foam composites

Table 0-12: Thermogravimetric Analysis of foam composites

Sample	PDT[a] (℃)	SDT[b] (℃)	%Residual weight at 800℃
FA0	277.02	428.76	9.31
FA-F6	270.02	444.73	19.48
FA-C6	275.05	446.68	18.76
FA-F40	265.23	438.25	37.13
FA-C40	271.21	438.18	40.72

[a] PDT- Primary Decomposition Temperature; [b] SDT-Secondary Decomposition Temperature

DSC results including glass transition temperature (T_g) and degree of gelation of the composites are reported in Table 5-7. The results suggest that incorporating FA as filler does not impact the Tg of the PVC foam composites significantly. This behavior is similar to the results observed in PVC/cumbaru filler and PVC/Carbon fiber composite systems reported by Iulianell and Rathy; respectively [Iulianell et al. (2013); Rathy et al. (2012)].

The addition of FA causes a decrease in the degree of gelation. Considering the composites with 6phr FA, it can be seen that class C filled samples show higher degree of gelation, which shows better fusion of particles with the matrix. This result can be also seen in samples with 40phr FA-C composites. This observation may be the result of better interfacial interaction between FA-C and PVC matrix at lower loading which can accelerate the gelled network formation.

Table 0-13: Tg values and percentage of gelation obtained from DSC of PVC foam composites

Sample	Tg	%Gelation
FA0	82.60	85.63
FA-F6	83.40	80.54
FA-C6	83.22	88.27
FA-F40	83.55	62.94
FA-C40	82.60	79.50

5.3.4. Viscoelastic properties

Comparison between viscoelastic properties of composites as shown in Figure 5-38 represents that the magnitude of elastic modulus, E′, seems to increase significantly with the incorporation of FA filler. This increase indicates an improvement of the stiffness with further loading of FA, which is in accordance with the expectations of the common behavior of rigid spherical particle filled composites [Gamage et al. (2013)]. The increase seems to be more remarkable in class C filled

composites compared to the ones containing FA-F. The storage modulus of FA-C6 at 50ºC is approximately 475MPa which is 6% higher than FA-F6 and 58% higher than FA0. Whereas, storage modulus of 40phr FA loaded samples are about the same. At higher temperatures, such as 70ºC, FA-C40 shows higher storage modulus. This may be due to the fact that it is well below the glass transition temperature of the PVC foam composites and the storage modulus is a measure of the stored energy of the material rendering it more elastic. This behavior is in line to the higher tensile modulus values of FA-C composites.

The peak intensity of loss modulus (E") is found to decrease with the addition of 6phr FA, irrespective of the type of fly ash (FA-F or FA-C) used in the PVC foam. However, in highly loaded composites; i.e., FA-F40 and FA-C40, the loss modulus was found to improve. This phenomenon may be attributed to the enhancement in the energy dissipation ability as a result of the presence of spherical filler in the composites and also the increase in the polymer-filler and filler-filler slippage at T_g [Qiao et al. (2011)].
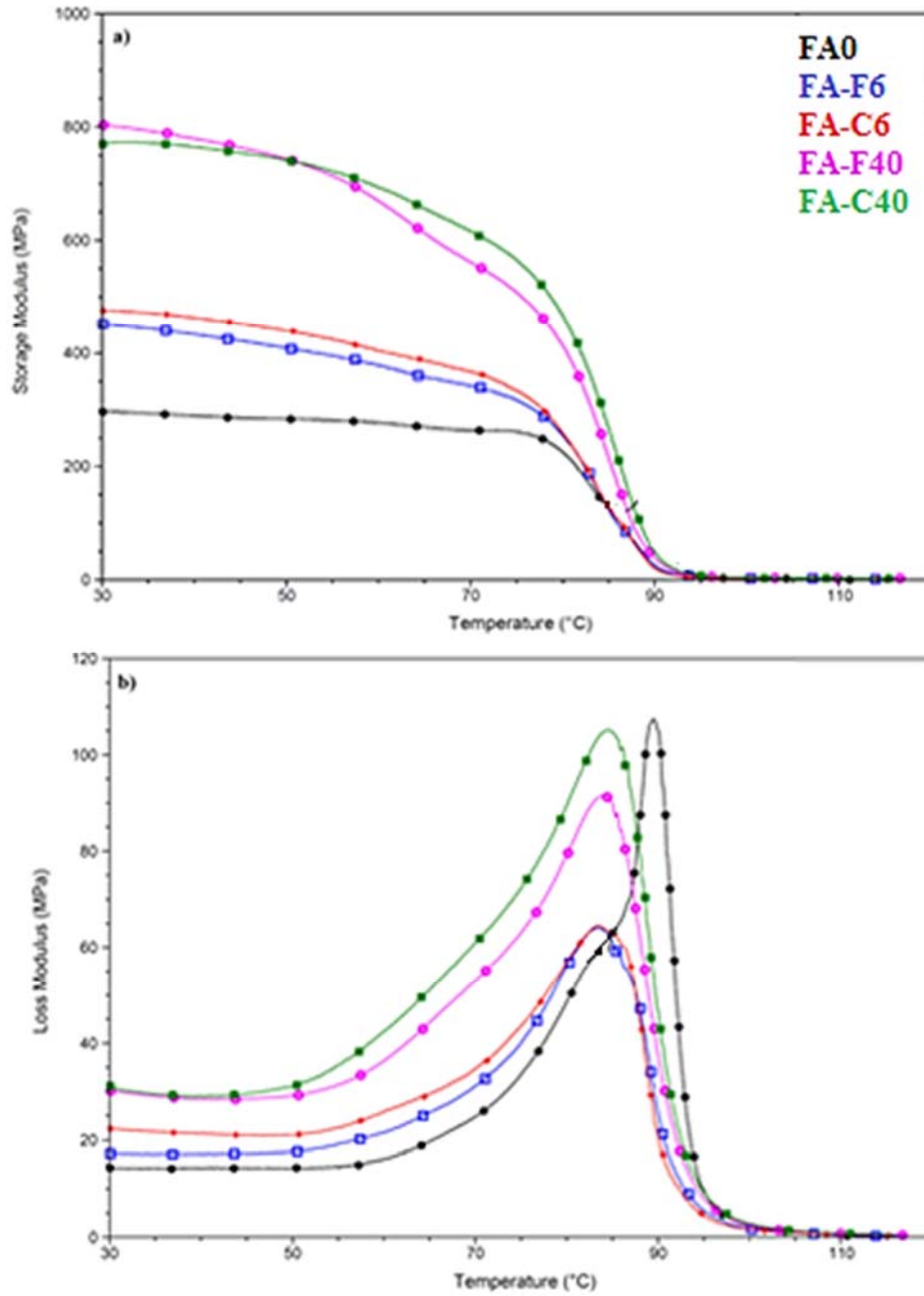
Figure 0-38: Dynamic mechanical behavior of PVC foam composites (a) storage modulus (E) and

(b) loss modulus (E″)

131

5.3.5. Structural and Interfacial Analysis

Recalled results of XRD ran on FA-F and FA-C are shown in Figure 5-39. As presented, FA-C has about 5wt% higher SiO_2 content and about two time higher CaO and MgO content compared to FA-F, while both have almost the same Al_2O_3. However, FA-F contains more than three time higher iron oxides than FA-C. According to mechanical, thermal and dynamic mechanical properties, FA-C provides better performance. As both FA-F and FA-C have almost the same surface area, the main reason of better resulted properties in FA-C could be due to its chemical composition.
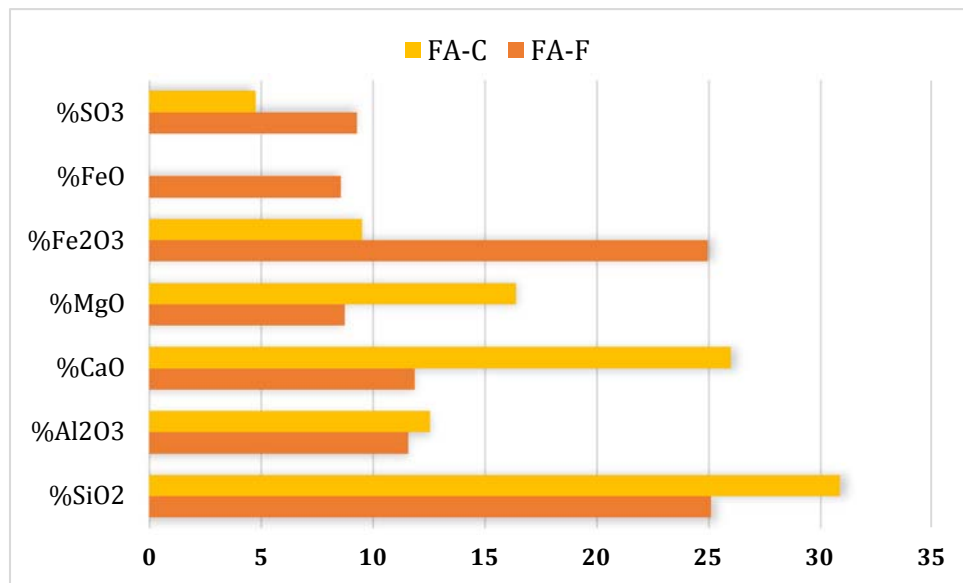
Figure 0-39- Weight percent of oxides in FA-F and FA-C

As mentioned elsewhere and shown in Figure 5-40, the main difference in between various fly ash characteristics at the far extremes of the classification relates to CaO content [Sutter (2004)]. XRD results presented in Figure 40 are consistent with ternary phase diagram shown in Figure 5-40.

132

SiO$_2$

SILICA FUME

CLASS F

CLASS C

FLY ASH

BLAST
FURNACE SLAG

PORTLAND
CEMENT

HIGH ALUMINA
CEMENT

CaO

Al$_2$O$_3$
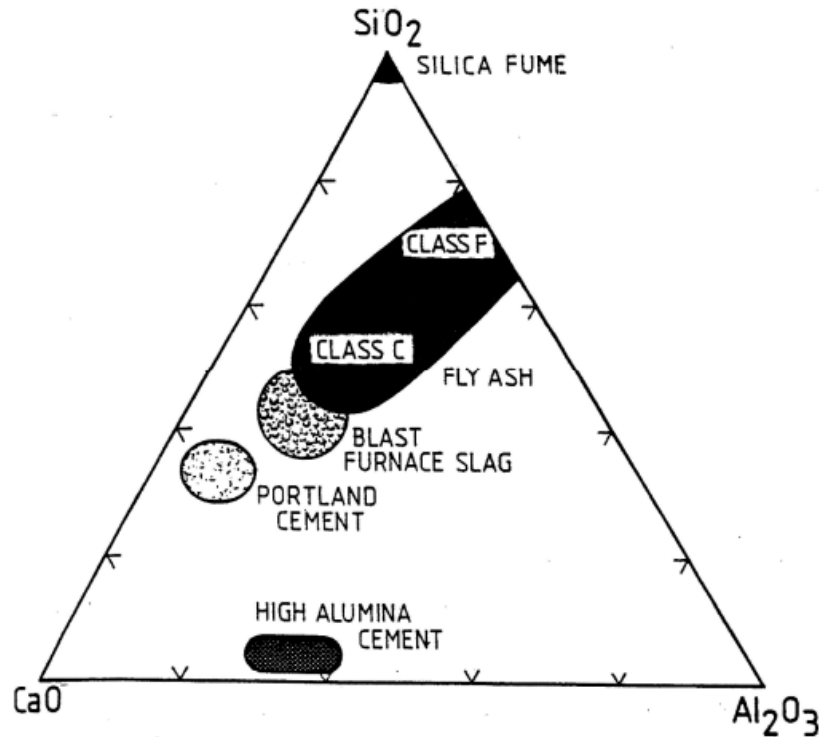
Figure 0-40- Ternary Phase Diagram in Fly Ash [Sutter (2004)]

Figure 5-41 shows the FTIR spectra of pure PVC and 40phr fly ash-reinforced composites. The characteristic IR bands of FA0 are classified into three regions which are respectively the range of 600-700 cm^{-1}, 900-1250 cm^{-1} and 1250-3000 cm^{-1}. These three regions are respectively assigned to (C-Cl) stretching, (C-C) stretching and C-H stretch bonds.

Peaks set in the range of 2800-3000 cm^{-1} correspond to C-H stretch bonds. The peak at higher wave number is the asymmetric stretch bond of C-H and the lower peak is the symmetric stretch bond of C-H. The CH$_2$ wagging, deformation and rocking were observed at around 1400, 1330 and 963cm^{-1}, respectively. The peak at 1250 cm^{-1} is attributed to the bending bond of C-H near Cl. The C-C stretch bond of the PVC backbone chain occurs in a range of 1000-1100 cm^{-1}. Finally, peaks

in the range of 600-650 cm^{-1} correspond to C-Cl gauche bonds [Bishoyee et al. (2010); Usta (2012); Patil et al. (2016)].

A comparison between the FTIR spectra of the fly ash reinforced composites with the pure samples, as a reference, shows that the C-H stretching and CH_2 bending peaks in the pure samples with wave numbers of approximately 2800-3000 cm^{-1} and 1400 cm^{-1}; respectively, are maximum and the peak intensity decreases by adding reinforcements.

Another difference is the slight shift of C-Cl peak from 607 cm^{-1} in FA0 to higher wavenumbers, 608 cm^{-1} and 610 cm^{-1} in in FA-F40 and FA-C40, respectively. This observation can be attributed to the dipolar interaction between C-Cl group of PVC and –OH group on the surface of metal oxides in fly ash [Chakrabarti et al. (2004)]. The higher shift in FA-C40 compared to FA-F40 can be also attributed to better interfacial interaction and physical bonding between class-C fly ash and PVC matrix.

The presence of hydroxyl (–OH) functional groups on the surface of metals and metal oxides plays a significant role in the formation of physical bonding and therefore interfacial interactions in between filler and polymer matrix [Nath et al. (2009); Leong et al. (2004); Mueller et al (2003)].
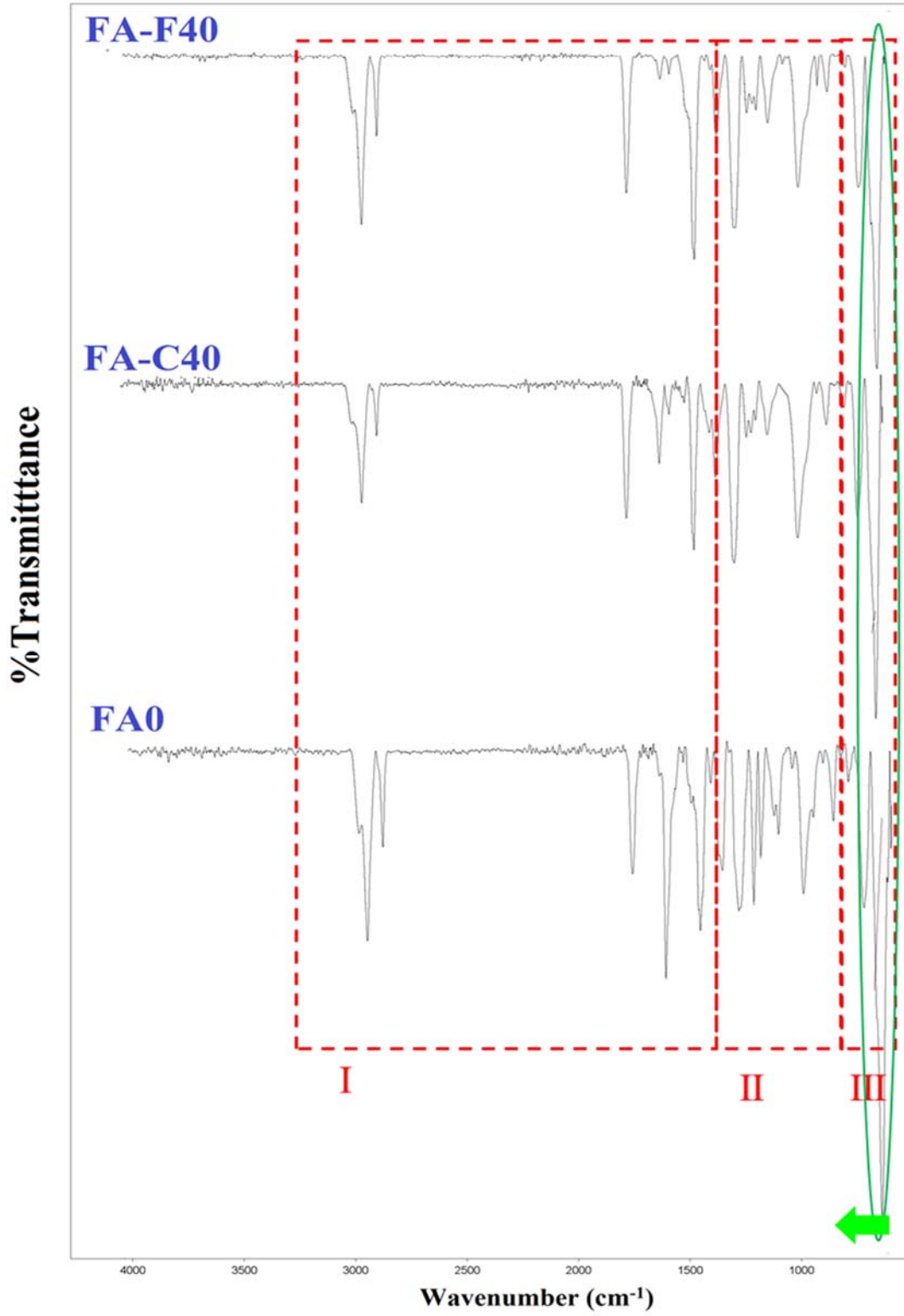
Figure 0-41- FTIR spectra of FA0, FA-C40 and FA-F40

XPS analysis was performed on the both classes of fly ash and their spectra are shown in Figure 5-42. As indicated, the major elements on FA-C and FA-F are silicon (Si), aluminum (Al), calcium (Ca), iron (Fe), oxygen (O) and carbon (C). XPS results are consistent with EDS and XRD results confirming the higher amount of Si and Ca elements and therefore their oxides in FA-C compared to FA-F. Si content in FA-F and FA-C were measured specifically and their results are shown in Figure 5-43 representing that FA-C has about 4wt% higher silicon content than FA-F.

As mentioned earlier, it is suspected the main reason of interfacial interaction between fly ash and PVC matrix and the formed physical bonds be due hydroxyl (-OH) groups on the fly ash surface [Nath et al. (2009)]. The presence of –OH groups on the surface of silica powder has been identified elsewhere [Nath et al. (2009); Leong et al. (2004); Mueller et al (2003)].

Thus XPS method was used to examine the presence of –OH functional groups in the range of binding energy 92-112 eV and results are presented in Figure 5-44. The binding energy of 2p Si is a clear evidence for the presence of Si-OH bonding states as also reported elsewhere.

The binding energy of SiO_2 is 103.4 eV, which in our results it is measured at 105.4 eV due to carbon peak position. SiO_2 peak shows a shoulder at binding energy of 103.4 eV which is attributed to the combined peaks of –OH and –O– attached to quartz (SiO_2) and mullite. The –OH group on the surface of fly ash is considered as the main in the formation of interfacial interactions polymer matrix [Nath et al. (2009)].
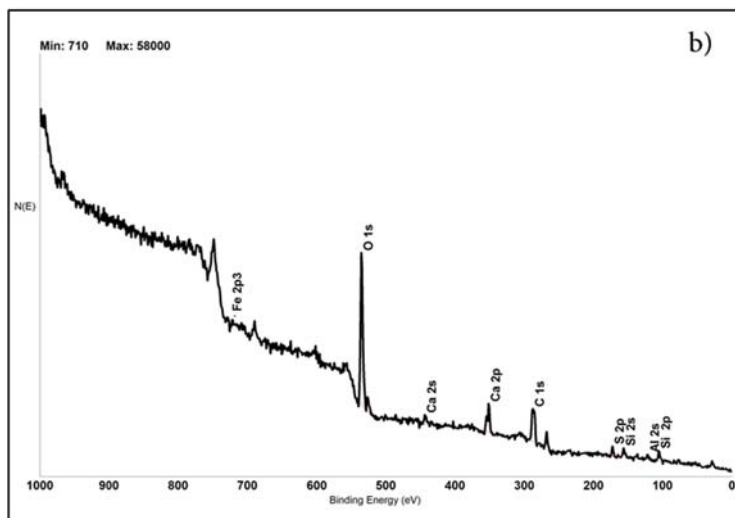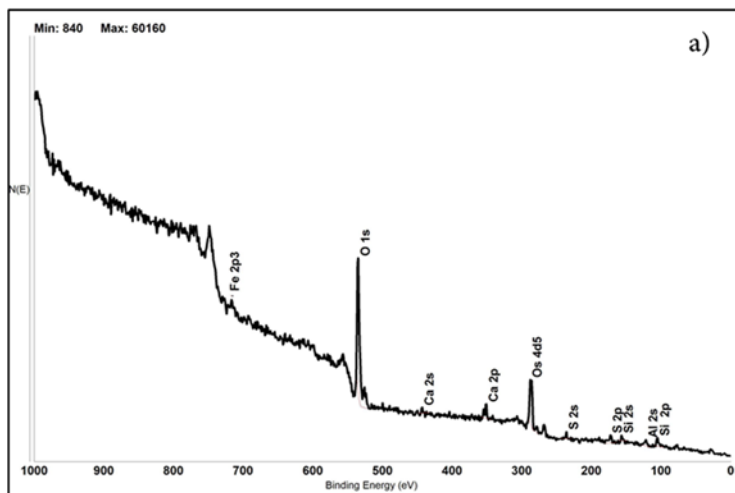
Figure 0-42- XRS spectra of a) FA-F and b) FA-C
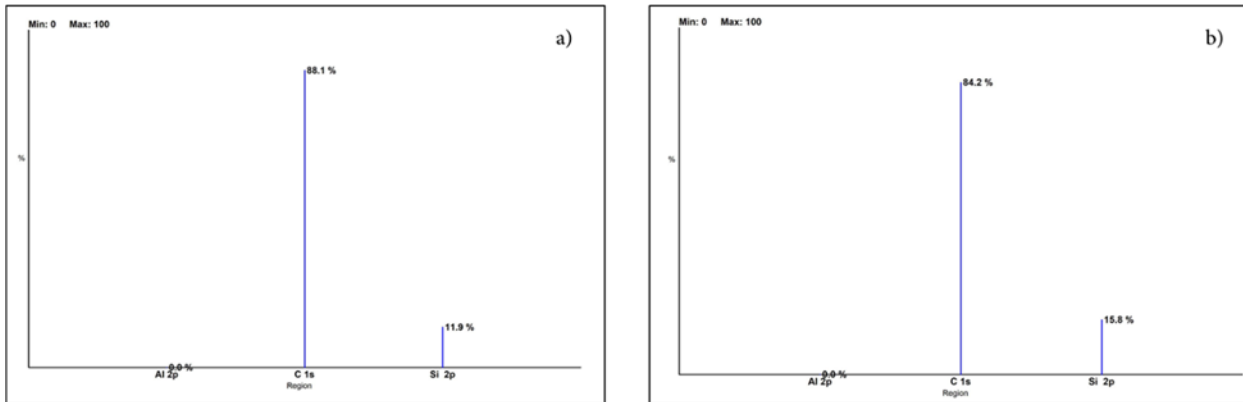
Figure 0-43- Si content in a) FA-F and b) FA-C measured by XPS
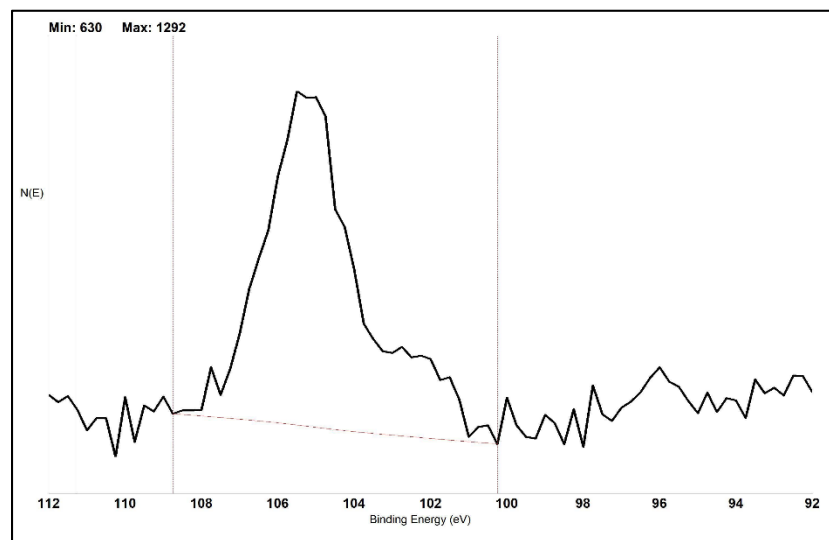
Figure 0-44- XPS spectra of fly ash showing a combined peak of hydroxides and oxides of silicon

5.3.6. Quantitative evaluation of Interfacial Interaction

Interfacial interaction between the reinforcement phase and the polymer matrix plays a significant role in polymer composites in terms of filler dispersion and agglomeration within the polymer matrix and also the stress transfer along the interface. Consequently, it affects the physical characteristics and the macroscopic properties of the composites [Pedrazzoli et al. (2015)].

Although the measurement of interfacial adhesion is an important task in the development of composites, the absolute quantification of interfacial interaction is complicated [Nath et al. (2009)]. Mechanical properties can be correlated with the interfacial interaction parameters in the composites. Pukanszky presented a model which relates interfacial adhesion and tensile properties as shown in Equation 5-4.

$$\frac{\sigma_{y,c}}{\sigma_{y,m}} = \frac{1-\varphi_f}{1+2.5\varphi_f} \exp(B\varphi_f)$$ **Equation 0-4**

where φ_f, $\sigma_{y,c}$ and $\sigma_{y,m}$ are the volume fraction of the filler, and tensile strength of the composite and polymer matrix; respectively. The parameter B is an interaction parameter that is related to the macroscopic characteristics of the filler-matrix interface and interphase. $\frac{1-\varphi_f}{1+2.5\varphi_f}$ is related to the decrease in effective load bearing cross-section, whereas the exponential term represents all other effects resulting in an increase of the tensile strength and interfacial interaction. High value of B indicate a higher tensile strength, while low values implies a weaker strength. B can be calculated by Equation 5-5 as the following:

$$B = (1 + A_f \rho_f t) \ln(\frac{\sigma_{y,i}}{\sigma_{y,m}})$$ **Equation 0-5**

where t is the thickness of the interphase, $\sigma_{y,i}$ is the strength of interaction, A_f and ρ_f are density and surface area of the filler [Nath et al. (2009); Pedrazzoli et al. (2016); Metın et al. (2004); Leong et al. (2003); Rostami et al. (2012); Firoozian et al. (2010)]. The calculated B parameter for all composites is presented in Table 5-14. As shown the evaluated B parameter also confirms the better interfacial interaction in class-C reinforced composite compared to class-F.

Table 0-14- Interfacial parameter values (B) in the composites calculated using Pukanszky model

Sample	Tensile Strength (MPa)	Volume Fraction φ_f	Interfacial Parameter (B)
FA0	9.06	-	-
FA-F6	9.11	0.01	3.59
FA-C6	12.05	0.01	10.38

5.3.7. Microstructural and Morphological Properties

Microstructure analysis was conducted on PVC foam composites to evaluate the interfacial interaction between FA particles and foam matrix, and also to determine the state of dispersion and distribution of FA particles in the composites.

Line-scan SEM/EDS of the fracture surfaces for PVC foam reinforced with 40phr class F or class-C fly ash are shown in Figure 5-45. In both samples a line was drawn starting from fly ash surface to the matrix with the purpose of identifying elemental concentration at the interface of the composites. SEM was used to study the fracture surfaces to identify the strength interface between the filler and matrix. In other words, as SEM images belongs to the fracture surfaces, it indicates that the remained particles within polymer matrix have a good interaction with the polymer, while the observed debonding areas belong to the particles that had a poor adhesion and consequently particle detachment occurred in those areas.

Line-scan on the interface of both FA-F and FA-C show that Si, as the main element of quartz crystal phase, has the highest concentration at the interface of the composites. High concentration of Si in the interface is consistent with the previously presented results of interfacial study showing that

–OH groups on SiO_2 surface can effectively improve interfacial adhesion and that is the main reason of good adhesion of fly ash with the matrix.

In addition, as shown the calcium concentration in the interface of FA-C40 is the second highest concentration representing that it is also an effective element in terms of interfacial interaction improvement and therefore the better observed mechanical properties in class-C contained composites can relate to its calcium content; the higher the calcium content is the better mechanical properties would be.

As seen in Figures 5-46a-e, the amount of visible FA particles was high in the composites containing higher amounts (40phr) of FA in comparison to the ones containing lower amounts (6phr) of FA. A good distribution can be seen in the composites at lower loadings [Nath et al. (2009); Das and Satapathy (2011)]. However, in FA-F40 and FA-C40, particle agglomeration can be seen in some parts of the SEM image (Figures 5-46b and 20d).

The presence of tightly embedded and mechanically interlocked FA particles within the PVC matrix in all composites indicates strong interaction between filler and matrix and also good dispersion of filler particles. In composites FA-F40 and FA-C40, filler debonding areas on the fractured surface can be noticed. This may be due to high filler loading and detachment of FA surfaces from the PVC matrix.
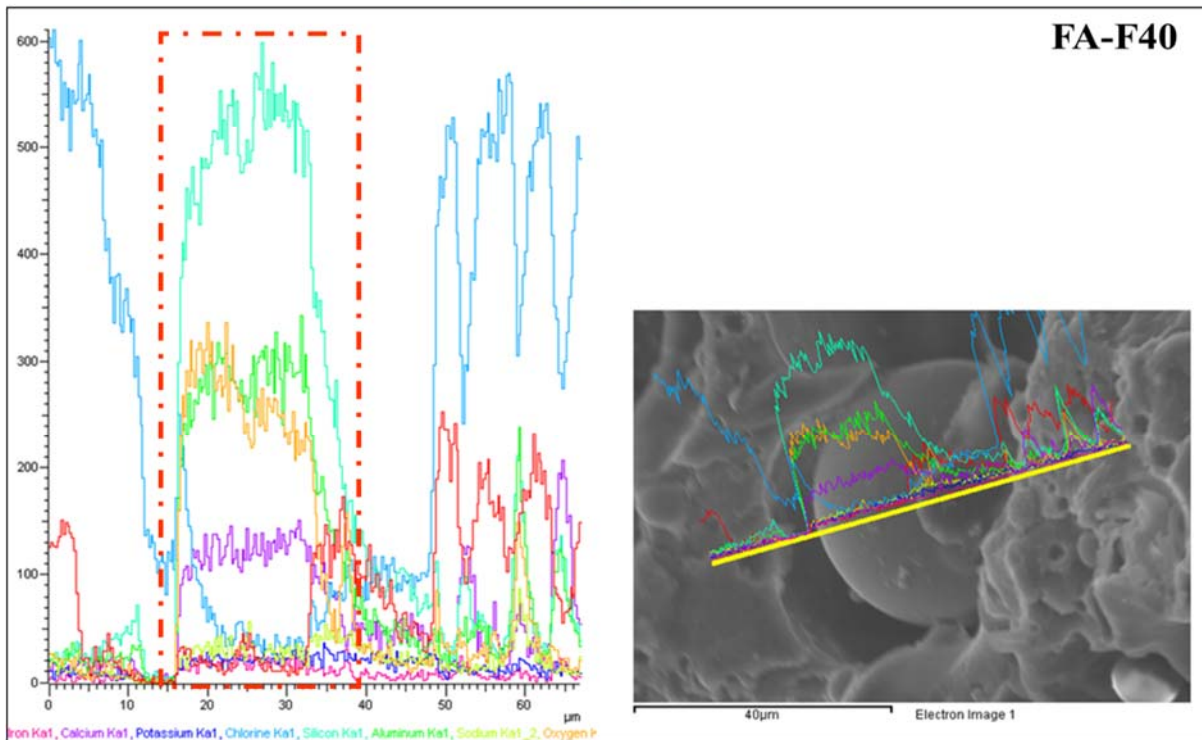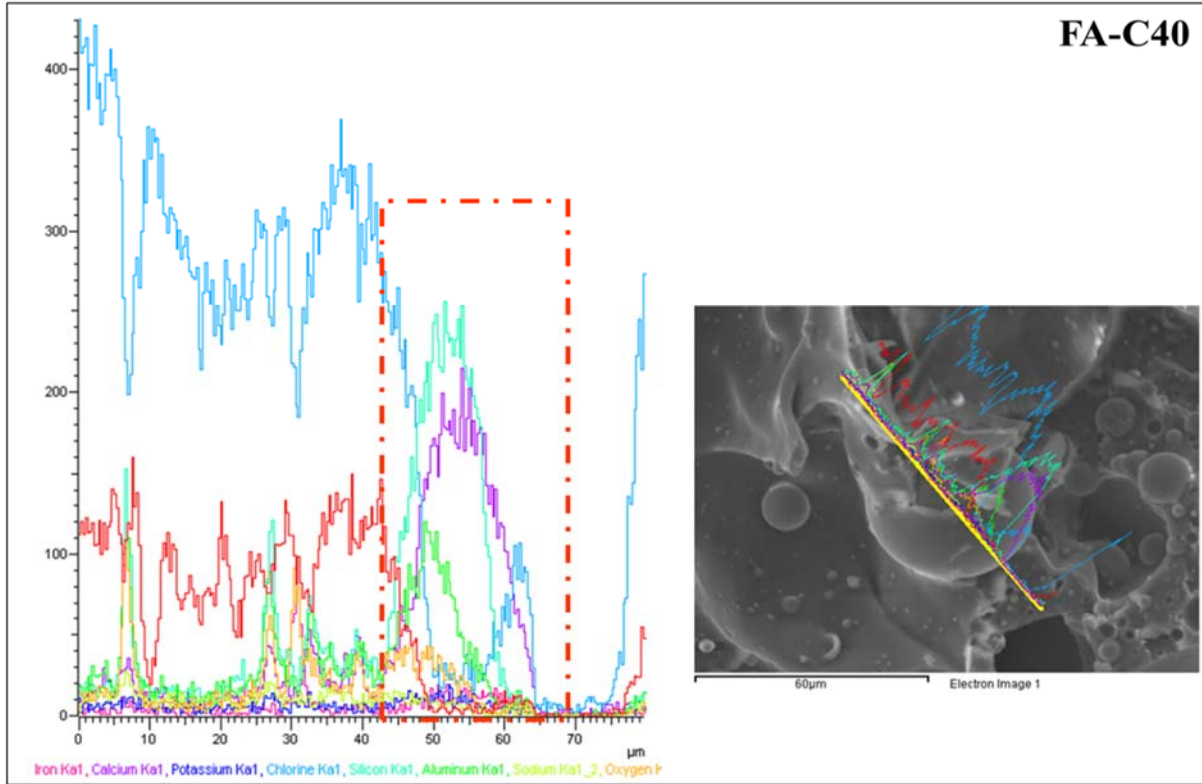
Figure 0-45-SEM-line scan of the fracture surface of FA-C40 (top) and FA-F40 (bottom).

142
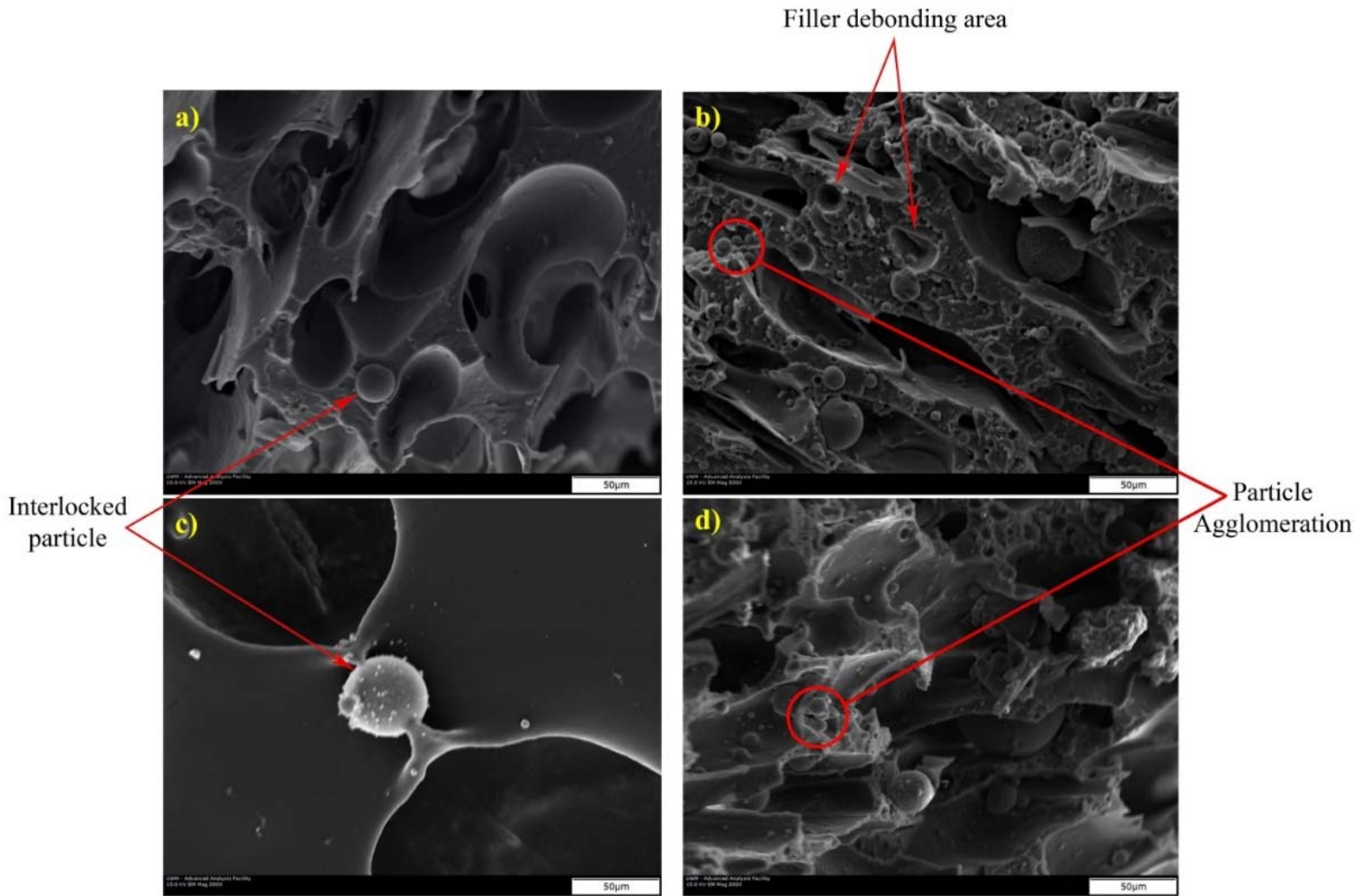
Figure 0-46: SEM micrograph of the PVC foam composites, a) FA-F6, b) FA-C6, c) FA-F40, and

d) FA-C40

5.4. Evaluate Fly Ash Particle Size Effect on its Chemical Composition and Rigid PVC Composites Performance

5.4.1 Mechanical Properties

The effect of fly ash particle size on the tensile properties of rigid PVC composites is shown in Figure 5-47. 10wt% fly ash incorporation into rigid PVC matrix improves the young's modulus by more than 30%. Comparison between the Young's modulus of 25-FA-F10 and 50-FA-F10 reveals that the composite filled with the larger particles is slightly stiffer than that of filled with the smaller. It could be due to the higher hardness in 50μm particle size fly ash which is measured and confirmed by nanoindentator. The nanoindentation results will be discussed later.

It is also noticeable that both composites prepared with 25μm and 50μfly ash (25-FA-F10 and 50-FA-F10, respectively) exhibit higher modulus than the one loaded with a wide particle size distribution fly ash, FA-F10. This can be attributed to the particle size uniformity and therefore their better dispersion and homogeneity within the polymer matrix.

Tensile strength is significantly influenced by the fly ash particle size. 25-FA-F10 has the highest tensile strength among all composites. An improved tensile strength in FA-F10 and 25-FA-F10, compared to the pure sample (r-PVC), confirms the existence of a sufficient load transfer from the polymer matrix into the fly ash particles as a result of good interfacial bonding between them [[Cho et al. (2006); Sharma and Mahanwar (2010), Bose and Mahanwar (2004)]. Since the surface area is higher in the smaller particles, there will be better filler-polymer interfacial adhesion and load transfer; and hence better mechanical properties are expected, as shown in Figure 5-47.

Although the XRD characterization of fly ash particles, presented in Table 5-7, show that 50μm sized fly ash contains much more SiO_2 than the 25μm particles, the enhanced properties in 25-FA-

F50 can be attributed to its higher surface area and better fly ash dispersion. The density of hydroxyl functional groups on SiO_2 surface is found to be size and surface area dependent; the higher surface area of the particles, the more hydroxyl group density on the surface [Mueller et al. (2003)]. In addition, 25-FA-F has higher CaO content compared with 50μm particles which is found to be very effective in mechanical properties improvement and toughening of the polymer composites [Adeosun et al. (2013); Usman et al. (2012); Zuiderduin and Gaymans (2005); Lazzeri et al. (2005)]].

It can also be observed that the elongation at break decreases with the addition of fly ash. The decrease in the percentage of elongation for 25-FA-F10 with smaller particles is less than what is observed with the larger particles of 50-FA-F10. This can be attributed to a better fly ash polymer interaction and therefore more uniform and homogenized mictrostructure in the case of 25-FA-F10 than 50-FA-F10. Similarly, the lower elongation in 50-FA-F10 can be attributed to the poor wetting of the polymer on the fly ash surface due to the fly ash large particle size [Deshmukh et al. (2010)], which can result in a higher chance of filler detachment from the polymer matrix.
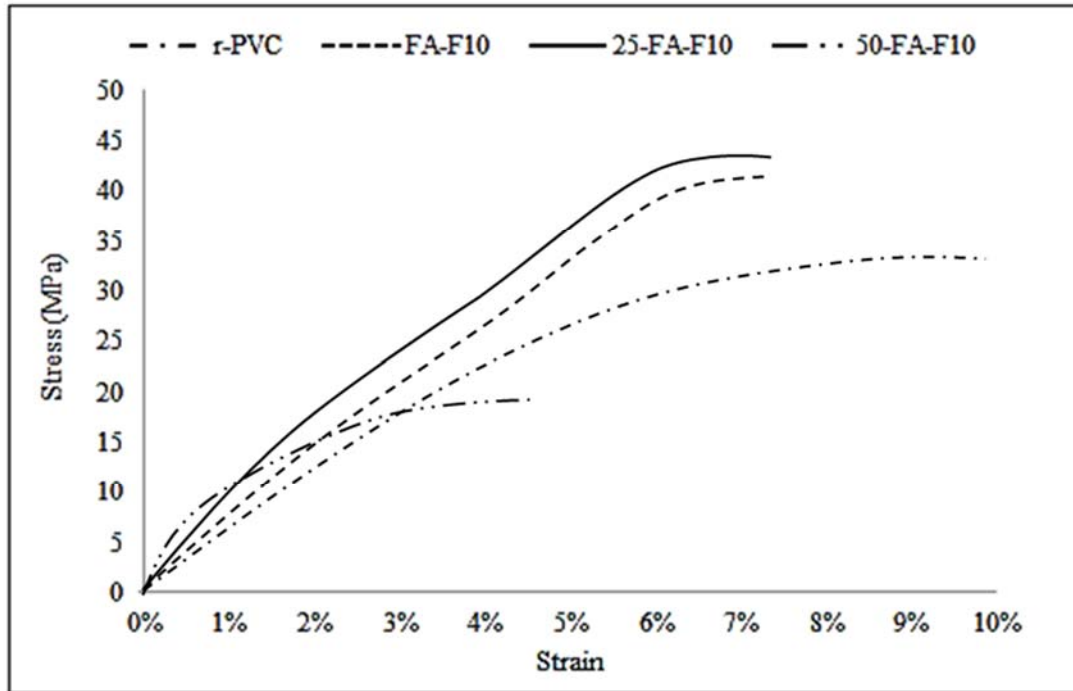
Figure 0-47- Stress versus strain graphs of fly ash reinforced composites

5.4.2. Structural Analysis

According to fly ash particles XRD analysis as presented in Figure 5-48, chemical composition is highly particle size dependent; the larger particles (50micron) contains more SiO_2 and iron oxides, while the smaller particles (25micron) consists of higher amount of calcium oxide.

The -OH surface density of SiO$_2$, an effective oxide in enhancing the interfacial interaction, is highly dependent on the particle size [Mueller et al. (2003)]. Since XRD is insensitive to the surface area; therefore, by considering the effect of surface area in each fly ash, 25-FA-F with the highest surface area is expected to have the highest SiO$_2$ content, and the highest –OH groups on its surface. Although the density of –OH groups should be measured accurately, it has a direct relationship with the surface area.
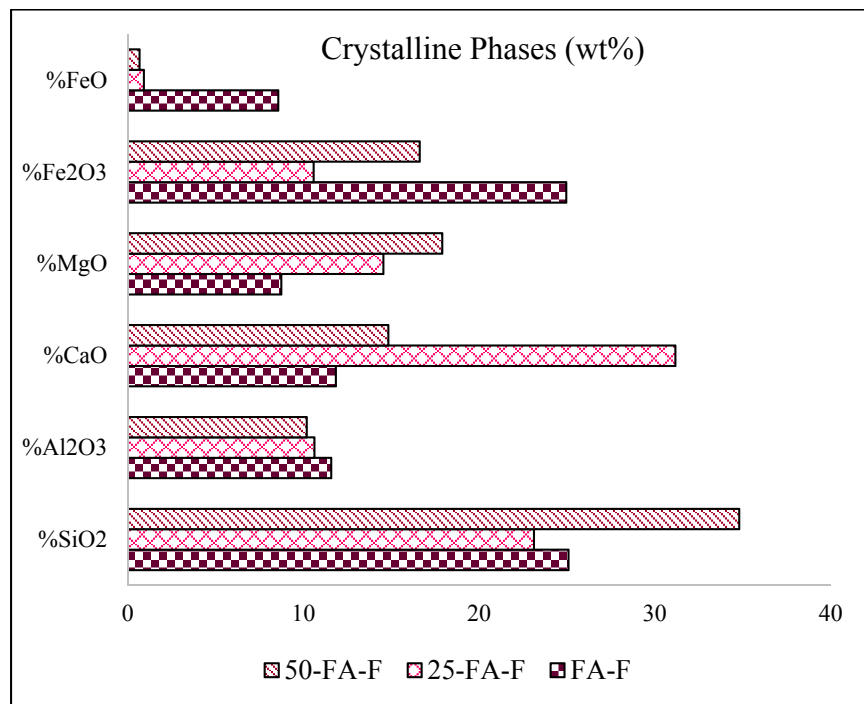
Figure 0-48- Crystalline phase content in FA-F, 25-FA-F and 50-FA-F analyzed by XRD

In addition, a comparison between the chemical composition of different particle sized fly ash shows that the smaller sized particles, 25-FA-F, contain more calcium oxide than the larger ones, 50-FA-F. Calcium carbonate (CaCO$_3$) and calcium oxide (CaO) have almost the similar effects on polymer composite properties as CaCO$_3$ is basically can be formed by a reaction between CaO and CO$_2$ [Qin and Ye (2015)]. It is also well known that the incorporation of calcium carbonate and/or

calcium oxide as a filler has dual purposes of reducing material cost as well as improving its strength, rigidity, durability and hardness [Adeosun et al. (2013); Usman et al. (2012)]. It is also being used as an impact modifier to polymers [Zuiderduin and Gaymans (2005); Lazzeri et al. (2005)]. Therefore, the higher the CaO content in fly ash, the better are the expected mechanical properties.

Weight percent of silicon in 25-FA-F and 50-FA-F are respectively 10wt% and 14wt% that are measured by XPS. This result also confirms the size dependency of chemical composition in fly ash. In addition, typical XPS spectrum of fly ash[5] is shown in Figure 5-49, where the presence of the peak shoulder is a clear evidence of –OH functional groups presence with the binding energy of 103.4eV [Nath et al. (2009)]. Although the -OH group presence can be confirmed by XPS, its surface density regarding particle size difference cannot be measured. FTIR and TGA is suggested as an accurate method to determine it [Muller et al. (2003)].
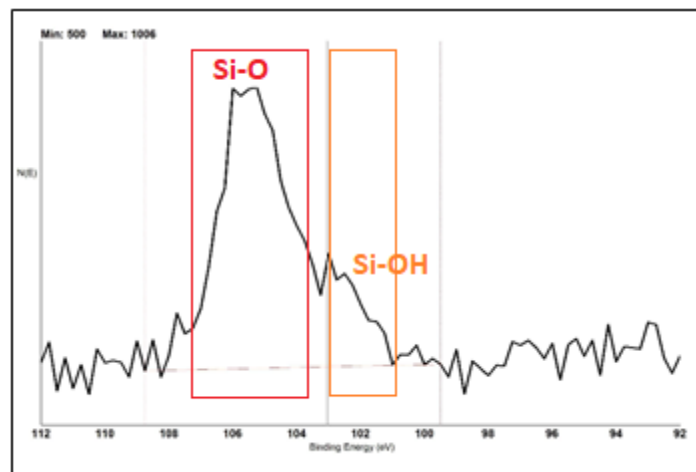
Figure 0-49- Typical XPS spectra of fly ash showing a combined peak of hydroxides and oxides of silicon

---

[5] XPS was ran on both 25-FA-F and 50-FA-F and as their spectrums were quite similar showing the presence of Si-OH group, only one of them is presented in this paper.

FTIR spectrums of r-PVC, 25-FA-F10 and 50-FA-F10 are shown in Figure 5-50. The characteristic IR bands of r-PVC are classified into three regions which are in the range of 600-700 cm^{-1}, 900-1250 cm^{-1} and 1250-3000 cm^{-1}; respectively. These three regions are respectively assigned to (C-Cl) stretching, (C-C) stretching and C-H stretch bonds.

Peaks set in the range of 2800-3000 cm^{-1} correspond to C-H stretch bonds. The peak at higher wave number is the asymmetric stretch bond of C-H and the lower peak is the symmetric stretch bond of C-H. The CH_2 wagging, deformation and rocking were observed at around 1400, 1330 and 963 cm^{-1}; respectively. The peak at 1250 cm^{-1} is attributed to the bending bond of C-H near Cl. The C-C stretch bond of the PVC backbone chain occurs in the range of 1000-1100 cm^{-1}. Finally, peaks in the range of 600-650cm^{-1} correspond to C-Cl gauche bonds [Bishoyee et al. (2010); Usta (2012); Patil et al. (2016)].

A comparison between the FTIR spectra of the fly ash reinforced composites with the pure PVC resin, as a reference, shows that C-Cl peak shifts from 607 cm^{-1} in r-PVC to the higher wavenumbers, 608cm^{-1} and 610cm^{-1} in 50-FA-F10 and 25-FA-F10; respectively. This observation can be attributed to the dipolar interaction between C-Cl group of PVC and –OH group on the surface of metal oxides in fly ash [Chakrabarti et al. (2004)]. As was discussed earlier, –OH group on the surface of SiO_2 plays a significant role in the formation of physical bonding and interfacial interaction between fly ash and the polymer matrix; thus the higher shift of C-Cl peak in 25-FA-F10 can be attributed to the higher density of –OH groups on the 25μm sized fly ash which results in a better physical bonding with the PVC matrix and a higher enhancement in mechanical properties. Higher –OH density in 25μm sized fly ash was also confirmed by FTIR analysis, as shown in Figure 5-51. The presence of a broad peak at wavenumbers around 3400 cm^{-1} indicates the presence of silanol group [Thongsang

and Sombatsompop (2006)], which is found in 25-FA-F. The higher the intensity of this peak indicates a higher density of –OH group on the surface.
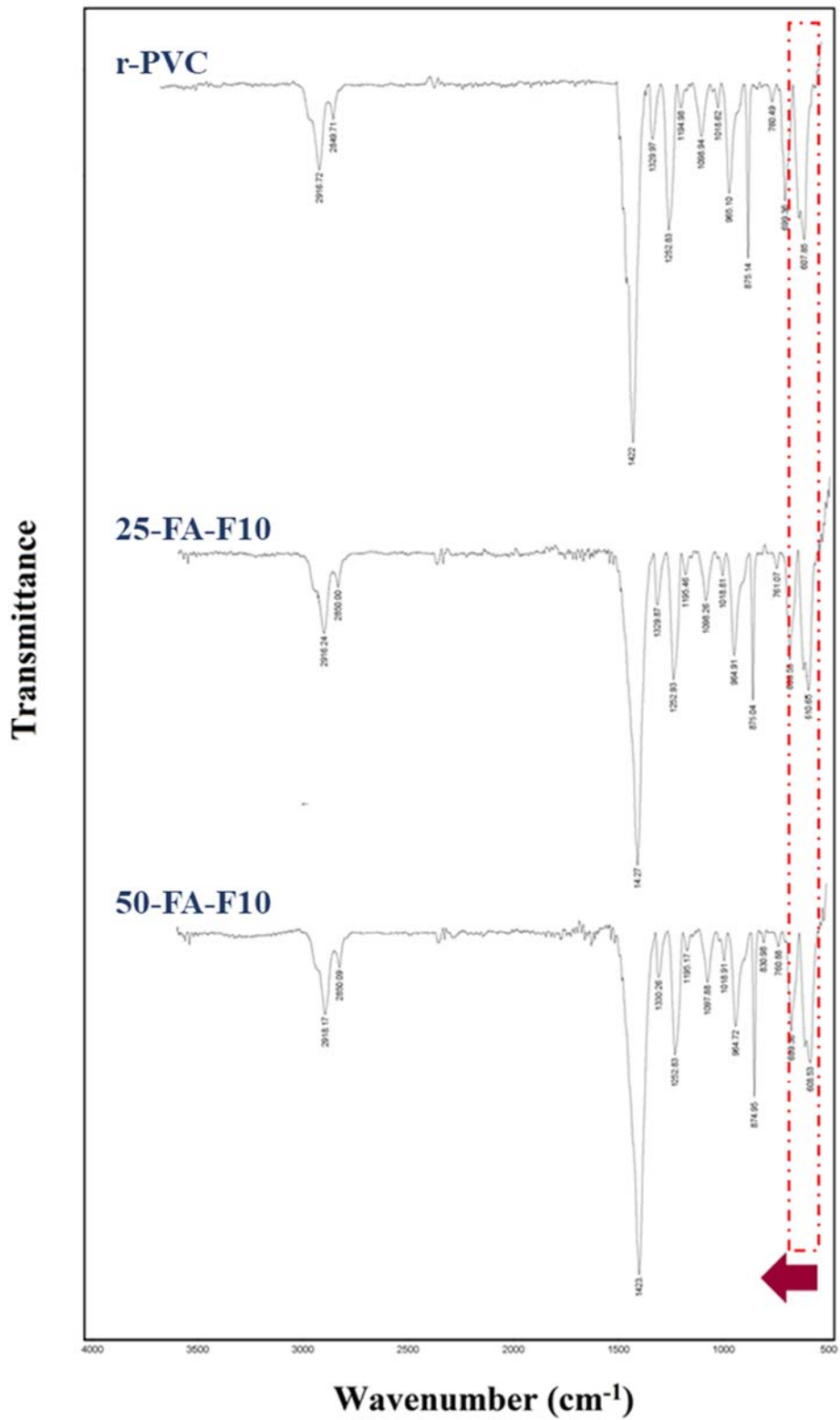
Figure 0-50- FTIR spectrum of r-PVC, 25-FA-F10, and 50-FA-F10
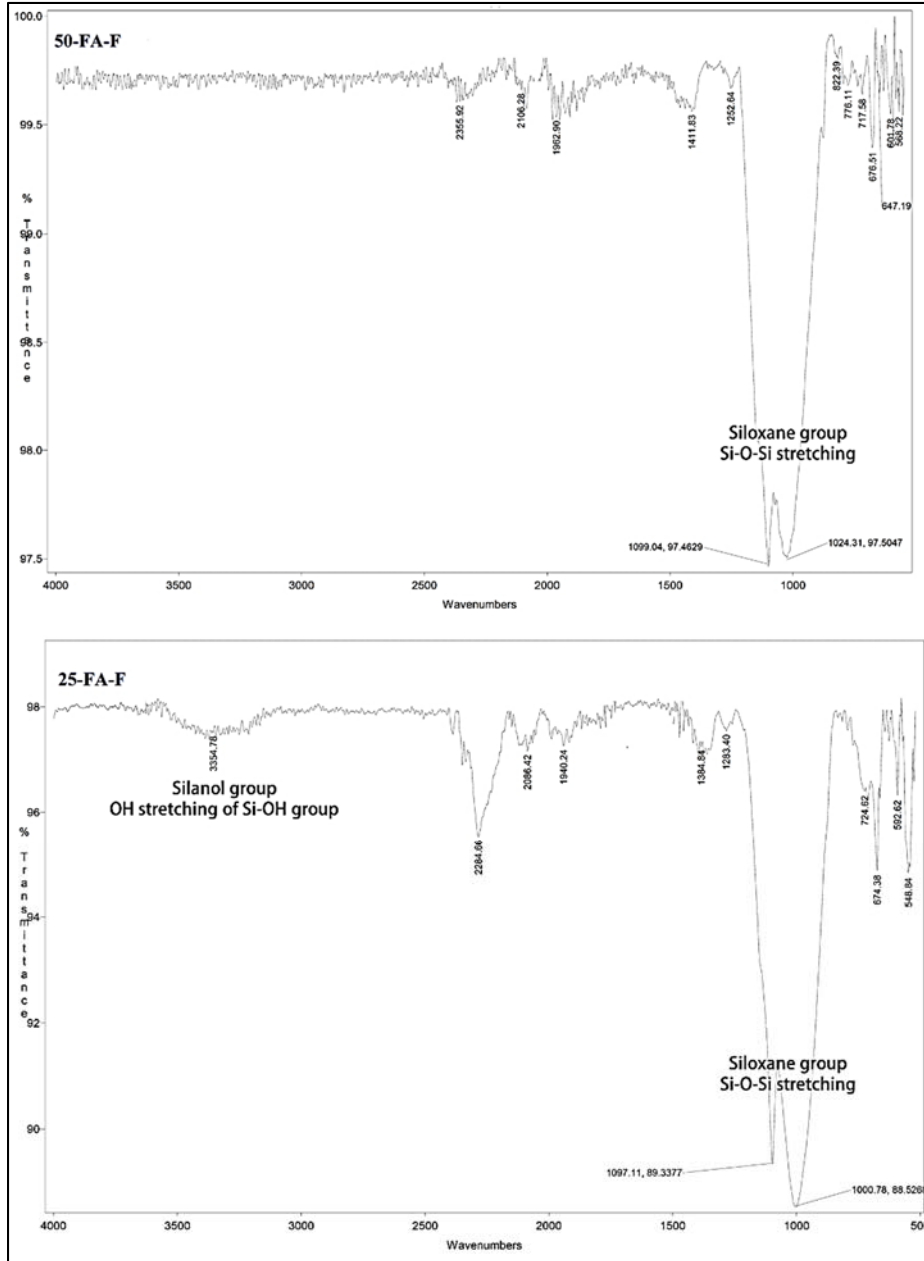
Figure 0-51- FTIR spectrum of 25-FA-F and 50-FA-F.

5.4.3. Viscoelastic Properties

Viscoelastic properties of the composites characterized by DMA and the result is shown in Figures 5-52 and 5-53. . The variation of elastic modulus versus temperature mainly consists of three

main zones; glassy, transition and high-temperature regions. These correspond, respectively, to the composite modulus affected by filler stiffness, glass-transition of the composite due to the micro-Brownian movement of the polymer chains, and the rubbery region related to thermal mechanical stability [Ghasemin et al. (2009); Ghasemi and Farsi (2010)].

A comparison between elastic modulus, E′, of the composites as shown in Figure 5-52, shows that fly ash incorporation improves the elastic modulus below glass transition temperature, Tg, which is an indication of the stiffness improvement. This observation is in accordance with the expectations of the common behavior of composites with rigid spherical particle fillers [Gamage et al. (2013)].

A comparison between the 10wt% fly ash reinforced composites shows that the stiffness in both of the 25-FA-F10 and 50-FA-F10 composites are comparable and higher than FA-F10. This observation is consistent with the Young's modulus measurements by tensile test. As mentioned earlier, the higher stiffness in 25-FA-F10 and 50-FA-F10 compared to FA-F10 can be attributed to their particle size uniformity and better dispersion and homogeneity within the polymer matrix. It should be also noted that the slightly higher stiffness in 50-FA-F10 compared to 25-FA-F10 at temperatures lower than 75°C can be attributed to a higher hardness of 50μm size particle. This is also verified by Nanoindent characterization which is presented in the following section.

Although at the temperatures below 75°C the storage modulus of 50-FA-F10 is slightly higher than 25-FA-F10, which is due to the higher hardness of 50μm fly ash, 25-FA-F10 composite shows the higher elastic modulus at the temperatures above 75°C. The storage modulus of particulate filled polymer composites above Tg is highly influenced by the interfacial interaction between the particles and the polymer matrix [Das and Satapathy (2011); Gummadi et al. (2012)]. As presented in the

153

DMA results, the shift of E′ to higher temperatures above Tg indicates better interfacial interaction in the case of 25µm sized particles.
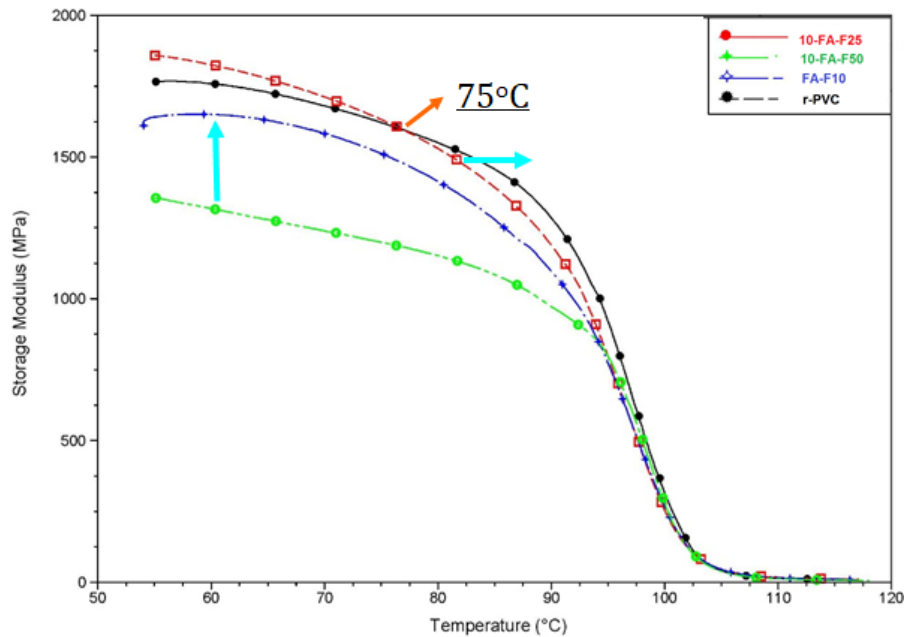
Figure 0-52- Storage modulus of PVC/Fly ash composites versus temperature

The peak intensity of loss modulus (E″) as shown in Figure 5-53 is found to increase with the addition of 10wt% FA, irrespective of the size of fly ash used in the PVC composite, which means that the energy damping capability of the composites is more function of the fly ash content rather than its particle size. This phenomenon may be attributed to the enhancement in the energy dissipation ability as a result of the presence of spherical fillers in the composites and also the increase in the polymer-filler and filler-filler slippage at T_g [Qiao et al. (2011)].

In addition, a comparison between the maxima of loss modulus in the composites shows that the glass transition temperature in 25-FA-F10 shifts higher, which is an indication of a good interfacial interaction between fly ash particles and the polymer matrix [Ghasemi et al. (2009)].
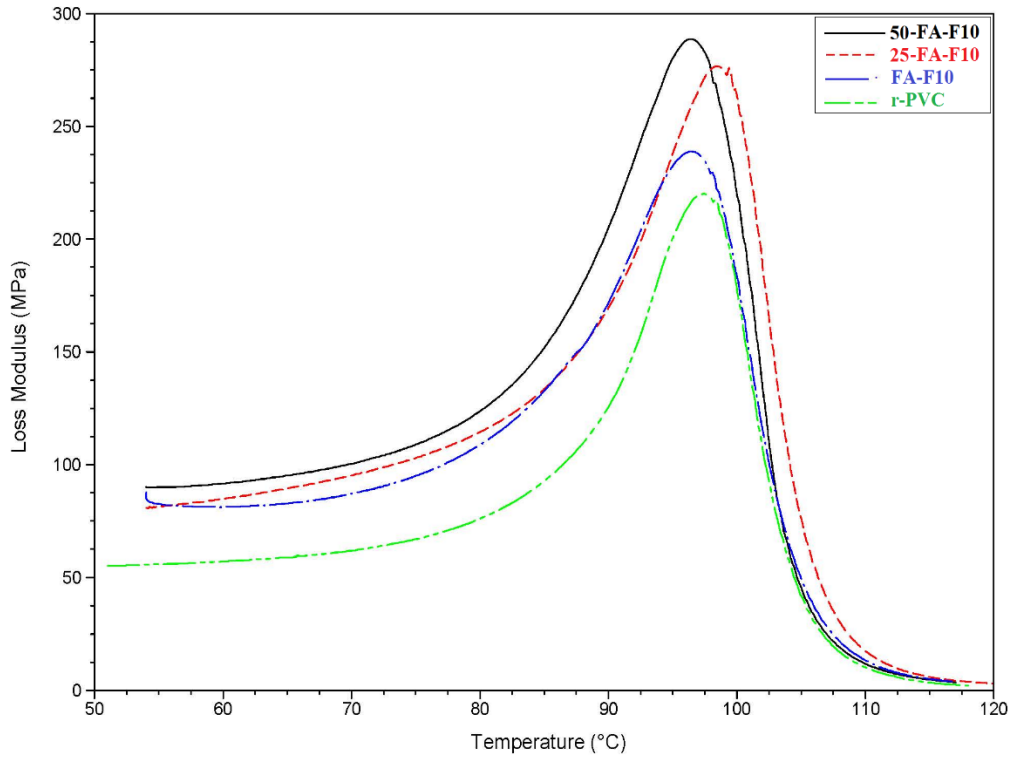
Figure 0-53- Loss modulus of PVC/Fly ash composites versus temperature

5.4.4. Experimental Evaluation of Interfacial Interaction

The local hardness and elastic modulus of r-PVC, 25-FA-F10 and 50-FA-F10 composites were evaluated by the continuous stiffness measurement during loading/unloading cycles using a nanoindenter. For each composite, five indentations were made at the surface of fly ash and the polymer-fly ash interface. In addition, measurements were taken for pure rigid PVC matrix for comparison. All the measurements were carried out at room temperature and the values are reported in Table 5-15. A typical load-displacement curve of the PVC/fly ash composites is shown in Figure 5-54.

155

A comparison between the hardness and modulus of two particle sized fly ash reveals that 50-FA-F has four times and seven times higher modulus and hardness than 25-FA-F; respectively. Therefore, the elastic modulus and hardness of fly ash, as well as its chemical composition are dependent on the particle size. XRD characterization of fly ash particles, which was presented earlier in Table 5-7, show that 50μm fly ash contains more quartz, iron oxides and magnesium oxide than 25 μm fly ash, while 25μm sized fly ash contains significantly more calcium oxide than that of 50μm fly ash. Referring to the hardness values of each mentioned pure oxide [Ciullo (1996)], the hardness of the existing oxides can be arranged from the greatest to the lowest as quartz, iron oxides, magnesium oxide and lime. Therefore, it is expected that 25-FA-F with the higher content of softer phases exhibits a lower hardness compared with 50-FA-F. This observation is also consistent with the storage modulus below T_g that was measured by DMA.

A comparison between the interfacial hardness and elastic modulus in both composites, 25-FA-F10 and 50-FA-F10, with the pure matrix, r-PVC, shows that the incorporation of fly ash enhances the mechanical properties of the composites, irrespective of the particle size, indicating a good interfacial interaction between the filler and the polymer matrix. The higher values of hardness and elastic modulus in 50-FA-F10 composites are essentially due to the incorporation of a harder filler in the case of 25-FA-F10.
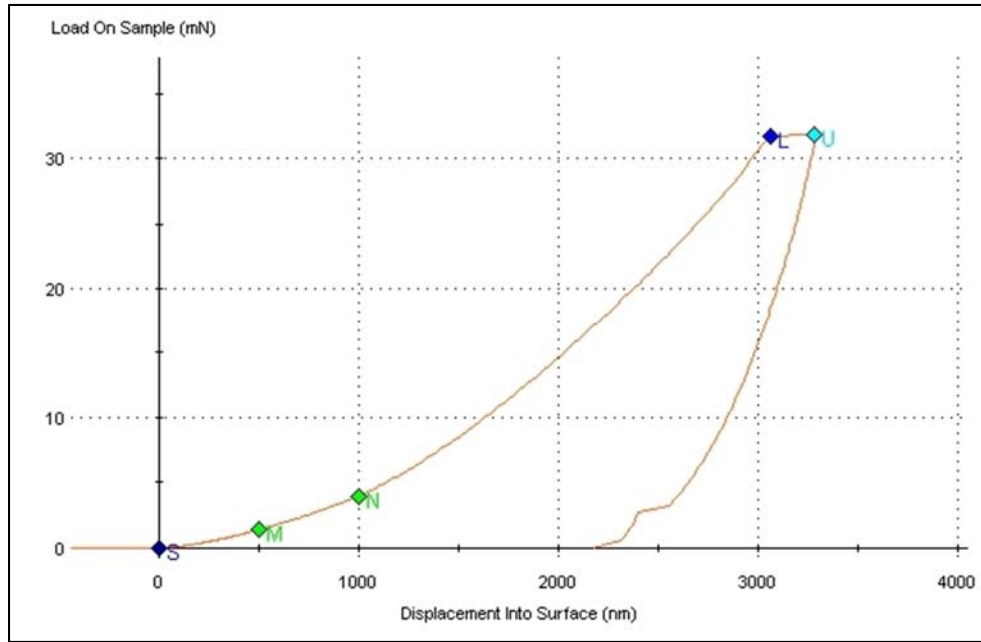
Figure 0-54- A typical load-displacement curve obtained during nano-indentation of a PVC/Fly ash composite

Table 0-15- Nanoindent measured properties of PVC/Fly ash composites

	r-PVC	25-FA-F	25-FA-F10	50-FA-F	50-FA-F10
Hardness (MPa)	40	250	100	1000	150
Elastic Modulus (GPa)	0.3	1.5	0.1	11	4.3

5.4.5. Quantitative evaluation of Interfacial Interaction

Interfacial interactions between PVC matrix and fly ash particles can be estimated using mechanical and viscoelastic data. Tensile properties are correlated with the interfacial interaction parameter (B) in composites using Pukanszky model as presented in Equation 5-4. The calculated interfacial parameters of the composites are listed in Table 5-16.

The calculated interfacial adhesion coefficient (B) has the lowest and highest values in 50-FA-F10 and 25-FA-F10 composites; respectively, as presented in Table 5-16. The negative value of B calculated for 50-FA-F10 has also been reported by other researchers [Százdi et al. (2006); (2007)]. This observation can be attributed to the incorporation of the large particles in 50-FA-F10 which results in poor polymer chains wetting on the particles surface and therefore early failure. In other words, fly ash particles are not well bonded to the polymer matrix and therefore cannot carry their share of the load [Adams (1993)].

Table 0-16- Interfacial parameter values (B) in the composites calculated using Pukanszky model

Samples ID	Tensile Strength (MPa)	Volume Fraction φ_f	Interfacial Parameter (B)
r-PVC	34	-	-
FA-F10	40	0.06	6.07
25-FA-F10	45	0.058	8.16
50-FA-F10	17	0.071	-6.42

DMA can also be used to evaluate interfacial strength by calculating an adhesion factor. This method was developed by Kubat [Kubat et al. (1990)] and based on their assumptions, mechanical loss factor (tan δ_c) of the composite can be written as:

$$tan\ \delta_c = V_f tan\ \delta_f + V_i tan\ \delta_i + V_m tan\ \delta_m \qquad \textbf{Equation 0-6}$$

where, the *f, i*, and *m* respectively subscript filler, interphase, and matrix, and *V* is the volume fraction. δ_f is almost zero and since the volume fraction of the interphase is rather small, Equation 5-6 can be simplified as:

$$\frac{tan\,\delta_c}{tan\,\delta_m} \approx \left(1 - V_f\right)(1 + A)$$ **Equation 0-7**

$$A = \frac{V_i}{1-V_f}\,\frac{tan\,\delta_c}{tan\,\delta_m}$$ **Equation 0-8**

where, Equation 5-8 can be rewritten as given in Equation 5-9:

$$A = \frac{1}{1-V_f}\,\frac{tan\,\delta_c}{tan\,\delta_m} - 1$$ **Equation 0-9**

The adhesion factor (A) can be calculated from DMA data, and its lower values represent strong interactions between the filler and polymer matrix due to a reduction of macromolecular mobility in the vicinity of the filler surface [Ghasemi and Farsi (2010); Ghasemi et al. (2009)].

The adhesion factor versus temperature is shown in Figure 5-55. Adhesion factor reaches the maximum in both 25-FA-F10 and 50-FA-F10 composites at around glass transition temperature due to the high mobility of the polymer chains. It is also noticeable that 25-FA-F10 exhibits a lower adhesion factor and higher Tg than 50-FA-F10 across all temperature range, which indicates the presence of a strong interaction between fly ash and the polymer matrix. In other words, lower values of adhesion factor indicate that the polymer chains mobility is restricted by the existence of a strong interaction between fly ash particles and the PVC matrix which results in the shift of Tg to higher temperatures.
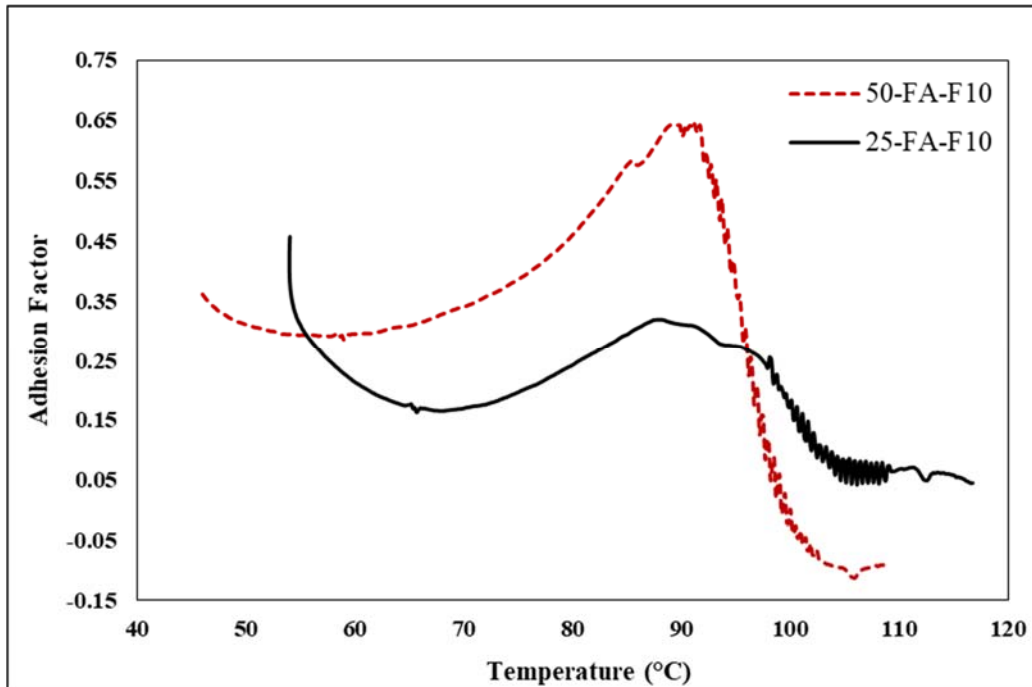
Figure 0-55- Adhesion factor versus temperature for PVC/Fly ash composites

5.4.6. Fracture Morphology

SEM images and EDX spectra of the fractured surfaces by tensile test of the fly ash filled PVC composites are shown in Figure 5-56. Generally, composites may fail due to the presence of either voids or air bubbles, poor wetting of polymer on the surface of reinforcing particles, or poor adhesion between the filler and the polymer.

In the SEM images of the tensile fractured composites, debonding of some of fly ash particles is obvious, while the rest are well bonded and interlocked in the matrix. Filler detachment occurs as a result of poor interfacial interaction. Since the properties of the reinforced fly ash composites depend significantly on the fly ash chemical composition, some elements or chemical composition might be more effective in terms of the properties enhancement. EDX spectra on the fractured surfaces of the

160

composites show that silicon, aluminum, and calcium are three main elements remained well bonded within the polymer matrix.

SEM line scan of the fractured composite is shown in Figure 5-57. . Elemental characterization of the composite among a line starting from PVC matrix and passing through two interlocked particles also confirms that the concentration of silicon, aluminum, and calcium elements remains the highest within the whole line. This observation is consistent with the results presented earlier showing that silicon and calcium, the two main elements of quartz and calcium oxide phases, in the fly ash play significant roles in the composite properties improvement.
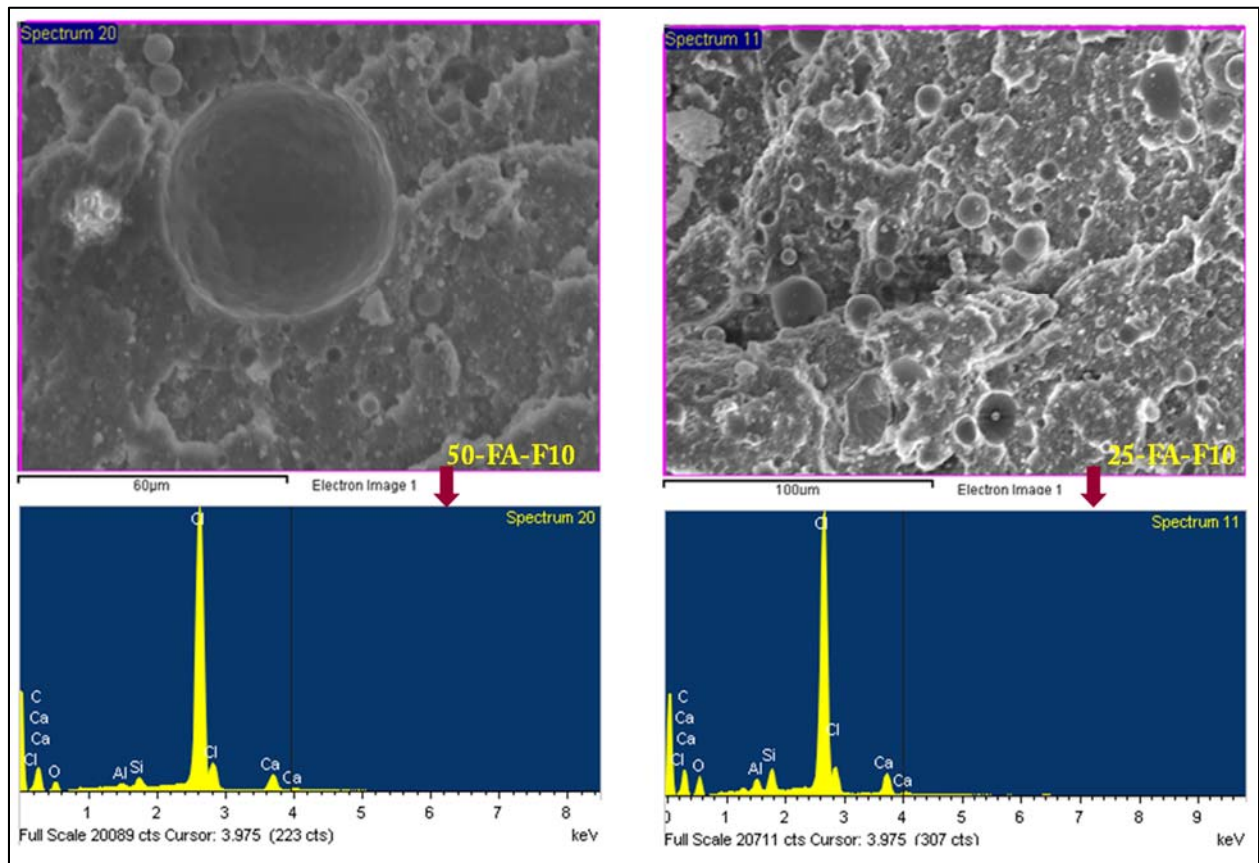
Figure 0-56-SEM/EDS of tensile fracture surface of 25-FA-F10 and 50-FA-F10

161
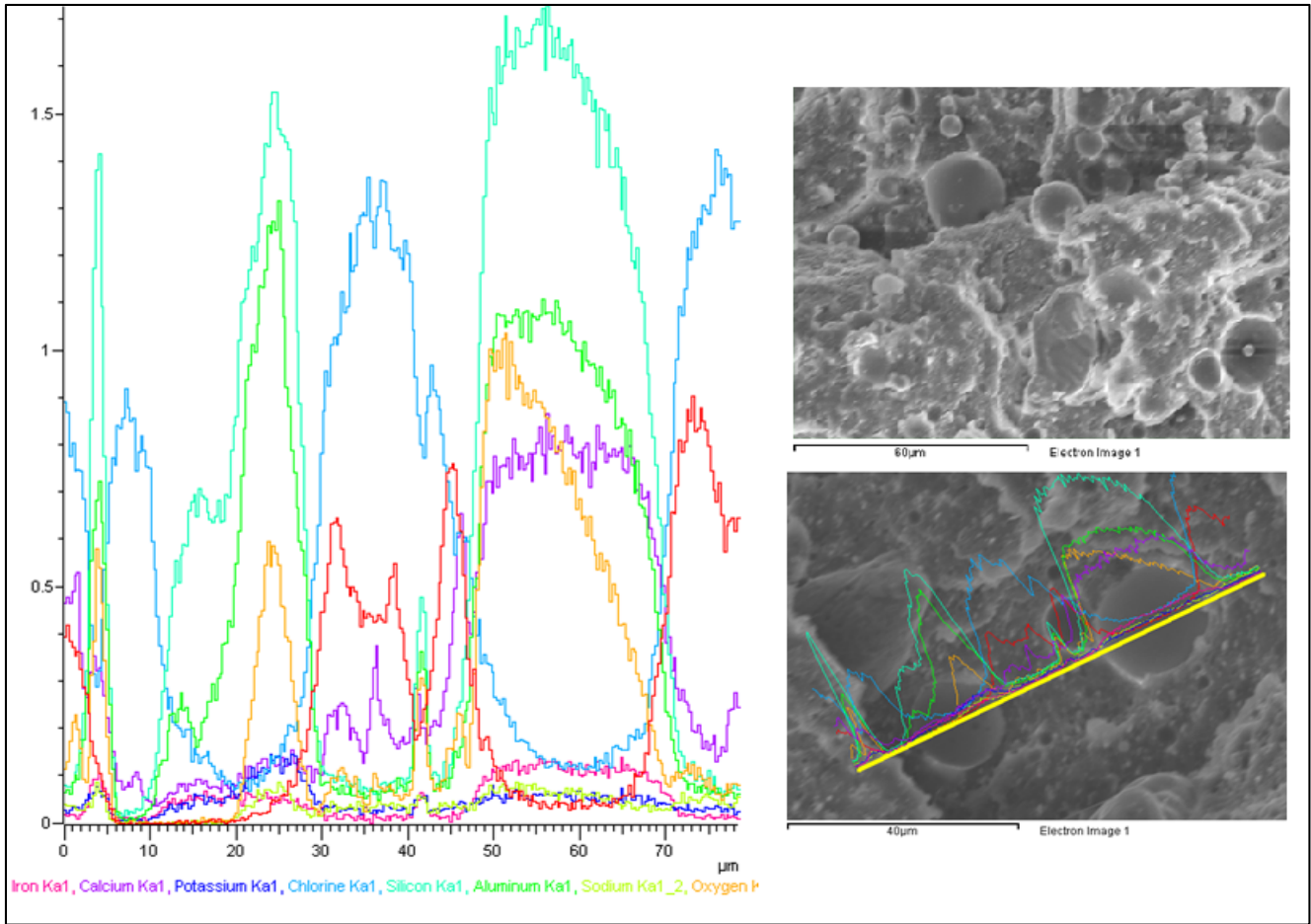
Figure 0-57- SEM-Line scan of PVC/Fly ash composites

5.5. Evaluate Recyclability and Reprocessability of Recycled-PVC/Fly Ash Foam Composites

5.5.1. Physical Properties

Density of the foam composites their trends of variation with varying amounts of regrind and fly ash are shown in Figures 5-58a) and b); respectively. It can be observed that the density increases proportionally as the regrind percentage or fly ash content in the composite increases; whereas the improvement of density values with varying fly ash content is more significant in comparison with density variation with increasing regrind amount.

In fact, cell growth can be physically hindered in the presence of fly ash particles, which results in smaller cell size, thicker cell walls, and higher foam density. On the other hand; since the nucleation, growth, and morphology of the foam cells are determined by the blowing agents concentration, the addition of foam regrind results in the scarcity of blowing agents and consequently a denser foam structure. These observations has been confirmed by SEM images, which are shown in Figure 5-66
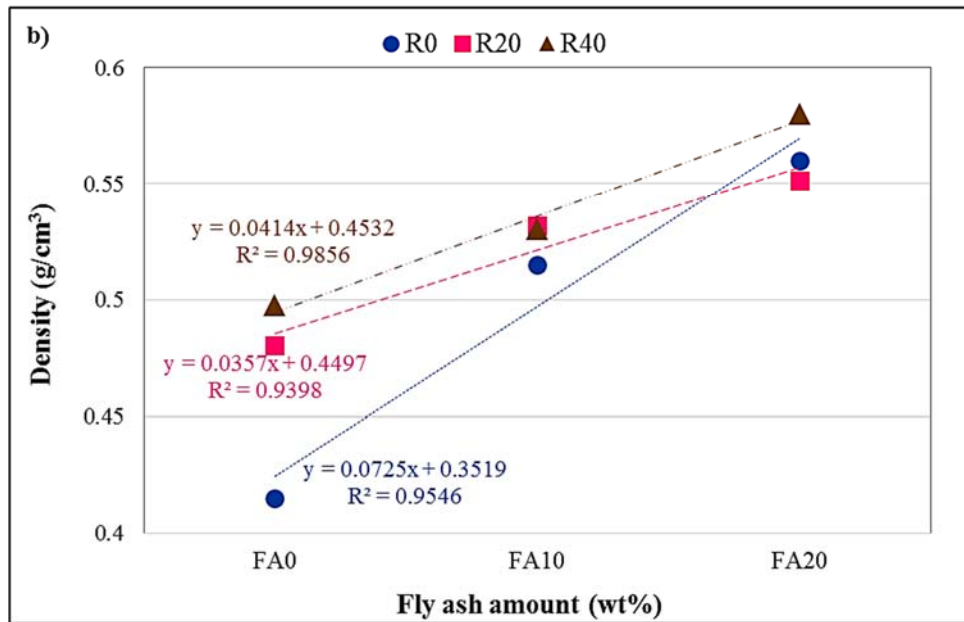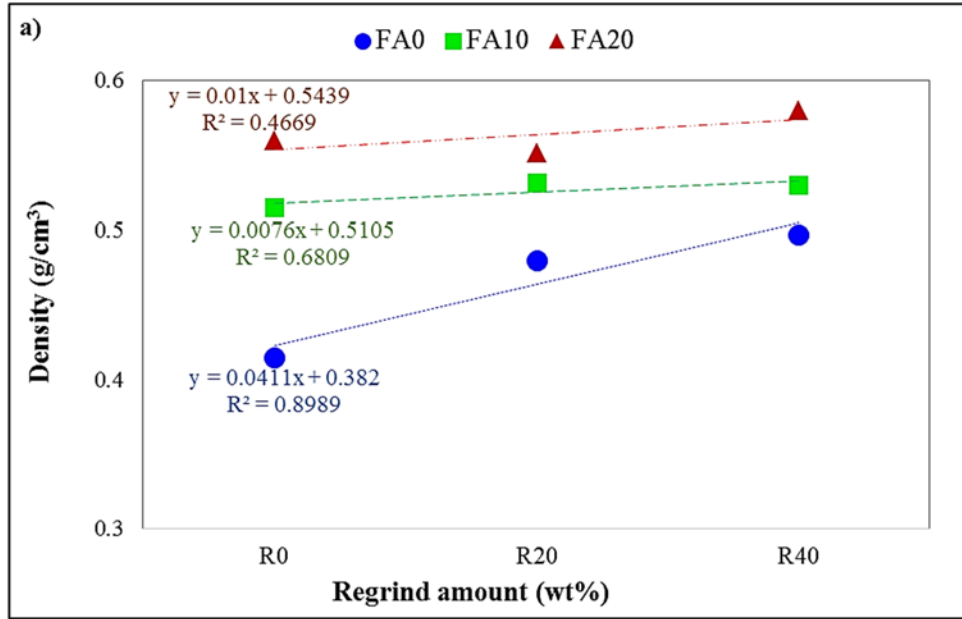
Figure 0-58-: Effect of a) Regrind amount (wt%), and b) Fly ash amount (wt%) on the density of PVC foam composites

5.5.2. Processing Properties

The torque rheometer curve for one of the PVC foam composites is shown in Figure 5-59. The first maximum peak is the loading peak (point A). Afterwards, the torque curve drops to a minimum value (point B), where PVC sub-grains and agglomerates slide over each other and the gelation process begins. This value is a relative value for the melt viscosity. Following point B, the torque reaches its maximum at point X, which is known as the fusion or gelation torque. At point X, the polymer is in a void-free state and starts to melt at the interface between the compacted polymer and the hot mixer chamber surface. The torque curve starts to drop until it reaches a constant value after a certain time, t_E. At this point, the polymer melt is in a homogenous state where an equilibrium between the friction heat and the temperature of the chamber is reached [Piszczek et al. (2004) (2010); Tomaszewska (2005); Tomaszewska et al. (2004) (2007) (2008) (2012); Piszczek et al. (2007)].
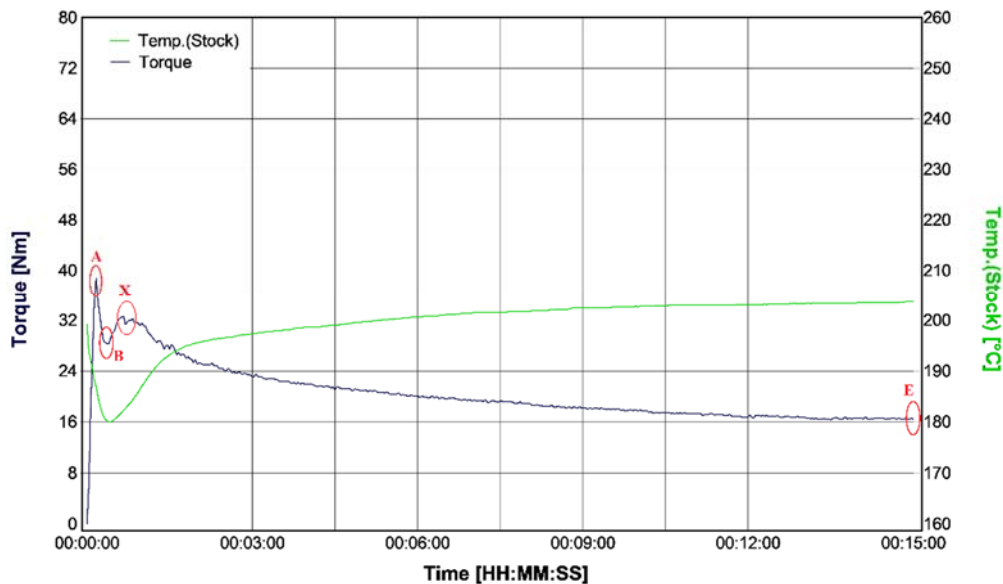
Figure 0-59-Torque rheometer curve of a PVC compound

The trends of variation in the minimum torque (point B) with varying regrind and fly ash concentrations are presented in Figures 5-60a and 5-60b; respectively.

As shown in Figure 5-60a, point B values increase with increasing the regrind concentration due to higher viscosities. As mentioned earlier, at point B, PVC subgrains and agglomerates slide over each other to form a three dimensional network of polymer chains. Since the regrind is a processed polymer with larger grains than the virgin powder, the viscosity increases with increasing the regrind loadings in the composites.

On the other hand, the minimum torque shows a decreasing trend with increasing fly ash content, as shown in Figure 5-60b. Since fly ash powder consists of solid particles, a higher concentration of fly ash particles in the PVC composites results in a higher shear in the compound and, consequently, a lower viscosity. In fact, the regrind amount and fly ash content in the PVC composites show a counterbalance effect on the minimum torque values. For example, in FA0-R0 composites, the minimum torque is about 24.5N.m and this value increases to 36.4N.m by adding 40wt% regrind to the PVC foam. However; in FA20-R0 composite, the minimum torque is about 19N.m and it increases to 30.2 N.m by adding 40wt% regrind. Therefore, varying the fly ash and regrind concentrations in the PVC composites can control the viscosity and minimize the processing difficulties associated with high melt viscosities.
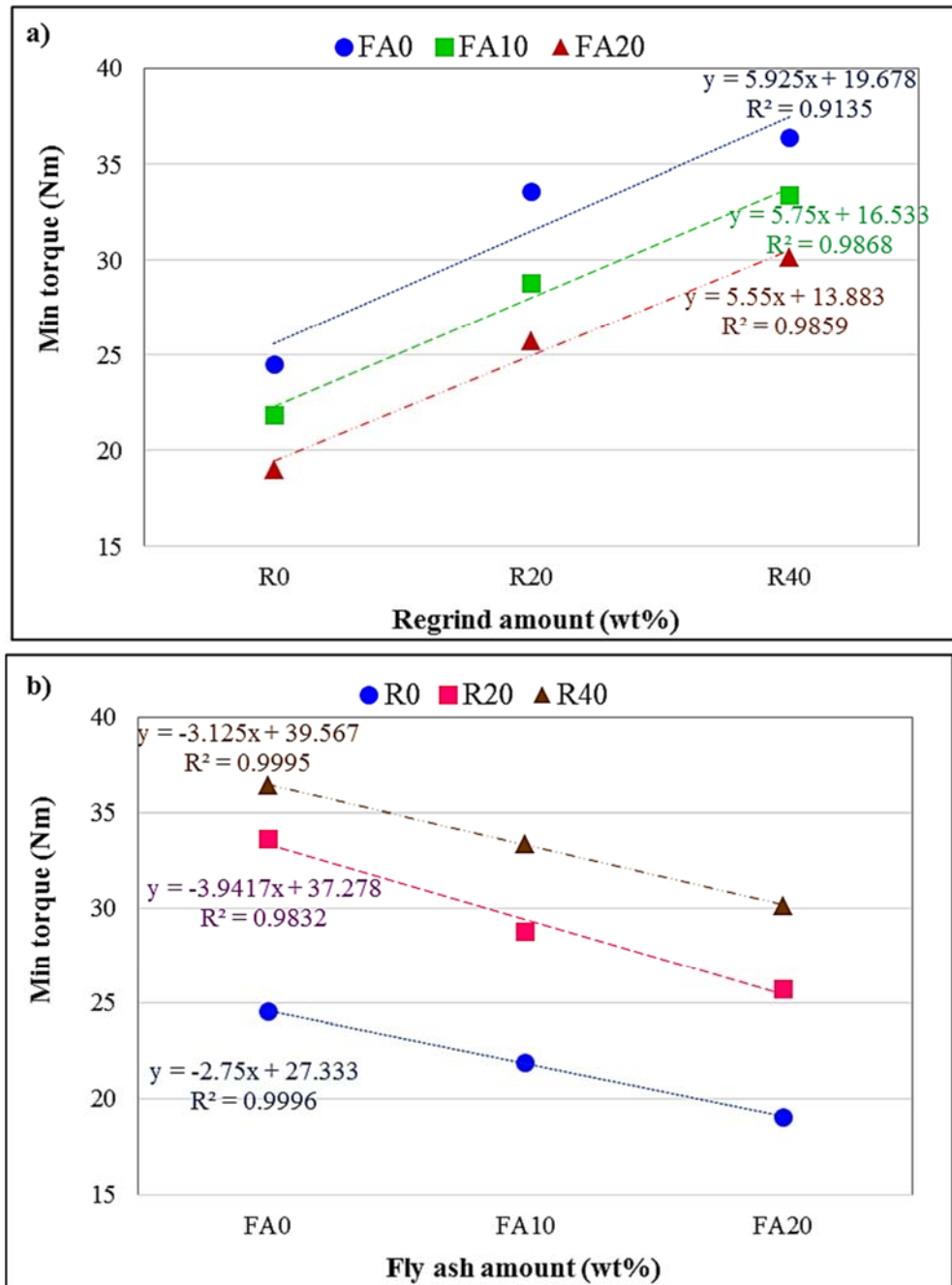
Figure 0-60- Minimum torque variation with varying a) regrind amount (wt%), and b) fly ash amount (wt%)

167

The trends of variation in the maximum torque (point X) with varying regrind and fly ash concentrations are presented in Figures 5-61a and 5-61b; respectively.

Increasing the regrind content in PVC composites increases the maximum torque values, as shown in Figure 5-61a. To achieve a uniform melt structure at point X, the virgin powder and regrind particles must be compacted together. Since the regrind has a more compact and densified structure, with a higher melting point compared to virgin PVC, adding more regrind to the virgin compounds necessitates a higher torque to break the grain boundaries and agglomerates in order to form a network of polymer chain entanglements. However; the maximum torque shows an inverse trend as the fly ash content is increased, as shown in Figure 5-61b. This may be attributed to a higher applied shear stress in PVC composites with the presence of fly ash particles, which results in a gelled structure at lower torque levels.
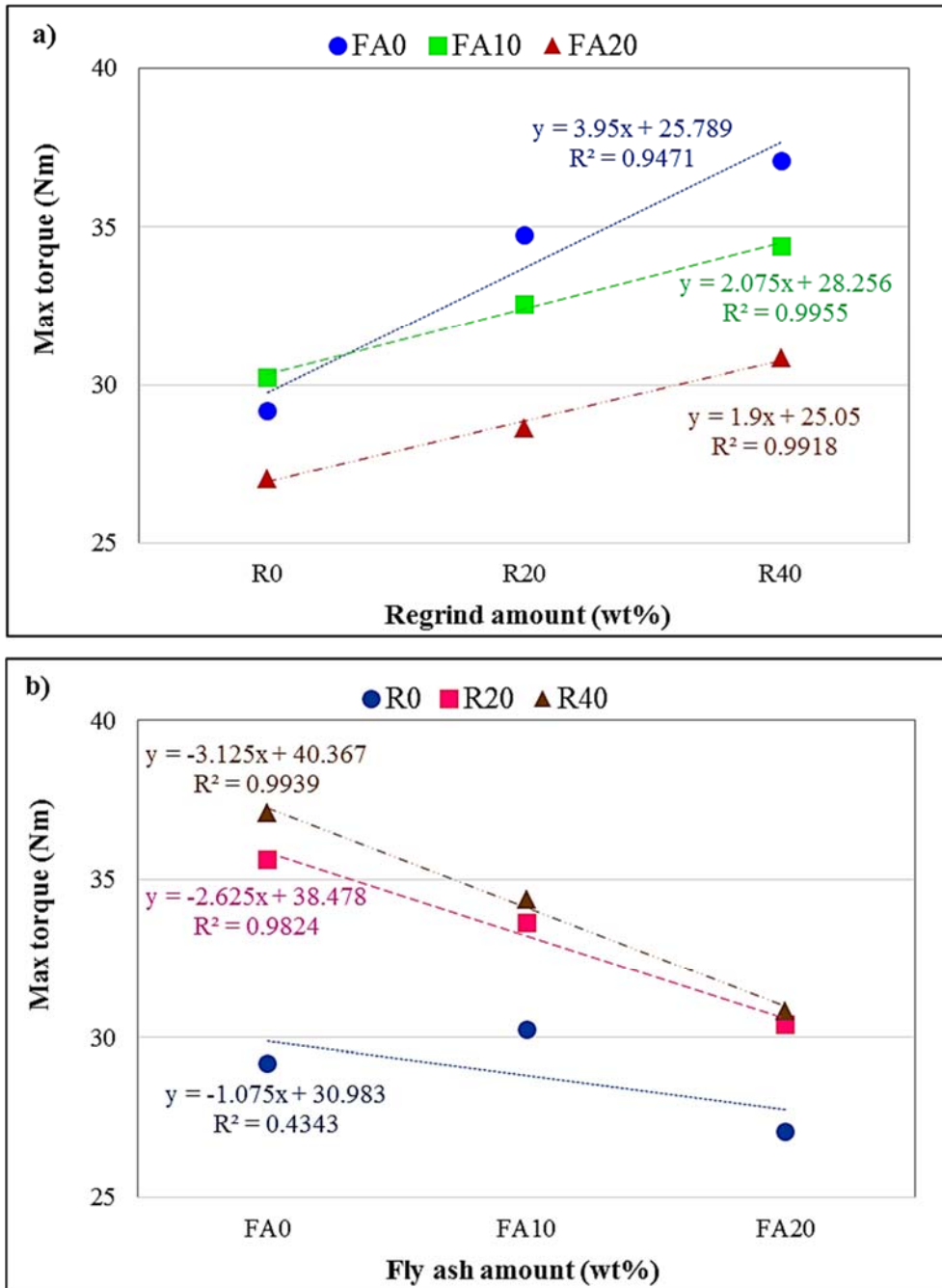
Figure 0-61- Maximum torque variation with varying a) regrind amount (wt%), and b) fly ash amount (wt%)

5.5.3. Mechanical Properties

The ultimate tensile strength (UTS) at various levels of regrind and fly ash contents is shown in Figure 5-62. It can be observed that by adding fly ash to pure PVC foam, the tensile strength decreases, which may be attributed to micro crack formation due to stress concentration points in fly ash filled samples.

A comparison of the tensile strength of composites with 0wt% fly ash content shows that by adding 20wt% regrind, the tensile strength increases, while it drops slightly with the addition of 40wt% regrind. Regrinds mainly have gelled structure and more heat is needed to melt them and make a uniform melt structure than their previous melting temperature. Since mixing results show that increasing regrind amounts give rise to increasing viscosity, adding more regrind to virgin materials hinders the mixing quality and may result in some remaining un-melted regrinds in the processed foam samples. The un-melted solids can cause stress concentration during tensile testing and therefore reduce the tensile strength.

Whereas; this effect is not observed in fly ash loaded samples, because the presence of fly ash particles in the samples results in decreasing the melt viscosity, which can help in having more uniform melt structure during mixing. Whereas; in fly ash reinforced composites, the tensile strength exhibits an increasing trend with increasing the regrind content. Failure to achieve the optimum level of gelation or fusion can cause a variety of faults, as well as failure to obtain maximum mechanical properties [Ditta et al. (2004)].

However, increasing UTS with increasing the regrind content can be attributed to a higher degree of gelation combined with a good dispersion of regrind in virgin PVC without an increase in stress

170

concentration due to the addition of regrind. Moreover, the increasing trend in tensile strength with

increasing the regrind content indicates a uniform cell structure even after the addition of 40wt% of

regrind to the composites.
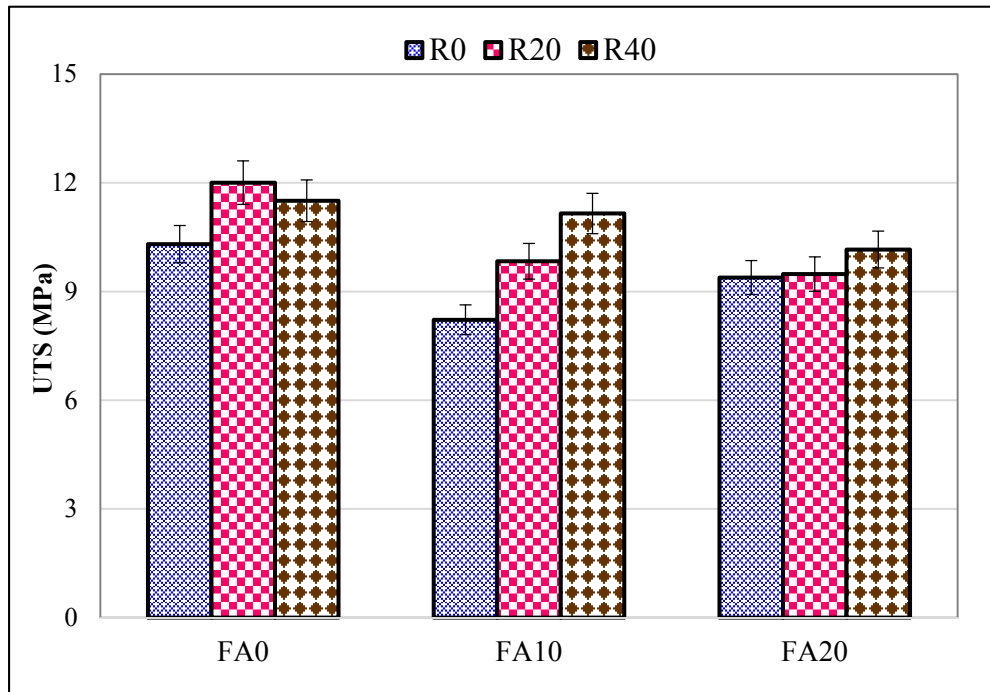
Figure 0-62- Effect of regrind amount (wt%) and fly ash amount (wt%) on the Ultimate Tensile Strength (UTS) of PVC

foam composites

The reduction of area in PVC foam composites, which shows ductility variation of composites

due to changing fly ash and regrind contents, is presented in Figure 5-63. It can be observed that as

the fly ash concentration increases, the ductility of fly ash filled composites decreases, significantly.

The rate of reduction of area in PVC reinforced composites with the addition of 10wt% and 20wt%

fly ash is 66% and 79%; respectively. This reduction is attributed to the restriction of polymer chain

movement and displacement due to proper filler and matrix bonding.

On the other hand, a comparison between the reductions of area in the composites with higher regrind content indicates that in virgin PVC foam composites, the ductility decreases proportionally with the addition of regrind. In the composites containing fly ash particles, the reduction of area improves slightly with adding 20% regrind, which presents a ductility improvement in the presence of regrind. Meanwhile, adding more than 20% regrind results in a lower reduction in area. This can be attributed to the increased rigidity imparted by fly ash content in the 40% regrind loaded, fly ash reinforced, foams which may lower the polymer mobility as a result of strong interaction between fly ash particles and the polymer matrix.
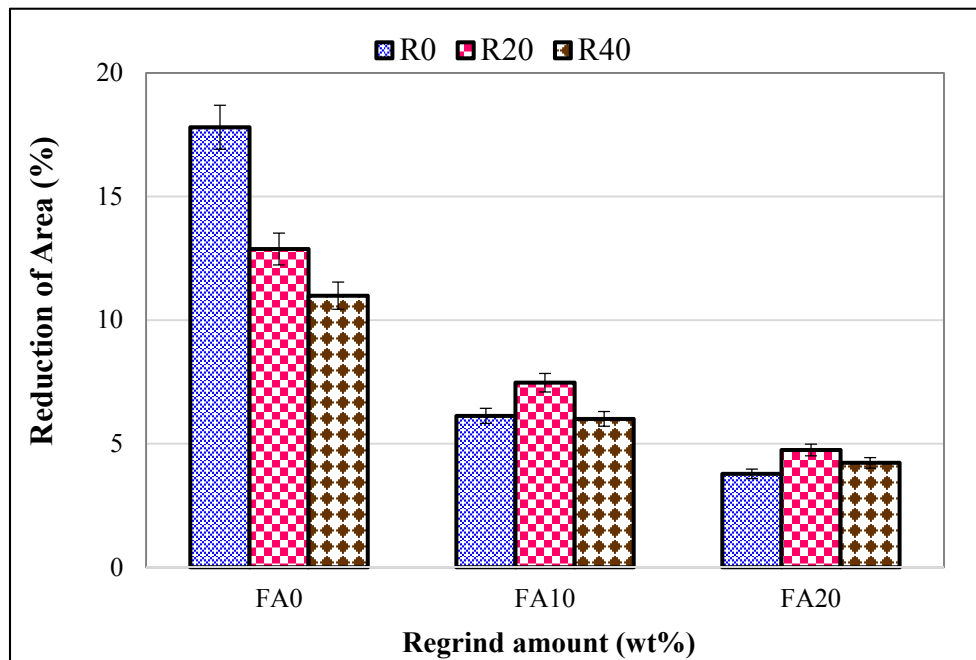
Figure 0-63-Effect of regrind amount (wt%) and fly ash amount (wt%) on the reduction of area (%) of PVC foam composites
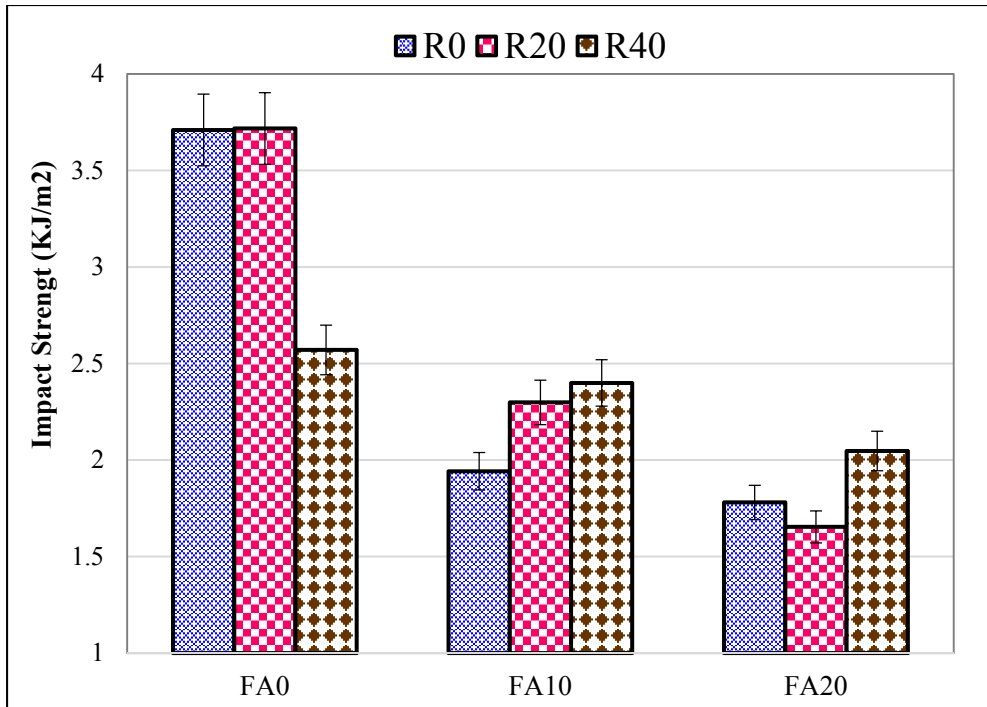
Figure 0-64- Effect of a regrind amount (wt%) and fly ash amount (wt%) on the impact strength of PVC foam composites

The measured notched charpy impact strength for PVC foam composites with varying fly ash and regrind content is shown in Figure 5-64. In the notched samples, the impact strength represents the resistance to crack propagation due to the triaxial stress field ahead of the notch. The test results show that by adding fly ash particles to PVC foam, the impact strength decreases, which may be attributed to the higher brittleness of the composites compared to the pure sample, FA0-R0, due to the higher reinforcement rigidity. Moreover, immobilization of polymer chains in the reinforced composites, due to the fly ash and matrix bonding, inhibits the growth of plastic deformation, and therefore increases the tendency for crack propagation, which yields lower impact strength than pure samples. On the other hand, by adding 20wt% regrind to unreinforced pure foam, the impact strength

changes marginally, while more addition of regrind results in a significant decrease in the impact strength.

However, in fly ash reinforced composites, impact strength improves generally with the addition and increasing regrind content. Meanwhile, this observation does not apply for FA20-R20 which shows 7.3% lower impact strength compared to FA20-R0. Since all samples obey a trend and only FA20-R20 is off-trend, the reduction in impact strength observed with FA20-R20 compared to FA20-R0 is considered as an anomaly in the experimental measurements.

It is generally accepted that one of the main parameters in determining the foam structure is the melt viscosity. At a higher melt viscosity, the cell nucleation and growth is limited. As shown in Figure 5-60a, FA0-R0 has higher melt viscosity compared to fly ash reinforced foams and its value increases with increasing the regrind content. Whereas; FA0-R20 has higher melt viscosity than FA0-R0, it shows the same impact strength as FA0-R20 which indicates that this sample has a uniform foam structure. Adding 40% regrind to FA0 results in increasing melt viscosity by about 48% and decreasing impact strength which may be due to the nonuniformity of its foam structure. Good interaction between fly ash particles and polymer matrix can hinder the polymer chain mobility which results in decreasing impact strength.

Moreover, fly ash particles act as nucleating agents during the foaming process and therefore the more fly ash addition, the higher cellular structure is achieved. On the other hand, by adding fly ash, melt viscosity drops and nucleates can grow faster, thus resulting in bigger cells with a narrower wall thickness. This in turn can result in faster crack propagation and lower impact strength. However, in fly ash reinforced composites containing regrind, and due to the counterbalance effect

174

of fly ash and regrind on the melt viscosity, slower cell growth with stronger and thicker cell walls are expected which can slow down the crack propagation rate and improve the impact strength.

5.5.4. Viscoelastic Properties

Figure 5-65 shows that E′ of PVC foam composites at 50°C, well below the glass transition temperature, improves significantly with the incorporation of fly ash particles and it increases with increasing fly ash content. This behavior can be attributed to the higher stiffness and rigidity of fly ash particles compared to pure PVC foam. The maximum storage modulus that is achieved by incorporating 20wt% fly ash is about 462MPa, which represents 53% improvement over pure composition, FA0-R0.

Moreover, it can be seen that by adding and increasing the regrind content, the storage modulus of PVC composites exhibits an increasing trend in most cases. For example, the extent of increase in E′ in FA10-R40 is approximately 47% compared to FA10-R0 and 12% compared to FA10-R20. Whereas, in FA20-R40, the storage modulus decreases by about 11% compared to FA20-R20, which is still 4% higher than the storage modulus of FA20-R0. Increasing the storage modulus with the addition and increasing the amount of regrind confirms a good stress transformation between the polymer matrix and fly ash particles. In addition, the increasing trend in storage modulus indicates that the matrix structure of mixed PVC regrind and virgin resin is uniform due to a high degree of gelation, and a good bonding with fly ash particles.
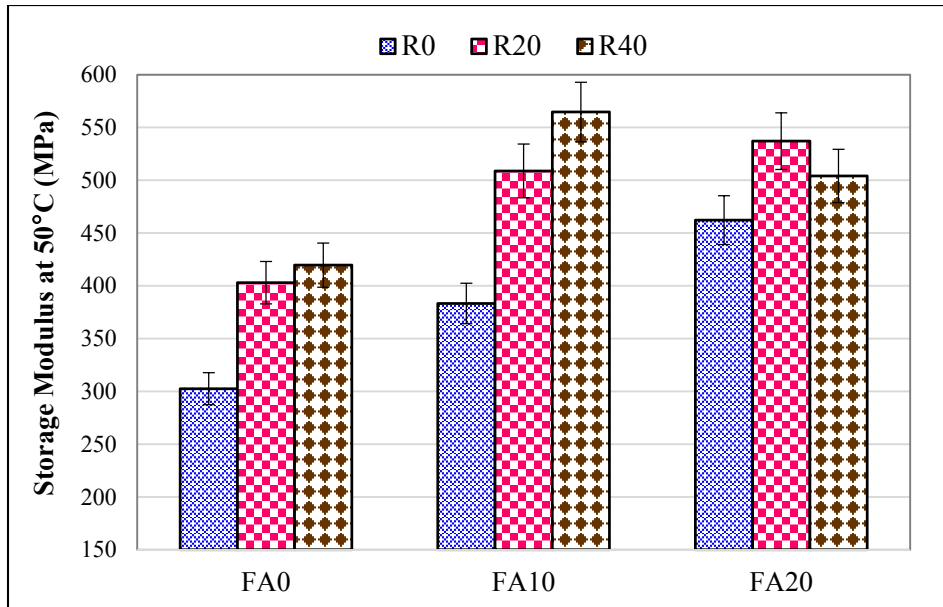
Figure 0-65- Effect of a regrind amount (wt%) and fly ash amount (wt%) on the storage modulus of PVC foam

composites

5.5.5. Morphological Properties

The SEM micrographs of PVC foam composites are shown in Figure 5-66. A comparison between FA0-R0 (Figure 5-66a) and FA0-R40 (Figure 5-66b), reveals that the cell structures and sizes do not change significantly even with the addition of 40wt% regrind. It can be also observed that by adding 40wt% regrind to FA0, the ratio of foam cells to cell walls decreases slightly, which can be the reason for increasing the foam density with increasing the regrind content. Figures 5-66c and 5-66d show the SEM micrographs of the tensile test fractured surfaces of FA10-R40 and FA20-R40; respectively. The highly regrind-loaded composites show ductile fractures, observed from the orientation or elongation of the PVC molecules (represented by circles in Figure 5-66c and 5-66d). It indicates that the regrind particles are well dispersed in the virgin PVC matrix and all their grains

176

boundaries and agglomerates are eliminated during mixing. A high degree of mixing in the presence

of regrind is the main reason to improved mechanical properties of the composites.
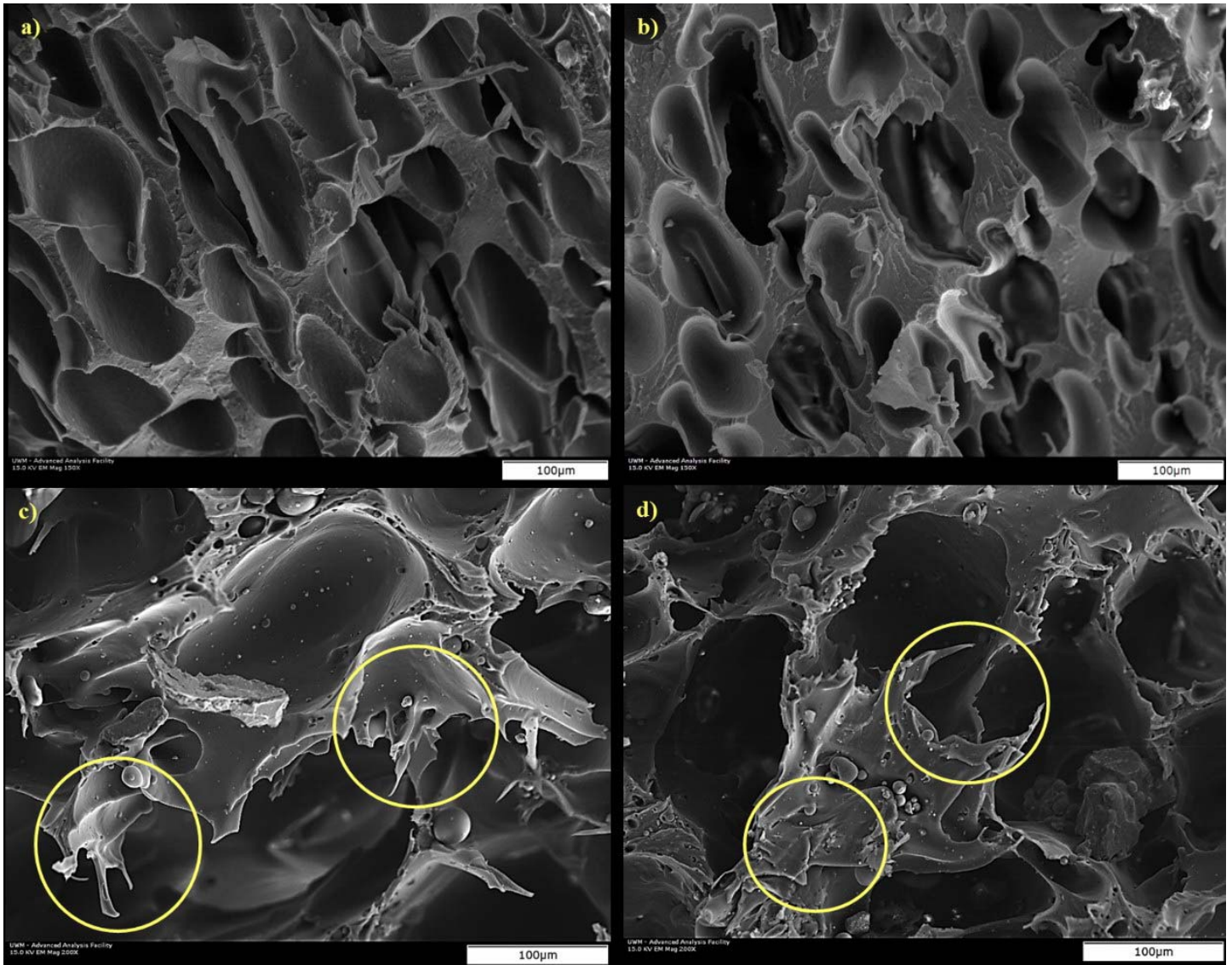
Figure 0-66- SEM micrographs of: a) FA0-R0 (150X), b) FA0-R40 (150X), c) FA10-R40 (200X), and d)

FA20-R40 (200X)

177

Chapter 6- Conclusions and Recommendations for Future Work

6.1. Conclusions

- Fly ash elemental and chemical composition is significantly dependent on its class and particle size. The smaller particle size has higher calcium oxide and less carbon contents. In addition, higher calcium oxide and silicon oxide was identified in class-C, while the amount of iron oxides in class-F is higher.

- Cell growth of the polymer foam is physically hindered in the presence of fly ash particles which results in an increase of the foam density and a decrease of cell size and cell size distribution.

- Mechanical properties; such as tensile and flexural strengths and modulus, improved, indicating that fly ash particles are properly incorporated into the PVC matrix.

- Ductility and impact strength of the composites decreased by fly ash particles addition, while their variation by increasing fly ash content was not significant indicating existence of a good interaction and a proper distribution of the particles within the polymer matrix.

- Fracture surface morphology confirmed a good dispersion, distribution, and interaction between fly ash and PVC matrix; whereas an agglomeration, particle detachment, and debonding was observed in the highly loaded composites.

- Thermal decomposition studies showed that the dehydrochlorination of PVC is accelerated in the presence of fly ash, while the main backbone crack is enhanced. It was also evident that CaO and Fe_2O_3 are reactive to chlorine radical and form metal chloride as a product instead of HCl. While SiO_2 and Al_2O_3 were found to be non-reactive.

- Kinetic studies confirmed higher activation energy in the first step of decomposition of the pure PVC foam compared with that of fly ash loaded, while the estimated activation energy of the second step in the composite contained fly ash was significantly higher.

- Class-C contained PVC foams represented lower density and much better mechanical, viscoelastic, thermal and morphological properties than that of class-F contained ones. The main reason of the better class-C performance was found to be related to its higher SiO_2 and CaO content.

- Interfacial interaction of the composites estimated using Pukanszky developed model confirmed the better interfacial interaction in class-C reinforced composite compared to class-F.

- Structural analysis confirmed the presence of hydroxyl (–OH) functional groups on the surface of SiO_2, which plays the main role in the formation of physical bonding and therefore interfacial interactions between fly ash particles and polymer matrix.

- Morphological studies of the fracture surfaces using SEM/EDS line-scan confirmed the effectiveness of silicon and calcium elements in the composited properties improvement due to their high concentration in the well-bonded particles.

- Although the characterized amount of silicon oxide in 25micron sized particles was lower than 50miron, performance of the composite contained smaller particles was found to be better. The main reason is due to the dependency of –OH group concentration in SiO_2 on the particles size and surface area. The higher surface area in the particles, the more hydroxyl groups was determined on the particles surface.

- Studies of the reprocessability and recyclability of PVC foam composites containing fly ash showed that by adding more regrind, the maximum and minimum torque values increase. Meanwhile, increasing fly ash content decreases the melt viscosity and improves processability. By adding both regrind and fly ash, the viscosity of the compound can be controlled and good mixing properties can be achieved.

- It was also observed that by adding more regrind, the mechanical properties improve, which indicates a good gelation in the composites containing both virgin and regrind of PVC/fly ash foam. It is concluded that reprocessing of PVC foam composites including up to 40wt% regrind is feasible.

- It can also be concluded the higher contents of SiO_2 and CaO in fly ash is determined, the better performance of their composites will be expected. Besides, the higher CaO and Fe_2O_3 contents in fly ash, the better thermal stability of polyene backbone is expected.

6.2. Recommendations for Future Work

This study can be further improved if surface treated fly ash is used. It is expected surface treated fly ash with the smaller and narrower size range and therefore higher surface area improves the properties of the prepared composites. Our preliminary results of fly ash surface treatment using 3molar NaOH solution showed the surface area improved more than 6 times and the particle size became narrower. Therefore, surface treatment of fly ash using not only base solution, but also other acidic solution can also be included into consideration.

Considering surface treatment of fly ash using silane-coulping agent in order to increase –OH functional group concentration and therefore improve interaction with polymer matrix may enhance the composites performance.

Studying the effect of other chemical phases such as magnesium oxide and aluminum oxide in details on the prepared composite performance can also be considered.

As our results showed a significant dependency of the final properties on the fly ash chemical composition, it would be beneficial to work more on the possibility of fly ash purification in terms of more favorable phases such as quartz and lime for better interfacial and mechanical properties and iron oxide and calcium oxide for better thermal properties.

Chapter 7- References

- S. T. Lee, "Foam extrusion, Principles and practice", (2000).

- Deloitte & Touche Regional Consulting Services Limited "PVC markets of Europe and South-East Asia: analysis of profitability and production cost", 2010.

- S. T. Lee, C. B. Park, "Polymeric Foams", (2006).

- Wallenberger, F. T., Watson, J. C., and Li, H. (2001), Glass fibers. Materials Park, OH: ASM International, pp. 27-34.

- K. Sivertsen, "Polymer Foams, J. Polymer Physics", (2007).

- S. T. Lee, "Polymeric Foams, Mechanisms and Materials", (2000).

- NEXTOOL, "PVC Foam Extrusion", (2009).

- M. Jährling, "Examining the Fusion and Degradation Behavior of PVC Dry Blends with the HAAKE PolyLab QC", Thermo Fisher Scientific, Karlsruhe Germany, (2009).

- K. Piszczek, J. Tomaszewska, and T. Sterzyn´ ski, "The universal temperature parameter of rigid PVC gelation in Brabender kneader", J. Polimery, 49, (2004).

- J. Tomaszewska, "Gelation of suspension PVC with small amount of plasticizer compounds", J. POLIMERY, 50, (2005).

- J. Tomaszewska, T. Sterzyn´ ski, K. Piszczek, "Rigid Poly (Vinyl Chloride) (PVC) Gelation in the Brabender Measuring Mixer. I. Equilibrium State between Sliding, Breaking, and Gelation of PVC", J. Applied Polymer Science, Vol. 93, 966–971, (2004).

- K. Piszczek, J. Tomaszewska, and T. Sterzyn´ ski, "Rigid Poly (vinyl chloride) (PVC) Gelation in the Brabender Measuring Mixer. II. Description of PVC Gelation in the Torque Inflection Point", J. Applied Polymer Science, Vol. 103, 3688–3693 (2007).

184

- J. Tomaszewska, T. Sterzyn´ ski, K. Piszczek, "The influence of the chamber temperature in the Brabender measuring mixer on the state of equilibrium of the torque of rigid poly (vinyl chloride)", J. POLIMERY, 53, (2008).

- Tomaszewska J., Sterzyn´ ski T., Piszczek K. (2007) "Rigid Poly (vinyl chloride) Gelation in a Brabender Measuring Mixer. III. Transformation in the Torque Maximum", J. Applied Polymer Science, Vol. 106, 3158–3164.

- K. Piszczek, J. Tomaszewska, T. Sterzyn´ ski, "The influence of temperature of poly (vinyl chloride) melt on the equilibrium state of gelation process", J. POLIMERY, 55, (2010).

- J. Tomaszewska, K. Piszczek, "Processing of Precipitated Nongranular PVC in the Brabender Measuring Mixer", J. Vinyl and Additive Technology, Vol 10, (2012).

- N. Sombatsompop, and S. Thongsang, *J. Appl. Polym. Sci.*, 82(10), 2478 (2001).

- E. B. Rabinovitch, J. D. Isner, J. A. SIDOR, and D. J. Wiedl, "Effect of Extrusion Conditions on Rigid PVC Foam" J. Vinyl and Additive Technology, Vol. 3, No. 3, (1997).

- N. L. Thomas, (2004a) Rigid PVC foam, formulating for sustainability. In: 6th International Conference on Blowing Agent and Foaming Processes, 10–11 May, Hamburg, Germany, pp.179–189.

- D. Eaves, (2004) "Handbook of Polymer Foams", Shawbury: Rapra Technology Limited.

- N. L. Thomas, (2004b) Cellular PVC-U, Current technology and future challenges. In: Proceedings of 6th International Conference of Blowing Agent and Foaming Process, 16–17 May, Munich, Germany, pp. 1–12. .

- J. L. Throne, "Thermoplastic Foam extrusion", (2003).

- Nexttool, "PVC Foam Extrusion", 2004.

185

- Bahar Azimpour, Frederic Marchand. Effect of Calcium Carbonate Particle Size on PVC Foam. JOURNAL OF VINYL & ADDITIVE TECHNOLOGY; 2006; 12(2), 55-57.

- British plastic and rubber (2003), Mineral fillers for PVC reinforcement (compounding), British plastic and rubber publication, November, 2003, pp. 4–6.

- Jiang H, Kamdem D. (2004) Development of poly (vinyl chloride)/wood composites. A literature review. J Vinyl Addit Techn; 10(2): 59-69.

- Swain, S. K., Dash, S., Kisku, S. K., & Singh, R. K. (2014). Thermal and oxygen barrier properties of chitosan bionanocomposites by reinforcement of calcium carbonate nanopowder. Journal of Materials Science & Technology, 30(8), 791-795.

- Ráthy, I., Kuki, Á., Borda, J., Deák, G., Zsuga, M., Marossy, K., and Kéki, S. (2012) Preparation and characterization of poly(vinyl chloride)– continuous carbon fiber composites. J. Appl. Polym. Sci.; 124(1): 190-194.

- Deshmukh, S. P., Rao, A. C., Gaval, V. R., and Mahanwar, P. A. (2011) Mica-Filled PVC Composites: Effect of Particle Size, Filler Concentration, and Surface Treatment of the Filler, on Mechanical and Electrical Properties of the Composites, J THERMOPLAST COMPOS; 24: 583.

- Katz, H., Mileski, H. (1987), Handbook of Fillers for Plastics. New York, pp. 132-152.

- White L, J. (1990), Principles of Polymer Engineering Rheology. USA. 1990.

- Kinsella, M., Murray, D., Crane, D., Mancinelli, J., and Kranjc, M. (2001),In: International SAMPE Technical Conference, November, 33, pp. 1644-1657.

- Zhou, Y. S., Liu, S., Liu, J. H., Sun, J. L., and Zhou, M. J. Rheological and Mechanical Properties of Fly Ash Microspheres Modified PVC. J Plastics 2012; 6: 008.

- Sushma, S. P., and Kumar, A. K. Hardness and Tensile Testing of PVC and Fly Ash Composite. Advance Research and Innovations in Mechanical, Material Science, Industrial Engineering and Management- ICARMMIEM-2014.

- Nath DCD, Bandyopadhyay S, Boughton P, Yu A, Blackburn D and White C. High-strength biodegradable poly(vinyl alcohol)/fly ash composite films. J Appl Polym Sci, (2010c) 117:114–121.

- Rohatgi PK, Matsunaga T, Gupta N (2009) Compressive and Ultrasonic Properties of Polyester/Fly Ash Composites, J Mat Sci 44(6): 1485-1493.

- Labella M, Zeltmann SE, Shunmugasamy VC, Gupta N, Rohatgi PK (2014) Mechanical and thermal properties of fly ash/vinyl ester syntactic foams. J. Fuel 121: 240–249.

- Jin-hu, D., Zhen-wu, S., Shou-jie, Y., and Ben-li, Q. The Properties Research of PVC/Fly Ash Composite Board. China Plastics Industry 2011; 5: 113-116.

- Senapati AK, Bhatta A, Mohanty S, Mishra PC, Routra BC (2014) An Extensive Literature Review on the Usage of Fly Ash as a Reinforcing Agent for Different Matrices. Int J Innov Sci Mod Eng 2(3); 4-9.

- Chow JD, Chai WL, Yeh CM and Chuang FS. Recycling and Application Characteristics of Fly Ash from Municipal Solid Waste Incinerator Blended with Polyurethane Foam. J Environ Eng Sci, 2008; 25(4): 461-471.

- Guhanathan S and Sarojadevi M. Studies on interface in polyester/fly-ash particulate composites. J Comp Interface, 2004; 11:43–66

- Bishoyee N, Dash A, Mishra A, Patra S and Mahapatra SS. A Grey-Based Taguchi Approach for Characterization of Erosive Wear Phenomenon of Glass–Polyester Fly Ash Filled Composites. J Polym Environ, 2010; 18:177–187

- N. Usta. Investigation of Fire Behavior of Rigid Polyurethane Foams Containing Fly Ash and Intumescent Flame Retardant by Using a Cone Calorimeter. J Appl Polym Sci, 2012; 124, 3372–3382.

- Vijaykumar HK, Prashanth M, Saheb S and Nayak V. Experimental Investigation of the Tensile strength and Compressive strength of Fly Ash Core Sandwiched Composite Material. J Int org Sci Res, 2014; 4(6): 1-10.

- Wasekar PA, Kadam PG, Mhaske ST(2012) Effect of Cenosphere Concentration on the Mechanical, Thermal, Rheological and Morphological Properties of Nylon 6, J Minerals and Materials Characterization and Engineering 11: 807-812.

- Guptaa N, Woldesenbetb E and Mensah P. Compression properties of syntactic foams: effect of cenosphere radius ratio and specimen aspect ratio. J Composites: Part A, 2004; 35: 103–111.

- Kulkarni MB, Bambole VA, Mahanwar PA (2014) Effect of particle size of fly ash cenospheres on the properties of acrylonitrile butadiene styrene-filled composites, J Thermoplast Compos Mater 27(2): 251-267.

- Chauhan SR, Thakur S (2012) Effect of Micro Size Cenosphere Particles Reinforcement on Tribological Characteristics of Vinylester Composites under Dry Sliding Conditions, J Minerals and Materials Characterization and Engineering 11: 938-946.

- Manjunath BR, Sadasivamurthy P, Reddy PV, Haridas RK (2013) Studies on Cenospheres as Fillers for PVC Compounds for Applications in Electrical Cables, J American Institute of Chemists 86(1): 10- 14.

- Aashis SR,Saravanan S, Kishore, Praveen CR, Madras G (2014) Dielectric Impedance Studies of Poly(vinyl butyral)–Cenosphere Composite Films, Polym Compos 35:1636-1643.

- Thakur S, Chauhan SR (2013) Study on mechanical and tribological behavior of cenosphere filled vinylester composites- A Taguchi method. Indian J Eng Mater Sci 20: 539-548.

- Chand N, Sharma P, Fahim M (2011) Abrasive Wear Behavior of LDPE Filled with Silane Treated Flyash Cenospheres, J Compos Interfaces 18: 575–586.

- [54] Chand N, Sharma P, Fahim M (2010) Correlation of mechanical and tribological properties of organosilane modified cenosphere filled high density polyethylene, J Mat Sci Eng 527: 5873-5878.

- Sharma J, Chand N, Bapat MN (2012) Effect of cenosphere on dielectric properties of low density polyethylene, Results Phys 2: 26–33

- Ismail K.N., Hussin K., Idris M. S., "Physical, chemical and mineralogical properties of fly ash", 2007, J. Nuclear and Related technology, 4, 47-51.

- Anandhan S, Sundar SM, Senthil T, Mahendran AR and Shibulal GS. Extruded poly(ethylene-co-octene)/fly ash composites-value added products from an environmental pollutant. J Polym Res, 2012; 19:9840-9851.

- Nath DCD, Bandyopadhyay S, Yu A, Zeng Q and Das T, Blackburn D, White C. Structure–property interface correlation of fly ash–isotactic polypropylene composites. J Mater Sci, 2009; 44:6078–6089.

- Nath DCD, Bandyopadhyay S, Yu A, Blackburn D and White C. Novel observations on kinetics of nonisothermal crystallization in fly ash filled isotactic-polypropylene composites. J Appl Polym Sci. (2010a); 115:1510–1517.

- Nath DCD, Bandyopadhyay S, Yu A, Blackburn D and White C. High strength bio-composite films of poly(vinyl alcohol) reinforced with chemically modified-fly ash. J Mater Sci, (2010d); 45:1354–1360.

- Doddamani MR and Kulkarni SM. Dynamic response of fly ash reinforced functionally graded rubber composite sandwiches- a Taguchi approach. Int J Eng Sci Tech, 2011; 3(1):166-182.

- S. Ditta, A.J. Wilkinson, G.M. McNally, and W.R. Murphy, *J. Vinyl & Addit. Technol.*, 10(4), 174 (2004).

- D. Braun, *J. Progress in polymer science*, 27(10), 2171(2002).

- N. Sombatsompop, and K. Sungsanit, *J. Appl. Polym. Sci.*, 92(1), 84 (2004).

- S. Ulutan, *J. Appl. Polym. Sci.*, 69(5), 865 (1998).

- Deshmukh, S. P., and A. C. Rao. Mica Filled PVC Composites: Performance Enhancement in Dielectric and Mechanical Properties with Treated/Untreated Mica of Different Particle Size and Different Concentration. *JMMCE* 2012; 11(02): 169.

- Wang, X., You, F., Zhang, F. S., Li, J., and Guo, S. Experimental and theoretic studies on sound transmission loss of laminated mica filled poly (vinyl chloride) composites. J Appl Polym Sci 2011; 122(2): 1427-1433.

- Jiang, H., Pascal K. D., Bezubic, B. and Ruede, P. Mechanical properties of poly(vinyl chloride)/wood flour/glass fiber hybrid composites. *J Vinyl Addit Technol* 2003; 9: 138–145.

- Tungjitpornkull, S., and N. Sombatsompop. Processing technique and fiber orientation angle affecting the mechanical properties of E-glass fiber reinforced wood/PVC composites. *J Mater Process Tech* 2009; 209 (6): 3079-3088.

- Tungjitpornkull, N., Chaochanchaikul, K., Sombatsompop, N. Mechanical Characterization of E-Chopped Strand Glass Fiber Reinforced Wood/PVC Composites. *J Thermoplast Compos* 2007; 20(6): 535-550.

- Matuana, L. M., Park, C. B. and Balatinecz, J. J. Cell morphology and property relationships of microcellular foamed PVC/wood-fiber composites. *J Polym Eng Sci* 1998, 38: 1862–1872.

- Sreekanth, M.S. and Bambole, V.A. (2009) Effect of Particle Size and Concentration of Fly ash on Properties of Polyester Thermoplastic Elastomer Composites. Journal of Minerals & Materials Characterization & Engineering, 8, 237-248.

- Matsunaga T, Kim JK, Hardcastle S and Rohatgi PK. Crystalinity and selected properties of fly ash particles. *J Mat Sci Eng*, 2002;A325: 333-343.

- White SC and Case ED. Characterization of fly ash from coal-fired power plants. *J Mat Sci*, 1990; 25: 5215-5219.

- Gamage, N., Liyanage, K., Fragomeni, S. and Setunge, S., 2013. Overview of different types of fly ash and their use as a building and construction material.

- Khairul NI, Kamarudin H and Mohd SI. Physical, chemical, and mineralogical properties of fly ash. *J Nucl Relat Tech*, 2007; 4: 47-51.

- Drozhzhin VS, Danilin LD, Pikulin IV, Khovrin AN, Maximova NV, Regiushev SA, Pimenov VG (2005) Functional Materials on the Basis of Cenosphere. WOCA Conference, Kentucky, April, 1-9.

191

- Kadam P, Pawar B, Mhaske S (2013) Studies in effect of low concentration of cenosphere on mechanical, thermal, electrical, crystallinity, colorimetric and morphological properties of epoxy cured with triethylenettramine. J Minerals and Materials Characterization and Engineering 1: 117-123.

- Das A, Satapathy BK (2011) Structural, thermal, mechanical and dynamic mechanical properties of cenosphere filled polypropylene composites. J Mat Des 32: 1477–1484.

- Qiao J, Amirkhizi AV, Schaaf K and Nemat-Nasser S. Dynamic Mechanical Analysis of Fly Ash Filled Polyurea Elastomer. J Eng Mat Tech, 2011; 133: 110161-110167.

- Deepthi MV, Sharma M, Sailaja RRN, Anantha P, Sampathkumaran P and Seetharamu S, Mechanical and thermal characteristics of high density polyethylene–fly ash Cenospheres composites. J Mat Des, 2010; 31:2051–2060.

- Nath DCD, Bandyopadhyay S, Yu A, Blackburn D, White C and Varughese S. Isothermal crystallization kinetics of fly ash filled iso-polypropylene composite-and a new physical approach. J Therm Anal Calorim. (2010b); 99:423–429.

- Y. Yoo, S. S. Kim, J. C. Won, K. Y. Choi, and J. H. Lee, *J. Polymer Bulletin*, 52(5), 373 (2004).

- Sahin, E.; Mahlicli, F. Y., Yetgin, S.; Balko¨se, D., J. Appl. Polym. Sci. 2012, 125, 1448–1455.

- Gummadi, J.; Kumar G.V.; Rajesh G. Intern. J. Modern Eng. Research (IJMER). 2012, 2(4): 2584-2590

- Parvaiz M. R.; Mohanty S.; Nayak K. S.; Mahanwar P. A. J. Min. Mater. Charac. Eng. 2010; 9(1): 25-41.

- Mudassir, H.; Lee, M. Progress in Natural Science: Materials International. 2014, 24(6): 579-587.

- Fillot, L.A.; Hajji, P. J. Vin. Add. Tech. 2006, 10, 108-114.

- Cruz, J.; Graman, P. Soc. Plas. Eng. 2009, 10, 1-3.

- Piszczek, K.; Tomaszewska, J.; Sterzynski, T. J. Polimery 2010, 55(2), 678-680.

- Iulianelli, C.G.V.; Maciel, P.M.C.; Tavares, M.I.B. J. Macromol. Symp. 2011; 299(300), 227–233.

- Ra´thy, I.; Kuki, A.; Borda, J. J. Appl. Polym. Sci., 2012, 124, 190–194.

- Helmuth, R. (1987). Fly ash in cement and concrete (No. SP040. 01T).

- Halstead, W. J. (1986). Use of fly ash in concrete. NCHRP Synthesis of Highway Practice, (127).

- Owens, P. L. (1979). Fly ash and its usage in concrete. Concrete, 13(7).

- Dubey, A. M. S. (2015). A review on the study of compressive strength of concrete due to partial replacement of ordinary portland cement with ground granulated blast furnace slag and fly ash. South Asia Journal of Multidisciplinary Studies, 1(10).

- Singh, K. and Benipal, G.S., 2015. Strengthening of cement concrete using fly ash and metakoline: A review. Volume, 3, pp.722-725.

- Lodi PC and Souza BBD. Thermo-gravimetric Analysis (TGA) after Different Exposures of High Density Polyethylene (HDPE) and Poly Vinyl Chloride (PVC) Geomembranes. Elec J Geotech Eng, 2012; 17:3339-3349.

- E. B. Rabinovitch *and* P.C. Booth, J. Vinyl Technology, Vol. 12, (1990).

- Fu, S. Y., Feng, X. Q., Lauke, B., & Mai, Y. W. (2008). Effects of particle size, particle/matrix interface adhesion and particle loading on mechanical properties of particulate–polymer composites. Composites Part B: Engineering, 39(6), 933-961.

- Shawabkeh, R., Khan, M. J., Al-Juhani, A. A., Wahhab, H. I. A. A., & Hussein, I. A. (2011). Enhancement of surface properties of oil fly ash by chemical treatment. Applied Surface Science, 258(5), 1643-1650.

- McCarthy, M. J., Jones, M. R., Zheng, L., Robl, T. L., & Groppo, J. G. (2013). Characterising long-term wet-stored fly ash following carbon and particle size separation. Fuel, 111, 430-441.

- Stellacci, P., Liberti, L., Notarnicola, M., & Bishop, P. L. (2009). Valorization of coal fly ash by mechano-chemical activation: Part I. Enhancing adsorption capacity. Chemical Engineering Journal, 149(1), 11-18.

- Patil, A. G., Mahendran, A., Selvakumar, M., & Anandhan, S. (2016). Ductility and Flame Retardancy Enhancement of PVC by Nanostructured Fly Ash. Silicon, 1-11.

- Dharmalingam, U., Dhanasekaran, M., Balasubramanian, K., & Kandasamy, R. (2015). Surface treated fly ash filled modified epoxy composites. Polímeros, 25(6), 540-546.

- Paul, K. T., Satpathy, S. K., Manna, I., Chakraborty, K. K., & Nando, G. B. (2007). Preparation and characterization of nano structured materials from fly ash: A waste from thermal power stations, by high energy ball milling. Nanoscale Research Letters, 2(8), 397.

- Li, H., Chen, Y., Cao, Y., Liu, G., & Li, B. (2016). Comparative study on the characteristics of ball-milled coal fly ash. Journal of Thermal Analysis and Calorimetry, 124(2), 839-846.

- Tham, D. Q., Thu Trang, N. T., Chinh, N. T., Mai, T. T., Giang, N. V., Kim Dung, N. T., & Hoang, T. (2016). Fabrication and characterization of masterbatches made from poly (vinyl chloride) and modified fly ash. Vietnam Journal of Chemistry, 54(2), 217.

- Kulkarni, S. M. (2002). Effects of surface treatments and size of fly ash particles on the compressive properties of epoxy based particulate composites. Journal of materials science, 37(20), 4321-4326.

- Feldman, D. (2002). Polymer weathering: photo-oxidation. Journal of Polymers and the Environment, 10(4), 163-173.

- Kim, Changhwan, Wootae Ki, SangMyung Kim, and Jinyong Shin. "The Influence of Weathering Conditions on the Outer Membrane of Biogas with Plasticized PVC." 47, no. 2 (2014): 57-62.

- Chaochanchaikul, Kantima, Vichai Rosarpitak, and Narongrit Sombatsompop. "Photodegradation profiles of PVC compound and wood/PVC composites under UV weathering." Express Polym. Lett 7, no. 2 (2013): 146-160.

- Yang, Xudong, Xiaowei Xu, Yongsheng Yan, and Fangjuan Wang. "Photo-Oxidation of PVC-Coated Membrane Material Under Different Light Sources [dagger]." Asian Journal of Chemistry 26, no. 17 (2014): 5777.

- Shin, Myoungsu, Kyuhun Kim, Seong-Woo Gwon, and Soowon Cha. "Durability of sustainable sulfur concrete with fly ash and recycled aggregate against chemical and weathering environments." Construction and building materials 69 (2014): 167-176.

- Goh, C. K., Valavan, S. E., Low, T. K., & Tang, L. H. (2016). Effects of different surface modification and contents on municipal solid waste incineration fly ash/epoxy composites. Waste Management.

- Shanmugam, Nagendiran, Ibnelwaleed A. Hussein, Adel Badghaish, Abdelrahman Nasr Shuaib, Sarfaraz Ahmed Furquan, and Mohammed H. Al-Mehthel. "Evaluation of oil fly ash as a light stabilizer for epoxy composites: Accelerated weathering study." Polymer Degradation and Stability 112 (2015): 94-103.

- Ceskaa, Global Polymer Foam Market, https://www.ceskaa.com/market-research-reports/global-polymer-foam-market-report-2015-2020/, (2016), Accessed 5 April 2017

- Carnachan, R. J., Emulsion-derived (Poly HIPE) foams for structural materials applications, Dissertation, University of Durham, (2004).

- Hess K., Hinchcliffe S., Fracture Behavior of Polyvinyl Chloride Foam: A Literature Review, University of Colorado Boulder, (2014)

- Wikipedia, https://en.wikipedia.org/wiki/Polyvinyl_chloride, Accessed 10 April 2017.

- Annapragada S. K., Mechanism of foaming on polymer-paperboard composites, Georgia Institute of Technology Dissertation, 2007.

- Wikipedia, https://en.wikipedia.org/wiki/Azodicarbonamide, Accessed 5 March 2017

- Thomas, N.L. Handbook of Polymer Foams; Eds. D. Eaves; Rapra, Shrewsbury;UK; (2004c); Chapter 6, pp123-153.

- Aurora plastics, http://www.auroraplastics.com/products/auroralite-pvc-cellular-foam/, Accessed 5 April (2017).

- Qingdao extrusion Technology, http://www.extruder.com.cn/sheet/en/PVC-celuka-foam-sheet-extrusion-line.htm, Accessed 5 April (2017).

- Materion, "Processing PVC with MoldMAX Tools", (2011).

- Mining Media International, http://www.concreteproducts.com/news/news-scope/9513-post-epa-rule-fly-ash-consumption-eclipses-pre-recession-level.html#.WPDyC_nyvIU, Accessed 10 April (2017).

- Ramezanpour, A.A., Cement Replacement Materials, Properties, Durability, Sustainability, Chapter 2, PP 47-153, (2014).

- Anantharaman S., Sulfate and alkali silica resistance of class c & f fly ash replaced blended cements, Dissertation, Arizona State University, (2008).

- Thomas M., Optimizing the Use of Fly Ash in Concrete, Portland Cement Association, 2007.

- ASTM C618-92a. Standard Specification for Fly Ash and Raw or Calcined Natural Pozzolan for Use as Mineral Admixture in Portland Cement Concrete" American Society for Testing and Materials, Annual Book of ASTM Standards, Volume 04.02.

- American Coal Ash Association, Fly Ash Facts for Highway Engineer, Reported 13 June 2003.

- Hardjito D., Rangan B. V., Development and properties of low-calcium fly ash-based geopolymer concrete, Dissertation, Curtin University of Technology, Research Report GC 1, 2005.

- Ramme Tharaniyil, Coal Combustion Products Utilization Handbook, We Energies, Third Edition, 2013.

- Canadian Standards Association, Supplementary cementing materials and their use in concrete construction. CSA, Rexdale, ON, CAN-A23.5-M82, 1982.

- Sayhan İ., Use of fly ash as an alternative filler material in PVC-plastisols, Dissertation, İzmir Institute of Technology, 2010.

- Sen S., Physical properties of cenosphere, Dissertation National Institute of Technology, Rourkela, 2014.

- BetterChemText, http://abetterchemtext.com/Condensed/quartz.htm, Accessed April 2017.

- StackExchange, https://chemistry.stackexchange.com/questions/9730/why-dont-molecules-of-ionic-compounds-exist, Accessed April 2017.

- Wu, W., Wu, Z., Yu, T., Jiang, C. and Kim, W.S., (2015). Recent progress on magnetic iron oxide nanoparticles: synthesis, surface functional strategies and biomedical applications. Science and technology of advanced materials, 16(2), p.023501.

- 123Stock Photos, https://www.123rf.com/photo_40236097_calcium-oxide-cao-quicklime-burnt-lime--crystal-structure-essential-ingredient-of-cement-oxygen-atom.html, Accessed April 2017.

- Liu, Y.C., He, H., Xu, W.Q. and Yu, Y.B., (2007). Mechanism of heterogeneous reaction of carbonyl sulfide on magnesium oxide. Journal of Physical Chemistry A, 111(20), pp.4333-4339.

- A.L. Kelly, R.M. Rose, R. Spares, P.D. Coates, and S.J. Weston, J. Vinyl Addit. Technol., 11(3), 119 (2002).

- Ghanbar S, Yousefzade O, Hemmati F, et al. Microstructure and thermal stability of polypropylene/ bagasse composite foams: design of optimum void fraction using response surface methodology. JTCM 2014; 1(1): 1–18.

- Gdoutos EE, Daniel MI and Wang K. Multiaxial characterization and modeling of a PVC cellular foam. JTCM 2001; 14(5): 365–373.

- Matuana LM and Li Q. Statistical modeling and response surface optimization of extruded HDPE/wood-flour composite foams. JTCM 2004; 14(2): 185–199.

- Zarandi, F., Amin, M. and Pillai, K.M., 2017. Spontaneous Imbibition of Liquid in Glass fiber Wicks, Part II: Validation of a Diffuse-front Model. AIChE Journal.

- Kord B. Preparation and characterization of lignocellulosic material filled polyethylene composite foams. JTCM 2012; 25(8): 917–926.

- Mohammadian, Z., Rezaei, M. and Azdast, T., 2016. Microstructure, physical, and mechanical properties of LDPE/UHMWPE blend foams: An experimental design methodology. Journal of Thermoplastic Composite Materials, 29(9), pp.1229-1260.

- Ma J, Duan Z, Xue C, et al. Morphology and mechanical properties of EVA/OMMT nanocomposites foams. JCTM 2013; 26(4): 555–569.

- Bose S and Mahanwar PA. Effect of fly ash on the mechanical, thermal, dielectric, rheological and morphological properties of filled nylon 6. JMMCE 2004; 3(2): 65–89.

- Liu, P., Zhao, M. and Guo, J., (2006). Thermal stabilities of poly (vinyl chloride)/calcium carbonate (PVC/CaCO3) composites. Journal of Macromolecular Science, Part B: Physics, 45(6), pp.1135-1140.

- Wikipedia BET theory, http://cme.nuk.edu.tw/files/personal_subject/418_e3ca1589.pdf, Accessed May 2017.

- Behera, R.K., 2010. Characterization of Fly ash for their effective management and utilization (Doctoral dissertation, NATIONAL INSTITUTE OF TECHNOLOGY ROURKELA).

- Brown, R.C. and Dykstra, J., (1995) Systematic errors in the use of loss-on-ignition to measure unburned carbon in fly ash. Fuel, 74(4), pp.570-574.

- Ranjbar, N., Mehrali, M., Behnia, A., Pordsari, A.J., Mehrali, M., Alengaram, U.J. and Jumaat, M.Z., 2016. A comprehensive study of the polypropylene fiber reinforced fly ash based geopolymer. PloS one, 11(1), p.e0147546.

- Fauzi, A., Nuruddin, M.F., Malkawi, A.B. and Abdullah, M.M.A.B., 2016. Study of Fly Ash Characterization as a Cementitious Material. Procedia Engineering, 148, pp.487-493.

- Sin, M.C., Tan, I.K.P., Annuar, M.S.M. and Gan, S.N., 2012. Thermal behaviour and thermodegradation kinetics of poly (vinyl chloride) plasticized with polymeric and oligomeric medium-chain-length poly (3-hydroxyalkanoates). Polymer degradation and stability, 97(11), pp.2118-2127.

- Inoue, T., Miyazaki, M., Kamitani, M., Kano, J. and Saito, F., 2004. Mechanochemical dechlorination of polyvinyl chloride by co-grinding with various metal oxides. Advanced Powder Technology, 15(2), pp.215-225.

- Sivalingam, G. and Madras, G., 2004. Effect of metal oxides/chlorides on the thermal degradation of poly (vinyl chloride), poly (bisphenol A carbonate), and their blends. Industrial & engineering chemistry research, 43(24), pp.7716-7722.

- Uegaki, Y. and Nakagawa, T., 1977. Thermal dehydrochlorination of poly (vinyl chloride). I. Effect of iron oxide on the rate of dehydrochlorination. Journal of Applied Polymer Science, 21(4), pp.96

- Gupta, M.C. and Viswanath, S.G., 1998. Role of metal oxides in the thermal degradation of poly (vinyl chloride). Industrial & engineering chemistry research, 37(7), pp.2707-2712.5-973.

- Hassan, A., Bakar, A.A., Wahit, M.U. and TUEEN, B., 2009. Structure-properties relationship of hybrid talc/calcium carbonate filled impact modified PVC composites.

- Zeng, X.F., Wang, W.Y., Wang, G.Q. and Chen, J.F., 2008. Influence of the diameter of CaCO3 particles on the mechanical and rheological properties of PVC composites. Journal of Materials Science, 43(10), pp.3505-3509.

- Hashim, P.D.S., Hassan, P.D.A., Yen, C.S., Penyelidikan, N. and Polimer, J.K., (2006), Mechanical, Chemical and Flammability Properties of ABS/PVC Blends, UNIVERSITI TEKNOLOGI MALAYSIA.

- Gandhi S, Abiramipriya P, Pooja N, Juliat Latha Jeyakumari J, Yelil Arasi A, Dhanalakshmi V, Gopinathan Nair MR, Anbarasan R. Synthesis and characterizations of nano sized MgO and its nanocomposite with poly(vinyl alcohol), Journal of Non-Crystalline Solids, 357, 2011, 181–185.

- Yan X, He Q, Zhang X, Gu H, Chen H, Wang Q, Sun L, Wei S, Guo Z. Magnetic Polystyrene Nanocomposites Reinforced with Magnetite Nanoparticles, Macromol. Mater. Eng, 299, 2014, 485–494.

- Hachani, S.E., Meghezzi, A., Nebbache, N. and Slimani, M., (2016) Impact of Magnesium Oxide incorporation on tensile and hardness properties of Polystyrene/Magnesium Oxide composites, Journal of Chemical and Pharmaceutical Sciences, 9(4), 2664-67.

- Leong, Y.W., Bakar, A., Ishak, Z.A., Ariffin, A. and Pukanszky, B., 2004. Comparison of the mechanical properties and interfacial interactions between talc, kaolin, and calcium carbonate filled polypropylene composites. Journal of Applied Polymer Science, 91(5), pp.3315-3326.

- Mueller, R., Kammler, H.K., Wegner, K. and Pratsinis, S.E., 2003. OH surface density of SiO2 and TiO2 by thermogravimetric analysis. Langmuir, 19(1), pp.160-165.

- Sutter L., (2004), Class C and Class F Fly Ash: Comparisons, Applications, and Performance, Michigan Technological University.

- Rupa Chakrabarti, Molay Das and Debabrata Chakraborty, Inc. J Appl Polym Sci., 93, 2721-2730, 2004.

- Pedrazzoli, D., Pegoretti, A. and Kalaitzidou, K., 2015. Interfacial interactions in silica-reinforced polypropylene nanocomposites and their impact on the mechanical properties. Polymer Composites.

- Metın, D., Tihminlioğlu, F., Balköse, D. and Ülkü, S., 2004. The effect of interfacial interactions on the mechanical properties of polypropylene/natural zeolite composites. Composites Part A: Applied Science and Manufacturing, 35(1), pp.23-32.

- Rostami, M., Mohseni, M. and Ranjbar, Z., 2012. An attempt to quantitatively predict the interfacial adhesion of differently surface treated nanosilicas in a polyurethane coating

matrix using tensile strength and DMTA analysis. International Journal of Adhesion and Adhesives, 34, pp.24-31.

- Firoozian, P., Akil, H.M. and Abdul Khalil, H.P.S., 2010. Prediction of mechanical properties of mica-filled epoxy composite using various mechanical models. Journal of Reinforced Plastics and Composites, 29(15), pp.2368-2378.

- Adeosun, S.O., Usman, M.A., Ayoola, W.A. and Bodud, M.A., 2013. Physico-Mechanical Responses of Polypropylene-CaCO 3 Composite.

- Aguilera-Camacho, L.D., Hernández-Navarro, C., Moreno, K.J., García-Miranda, J.S. and Arizmendi-Morquecho, A., 2015. Improvement effects of CaO nanoparticles on tribological and microhardness properties of PMMA coating. Journal of Coatings Technology and Research, 12(2), pp.347-355.

- Usman, M.A., Adeosun, S.O. and Osifeso, G.O., 2012. Optimum calcium carbonate filler concentration for flexible polyurethane foam composite. Journal of Minerals and Materials Characterization and Engineering, 11(03), p.311.

- Zuiderduin, C.J. and Gaymans, R.J., 2005. Toughening of polypropylene with calcium carbonate particles. Polymeric Materials Science and Engineering, 93.

- Lazzeri, A., Zebarjad, S.M., Pracella, M., Cavalier, K. and Rosa, R., 2005. Filler toughening of plastics. Part 1—the effect of surface interactions on physico-mechanical properties and rheological behavior of ultrafine CaCO3/HDPE nanocomposites. Polymer, 46(3), pp.827-844.

203

- Cho, J., Joshi, M.S. and Sun, C.T., 2006. Effect of inclusion size on mechanical properties of polymeric composites with micro and nano particles. Composites Science and Technology, 66(13), pp.1941-1952.

- Sharma, A.K. and Mahanwar, P.A., 2010. Effect of particle size of fly ash on recycled poly (ethylene terephthalate)/fly ash composites. International Journal of Plastics Technology, 14(1), pp.53-64.

- Thongsang, S. and Sombatsompop, N., 2006. Effect of NaOH and Si69 treatments on the properties of fly ash/natural rubber composites. Polymer composites, 27(1), pp.30-40.

- Ghasemi, I., Azizi, H. and Naeimian, N., 2009. Investigation of the dynamic mechanical behavior of polypropylene/(wood flour)/(kenaf fiber) hybrid composites. Journal of Vinyl and Additive Technology, 15(2), pp.113-119.

- Ghasemi, I. and Farsi, M., 2010. Interfacial behavior of wood plastic composite: effect of chemical treatment on wood fibers. Iranian Polymer Journal, 19(10), pp.811-818.

- Zare, Y., Daraei, A., Vatani, M. and Aghasafari, P., 2014. An analysis of interfacial adhesion in nanocomposites from recycled polymers. Computational Materials Science, 81, pp.612-616.

- Százdi, L., Pukánszky, B. and Vancso, G.J., 2006. Quantitative estimation of the reinforcing effect of layered silicates in PP nanocomposites. Polymer, 47(13), pp.4638-4648.

- Százdi, L., Pozsgay, A. and Pukánszky, B., 2007. Factors and processes influencing the reinforcing effect of layered silicates in polymer nanocomposites. European Polymer Journal, 43(2), pp.345-359.

- Adams, J.M., 1993. Particle size and shape effects in materials science: examples from polymer and paper systems. Clay Minerals, 28(4), pp.509-530.

- Kubat, J., Rigdahl, M. and Welander, M., 1990. Characterization of interfacial interactions in high density polyethylene filled with glass spheres using dynamic-mechanical analysis. Journal of Applied Polymer Science, 39(7), pp.1527-1539.

- Ciullo, P.A., 1996. Industrial minerals and their uses: a handbook and formulary. William Andrew.

- Qin, Q.H., 2015. 1–Introduction to the composite and its toughening mechanisms. Toughening mechanisms in composite materials, pp.1-32.

Chapter 9- Appendices

Appendix A) Preliminary results of fly ash surface treatment by NaOH solution

8A.1. Fly Ash Surface Treatment

Class-F fly ash powder is surface treated using alkaline solution. First, 3M NaOH solution was prepared. Then, 25micorn particle sized fly ash was mixed with NaOH solution in the ratio of 1:3 in a 500ml flask with reflux condenser under stirring at 500rpm for 4 hours at 60°C. The alkali treated fly ash was washed with DI water until neutral pH followed by vacuum filtration. Then it was dried in a vacuum oven at 90°C overnight.

8A.2. Preliminary results

Surface treating of fly ash, N-(25-FA-F), decreases its specific gravity, which is due to formation of highly porous media during surface treatment of fly ash with NaOH solution. The measure surface gravity of N-25-FA-F is 1.7, which in comparison with the specific gravity of 25miron sized fly ash, 2.1, is much lower.

BET results are also reported in Table 8-1. Alkali-surface treated fly ash has an about six times larger BET surface area, ten times larger BJH cumulative surface area of pores and thirty times larger pore volume in comparison with 25-FA-F. The significant difference between the values of the specific surface area in 25-FA-F and N-(25-FA-F) can be explained by the presence of the smaller particles with the porous structure of due to alkali surface treatment of fly ash.

XRD spectrum of N-25-FA-F is also shown in Figure 8-1. It seems that alkali surface treatment purifies N-(25-FA-F) with more of quartz, mullite, iron oxide and calcium oxide crystals as

compared to 25-FA-F. It is also noticeable percentage of crystalline phase increases from 40.9 to 47.4 as per of alkali treatment. These results are consistent with EDX results presented earlier.

Table 0-1- 25micorn sized treated and untreated Fly ash physical properties

	BET Surface Area m²/g	BJH cumulative surface area of pores (17-3000Å diameter) m²/g	Pore Volume mm³/g	Pore Size Å
25-FA-F	7.86	5.28	8.55	43.48
N-25-FA-F	47.64	50.01	260.29	218.55
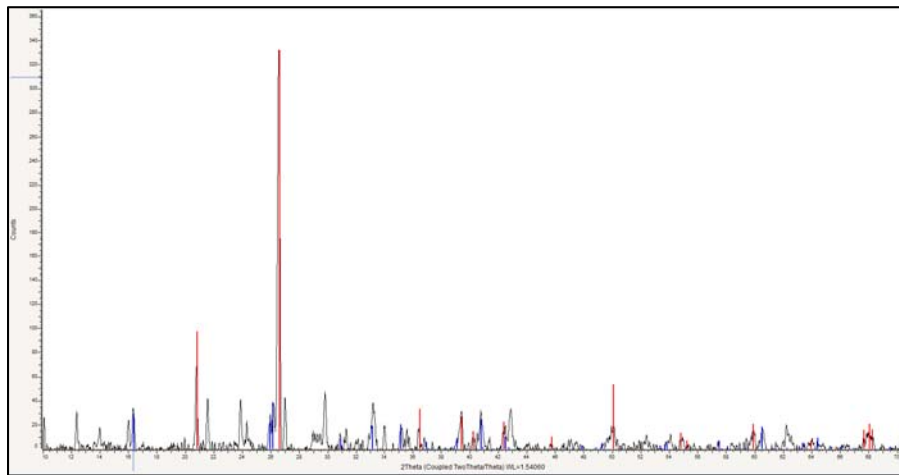
Figure 0-1- XRD Spectrum of surface treated fly ash, N-(25-FA-F)

SEM images i9n Figure 8-2 also show morphology of alkali surface treated fly ash, N-(25-FA-F). Comparing morphology of N-25-FA-F with 25-FA-F (Figure 5-7) reveals that the spherical structure of fresh fly ash has been destroyed during treatment and the average particle size was reduced. During alkali treatment, both amorphous and crystalline phases will be dissolved and thereafter recrystallization occurs which consequently results in increase of the amount of crystallinity.
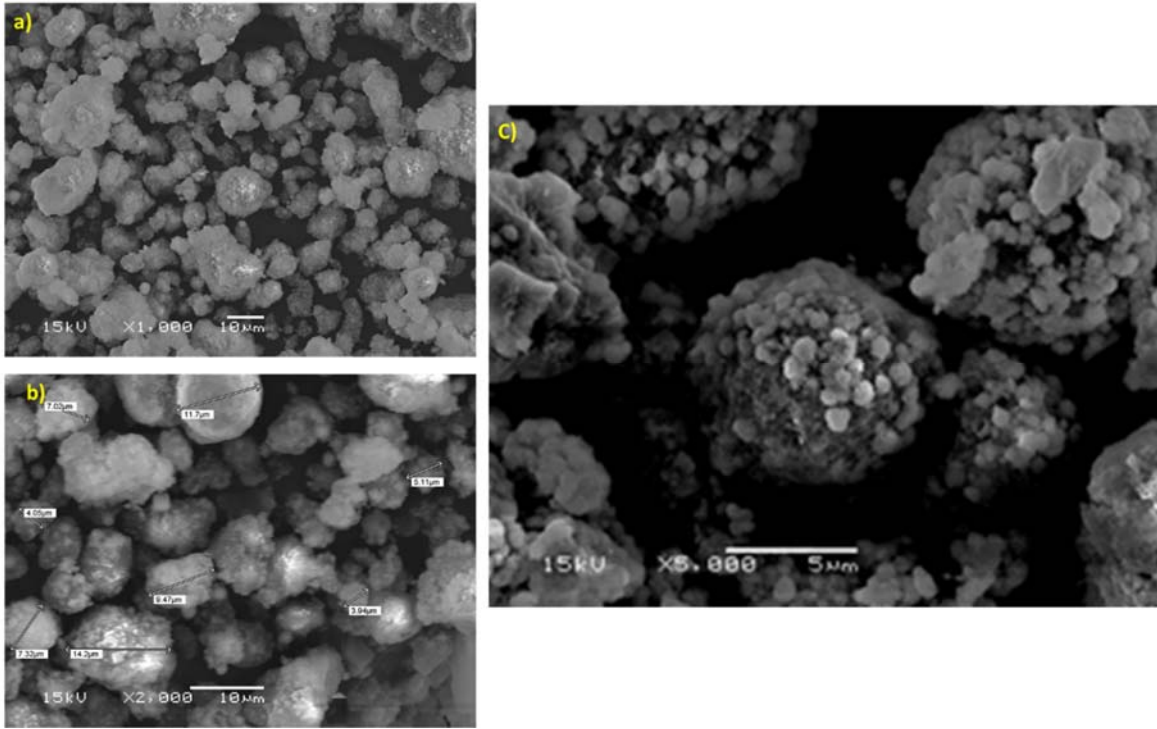
Figure 0-2-SEM image of surface treated fly ash, N-25-FA-F

Appendix B) Effect of Cenosphere Fly Ash on the Thermal, Mechanical, and Morphological Properties of Rigid PVC Foam Composites

8B.1. Experimental: *Preparation of PVC/Cenosphere foam*

PVC foam compounds were prepared using a high shear mixer (Gunther Pepenmeier, Machinen-u. Detmoid, Type: TSHK). The stabilizer was added at 52ºC, cenospheres and processing aids were added to the PVC resin at 52ºC and 58ºC; respectively. Finally, the lubricants and the blowing agents were added at 66ºC. PVC foam compounds containing 0, 6, 12, and 18phr cenosphere were extruded by using a 1.25 inch, 20:1 (L/D) single screw extruder (Themoplas New England Wire Machinery Co. Inc.) at a screw speed of 60 rpm. The extrusion temperature profile used for mixing was in the range of 158 to 175 °C. The compound formulations and sample codes are listed in Table 8-2. The sample without cenosphere is called pure and the other samples are named based on TG type cenosphere content.

Table 0-2: PVC foam composites formulation

Raw Materials (phr)	Pure	TG6	TG12	TG18
PVC resin	100	100	100	100
TG-cenosphere	0	6	12	18

8B.2. Results and Discussion

8B.2.1. Cenosphere Characterization

The density of the cenosphere was measured to be 0.75 g/cm^3 with a particle size ranging from 5 to 500µm. The SEM micrograph of cenosphere, shown in Figure 8-3, confirms a wide particle size distribution. The elemental and chemical compositions of cenosphere were characterized by SEM-EDX and XRD as shown in Figure 8-4 and Figure 8-5; respectively. XRD result shows that the cenospheres contain mainly Quartz and Mullite crystal phases
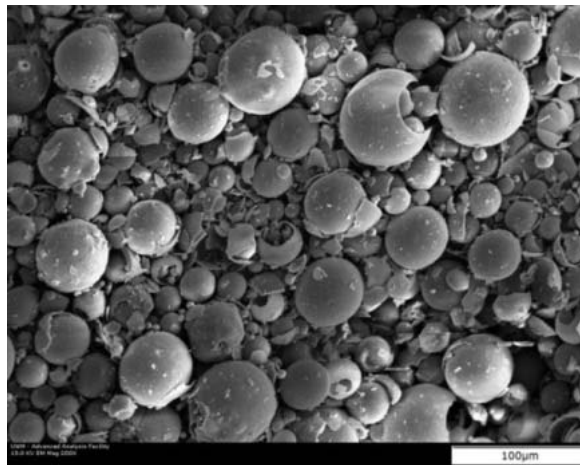
Figure 0-3: SEM micrograph of Cenospheres

Component	Content (Wt. %)
Silicon	35.91
Oxygen	27.87
Aluminum	21.78
Iron	5.16
Calcium	2.31
Magnesium	1.56
Sulfur	1.13
Potassium	0.95
Sodium	0.62
Carbon	0.57
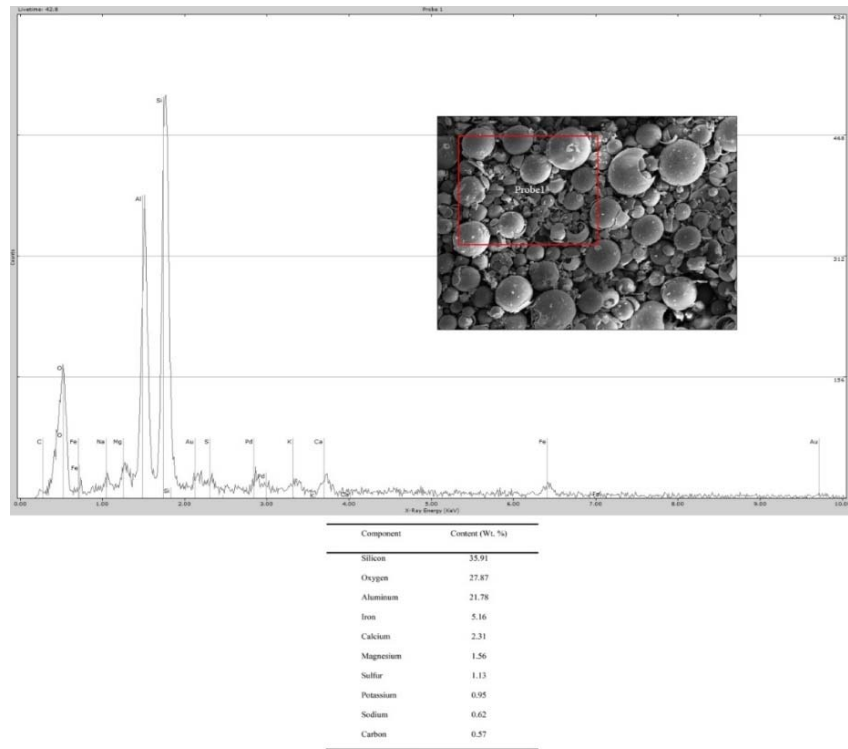
Figure 0-4: Elemental composition of cenosphere characterized by SEM/EDX

Crystal Phase	K	I	X_i (%)
Quartz	3.06	1500	30
Mullite	1	1100	69
Other Phases	-	-	1
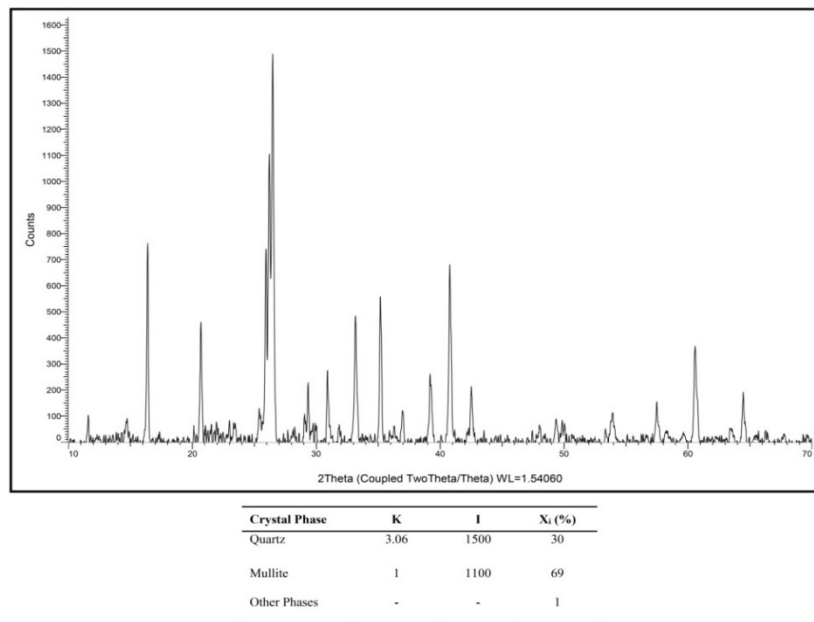
Figure 0-5: X-Ray diffraction spectrum and weight percentage of crystal phases of cenosphere

212

8B.3. PVC foam – Cenosphere Composite Characterization

8B.3.1. Physical properties

The measured density of the PVC foam composites are presented in Figure 4 and summarized in Table 8-3. The results show that the foam density increases by increasing the cenosphere content; indicating a denser composite microstructure with higher cenosphere loadings. By adding more filler, foaming process is hindered, thus resulting in smaller cells and denser matrix. This observation is consistent with the SEM images shown in Figure 8-6.
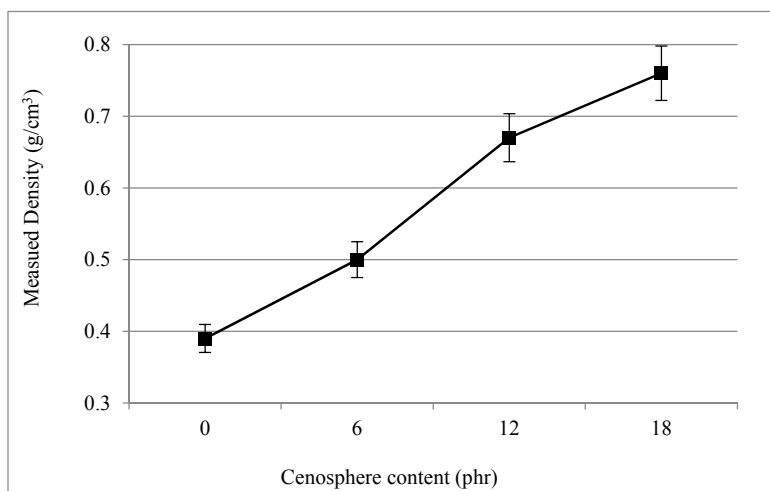
Figure 0-6: Measured Density of PVC foam composites versus cenosphere content (phr)

Table 0-3: Density of PVC foam composites

Sample	Pure	TG6	TG12	TG18
Measured Density (g/cm^3)	0.39	0.50	0.67	0.76

8B.3.2. Mechanical Properties

The tensile strength and tensile modulus of the foam composites as a function of the cenosphere content, are shown in Figures 8-7 and 8-8; respectively. It is evident that the tensile strength increases as the filler content increases in the composites, an indication of high strength and bonding energy between the filler and the matrix. Similarly, the incorporation of higher amounts of cenospheres in PVC foam, improves the elastic modulus of the composites. The higher tensile strength and elastic modulus of the composites may also be due to the strong interphase interaction between the PVC membranes and the cenospheres, which reduces the stress concentration sites under tensile loading.
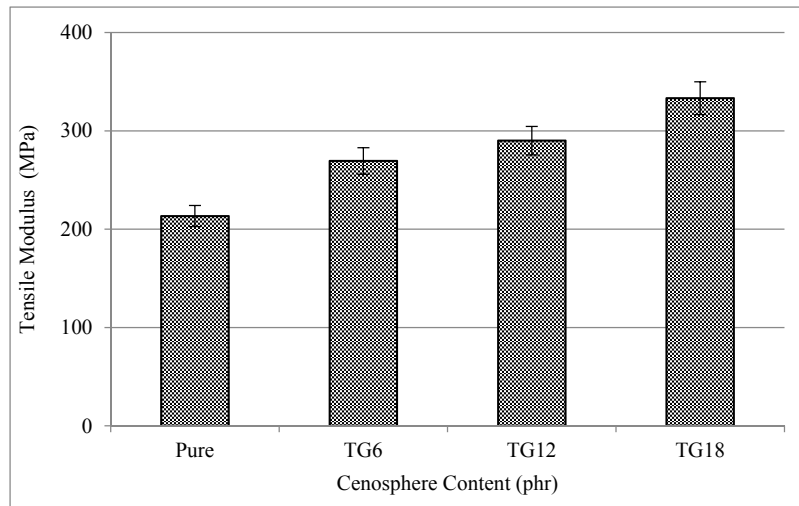
Figure 0-7: Tensile modulus of PVC-Cenosphere foam composites
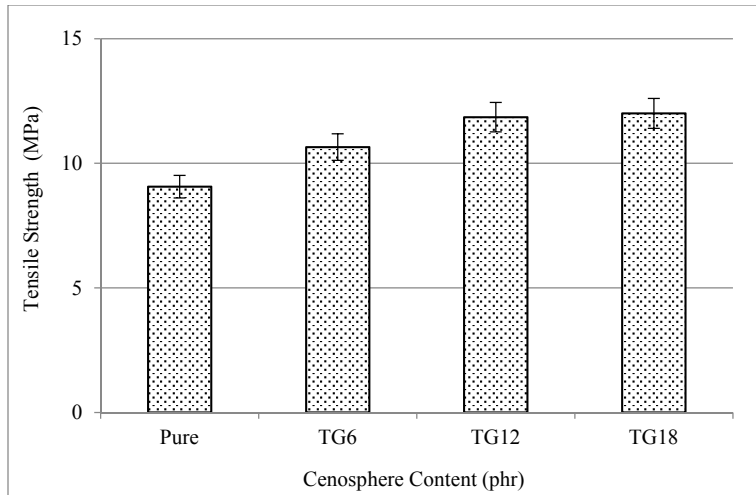
Figure 0-8: Tensile strength of PVC-Cenosphere foam composites

The effect of cenosphere content on the flexural strength and modulus of PVC foam composites are presented in Figures 8-9 and 8-10; respectively. The flexural modulus was found to increase 136% by adding 6phr cenospheres compared to pure samples, reaching up to 220% increase with 18phr cenosphere composites. The increase in flexural modulus indicates higher stiffness of the composites. Similarly, adding cenosphere particles to the PVC foam matrix increases flexural strength up to 24% in the samples with 18phr cenospheres. The increase in both the flexural strength and modulus in the presence of cenospheres indicates good interfacial interaction between the filler and the polymer matrix. Also, it indicates minimum aggregation of the cenosphere particles and good dispersion in the PVC matrix.
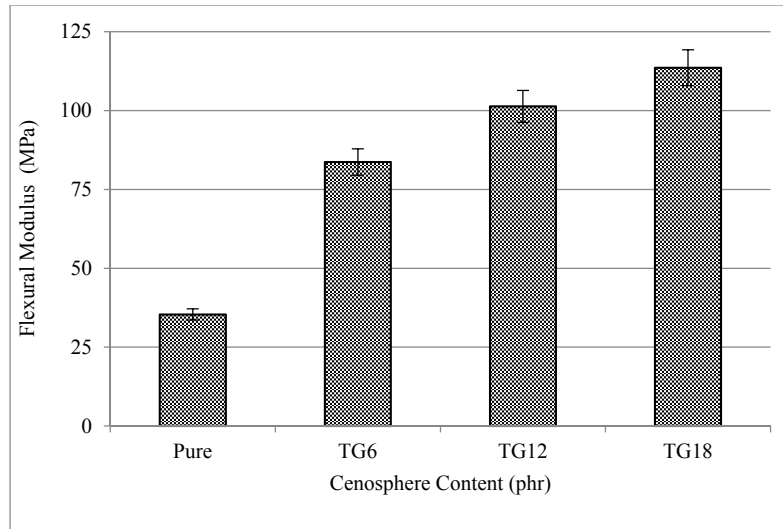
Figure 0-9: Flexural modulus of PVC-Cenosphere foam composites
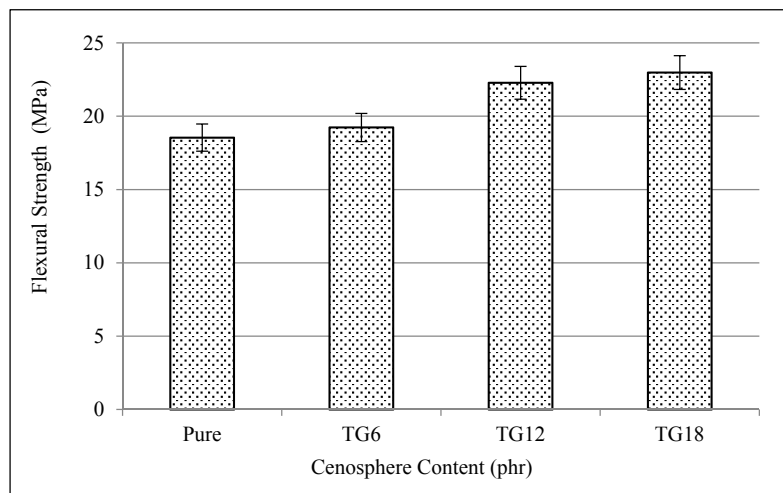
Figure 0-10: Flexural strength of PVC-Cenosphere foam composites

The effect of cenospheres on the impact strength of the composites is shown in Figure 8-11. By adding 6phr cenosphere particles, the impact strength and impact energy decrease. This can be attributed to the formation of stress concentration sites as a result of the strong interfacial bonding between the cenosphere particles and the matrix. On the other hand, due to the unique spherical

216

shape of the cenospheres, the particles cannot transfer the applied load easily and it causes a decrease in the impact energy to break and impact strength. By increasing the cenosphere content above 6phr, the impact energy and strength are almost steady or nearly unaffected, which indicates more efficient load transfer in the composites containing higher loading of cenosphere particles.
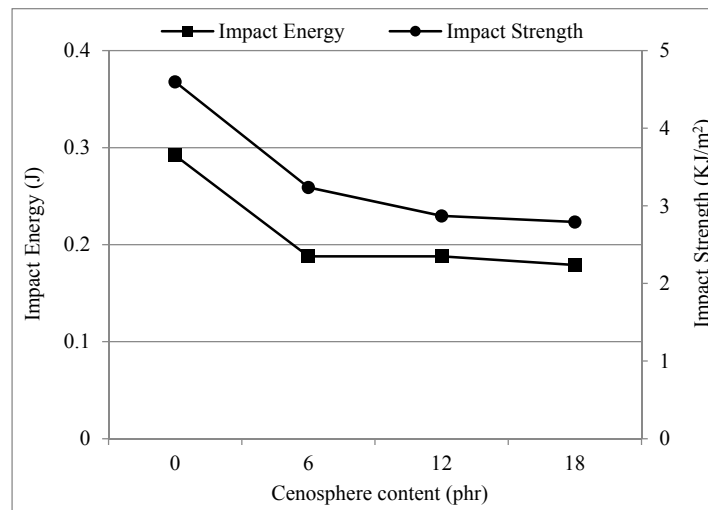
Figure 0-11: Impact strength and energy of PVC-Cenosphere foam composites

The mechanical properties of the PVC/cenosphere foam composites are summarized in Table 8-4.

Table 0-4: Summary of the mechanical properties of PVC-Cenosphere foam composites

Sample	Tensile Strength (MPa)	Tensile Modulus (MPa)	Flexural Strength (MPa)	Flexural Modulus (MPa)	Impact Energy (J)	Impact strength (KJ/m^2)
Pure	9.06	213.35	18.54	35.358	0.29	4.6
TG6	10.65	269.37	19.23	83.69	0.188	3.24
TG12	11.85	290.04	22.28	101.33	0.188	2.87
TG18	12.00	333.18	22.98	113.59	0.179	2.79

8B.3.4. Thermal Properties

The results from TGA analysis of the PVC/cenosphere foam composites are shown in Figure 8-12 and the degradation temperatures are summarized in Table8-5. The pure samples show primary degradation temperature (PDT) and secondary degradation temperature (SDT) at 288.82°C and 428.76 °C; respectively. TGA analysis shows insignificant change in PDT of the composites compared to pure samples, i.e. ~3-5°C, which is attributed to the separation of chlorine from the polymer chains. Enthalpy of PDT increases by adding cenospheres to PVC matrix and this increment in TG18 is about 23°C, which is the maximum value. SDT is related to cracking of the hydrocarbon backbone, which is found to improve significantly in the case of cenosphere filled composites. It means that, in cenosphere filled samples more energy is required to break the hydrocarbon backbone indicating some bonding between the filler and the matrix.

A comparison between the final degradation enthalpies show that the enthalpy of polymer backbone breaking increases with increasing the cenosphere content. It shows a maximum value in TG18, which is almost 350% improvement compared to the pure samples. Cenosphere is a ceramic material and has hollow shaped structure; therefore by increasing the cenospheres content, the void portion of the cenospheres increases and the thermal conductivity decreases, and consequently the degradation temperature increases.

The residual weight in thermal degradation is the undecomposed inorganic filler and ash. Residual weight at 800°C is found to be 17.95% in pure samples indicating that the ash of the PVC compound and the residual weight in TG6 containing 6phr cenosphere is 18.97% which is only 5.68% higher than pure sample. This factor increases with increasing the cenosphere content up to 27.13% in TG18 which has the highest amount of cenosphere loading.

Table 0-5: Thermogravimetric Analysis (TGA) of foam specimens

Sample	PDT[a] (℃)	Enthalpy of PDT (J/g)	SDT[b] (℃)	Enthalpy of SDT (J/g)	%Residual weight at 800℃
Pure	288.82	110.6	440.70	9.74	17.95
TG6	284.55	128.3	451.85	17.35	18.97
TG12	283.50	125.1	453.77	27.63	23.4
TG18	285.09	143.8	457.18	43.99	27.13

[a] PDT- Initial Degradation Temperature; [b] SDT-Final Degradation Temperature
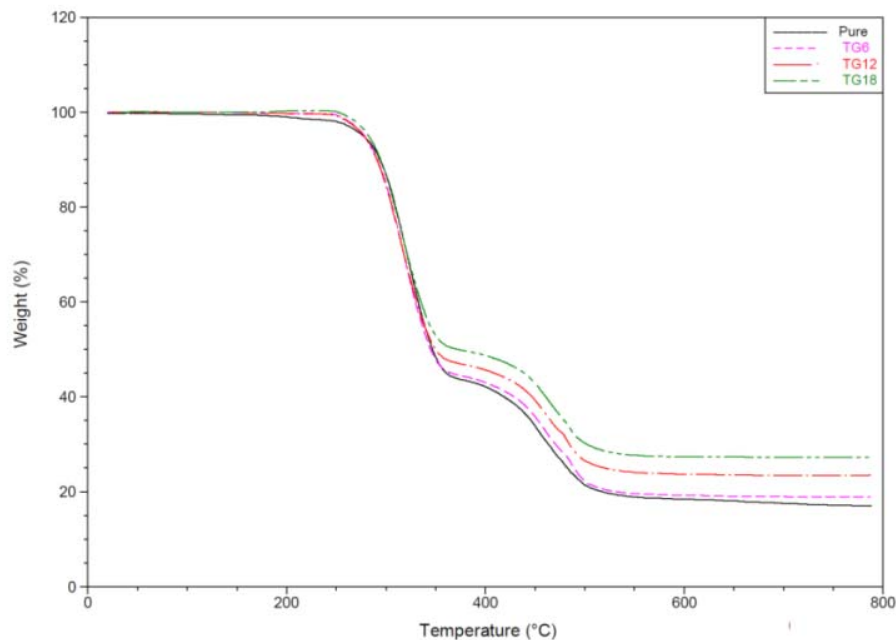
Figure 0-12: TGA curves of PVC/Cenosphere foam composites

Figure 8-13 shows DSC thermograms of PVC/cenosphere foam composites. Glass transition temperature (T_g) and percentage of gelation of the PVC foam composites don't seem to change significantly with the incorporation of cenospheres in the composites. This behavior was also observed in our previous work. PVC/natural filler and PVC/Carbon fiber composite systems

reported by Iulianelli et al. and Rathy et al.; respectively. The degree of gelation, initial (Tg_i), middle (Tg_m), and final T_g (Tg_f) values are reported in Table 8-6.
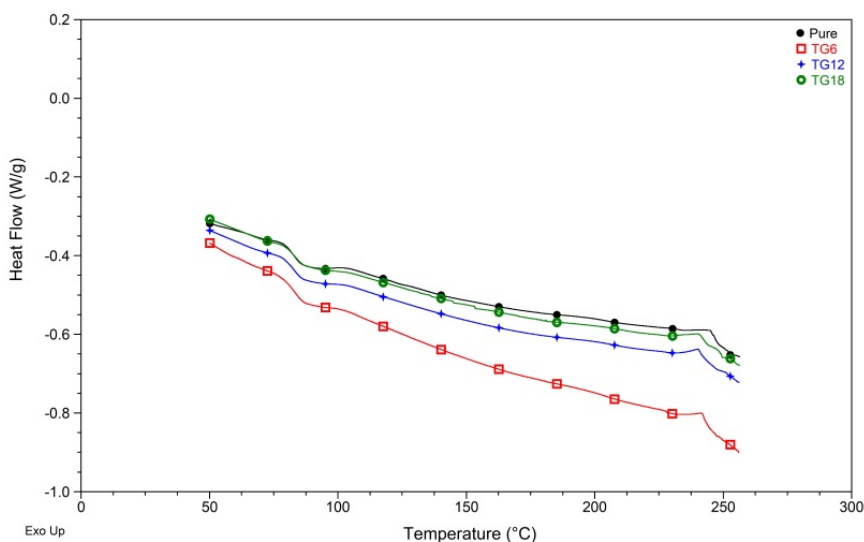
Figure 0-13- DSC curves of PVC/Cenosphere foam composites

Table 0-6: DSC analysis of PVC/Cenosphere foam composites

Sample	Tg_i	Tg_m	Tg_f	%Gelation
Pure	79.17	82.55	86.81	85.79%
TG6	78.71	83.61	86.33	77.43%
TG12	78.97	82.69	86.78	78.03%
TG18	80.02	83.45	86.91	82.17%

The viscoelastic properties of the PVC/cenosphere composites were determined by DMA analysis. These are reported in terms of variations of storage modulus (E'), which represents the elastic nature, and loss modulus (E"), which represents the viscous nature, as a function of temperature. E' and E" are presented in Figures 8-14a and 8-14b; respectively. The magnitude of E' seems to increase significantly with the incorporation of cenospheres. This increase indicates an

improvement of the stiffness in accordance with the expectations of the common behavior of composites filled with rigid spherical particles. The extent of increase of storage modulus in TG18 at 50 °C is approximately 180% compared to pure samples.

The peak intensity of loss modulus is found to increase with the addition of small amounts of cenospheres (6phr) to PVC foam. This phenomenon may be due to the enhancement in the energy dissipation ability as a result of the presence of spherical filler in the composites and also an increase in the polymer-filler and filler-filler slippage at Tg. Tg of the PVC/cenosphere foam composites was measured in two different ways; as the temperature at the peak of the loss modulus and as the temperature at the maximum of tanδ at about 1Hz frequency. Both values, reported in Table 8-7, are almost constant up to 12phr cenosphere loading, however it increases 1°C in TG18, which may be due to the segmental immobilization of the filler surface.

Table 0-7: Tg of PVC/Cenosphere foam composites as defined by
the peak of loss modulus curve and tanδ at 1Hz frequency

Sample	Pure	TG6	TG12	TG18
Tg (C) from E"	84.19	84.10	84.77	85.87
Tg (C) from tanδ	93.49	93.08	93.43	94.48
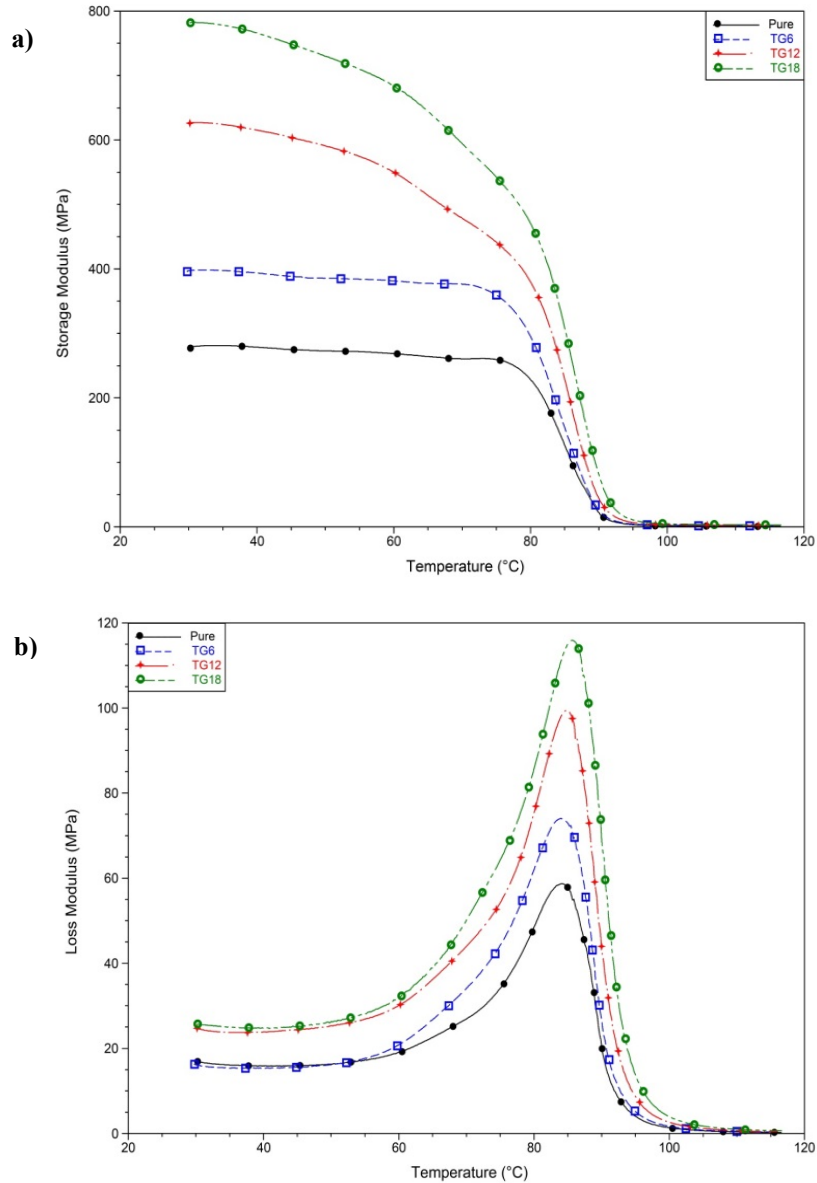
Figure 0-14: Dynamic mechanical analysis plots of PVC-cenosphere foam composites (a) storage modulus (E') and (b) loss modulus (E") versus temperature.

8B.3.5. Microstructural Properties

The interfacial interaction between the cenosphere particles and the foam matrix walls, as well as the state of dispersion and distribution of the cenospheres at the microstructural level were investigated by SEM. Figure 8-15 shows the SEM images of PVC foam composites with different

loadings of cenosphere particles. The difference in cenosphere loading in the samples between 6 to 18phr is visible in figures 8-15(a) to (c), at a constant magnification of 200x, indicating a good distribution of the cenospheres in the foam matrix. In addition, it is evident in figures (a)-(c) that the foam cell size decreases with increasing the cenosphere content due to the higher restriction to the foaming process.

At a higher magnification of 1000x, figures (d) to (f) show the presence of tightly embedded and physically interlocked cenosphere particles within the PVC matrix walls. This observation indicates a strong interaction between the filler and the matrix and also a good dispersion of cenosphere particles. By increasing the cenospheres content, the number of broken cenospheres is found to be higher, which is attributed to a shifting from ductile plastic deformation to brittle failure mechanism in the cenospheres during the foam cell formation.

8B.4. Conclusions

PVC-foam composites containing cenosphere fly ash were successfully extruded with up to 12phr loading without adversely affecting the properties of the foam. The addition of cenospheres resulted in an increase in the foam density. Both the tensile strength and modulus increased by incorporating cenosphere fly ash, indicating good interfacial bonding between the filler and the matrix. Flexural strength improved by increasing the cenospheres content, which is attributed to higher stiffness of the composites. Impact strength and impact energy remained almost constant with increasing the cenospheres content from 6phr to 18phr, which indicates efficient load transfer in the composites containing cenosphere particles.

The final and primary decomposition temperatures, measured by TGA, increased and slightly decreased; respectively, whereas the enthalpy in both temperatures increased by adding more

223

cenospheres. Dynamic mechanical analysis confirmed the increase in stiffness by increasing cenosphere content in the composites and also the presence of good interfacial adhesion between the cenosphere particles and the matrix. SEM images revealed good dispersion, distribution, and interaction between the cenosphere particles and the PVC matrix.
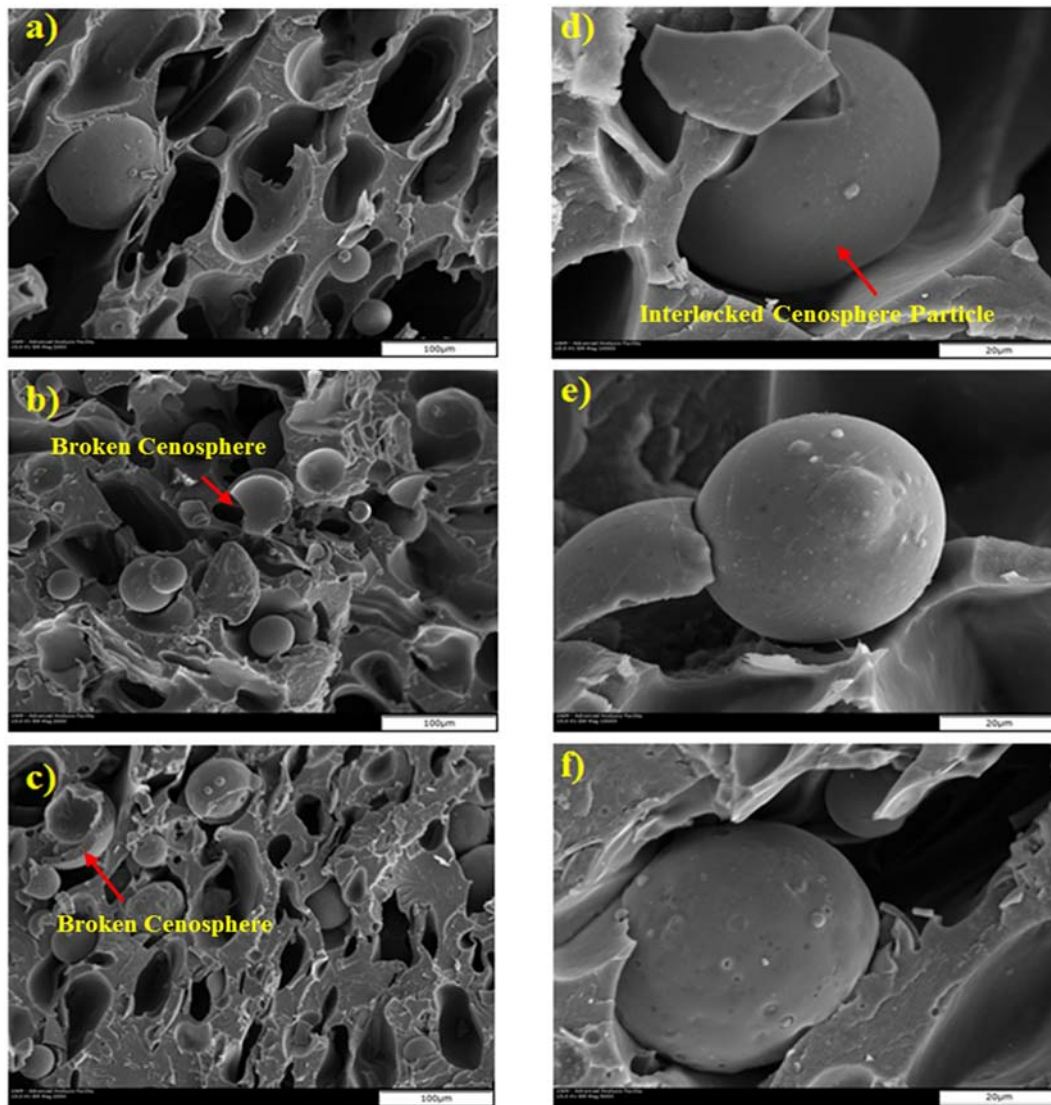

Figure 0-15: SEM images of PVC/Cenosphere composites, (a) TG6 (200x), (b) TG12 (200x), (c) TG18 (200x), (d) TG6 (1000x), (e) TG12 (1000x), (f) TG18 (1000x).

Appendix C) Properties of Rigid PVC Foam Composites Reinforced with Different Shape Fillers

8C.1. Experimental

8C.1.1. Materials

Phlogopite Mica PW80 was used as received from LKAB Minerals, Inc., USA. It has a plate-like structure with a size distribution ranging from 45 to 250µm and an average measured density of 0.25g/cm^3. It mainly consists of quartz, magnesium oxide, potassium oxide, and alumina. Milled and saline treated E-glass fibers, with a mean length of 1.6mm, an average diameter of 16µm, and a measured density of 0.3g/cm^3 were used as received from Fiber Glast Developments Corporation, USA. Fly ash particles were collected from WE Energies power plant in Oak Creek, Wisconsin, USA. Fly ash is a fine powder with a spherical structure and a wide particle size distribution ranging from 0.1 to 1000 µm with a measured density of 2.5g/cm^3. Based on chemical characterizations of fly ash reported in our previous work [31, 32], fly ash mainly contains quartz, mullite, hematite, magnetite, and lime. SEM micrographs of reinforcements are shown in Figure 8-16.
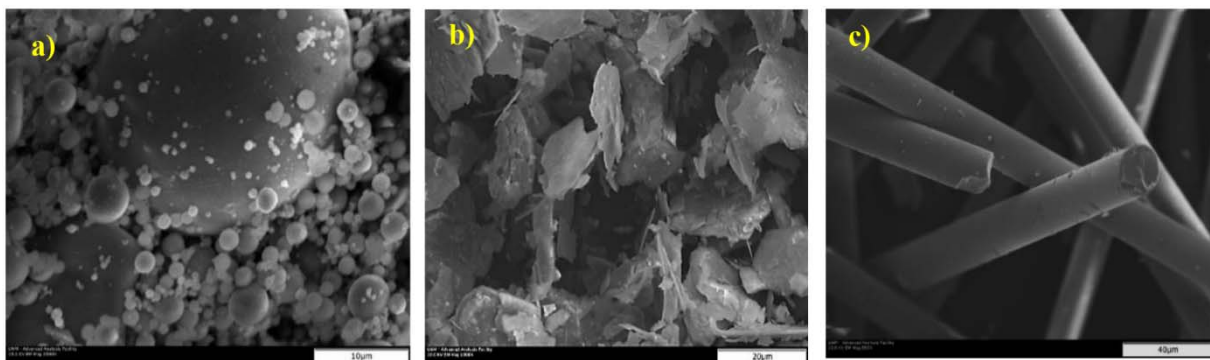

Figure 0-16-: SEM micrographs of a) Fly Ash, b) Mica, c) Glass Fibers

8C.1.2. Preparation of PVC/Fly ash foam composites

PVC foam compound was prepared using a high shear mixer (Gunther Pepenmeier, Type: TSHK). The stabilizer was added at 52ºC, reinforcing fillers and processing aids were added to the PVC resin at 52ºC and 58ºC; respectively. Finally, the lubricants and the blowing agents were added at 66ºC. PVC foam compounds containing 0, 10, and 20wt% reinforcement were prepared by using single screw extruder (Thermoplas New England Wire Machinery Co. Inc.) with L/D ratio of 20:1 and a screw speed of 60 rpm. The temperature profile in the extruder barrel was maintained in the range of 158 to 175ºC. The extrudate was air cooled and cut using an automated cutter. The composite formulations and sample codes, based on the reinforcement content and type, are listed in Table 8-8. In the sample code, FA-, M-, and GF- correspond to the samples containing Fly ash, Mica and Glass Fiber; respectively.

Table 0-8 -PVC foam composites formulation

Sample Code	PVC resin	FA	Mica	Glass Fiber
Pure	100	0	0	0
FA10	100	10	0	0
M10	100	0	10	0
GF10	100	0	0	10
FA20	100	20	0	0
M20	100	0	20	0
GF20	100	0	0	20

8C.3. Results and Discussion

8C.3.1. Mechanical Properties

Tensile properties of PVC foam composites are presented in Figure 8-17a. It can be observed that, by adding 10 wt% fly ash, tensile strength decreases, while it improves slightly with the addition of glass fibers or mica. This indicates that in M10 and GF10 composites, fillers carry their share of the load. At higher glass fiber and mica loadings, tensile strength drops by the rate of 8.26% and 16.12%; respectively. In fact, counterbalance phenomenon can affect tensile strength of a polymer composite; increasing the filler content results in an increase in the effective surface fracture energy, size of voids and filler particles agglomeration. Crack propagation path in a composite with a dispersed filler is longer, which results in partial energy absorption and consequently plastic deformation enhancement. Therefore, the surface fracture energy and the strength of the composites increase with increasing the volume percentage of the fillers. However, with increasing the filler content, the void fraction, caused by the polymer matrix detaching from the filler particles, becomes critically large to initiate the main crack. In addition, agglomeration of the dispersed filler particles increases with increasing the filler content, which results in decreasing the mechanical strength due to the lower strength of the agglomerates themselves.

A comparison between the trends of variation in tensile strength of the reinforced composites shows that the tensile strength in fly ash loaded composites increases with increasing fly ash content from 10wt% to 20wt%. In other words, PVC chain movements in 20wt% fly ash loaded composite are less restricted than M20 and GF20. This can be attributed to the spherical shape of fly ash particles, which provides less possibility of filler-polymer bonding as compared to longitudinal glass fibers or flaky mica fillers.

227

The reduction of area in PVC foam composites was also measured to show the ductility variation in the samples. As shown in Figure 8-17b, the ductility of the composites decreases with the addition and increasing the amount of filler, which indicates that brittleness increases in the PVC foam composites. The rate of reduction of area in PVC/mica composites is lower than glass fiber and fly ash composites, which represents higher toughness in these composites.
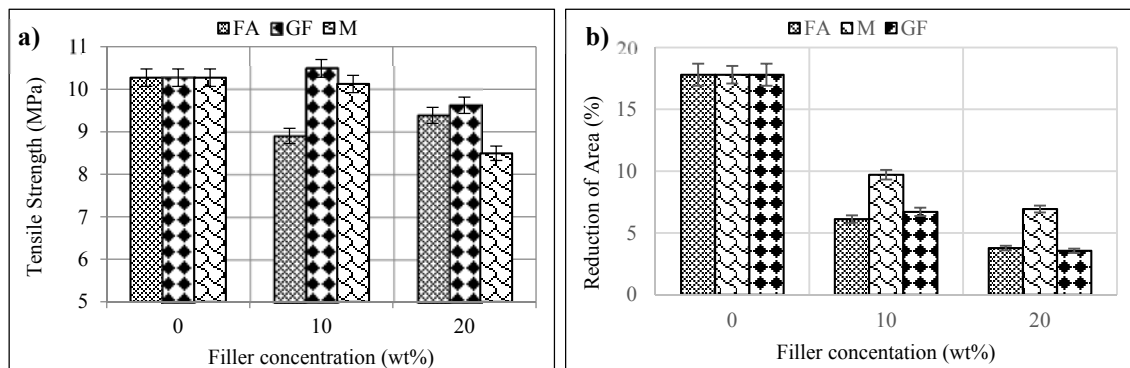

Figure 0-17-: a) Tensile Modulus, and b) Tensile Strength versus filler concentration

The flexural modulus exhibits an increasing trend in all PVC foam reinforced composites, as shown in Figure 8-18a. Since the modulus of the composites depends on the individual properties of the matrix components, i.e., filler and polymer, and since the modulus of fillers is generally higher than the polymer itself, the flexural modulus of the filled composites is higher than the pure samples. The trend of variation in the flexural strength of different filler composites, with varying concentrations, is presented in Figure 8-18b.

Flexural strength of PVC/glass fiber foam composites increases continuously with increasing the concentration of glass fibers; while in the case of mica and fly ash, the flexural strength increases up to 10wt%, but thereafter decreases. This phenomenon indicates that the saturation level of the filler matrix composition is determined by the filler agglomeration.

Mica plate's orientation is mostly parallel within the cell walls and their agglomeration in the foam walls starts at 20wt% mica content. Whereas, long glass fibers penetrate and interlock mainly across multiple cell walls along the length of the fibers; therefore it may have lower agglomeration tendency compared to other filled composites. SEM results of fly ash filled composites show that the fly ash particles can be in both foam walls and foam cells. It has lower possibility of agglomeration than the flaky shaped mica fillers due to its low surface energy. Therefore, mica and glass fibers have the lowest and the highest saturation level of filler matrix composition; respectively, whereas fly ash has a level which falls between those two due to its wide particle size range.
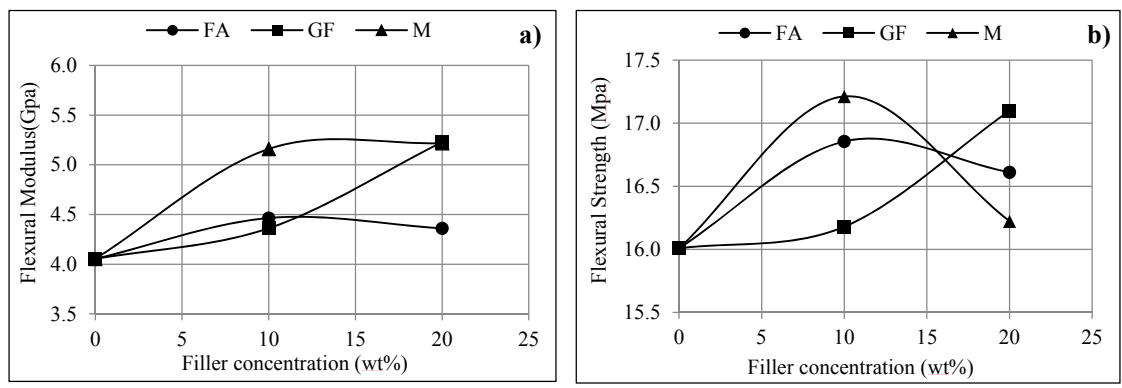
Figure 8-18- a) Flexural Modulus, and b) Flexural Strength versus filler concentration

In Figure 8-18b, it can also be observed that flexural strength increases and attains its maximum level at 10wt% mica content as compared to fly ash and glass fiber filled composites. The increase in flexural strength of M10 composites is attributed to the high aspect ratio of mica due to its platy shape, which results in a better interaction between the polymer chains and the filler surface. In addition, mica contains SiO_2 functional group, which can react with polymer chains through covalent bonds and make a high interfacial bonding with the PVC matrix. By incorporating 20wt% mica,

229

flexural strength drops significantly due to the higher tendency of agglomeration at higher loadings due to its high aspect ratio and surface area.

Charpy impact test measures the energy to break the test sample under banding condition. The measured notched charpy impact strength versus filler concentration of PVC foam composites with different types of filler is shown in Figure 8-19. In general, adding fillers to PVC foam decreases the impact strength, which may be attributed to the higher brittleness of the composites compared to the pure foam due to the higher reinforcement rigidity. Moreover, immobilization of polymer chains by fillers inhibits the growth of plastic deformation, which absorbs fracture energy. Therefore, in the composite samples, crack propagation tendency increases and hence causes lower impact strength than pure foams. A comparison between 10wt% filled composites show that FA10 and GF10 have the lowest and highest impact strength; respectively, which can be attributed to the low load transfer ability of spherical shape fly ash particles and high load transfer ability of longitudinal shape of glass fibers.
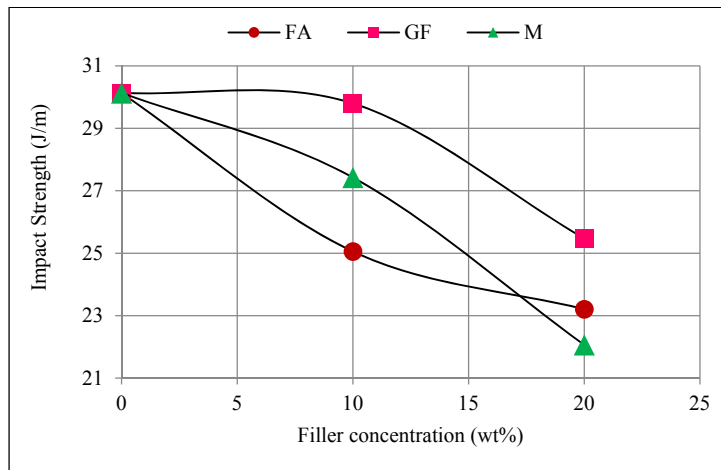

Figure 8-19 Charpy impact energy variation in PVC foam composites versus filler concentration

8C.3.2.Thermal Properties

Figure 8-20 shows thermal gravimetric (TG) thermograms of the PVC foam composites, where two major weight losses can be observed in all cases. Pure PVC foam is stable at low temperatures, while at about 270°C, its weight loss percentage suddenly drops to 50% and gradually decreases before 400°C. The second drastic drop occurs at around 450°C. The weight loss percentage remains constant at about 20% until the temperature reaches 800°C. The amount of the final ash shows an increasing trend with increasing the filler content, which is related to the undecomposed inorganic fillers and ash.
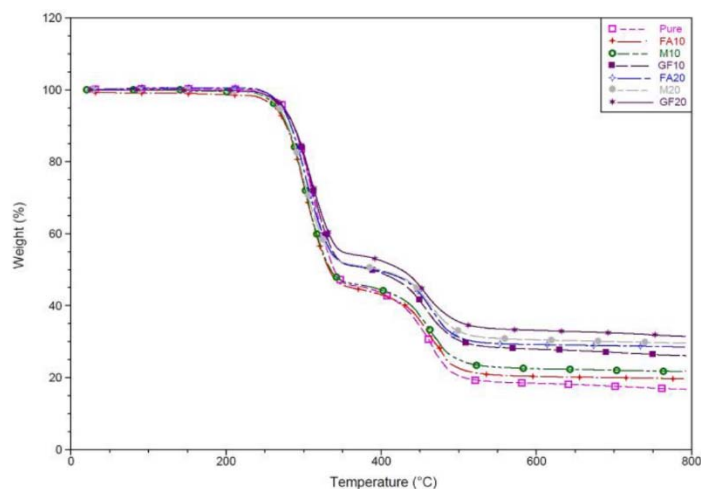
Figure 8-20- Thermal Gravimetric results of PVC composites

At the first decomposition step, separation of chlorine occurs. Adding a filler to PVC foam decreases the value of the first decomposition temperature (Figure 8-21a) and its rate varies with varying the filler type and concentration. Azodicarbonamide (AZO) is a known chemical blowing agent, which decomposes at 195-216°C during PVC foaming process to make a large volume of gases. The decomposition temperature decreases with adding finely dispersed filler additives by activating the blowing agent and providing nucleation sites for gas evolution. As is shown in Figure

6a, the rate of reduction in the first decomposition temperature in GF10 is about 0.45% and this value increases to 0.91% by adding 20wt% glass fiber to PVC foam. Therefore, the first decomposition temperature of PVC foam is relatively stable by adding up to 20wt% glass fiber. However, the first decomposition temperature drops approximately 7°C and 8°C in the presence of 10wt% fly ash and mica; respectively. Increasing fly ash content to 20wt% results in increasing the first decomposition temperature by about 1°C, while it remains constant in the case of mica filled composites. A comparison between the first decomposition temperatures of the composites show that HCl gas formation is more delayed in PVC/glass fiber composites, due to their highest temperature of the first decomposition
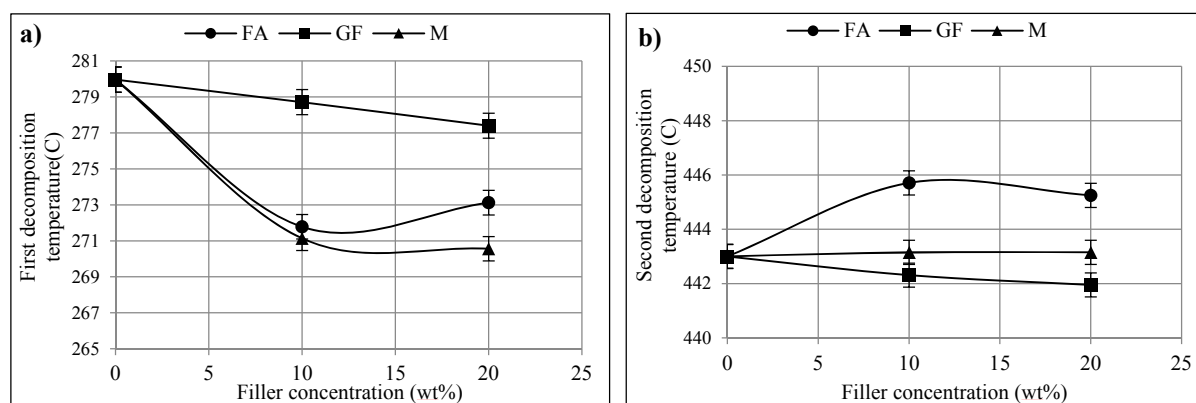
Figure 8-21- a) First Decomposition Temperature, and b) Second Decomposition Temperature variation versus filler concentration

The second decomposition temperature of PVC foam composites follows an increasing trend, as shown in Figure 8-21b. Thermal degradation of the polyene backbone occurs at this step, resulting in the formation of volatile aromatic compounds and a stable carbonaceous residue. In FA10, the second decomposition temperature improves by about 3°C from 443°C to 446°C and remains constant even after adding 20wt% fly ash, which shows the highest second decomposition

temperature value compared to other PVC foam composites. Fly ash particles are distributed in both cell walls and cell bubbles, while glass fibers are mainly dispersed through cell bubbles and mica flakes are dispersed in cell walls. Therefore, it is expected to have more interfacial interaction between fly ash and the matrix backbone in the case of fly ash filled composites. This can be the reason of higher thermal stability in fly ash reinforced composites compared to other composites. Whereas, the second decomposition temperature of GF10 is almost the same as pure samples; i.e. 443°C, which is the lowest temperature among PVC foam composites. The rate of hydrocarbon backbone cracking is the lowest in fly ash filled PVC composites due to their highest temperature of the second decomposition.

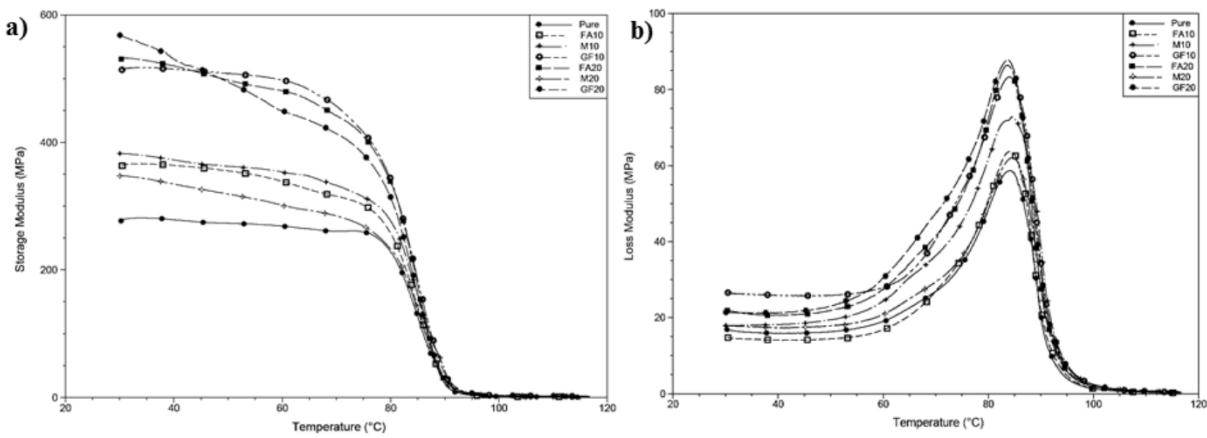*Figure 8-22- Dynamic mechanical behavior of PVC foam composites a) storage modulus (E'),*

and b) loss modulus (E'')

Figure 8-22a presents the effect of filler type and concentration on the storage modulus, E′, of the PVC foam composites, over a temperature range of 30°C to 120°C. As shown in Figure 8-22a, in both the glassy and rubbery regions, E′ of the PVC foam composites is higher than the pure

samples. According to the loss modulus presented in Figure 8-22b, the glass transition temperature is negligibly affected by the filler type and content.

As shown in Figure 8-23, at 50°C, well below the glass transition temperature, PVC foam composites reinforced with 10wt% glass fiber show the highest storage modulus of 499MPa. This improvement may be due to the longitudinal form of glass fibers with multiple cell walls interlocked structure. Whereas, the incorporation of 20wt% glass fiber in the PVC foam results in a reduction of storage modulus value to 448MPa, which may be due to an increasing tendency of agglomeration at higher glass fiber content. The incorporation of 10wt% mica in the PVC foam increases storage modulus and it drops thereafter, which may be due to low critical volume fraction in the flaky shape fillers. Whereas, the storage modulus of fly ash filled composites increases with increasing the fly ash content at nearly a constant rate. This can be attributed to the higher saturation level of the spherical shaped fillers, due to their lower surface area than platy and longitudinal fillers.

The storage modulus of the PVC foam composites at 85°C is also affected by the content and type of the filler. In 10wt% glass fiber and mica filled composites, the storage modulus is about 162MPa, an increase of about 35% when compared to pure PVC foams. Adding 20wt% glass fiber and mica to the matrix results in a reduction in the storage modulus above glass transition temperature. In the case of fly ash reinforced composites, incorporating 10wt% fly ash does not alter the storage modulus; significantly. Meanwhile, adding 20wt% fly ash increases the storage modulus by 41% and 48% compared to FA10 and pure foam; respectively.
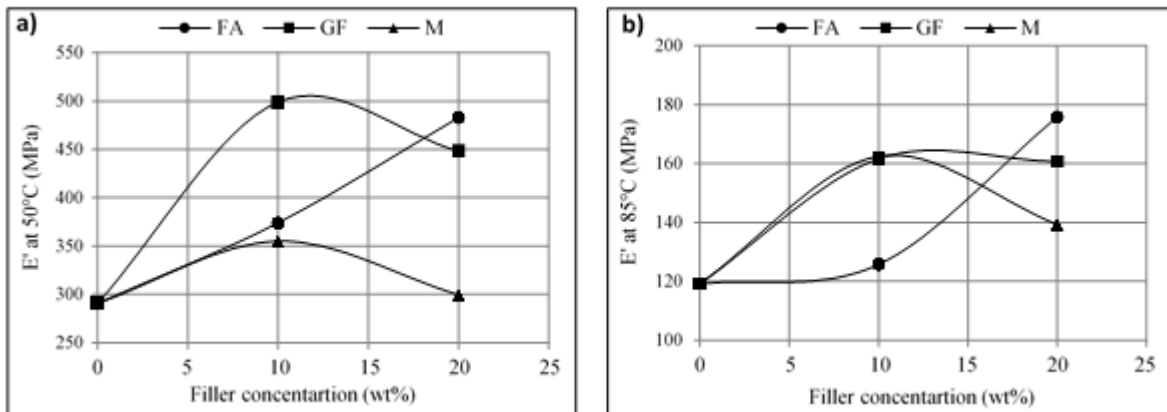
Figure 8-23- Storage modulus (E') of PVC foam composites a) below Tg at 50°C, and b) above Tg at 85°C versus filler concentration

8C.3.3. FTIR Spectroscopy

Figure 8-24 shows the FTIR spectra of PVC foam composites containing 0 and 10wt% of reinforcements. Peaks set in the range of 2800-3000 cm^{-1} correspond to C-H stretch bonds. The peak at higher wave number is the asymmetric stretch bond of C-H and the lower peak is the symmetric stretch bond of C-H. The peaks around 1400 cm^{-1} are assigned to C-H aliphatic bending bond. The peak at 1250 cm^{-1} is attributed to the bending bond of C-H near Cl. The C-C stretch bond of the PVC backbone chain occurs in a range of 1000-1100 cm^{-1}. Finally, peaks in the range of 600-650 cm^{-1} correspond to C-Cl gauche bonds.

A comparison between the FTIR spectra of the reinforced foam composites with the pure samples, as a reference, shows that the C-H stretching and CH2 bending peaks in the pure samples with wave numbers of approximately 2800-3000 cm^{-1} and 1400 cm^{-1}; respectively, are maximum and the peak intensity decreases by adding reinforcements. Another significant difference is the existence of a very wide and sharp peak in M10 samples with a wave number of approximately 1000

235

cm^{-1}, which can be attributed to an overlapping of the main characteristic peak of mica and C-C stretch bond of the main backbone.

8C.3.4. Microstructural Properties

Figure 8-25 presents SEM micrographs of the fractured surfaces of PVC foam tensile samples with various fillers. As shown in Figure 10a, glass fibers have a good interaction with the polymer matrix. They penetrate through foam cells and interlock them, which can be one of the main reasons of good mechanical strength of PVC/glass fiber composites. Increasing glass fiber content increases agglomeration tendency due to their high aspect ratio and low surface energy, which is shown in Figure 8-25b. Mica flakes are mainly dispersed through cell walls and since the cell wall thickness is small, the possibility of agglomeration increases in mica reinforced PVC foam composites at high loading (Figure 8-25c). Therefore, it is expected to see a low saturation level of mica filled composites to reach the maximum mechanical strength, which is confirmed by mechanical results. SEM micrograph of fly ash filled composites, presented in Figure 9d, show that fly ash particles are dispersed in both cell walls and cell voids, which exhibit less particle agglomerate formation compared to glass fibers and mica composites at the same loading levels.

8C.4.Conclusion

PVC foam composites reinforced with different fillers; i.e. glass fibers, mica, and fly ash, were prepared to investigate the effect of longitudinal, flaky, and spherical filler shapes on their mechanical, thermal, and microstructural properties. The tensile strength of PVC foam composites decreased at 10wt% fly ash content, while in mica and glass fiber composites it increased slightly. Mica and fly ash reinforced PVC foam composites exhibit greater flexural strength than glass fiber at 10wt% loading, whereas at 20wt% glass fiber reinforced composite show higher flexural strength

than both mica and fly ash reinforced composites. Charpy impact strength decreased with the addition of fillers in accordance with the higher rigidity of the reinforcements and this reduction was lower in glass fiber reinforced composites. TGA characterization of the composites showed that the increase of thermal stability in spherical fly ash composites, due to the good particles distribution, is more pronounced than mica and glass fiber foam composites. Dynamic mechanical studies indicated that storage modulus of mica and glass fiber reinforced composites have an increasing trend below and above glass transition temperature up to 10wt% loading, while in fly ash reinforced composites it increases with increasing filler content up to 20wt%. SEM images show fly ash particles to be uniformly distributed in the foam composites, while the mica flakes and glass fibers are mainly dispersed through cell walls and cell bubbles; respectively. Due to the narrower distribution areas of mica flakes and glass fibers compared to fly ash particles, the agglomeration possibility in mica and glass fiber reinforced composites is higher in comparison with PVC/fly ash foam composites.
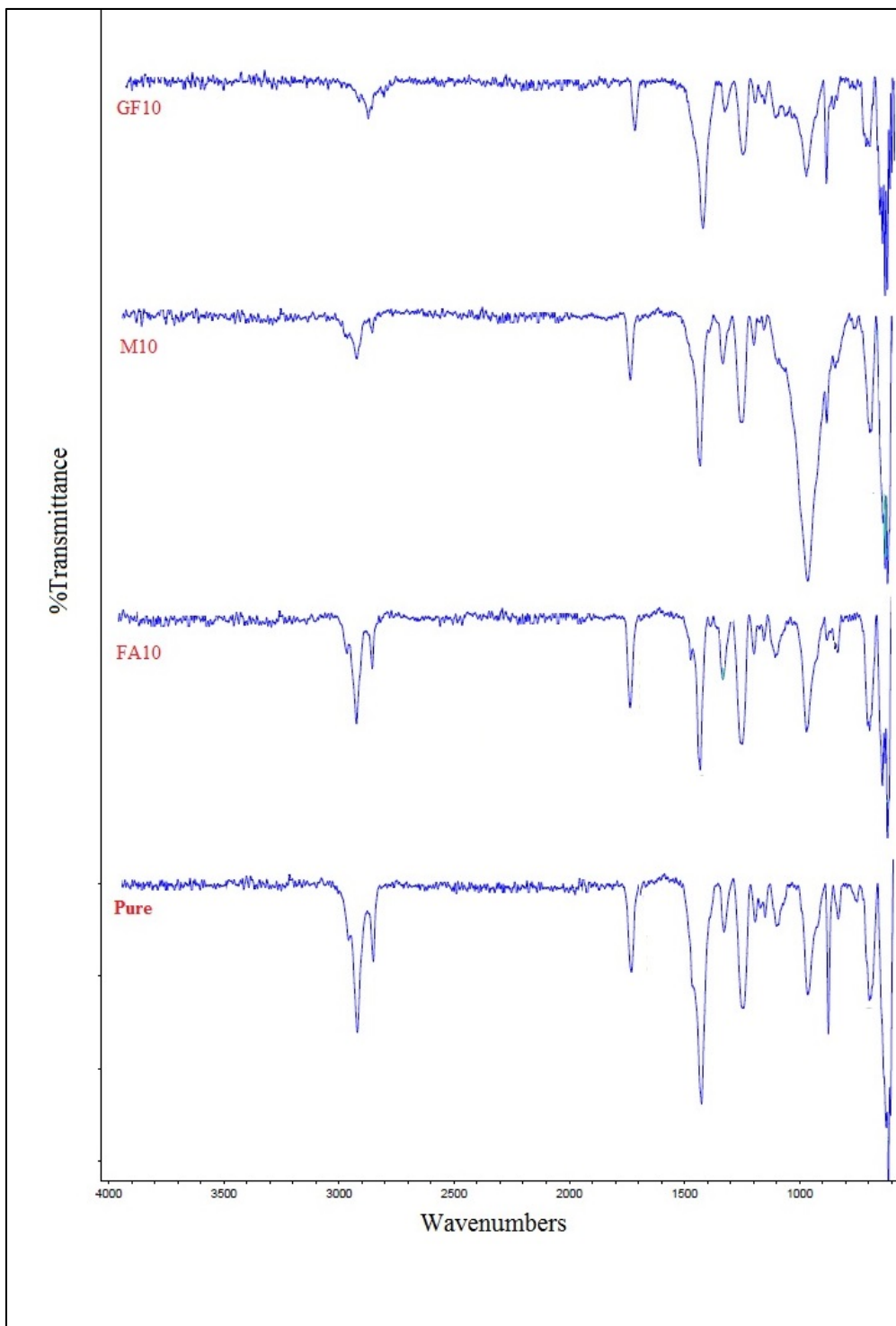
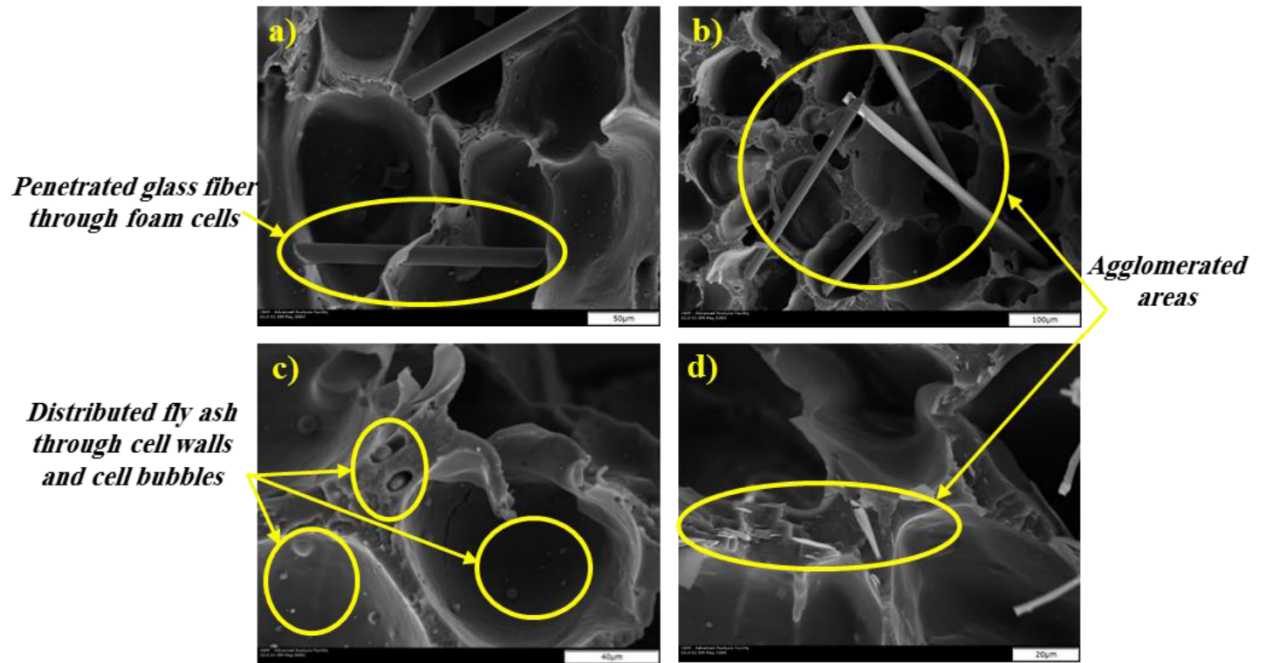*Figure 8-24- FTIR spectrum of pure, FA10, M10, and GF10 samples.*

238

Figure 8-29- SEM micrographs of a) GF10, b) GF20, c) FA20, and d) M20.

Curriculum Vitae

Parisa Khoshnoud

Place of Birth: Tehran, Iran

Education:

B.Sc., *Polymer Science and Engineering*, Science and Research Branch, Islamic Azad University, Tehran, Iran; August 2007.

M.Sc., *Polymer Engineering*, Amirkabir University of Technology (Tehran Polytechnic), Tehran, Iran; February 2011.

Ph.D., *Materials Science and Engineering*, University of Wisconsin in Milwaukee, USA, August 2017.

Dissertation Title: Polymer Foam /Fly ash Composites: Evaluation of Mechanical, Interfacial, Thermal, Viscoelastic and Microstructural properties

Internship: *SACO AEI Polymers*, Sheboygan, Wisconsin, February 2016-Present.

Work Experiences

August 2017- Present

- Research and Development Scientist*, SACO AEI Polymers*, Sheboygan, Wisconsin.

April 2011-June 2013
- Research and Development Engineer, Persian Chemicals Company, *working on esterification process, synthesizing Zinc stabilizers based on phthalates (aqueous and powder), oleates, and stearates, and synthesizing of Butyl Benzyl Phthalate (BBP) plasticizer*.

October 2009-April 2011
- Research and Development Engineer, Sepehran Polymer Company, *working on troubleshooting and improving injection molding process of PP, PE, PMMA, PC, and PVC using Mold Flow software.*

Peer Reviewed Journal Publications:

1) P. Khoshnoud, "Plastic Processing Technology at University of Wisconsin-Platteville", Baspar Magazine, 88, pp. 75- 77, 2009.

2) P. Khoshnoud, "Radiation cross-linked plastics: a versatile material solution for packaging, automotive, Electrotechnic and Electronics*", Baspar Magazine, 87, pp. 52 - 54, 2009.*

3) P. Khoshnoud, S. Gunashekar, M. Jamel, N. Abu-Zahra, "Evaluating the Performance of Class-F Fly Ash Reinforced PVC Foam Composites", *International Journal of Innovative Research in Science, Engineering and Technology,* (2015), 4(9), 9419-27.

4) P. Khoshnoud, N. Abu-Zahra, "Effect of Cenosphere Fly Ash on the Thermal, Mechanical, and Morphological Properties of Rigid PVC Foam Composites", *Journal of Research Updates in Polymer Science*, 2015, 4 (1), 1-14.

5) P. Khoshnoud, S. Gunashekar, M. Jamel, N. Abu-Zahra, "Comparative Analysis of Rigid PVC Foam Reinforced with Class-C and Class-F Fly Ash", *Journal of Minerals and Materials Characterization and Engineering*, 2014, 2, 554-565.

6) P. Khoshnoud, N. Abu-Zahra, "Properties of Rigid PVC Foam Composites Reinforced with Different Shape Fillers", *Journal of Thermoplastic Composite Materials*, 2016, 1-19.

7) P. Khoshnoud, J. Carl Wolgamott, N. Abu-Zahra, "Evaluating Recyclability of Fly Ash Reinforced PVC Foams", *Journal of Vinyl and Additive Technology*, 2016.

8) S. Golbad, P. Khoshnoud, N. Abu-Zahra, "Hydrothermal synthesis of hydroxy sodalite from fly ash for the removal of lead ions from water", *International Journal of Environmental Science and Technology*, 2016, pp. 1-8.

9) S. Golbad, P. Khoshnoud, N. Abu-Zahra, "Synthesis of 4A zeolite and characterization of calcium- and silver-exchanged forms", *Journal of Minerals and Materials Characterization and Engineering,* 2017, 5(5).

10) M. Jamel, P. Khoshnoud, S. Gunashekar, N. Abu-Zahra, " Enhancement of Dimensional Stability of Rigid PVC Foams using E-Glass Fibers", *Journal of Minerals and Materials Characterization and Engineering*, 2015, 3 (02), 65.

11) M. Jamel, P. Khoshnoud, S. Gunashekar, N. Abu-Zahra Mechanical "Properties and Dimensional Stability of Rigid PVC Foam Composites Filled with High Aspect Ratio Phlogopite Mica", *Journal of Minerals and Materials Characterization and Engineering*,

2015, 3 (04), 237.

12) M. Jamel, <u>P. Khoshnoud</u>, S. Gunashekar, N. Abu-Zahra, "Effect of E-Glass Fibers and Phlogopite Mica on the Mechanical Properties and Dimensional Stability of Rigid PVC Foams", *Journal of Polymer-Plastics Technology and Engineering*, 2015, 54 (15), 1560-1570.

13) <u>P. Khoshnoud</u>, N. Abu-Zahra, "The effect of particle size of fly ash on the interfacial interaction and performance of PVC/FA composites", *Journal of Composites Science and Technology,* submitted August 2017.

14) <u>P. Khoshnoud</u>, N. Abu-Zahra, "Kinetics of Thermal Decomposition in PVC/Fly Ash Composites", *Journal of Polymer Composites*, submitted August 2017.

15) <u>P. Khoshnoud</u>, N. Abu-Zahra, "Fly Ash Characterization: The effects of Fly Ash Class and Particle size on its Physical, Chemical, Structural, Thermal and Microstructural Properties", under revision.

Conference Papers:

1) Nidal H. Abu-Zahra, <u>Parisa Khoshnoud</u>, Murtatha Jamel, Subhashini Gunashekar, *ICMCE 2015: XIII International Conference on Materials and Chemical Engineering*, 2015, Jeddah, Jan. 25-26.

2) Nidal H. Abu-Zahra, Murtatha Jamel, <u>Parisa Khoshnoud</u>, Subhashini Gunashekar, *ICMCE 2015: XIII International Conference on Materials and Chemical Engineering*, 2015, Jeddah, Jan. 25-26.

3) <u>P. Khoshnoud</u>, A.A. Katbab, *Polymer Processing Science (PPS) conference*, Marrakech, 2011.

4) <u>P. Khoshnoud</u>, A.A. Katbab, *43th MACRO*, India, 2010.

5) <u>P. Khoshnoud</u>, A.A. Katbab, *32th Australian Polymer Science (APS) Conference*, Australia, 2010.

6) <u>P. Khoshnoud</u>, A.A. Katbab, *Polymer Processing Science (PPS) Conference*, Iran, 2010.

7) <u>P. Khoshnoud</u>, A.A. Katbab, *10th Iran International Rubber Industry conference*, 2010.